Toward High Precision Higgs-Boson Measurements at the International Linear e^+e^- Collider

The Higgs Working Group at Snowmass '05

S. Heinemeyer[ay*], S. Kanemura[b], H. Logan[c], A. Raspereza[d], T. Tait[e]

H. Baer[f], E.L. Berger[e], A. Birkedal[g], J.-C. Brient[h], M. Carena[i] J.A.R. Cembranos[j], S. Choi[k], S. Godfrey[c], J. Gunion[l], H.E. Haber[g], T. Han[m], H. Heath[n], S. Hesselbach[o], J. Kalinowski[p], W. Kilian[q], G. Moortgat-Pick[a], S. Moretti[r], S. Mrenna[i], M. Muhlleitner[s], F. Petriello[m], J. Reuter[q], M. Ronan[t], P. Skands[i], A. Sopczak[u], M. Spira[v], Z. Sullivan[e], C. Wagner[ew], G. Weiglein[x], P. Zerwas[o]

Abstract

This report reviews the properties of Higgs bosons in the Standard Model (SM) and its various extensions. We give an extensive overview of the potential of the ILC operated at center-of-mass energies up to 1 TeV (including the $\gamma\gamma$ collider option) for the determination of the Higgs boson properties. This includes the measurement of the Higgs boson mass, its couplings to SM fermions and gauge bosons, and the determination of the spin and the CP quantum numbers of the Higgs. We also discuss extensions of the SM, including heavy SM-like Higgs bosons, heavy Higgs bosons in the framework of Supersymmetry (SUSY) and more exotic scenarios. We review recent theoretical developments in the field of Higgs boson physics, and the impact of Higgs boson physics on cosmology in several SUSY frameworks is considered. The important questions as to what the ILC can contribute to Higgs boson physics after the LHC, the LHC/ILC interplay and synergy, are addressed. The impact of the accelerator and detector performance on the precision of measurements are discussed in detail and we propose a strategy to optimize future analyses. Open questions arising for the various topics are listed, and further topics of study and corresponding roadmaps are suggested.

*email: Sven.Heinemeyer@cern.ch

[a]CERN, TH division, Dept. of Physics, 1211 Geneva 23, Switzerland
[b]Department of Physics, Osaka University, Toyonaka, Osaka 560-0043, Japan
[c]Ottawa Carleton Inst. for Physics, Carleton University, Ottawa, Ontario K1S 5B6, Canada
[d]Max-Planck-Institut fr Physik, Föhringer Ring 6, 80805 München, Germany
[e]High Energy Physics Division, Argonne National Laboratory, Argonne, IL 60439, USA
[f]Dept. of Physics, Florida State University, Tallahassee, Florida 32306, USA
[g]Santa Cruz Institute for Particle Physics, Santa Cruz, CA 95064 USA
[h]Laboratoire Leprince-Ringuet, Ecole polytechnique, Palaiseau, France
[i]Theoretical Physics Department, Fermilab, Batavia, IL 60510, USA
[j]Department of Physics and Astronomy, University of California, Irvine, CA 92697, USA
[k]Department of Physics, Chonbuk National University, Chonju 561-756, Korea.
[l]Department of Physics. University of California at Davis, Davis CA 95616, USA
[m]Department of Physics, University of Wisconsin, Madison, WI, 53706, USA
[n]Physics Department, University of Bristol, Tyndall Ave, Bristol BS8 1TL, UK
[o]High Energy Physics, Uppsala University, Box 535, S-751 21 Uppsala, Sweden
[p]Institute of Theoretical Physics, Warsaw University, Hoza 69, 00681 Warsaw, Poland
[q]Deutsches Elektronen-Synchrotron DESY, D–22603 Hamburg, Germany
[r]School of Physics & Astronomy, Southampton University, Highfield SO17 1BJ, UK
[s]Laboratoire d'Annecy-Le-Vieux de Physique Théorique, LAPTH, Annecy-Le-Vieux, France
[t]Lawrence Berkeley National Laboratory, USA
[u]Department of Physics, Lancaster University, Lancaster, LA1 4YW, UK
[v]Paul Scherrer Institut, CH-5232 Villigen PSI, Switzerland
[w]Enrico Fermi Institute, University of Chicago, 5640 Ellis Ave., Chicago, IL 60637, USA
[x]Institute for Particle Physics Phenomenology, University of Durham, Durham DH1 3LE, UK
[y]Depto. de Física Teórica, Universidad de Zaragoza, 50009 Zaragoza, Spain

Contents

Chapter 1

Introduction

Elucidating the mechanism of electroweak symmetry breaking (EWSB), by which the electroweak gauge bosons and the fermions acquire masses, will be one of the main tasks of future collider experiments. Ultimately, all theoretical models rely on some form of the Higgs mechanism to explain EWSB through spontaneous symmetry breaking. In the Standard Model (SM) [1], this is postulated by introducing one fundamental scalar doublet field whose potential leads it to acquire a non-zero vacuum expectation value. Three of the real scalar components of the doublet are eaten by the gauge bosons, leaving one physical scalar particle referred to as Higgs boson [2]. Although this particle has eluded experimental observation so far, high precision measurements of electroweak observables provide indirect indications for a light Higgs boson. Updated electroweak data set an upper limit on the Higgs mass of about 200 GeV at 95% confidence level [3]. The preferred value of the Higgs boson mass as extracted from the global fits of electroweak observables is 91 GeV, with an experimental uncertainty of $+45$ and -32 GeV [3]. This result strongly depends on the assumption that the SM describes all physics up to high energy scales, and thus is not a proof that the SM Higgs boson actually exists. Rather, the results of electroweak fits serve as guidelines as to what mass range is to be expected. The results of experimental searches for the Higgs boson at LEP set a lower limit on the SM Higgs boson mass of about 114 GeV [4].

If a SM-like Higgs boson exists, it is expected to be seen at the Large Hadron Collider (LHC) at CERN [5]. To be certain the state observed is the Higgs boson, it is necessary to measure the couplings of this state to the W and Z gauge bosons, and to fermions such as the top and bottom quarks and the tau leptons. Progress along these lines will be achieved at the LHC [5–7], but the international linear e^+e^--collider (ILC) is absolutely essential for making precise measurements of a full set of these couplings and for establishing the nature of EWSB [8–11].

Many models beyond the SM, e.g., supersymmetric extensions of the SM, predict extended Higgs sectors containing more than one physical scalar state and therefore enriching Higgs boson phenomenology. A common feature of the models with such extended Higgs sectors is the existence of additional scalar bosons, such as charged Higgs bosons and CP-odd Higgs boson(s). Discovery of these extra scalar particles would be direct evidence for physics beyond the SM and be vital for our understanding of the structure of EWSB. Once these additional Higgs bosons are found, we would be able to test each new physics model by measuring details of their properties accurately at ILC. A $\gamma\gamma$ collider option provides further opportunity for the heavy Higgs search, where various properties of the heavy Higgs bosons, such as the CP-parity, can be explored.

In this report we address the following questions:

- What are the most important measurements that the ILC should perform in the subject of Higgs boson physics?

- What are the key measurements by which the ILC will add to what will be known already from the LHC?

- For each of these measurements, what criteria for the detectors are necessary to allow the measurements with the required precision?

- What are the open questions in the fields of theory, experimental analyses and detector developments that have to be addressed for a successful ILC program?

- For these open questions, what is the best way to answer them in a comprehensive and systematic way?

Consequently, we review the properties of Higgs bosons in various models in Sect. 2. This includes the possible mass ranges, as well as a general overview about production and decay modes. In Sect. 3 we give an extensive overview about the potential of the ILC operated at center-of-mass energies up to 1 TeV (including the $\gamma\gamma$ option) for the determination of the Higgs boson properties within the framework of the SM and its various extensions. This comprises the measurement of the Higgs boson mass, its couplings to SM fermions and gauge bosons, and the determination of the spin and the CP quantum numbers of the Higgs. The extensions of the SM that are analyzed in more detail are heavy SM-like Higgs bosons, heavy Higgs bosons in the framework of supersymmetry (SUSY) and further exotic scenarios. We review in Sect. 4 recent theoretical developments in the field of Higgs boson physics. This includes higher-order corrections to Higgs boson masses and production cross sections in the SM and the Minimal Supersymmetric Standard Model (MSSM), the possibility of CP-violation, as well as extensions of the MSSM such as the NMSSM, gauge-extended models, and Fat Higgs. We also summarize work on non-supersymmetric models, such as Little Higgs models, models with extra dimensions, and dimension-six Higgs operators. A list of Higgs related computer tools (spectrum generators, decay packages, event generators) is provided in Sect. 5. The important question of what the ILC can contribute to Higgs boson physics after the LHC, the LHC/ILC interplay and synergy, is discussed in Sect. 6. It is emphasized that if a Higgs-like state is discovered at the LHC and the ILC, independent of the realization of the Higgs mechanism, important synergistic effects arise from the interplay of LHC and ILC [12]. Higgs boson physics can also have an important impact on our understanding of cosmology. This is analyzed for the MSSM and the NMSSM case in Sect. 7. The above listed issues and analyses impose certain detector requirements to achieve the necessary precision. The impact of the accelerator and detector performance on the precision of measurements are analyzed in detail in Sect. 8. We propose a strategy to optimize future analyses. Open questions arising for the topics in the various chapters are listed, and further topics of study and corresponding roadmaps are suggested.

Chapter 2

Production and Decays of Higgs Bosons

In this section we review the experimental status of Higgs boson production and decay at the ILC and the photon collider (γC). For the corresponding theoretical results and developments, see Sect. 4.

2.1 The Higgs boson mass

2.1.1 Limits from theory

The Higgs boson h is yet to be discovered, and its mass m_h remains unknown. In the SM, m_h is a parameter which characterizes the property of the Higgs dynamics. Since $m_h \propto \sqrt{\lambda} v$ (λ is the quartic term in the Higgs potential, v denotes the vacuum expectation value), a light h means that the Higgs sector is weakly-interacting, while a heavy h corresponds to strong coupling. Although m_h is an unknown parameter, by imposing the requirement that the theory must be consistent up to a given value of the cutoff scale Λ, the allowed region of m_h can be predicted as a function of Λ [13]. Based on this requirement, a renormalization group analysis for the coupling constant λ gives upper and lower bounds on m_h for a given Λ. In the SM, for $\Lambda = 10^{19}$ GeV, the allowed region of m_h is evaluated as about $135 < m_h < 180$ GeV, while for $\Lambda = 10^3$ GeV it is about $m_h < 500$ GeV. The results are summarized in Fig. 2.1 [14], evaluated for $m_t = 175$ GeV.

Hence, as long as the SM Higgs sector is assumed, a light Higgs boson would indicate a weakly coupled theory with a high cut-off scale. Scenarios based on grand unified theories might correspond to this case. In such cases, supersymmetry would necessarily be required to reduce the problem of the large hierarchy between the weak scale and the scale Λ. On the contrary, a heavy Higgs boson with $m_h \sim$ several hundred GeV would imply a strongly-coupled Higgs sector with a low cutoff $\Lambda \sim \mathcal{O}(1)$ TeV. In such a case, the Higgs sector should be considered as an effective theory of a new dynamics at TeV scales. Therefore, from knowing the mass of the Higgs boson, a useful hint for new physics beyond the SM can be obtained. Figure 2.2 shows the mass range of the (lightest) Higgs boson under the assumption of $\Lambda = 10^{19}$ GeV in the SM [13], the minimal supersymmetric SM (MSSM) [15–17] (see also Sect. 4.1), some extended SUSY models [18] and the general two Higgs doublet model [19]. Due to its strong dependence on the other model parameters, the lightest Higgs boson mass in the MSSM and its extensions is one of the most important observables in the Higgs sector.
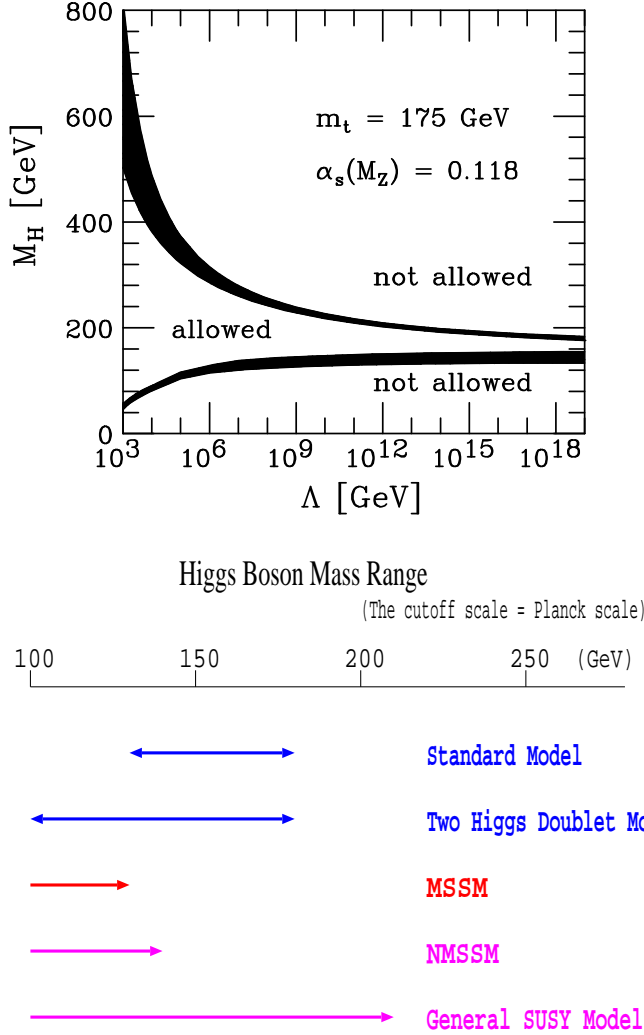
Figure 2.1: Summary of the uncertainties connected to the bounds on m_h. The upper solid area indicates the sum of theoretical uncertainties in the m_h upper bound for $m_t = 175$ GeV [14]. The upper edge corresponds to Higgs masses for which the SM Higgs sector ceases to be meaningful at scale Λ, and the lower edge indicates a value of m_h for which perturbation theory is certainly expected to be reliable at scale Λ. The lower solid area represents the theoretical uncertainties in the m_h lower bounds derived from stability requirements using $m_t = 175$ GeV and $\alpha_s = 0.118$.

Figure 2.2: Predictions of the mass range of a Higgs boson for various models [20]. The upper and lower bound of the Higgs boson mass is derived from an assumption that each model is valid up to the cut-off scale of the theory, which is taken to be 10^{19} GeV. For the MSSM case, the mass bound is obtained without reference to the cutoff scale.

2.1.2 Experimental limits on the SM Higgs boson mass

The mass of the SM Higgs boson is bounded from below by direct searches at LEP to be $M_H > 114.4$ GeV at the 95% C.L. [4]. An upper limit can be obtained from a global fit to all electroweak precision data [3]. Including the new experimental m_t value of $m_t = 172.7$ GeV [21], the fit yields $M_H = 91^{+45}_{-32}$ GeV with an upper limit of $M_H < 186$ GeV at the 95% C.L. The fit was performed under the assumption that the SM including the Higgs sector gives a correct description of the experimental data. Therefore it does *not* confirm the SM Higgs sector. Higgs masses larger than about 200 GeV are only possible if other new physics effects would compensate the effect of the heavy Higgs on the electroweak precision data, see e.g. [22, 23]. In most cases, some hints of these new physics effects are expected to be visible at either the LHC or ILC (or both).

2.2 Standard Model Higgs Production and Decays

In e^+e^- collisions, the SM Higgs boson is predominantly produced through the Higgs-strahlung process, $e^+e^- \to HZ$, and through vector boson fusion processes $e^+e^- \to \nu_e\bar{\nu}_e(e^+e^-)H$. The cross section of the main production mechanisms as a function of the Higgs boson mass is presented in Fig. 2.4 for the three representative centre-of-mass energies, 350, 500 and 800 GeV.

7
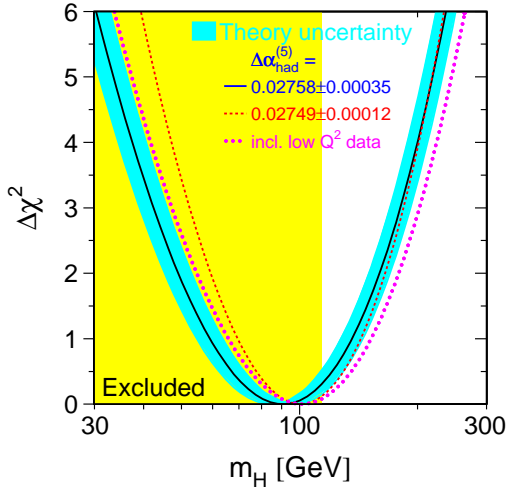
Figure 2.3: Global fit to all electroweak precision data within the SM [3] (including the new m_t value of $m_t = 172.7$ GeV). The fit yields $M_H = 91^{+45}_{-32}$ GeV with an upper limit of $M_H < 186$ GeV at the 95 % C.L. The fit was performed under the assumption that the SM including the Higgs sector gives a correct description of the experimental data.

The Higgs boson can be detected and its profile can be studied in detail over a wide mass range by exploiting various decay modes. Being responsible for generation of fermion and weak boson masses, the Higgs boson decays preferentially into the heaviest kinematically accessible final states. The dependence of the branching ratios of the SM Higgs boson on its mass is illustrated in Fig. 2.5.
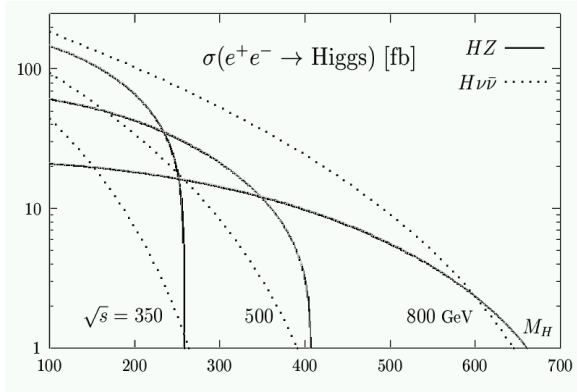
Figure 2.4: SM Higgs boson production cross sections as a functions of the Higgs boson mass.
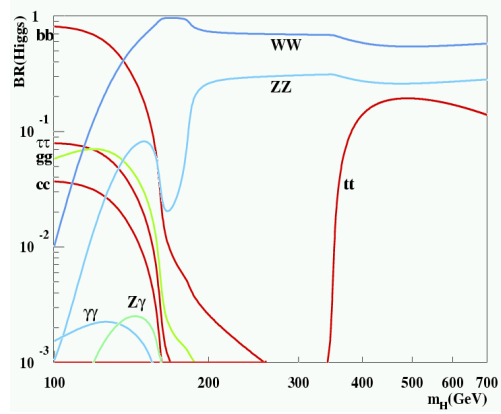
Figure 2.5: SM Higgs boson branching ratios as a functions of the Higgs boson mass.

2.3 Higgs Bosons in General Two Higgs Doublet Models

Among models with an extended Higgs sector, two Higgs doublet models are of particular interest, since this structure of the Higgs sector is required in MSSM [24, 25]. In CP-conserving two Higgs doublet models, spontaneous symmetry breaking gives rise to five physical scalar states: two CP-even Higgs bosons, the lighter one denoted h and heavier H, one CP-odd boson A and two charged bosons, $H^{\pm}$. At tree level in the MSSM, the mass spectrum is determined by $\tan \beta$ and the mass of CP-odd boson m_A. The mass of the light Higgs boson is constrained to be smaller than the

mass of the Z boson, $m_h < M_Z$. Higher order corrections, in particular from loops involving third generation fermions and their superpartners, move the upper limit on m_h up to about 135 GeV [16,17].

In addition to supersymmetry, there are lots of motivations to consider models with two Higgs doublets at the electroweak scale, such as top-color [26], Little Higgs models [27], some extra dimension models, and the model of gauge-Higgs unification [28]. Tiny neutrino masses (*e.g.*, the Zee model [29]), and extra CP violating phases which may be required for the realization of electroweak baryogenesis [30] also can be studied by introducing multi scalar doublets (plus singlets) at the electroweak scale. The analysis of phenomenology in the framework of the general two Higgs doublet model can make it possible to distinguish these nonstandard models.

In the CP-conserving MSSM and more general two Higgs doublet model, the cross sections of the Higgs-strahlung and weak boson fusion processes involving CP-even bosons scale with the coupling of the appropriate Higgs to gauge bosons relative to that in the SM. These couplings are given by

$$g_{hZZ,hWW} \sim \sin(\beta - \alpha), \qquad\qquad g_{HZZ,HWW} \sim \cos(\beta - \alpha), \qquad\qquad (2.1)$$

where α is the mixing angle in the CP-even sector. The set of tree level couplings between neutral Higgs particles and weak bosons is extended by two additional couplings,

$$g_{hAZ} \sim \cos(\beta - \alpha), \qquad\qquad g_{HAZ} \sim \sin(\beta - \alpha). \qquad\qquad (2.2)$$

As a consequence, in e^+e^- collisions, the Higgs-strahlung and fusion processes will be complemented by the associated Higgs boson pair production mechanisms, $e^+e^- \to h(H)A$. Neutral Higgs bosons can be also accessed via Yukawa processes, $e^+e^- \to H(A)b\bar{b}$, $e^+e^- \to H(A)t\bar{t}$. The former reaction is of particular importance, since it allows to extend the mass reach for neutral Higgs bosons up to values close to the collision centre-of-mass energy.

The MSSM exhibits a so-called decoupling limit as m_A becomes large, $m_A \gtrsim 200$ GeV. In this scenario, h approaches the properties of the SM Higgs boson, while H decouples from the weak bosons. As a consequence the H boson production via Higgs-strahlung or weak boson fusion processes gets suppressed, whereas the cross section of the process $e^+e^- \to HA$ reaches its maximal value. Another distinct feature of the decoupling limit is a tiny mass splitting between H and A, making it practically impossible to distinguish them by mass. For a large portion of MSSM parameter space, decoupling is realized and the decay properties of h are close to those of the SM Higgs boson, while H and A decay predominantly into the heaviest kinematically accessible fermions, $\tau^+\tau^-$, $b\bar{b}$ or $t\bar{t}$. However, scenarios are possible in which decay rates of heavy neutral Higgs bosons into supersymmetric particles become significant.

Charged Higgs bosons can be produced in e^+e^- collisions in pairs, $e^+e^- \to H^+H^-$. In this process, the mass reach for the charged Higgs boson is limited to half of centre-of-mass energy. Hence, it would be desirable to investigate also the rare processes of single charged Higgs boson production. The dominant processes of the single charged boson production are: $e^+e^- \to H^+b\bar{t}$, $e^+e^- \to H^+\tau^-\nu_\tau$, $e^+e^- \to H^+W^-$, $e^+e^- \to H^+e^-\bar{\nu}_e$. Recent theoretical calculations [31–34] showed that, in general, the parameter regions for which single charged Higgs boson production cross sections exceeds 0.1 fb are rather small beyond the pair production threshold. The main decay channels of the charged Higgs bosons are $H^+ \to c\bar{s}$, $H^+ \to \tau^+\nu_\tau$ and, if kinematically allowed, $H^+ \to t\bar{b}$.

Figure 2.6 shows contour plots of the production cross-sections in the m_A-$\tan\beta$ plane for the following processes: $e^+e^- \to ZH$, Ah, AH, H^+H^-, $W^\pm H^\mp$, $b\bar{b}A$, $b\bar{b}H$, $t\bar{t}A$, $t\bar{t}H$, and $\nu\bar{\nu}H$ [35]. In Figures 2.6 (a), (c), (d), (e) and (f), the mass reach for A, H, and $H^\pm$ at the ILC is determined by half of $\sqrt{s}$. In Figure 2.6(b), if the sensitivity reaches to 0.1fb, the discovery contours for

9

the $b\bar{b}A$ and $b\bar{b}H$ modes go beyond $\sqrt{s}/2$ for large $\tan\beta$. For $\tan\beta \lesssim 10$, the ZH (Ah) mode is available above $m_A > \sqrt{s}/2$. In Figure 2.6(c)-(f), cross-section contours of $e^+e^- \to t\bar{t}A$, $t\bar{t}H$, $b\bar{b}A$, and $b\bar{b}H$ exhibit a dependence on $\tan\beta$ for 350 GeV $\lesssim m_A \lesssim \sqrt{s}/2$. These processes include $e^+e^- \to AH$ followed by A or H decaying into a $b\bar{b}$ or $t\bar{t}$ quark pair. The $\tan\beta$ dependence shown in Figure 2.6(c)-(f) comes from the branching ratio of the heavy Higgs bosons. Figure 2.6(c)-(e) also shows that the ILC will cover the region of moderate $\tan\beta \lesssim 10$ and $M_A \lesssim \sqrt{s}/2$ where the detection of the heavy Higgs bosons at LHC is expected to be difficult. If kinematically allowed, the heavy Higgs bosons are expected to be found in several modes at the ILC. More details can be found in Sect. 4.2.
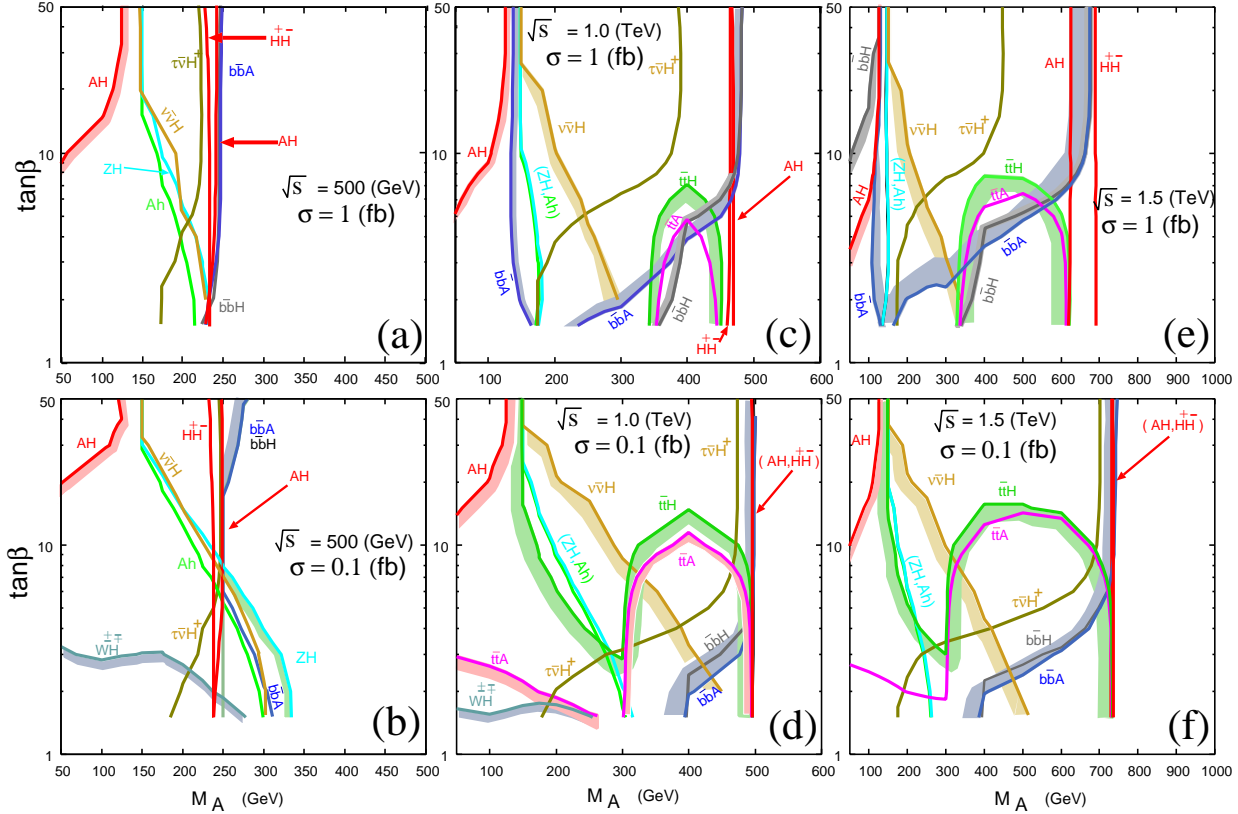
Figure 2.6: The cross-section contours: (a) for $\sqrt{s} = 500$ GeV and $\sigma = 1$ fb, (b) for $\sqrt{s} = 500$ GeV and $\sigma = 0.1$ fb, (c) for $\sqrt{s} = 1.0$ TeV and $\sigma = 1$ fb, (d) for $\sqrt{s} = 1.0$ TeV and $\sigma = 0.1$ fb, (e) for $\sqrt{s} = 1.5$ TeV and $\sigma = 1$ fb, and (f) for $\sqrt{s} = 1.5$ TeV and $\sigma = 0.1$ fb. GRACE/SUSY [36] is used to calculate the production cross-sections of the tree-level processes. One-loop induced production of W^+H^- is calculated as in Refs. [31, 32]. Masses of the Higgs bosons and the mixing angle of the neutral Higgs bosons are obtained by using FeynHiggs [37], where we assume the diagonal masses to be $(1 \text{ TeV})^2$ in the stop mass matrix and maximal stop mixing. HDECAY [38] is used to calculate decay widths of the Higgs bosons.

2.4 Higgs Boson Production at a $\gamma\gamma$ collider

At a $\gamma\gamma$ collider, neutral Higgs bosons can be produced resonantly in the s-channel. Although Higgs bosons do not couple to photons at tree level, Higgs boson production in $\gamma\gamma$ collisions becomes possible due to loop-induced couplings as illustrated in Fig. 2.7. As compared to the e^+e^-

collision option, the $\gamma\gamma$ collider, operated at the same centre-of-mass energy, has higher mass reach for the Higgs bosons, as the whole collision energy is available for the resonant production of the Higgs particles in the s-channel [39–42]. In addition, we can determine the CP parity of the heavy Higgs boson through the process $\gamma\gamma \to t\bar{t}$ by measuring the helicity of the top quark [43]. Along with other nice features, described later on in this report, the high-mass discovery potential of the $\gamma\gamma$ collider makes it a particularly attractive running option of the International Linear Collider facility.

Technical aspects related to the $\gamma\gamma$ collision option are highlighted in References [44–46].
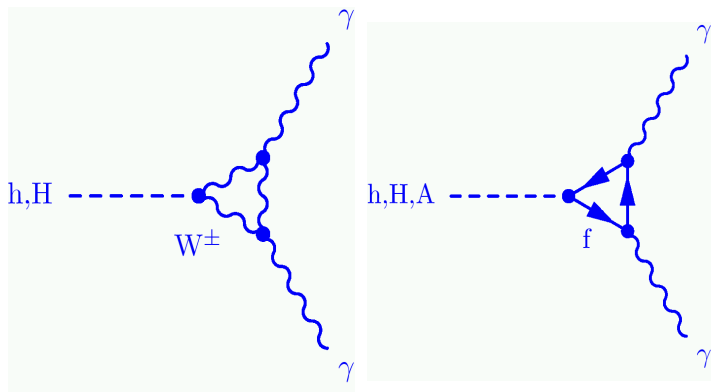
Figure 2.7: Loop-induced couplings of Higgs bosons to photons. Feynman diagram involving W boson loop (left plot). Feynman diagram involving charged fermion loop (right plot).

2.5 The role of polarization

For the ILC the possibility to have a polarized e^- beam is in the baseline design [47]. A polarization of up to 80% is foreseen. The possibility to have polarized e^+ as well is still under discussion. Here in principle a polarization of $\sim 60\%$ seems to be achievable. Polarization can be helpful in various aspects of Higgs boson physics.

- One of the major physics goals at the ILC is the precise analysis of all the properties of the Higgs particle. For a light Higgs the two major production processes, Higgs-strahlung, $e^+e^- \to HZ$, and WW fusion, $e^+e^- \to H\nu\bar{\nu}$, will have similar rates at $\sqrt{s} = 500$ GeV; see Sect. 2.2. Beam polarization will be important for background suppression and a better separation of the two processes. Furthermore, the determination of the general Higgs couplings is greatly improved when both beams are polarized [48].

- Searches for heavy SUSY Higgs particles can be extremely challenging for both the LHC and the ILC. Exploiting single Higgs-boson production in $e^+e^- \to \nu\bar{\nu}H$ extends the kinematical reach considerably. However, in the decoupling region, $M_A \gg M_Z$, the suppressed couplings of the heavy Higgs boson to SM gauge bosons lead to very small rates. This difficulty could be attenuated by accumulating a very high integrated luminosity, together with a further enhancement of the signal cross section by polarizing both beams, see also Sect. 4.2. Polarization can be decisive to discover MSSM Higgs bosons with low production cross sections [49]. Polarization of both the e^- and e^+ beams is important in this case.

- Compared with the case where only the electron beam is polarized, the polarization of both beams leads to a gain of about one order of magnitude in the accuracy of the effective weak mixing angle, $\sin^2\theta_{\mathrm{eff}}$ [50]. Within the SM, this has a dramatic effect on the indirect determination of the Higgs-boson mass, providing a highly sensitive consistency test of the

model that may possibly point towards large new-physics scales [51]. Within the MSSM, the large increase in the precision of $\sin^2\theta_{\text{eff}}$ will allow to obtain stringent indirect bounds on SUSY parameters [48]. This will constitute, in analogy to the SM case, a powerful consistency test of supersymmetry at the quantum level and may be crucial to constrain SUSY parameters that are not directly experimentally accessible [52, 53].

In order to fully exploit the possibility of beam polarization, several questions should be addressed in the above scenarios:

- What are the detector requirements for these measurements?

- What are the accelerator requirements?

- What are the theory requirements?

Partial answers are already available in Ref. [48].

Chapter 3

Measurements in the Higgs Sector at e^+e^- and $\gamma\gamma$ Colliders

In the following we review the Higgs boson sector measurements that can be performed at the ILC and the γC. The description of a SM-like Higgs boson (with mass below $\lesssim 140$ GeV) also applies to the lightest MSSM Higgs boson for large parts of the MSSM parameter space. The issue of heavy MSSM Higgs bosons is addressed separately.

3.1 Model Independent Determination of the Higgs-strahlung cross section

One of the nice features of the linear collider is its capability to detect the Higgs boson independent of its decay mode. Even if the Higgs boson decays into invisible particles[1], it can still be detected by exploiting the Higgs-strahlung production mechanism with subsequent decay of the Z into electron or muon pairs. The signal manifests itself as a peak in the distribution of invariant mass of the system recoiling against the electron or muon pair stemming from Z boson decay. This is illustrated in Fig. 3.1.

The results of the dedicated study [55] on model-independent measurement of the Higgs-strahlung cross-section, exploiting the $HZ \to X\ell^+\ell^-$ channel, are presented in Table 3.1. Combining the two final states $HZ \to Xe^+e^-$ and $HZ \to X\mu^+\mu^-$, the cross sections can be measured with statistical errors of 2.6 to 3.1% for Higgs masses from 120 to 160 GeV.

m_H (GeV)	σ (fb) $Z \to e^+e^-$	σ (fb) $Z \to \mu^+\mu^-$
120	5.26±0.18±0.13	5.35±0.21±0.13
140	4.38±0.18±0.11	4.39±0.17±0.10
160	3.68±0.17±0.09	3.52±0.15±0.08

Table 3.1: The results for the Higgs-strahlung cross-section measurement in the $HZ \to Xe^+e^-$ and $HZ \to X\mu^+\mu^-$ channels at $\sqrt{s} = 350$ GeV with an integrated luminosity of 500 fb^{-1}. The first error is statistical and the second is systematic.

---

[1]Scenarios of the Higgs boson decays into invisible particles are discussed in Sect. 3.10.2.
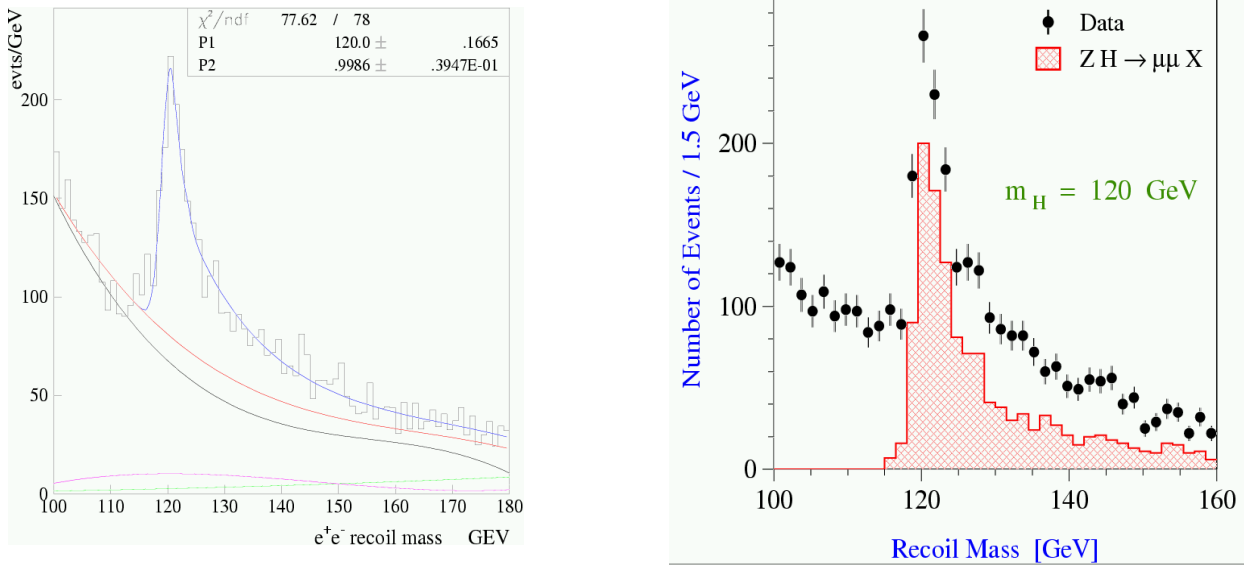
Figure 3.1: Distribution of the invariant mass of the system recoiling against a pair leptons in the channel $HZ \to Xe^+e^-$ [54] (left plot) and in the channel $HZ \to X\mu^+\mu^-$ [55] (right plot). The Higgs boson mass is 120 GeV. The left plot corresponds to the centre-of-mass energy of 340 and the right plot to 350 GeV. Assumed integrated luminosity is 500 fb^{-1} for both cases.

3.2   Determination of Higgs Boson Mass

The SM Higgs boson mass is a free parameter of the model and of great importance for the exploration of the EWSB mechanism. The prospects of Higgs mass measurement at a linear e^+e^- collider are investigated in References [56, 57]. The study presented in [56] focuses on the low and intermediate Higgs boson masses in the range from 120 to 180 GeV. The analysis utilizes Higgs boson decays into b-quark and W-boson pairs and Z boson decays into quark and charged lepton pairs. Considering hadronic decays of W bosons, four distinct topologies are covered: 2jet+2ℓ final states resulting from $HZ \to q\bar{q}\ell^+\ell^-$, 4jet from $HZ \to b\bar{b}q\bar{q}$, 4jet+2ℓ from $HZ \to WW\ell^+\ell^-$ and 6jet from $HZ \to WWq\bar{q}$. The study is performed for centre-of-mass energy of 350 GeV, assuming an integrated luminosity of 500 fb^{-1}. As an example, Fig. 3.2 shows the reconstructed Higgs boson mass spectra in the $HZ \to WWq\bar{q}$ channel for $m_H = 150$ GeV and the $HZ \to WW\ell^+\ell^-$ channel for $m_H = 180$ GeV.

From the fit of the resulting mass spectra, the Higgs boson mass can be extracted. Results of the analysis are summarized in Table 3.2.

| | $\Delta(m_H)$ in MeV | | |
Decay mode	120	150	180
$HZ \to q\bar{q}\ell^+\ell^-$	85	100	–
$HZ \to b\bar{b}q\bar{q}$	45	170	–
$HZ \to WW\ell^+\ell^-$	–	90	80
$HZ \to WWq\bar{q}$	–	100	150
Combined	40	65	70

Table 3.2: Uncertainties on the determination of m_H for $m_H = 120$, 150 and 180 GeV. For $m_H = 150$ GeV, the combination is done using the $HZ \to WW\ell^+\ell^-$ and $HZ \to WWq\bar{q}$ channels.

14
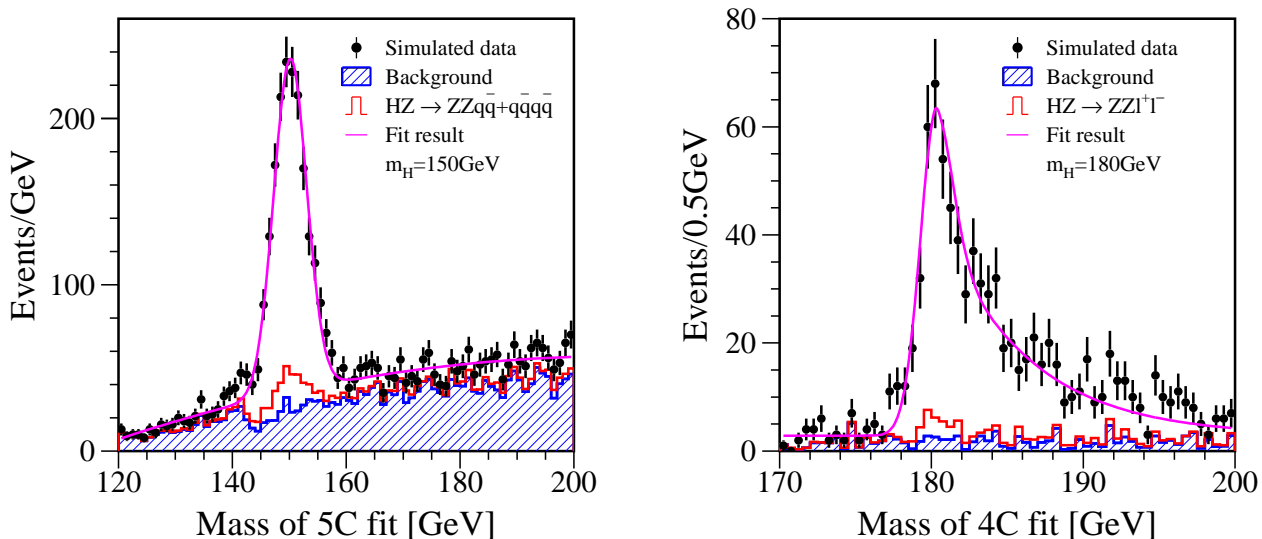
Figure 3.2: Distribution of the reconstructed Higgs boson mass in the $HZ \to WWq\bar{q}$ channel for $m_H = 150$ GeV (left plot) and in the $HZ \to WW\ell^+\ell^-$ channel for $m_H = 180$ GeV (right plot).

The study presented in Reference [57] focuses on a heavy Higgs boson with mass greater than 200 GeV. Exploiting 4jet+2ℓ final states stemming from $HZ \to WW(ZZ)\ell^+\ell^-$ decay modes, the Higgs boson mass is extracted from a lineshape analysis of the invariant mass of the hadronic system stemming from Higgs decays to weak boson pairs. The relative accuracy on the Higgs boson mass varies from 0.11 to 0.36% for m_H between 200 and 320 GeV. As discussed in Sect. 3.6, in the case of a heavy Higgs boson not only its mass but also its width can be determined with good accuracy from the mass lineshape analysis.

3.3 Measurements of the Higgs Boson Couplings to Gauge Bosons, Fermions and Itself

In the SM, the electroweak symmetry is spontaneously broken by introducing the Higgs doublet field. Its neutral component receives the vacuum expectation value (v). The weak gauge bosons then obtain their masses through the Higgs mechanism. At the same time, all quarks and charged leptons receive their masses from the Yukawa interactions with the Higgs field. Moreover, the Higgs boson (h) itself is also given its mass (m_h) by v through the self-interaction of the Higgs boson. All these masses of the SM particles are expressed as multiplication of coupling constants with v. Therefore, there is a universality between masses and coupling constants:

$$\frac{2m_W}{g} = \frac{\sqrt{2}m_t}{y_t} = \frac{\sqrt{2}m_b}{y_b} = \frac{\sqrt{2}m_\tau}{y_\tau} = ... = \frac{m_h}{\sqrt{2\lambda}} = v \simeq 246 \text{ GeV}, \tag{3.1}$$

where g is the weak gauge coupling, y_f is the Yukawa coupling constant to the fermion f, λ is the self-coupling constant of h, and m_i is the mass of the field i. Experimental validation of these relations would be a crucial step in establishment of the Higgs mechanism, the fermion mass generation mechanism, and the structure of the Higgs potential. This is visualized in Fig. 3.3, where the coupling of SM particles to the Higgs boson is shown as a function of their respective mass. Also shown are the prospective ILC precisions as discussed in the next sections. Information

on the triple Higgs coupling is crucial for the reconstruction of the Higgs potential by which the breaking of the electroweak symmetries is induced. The accurate measurement of the self-couplings can also be important to discriminate models.
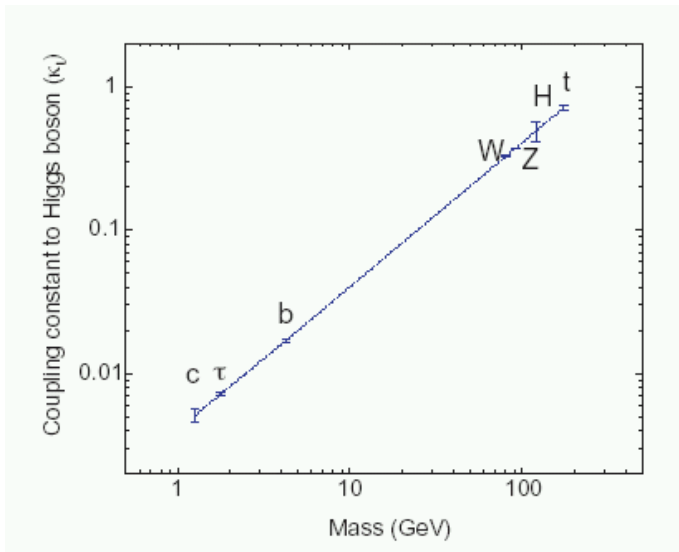
Figure 3.3: The couplings of the SM particles to the Higgs boson are shown as a function of their respective mass. Also shown are the prospective ILC precisions as discussed in the next sections.

3.3.1 Couplings to heavy SM gauge bosons

Couplings to Z and W bosons can be directly accessed by measuring Higgs production rates in the Higgs-strahlung and W boson fusion processes. The prospects for measuring the Higgs-strahlung cross section at ILC was discussed in Sect. 3.1. The feasibility of measuring W fusion cross section at centre-of-mass energies 350 and 500 GeV is investigated in Ref. [58]. The analysis utilizes the $H \to b\bar{b}$ decay mode and is based on the selection of final states characterized by two jets with the invariant mass compatible with m_H and missing energy carried by a pair of neutrinos[2]. Fig. 3.4 presents the spectrum of missing mass after applying a dedicated selection in the $e^+e^- \to H\nu_e\bar{\nu}_e \to b\bar{b}\nu_e\bar{\nu}_e$ channel.

The selected samples contain a large contribution from the Higgs-strahlung process followed by Higgs decays into b quarks and Z decays into neutrinos. However, the reconstructed missing mass clearly distinguishes between Higgs-strahlung and WW-fusion processes. The missing mass spectrum is then fitted with two normalization factors, quantifying contributions from the Higgs-strahlung and fusion processes, as free parameters. Results of the fits are given in Table 3.3.

Using a polarized electron beam will considerably enhance the Higgs production rate in the WW-fusion process and allow for improvement of the precision on the cross-section by a factor of 2 or better for electron beam polarization of 80% [58]. Polarization of the positron beam could lead to a further improvement; see also Ref. [48].

3.3.2 Higgs-photon coupling

The coupling of the Higgs boson to photons can be determined through the measurement of the resonant Higgs production rate in $\gamma\gamma$ collisions. Colliding photons of high energy are produced through the Compton back-scattering of laser light on high energy electron beams. The high

---

[2]This analysis assumes that values for the Higgs boson mass and $H \to b\bar{b}$ branching ratio will be already known from other channels.
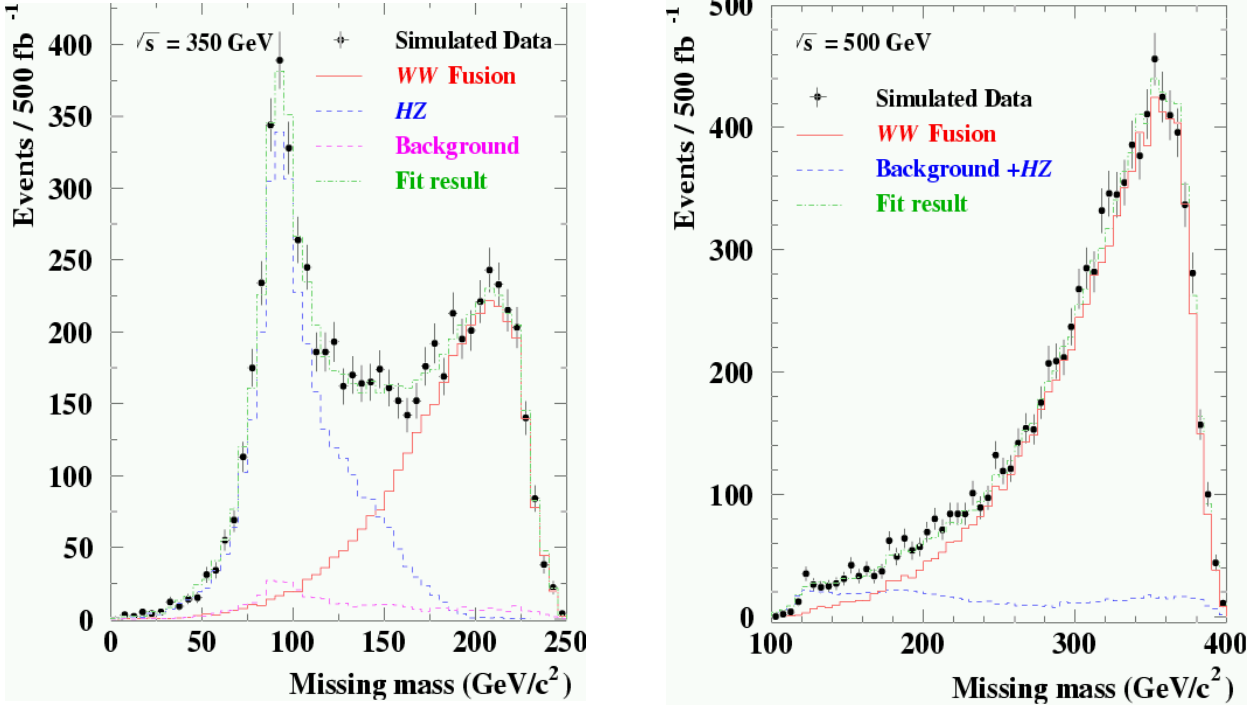
Figure 3.4: The missing mass spectrum in the $e^+e^- \to H(\nu_e\bar{\nu}_e) \to b\bar{b}\nu_e\bar{\nu}_e$ channel at $\sqrt{s} = 350$ GeV (left plot) and 500 GeV (right plot). Assumed integrated luminosity is 500 fb^{-1}.

$\sqrt{s}$ (GeV)	m_H (GeV)	$\Delta\sigma_{WW-\text{fusion}}$
	120	3.3%
350	140	4.7%
	120	2.8%
500	140	3.7%
	160	13.0%

Table 3.3: Results on the accuracy on the WW-fusion cross-section measurements in the $e^+e^- \to H\nu_e\bar{\nu}_e \to b\bar{b}\nu_e\bar{\nu}_e$ channel. An integrated luminosity of 500 fb^{-1} is assumed for each center-of-mass energy.

energy photon beams resulting from this process are not monochromatic. A number of simulation tools have been developed, allowing for estimation of the two-photon luminosity spectrum [59, 60]. As an example, Fig. 3.5 shows the resulting two-photon luminosity spectrum for a linear e^-e^- collider operated at $\sqrt{s} = 210$ GeV as simulated using the CIRCE2 program [60]. A Higgs boson produced in $\gamma\gamma$ collisions can be identified via its decays into b-quarks [61–63]. Fig. 3.6 presents the spectrum of the reconstructed Higgs boson mass in the channel $\gamma\gamma \to H \to b\bar{b}$ for $m_H = 120$ GeV and assuming integrated photon-photon luminosity of 410 fb^{-1} collected at a linear e^-e^- collider operated at center-of-mass energy 210 GeV [63]. Dedicated analyses [61–63] showed that the quantity $\Gamma(H \to \gamma\gamma)\text{BR}(H \to b\bar{b})$ can be measured with an accuracy of $2.1-7.8\%$ for $m_H = 120-160$ GeV, respectively. Combining this with the measurements of $H \to b\bar{b}$ in e^+e^- collisions, the partial decay width $\Gamma(H \to \gamma\gamma)$, and therefore the photonic coupling, of the Higgs boson can be extracted.

One potential caveat is that the reach analyses performed to date have assumed that the QCD
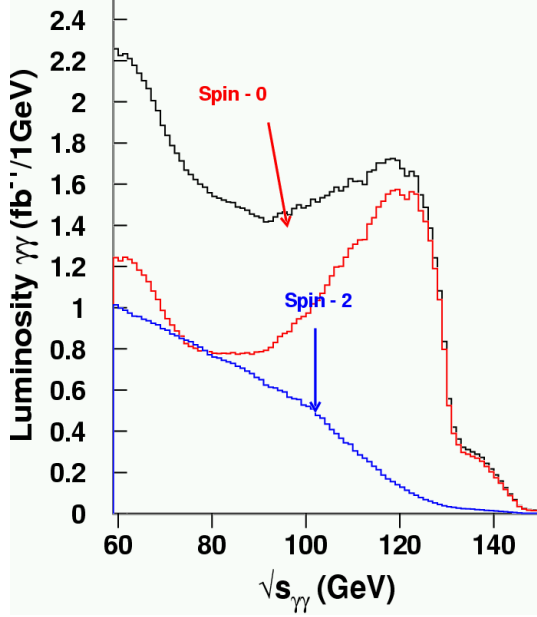
Figure 3.5: Luminosity spectra for the spin of the two colliding photons $J_z = 0$ and $J_z = 2$. Distribution is obtained with the CIRCE2 program for a linear $e^- e^-$ collider operated at center-of-mass energy of 210 GeV.
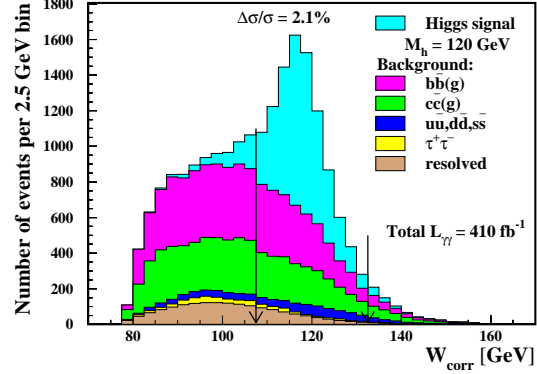
Figure 3.6: Reconstructed Higgs boson mass in the process $\gamma\gamma \to H \to b\bar{b}$ assuming integrated photon-photon luminosity of 410 fb^{-1} collected at a linear $e^- e^-$ collider operated at center-of-mass energy 210 GeV.

background is well-described by current theoretical estimates. A study during this Workshop (see [64] for details) of the QCD structure in the resolved portion of the background in Fig. 3.6 has demonstrated a factor of 5 uncertainty in that term, which raises the overall background uncertainty by a factor of 2. The origin of this large uncertainty is that the gluonic component of the photon is nearly unconstrained at these large energies. The gluon contribution will be well-measured by an *in situ* determination once the collider is running. Hence, at worst, a slightly larger luminosity may be required to obtain the high precision measurements of the photon coupling to the Higgs.

3.3.3 Higgs couplings to SM fermions

Information on Higgs couplings to SM fermions can be extracted through the measurements of the Higgs boson decay branching fractions. Two approaches for the measurements of Higgs branching fractions can be used:

- Extract topological cross sections, $\sigma(e^+e^- \to H\nu_e\bar{\nu}_e)\mathrm{BR}(H \to X)$ or $\sigma(e^+e^- \to HZ)\mathrm{BR}(H \to X)$ from the event rate measurement and then divide by the total Higgs-strahlung or WW-fusion cross-section as obtained from corresponding studies.

- Select unbiased inclusive samples of Higgs decays, e.g., events in the recoil peak in the $HZ \to X\ell^+\ell^-$ channel, and then determine from this sample the fractions of events corresponding to a given decay mode $H \to X$. Since in this direct method binomial (or generally multi-nomial) statistics is employed, the errors on the branching ratios are reduced by a factor of $\sqrt{1 - \mathrm{BR}(H \to X)}$.

Examples of the first approach are given by a number of analyses examining the potential of the linear collider for the measurement of the Higgs boson branching fractions into vector bosons

18

and hadrons [65–68]. These analyses exploit either WW-fusion or the Higgs-strahlung process with various possible Z boson decays. The approach based on binomial statistics is described in Reference [69]. Although relying only on Higgs-strahlung events with $Z \to \ell^+\ell^-$, this method yields errors very similar to the analyses based on the first approach, exploiting a variety of Z boson decays following $e^+e^- \to HZ$. Results on Higgs branching ratio measurements at $\sqrt{s} = 800$ GeV and below are given in Table 3.4.

m_H (GeV)	120	140	160	180	200	220
Decay	Relative precision (%)					
$b\bar{b}$	2.4(a)/1.9(e)	2.6(a)	6.5(a)	12.0(d)	17.0(d)	28.0(d)
$c\bar{c}$	8.3(a)/8.1(e)	19.0(a)				
$\tau^+\tau^-$	5.0(a)/7.1(e)	8.0(a)				
gg	5.5(a)/4.8(e)	14.0(a)				
WW	5.1(a)/3.6(e)	2.5(a)	2.1(a)			
ZZ		16.9(a)				
$\gamma\gamma$	23.0(b)/35.0(e)					
$Z\gamma$		27.0(c)				

Table 3.4: Precision on the Higgs boson branching ratio measurements [65–69]: (a) for 500 fb^{-1} at 350 GeV; (b) for 500 fb^{-1} at 500 GeV; (c) for 1 ab^{-1} at 500 GeV; (d) for 1 ab^{-1} at 800 GeV; (e) as for (a) but using binomial statistics method.

Recently, a dedicated analysis based on detailed flavor-tagging tools has been performed [70] to evaluate the linear collider potential for the measurement of hadronic decays of the light Higgs boson, $m_H = 120$ GeV. The study is based on selection of an inclusive sample of hadronic Higgs decays using the Higgs-strahlung process and exploiting all possible decay modes of the Z boson. Each selected event is assigned a quantified probability to contain b- or c-jets, referred to as b- and c-tag variables. The branching ratios $H \to b\bar{b}$, $H \to c\bar{c}$ and $H \to gg$ are determined from the fit of a two-dimensional distribution of b-tag versus c- tag variables (Fig. 8.5) with three free normalization parameters quantifying the fractions of $H \to b\bar{b}$, $H \to c\bar{c}$ and $H \to gg$ events in the final selected samples. Results of this study are presented in Table 3.5.

Decay	$Z \to \ell^+\ell^-$	$Z \to \nu\bar{\nu}$	$Z \to q\bar{q}$	Combined
	Relative precision (%)			
$H \to b\bar{b}$	3.0	2.1	1.5	1.1
$H \to c\bar{c}$	33.0	20.5	17.5	12.1
$H \to gg$	18.5	12.3	14.4	8.3

Table 3.5: Relative precision on the measurement of the hadronic branching ratios of Higgs for m_H = 120 GeV. Analysis is performed for $\sqrt{s}$ = 350 GeV, assuming an integrated luminosity of 500 fb^{-1}.

One can improve the precision of branching ratio measurements at higher e^+e^- collision energies. This is done taking advantage of the increase in the Higgs production rate with energy due to a $\log\sqrt{s}$ dependence of WW-fusion cross-section. Moreover, the specific luminosity is expected to increase with increasing center-of-mass energy. Both these factors will enhance the signal statistics, allowing not only to improve the precision on Higgs branching ratios for the major decay modes, but also to measure rare Higgs decays, e.g., $H \to \mu^+\mu^-$ [71]. An example of this signal is shown in Fig. 3.7.
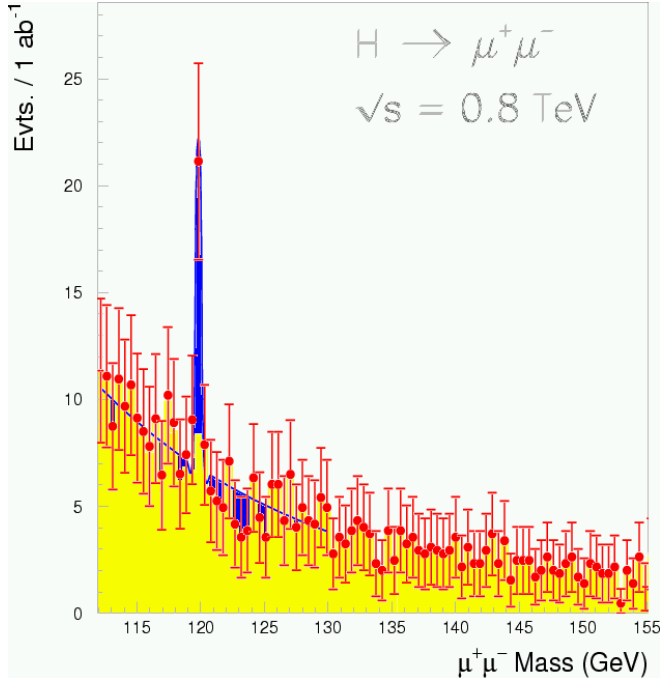
Figure 3.7: Invariant mass of the two muons in the selected sample of $H \to \mu^+\mu^-$ decays following WW-fusion process. Higgs boson mass is 120 GeV. Center-of-mass energy is 800 GeV. An integrated luminosity of 1 ab^{-1} is assumed.

3.3.4 Top Yukawa Couplings of the Higgs Boson

The top quark is exceptionally heavy as compared to the other quarks, with its mass being $m_t \sim v/\sqrt{2}$. The size of the top Yukawa coupling is nearly 1. The fact that the mass of the top quark is the same size as the scale of electroweak symmtry breaking may suggest that the physics of the top quark may be strongly related to the dynamics of the electroweak symmetry breaking. Therefore, the experimental determination of the top Yukawa coupling is expected to be a very sensitive probe of possible new physics that might be responsible for generating the top quark mass. For example, alternative models of electroweak symmetry breaking with new strong interactions, such as Technicolor and Topcolor models, substantially modify the top quark interaction with the Higgs sector and give rise to new signals that could be studied at the ILC.

If the Higgs boson mass is below 200 GeV, the top Yukawa coupling could be measured in associated $t\bar{t}H$ production, with an error of the order of 15% at the LHC [7] (with "mild" theory assumptions). At the ILC [72] in the SM the production cross section becomes maximal around $\sqrt{s} = 700$ GeV for $m_h = 120$ GeV. The expected accuracy for the top Yukawa coupling in the SM is 4.2% at $\sqrt{s} = 700$ GeV with $\int \mathcal{L} = 500$ fb^{-1}. An error of 5.5% can be achieved for $\sqrt{s} = 800$ GeV, $\int \mathcal{L} = 1000$ fb^{-1} and $m_h = 120$ GeV [8]. However, recent studies show that for this Higgs mass and integrated luminosity even at $\sqrt{s} = 500$ GeV a measurement at the 10% level might be possible [73]. For a combination of LHC and the 500 GeV ILC, see Sect. 6.2.1.

3.3.5 Higgs Boson Self-Couplings

Information about the structure of the Higgs potential will be obtained by measuring the triple Higgs boson coupling. Accurate information on this coupling is important to discriminate models beyond the SM. Even when the other Higgs boson couplings such as hZZ, hWW and $hf\bar{f}$ are in good agreement with the SM predictions, the Higgs self-couplings can significantly deviate from the SM prediction due to non-decoupling quantum effects of heavy particles. In the two Higgs doublet model, radiative corrections of O(100)% on the hhh coupling are possible if the additional

heavy Higgs bosons show a non-decoupling property [74]. Such a non-decoupling phenomenon is known to be required for a scenario of electroweak baryogenesis [30]. Therefore, the measurement of the triple Higgs boson coupling may be used to test such a model of the baryon asymmetry of the universe [75].

The hhh coupling can be measured via the double Higgs boson production processes $e^+e^- \to Zhh$ and also $e^+e^- \to \nu\bar{\nu}hh$ [76]. In these processes, in addition to the diagram involving the hhh coupling, there are double Higgs radiation diagrams which depend only on the hZZ or the hWW coupling. Hence, the production cross section is not simply proportional to the square of the self-coupling constant. Systematic studies on the self-coupling measurement have been performed for various values of m_h and $\sqrt{s}$ [77–79]. As seen in Figure 3.8 (left), the hhZ mode is sensitive to the deviation $\delta\lambda_3$ of the hhh coupling from the SM value in the low values of the invariant mass M_{hh} of the hh system [78]. A cut on M_{hh} is therefore useful to improve the sensitivity. For $\sqrt{s} \gtrsim$ 1 TeV, the sensitivity is further improved by using initial electron (and positron) polarization. The production cross section of the WW fusion process can be increased by up to a factor of 2 (4) in principle with electron (electron and positron) polarization.

For $\sqrt{s} = 500$ GeV, $e^+e^- \to Zhh$ has much larger cross section than the $e^+e^- \to \nu\bar{\nu}hh$ process. For a higher energy, the production cross section of the latter process is enhanced because of its t-channel nature, whereas $e^+e^- \to Zhh$ decreases as $1/s$. For $\sqrt{s} \gtrsim$ 1 TeV, the WW fusion process $e^+e^- \to \nu\bar{\nu}hh$ becomes important to determine the hhh coupling. The statistical errors in the hhh measurement are shown in Figure 3.8 (right) as a function of the Higgs boson mass from 100 to 200 GeV, assuming an integrated luminosity of 1 ab^{-1} [78]. Dashed (dotted, sold) lines are the results for the hhZ mode ($hh\nu\bar{\nu}$ mode, both modes combined). At $\sqrt{s} = 500$ GeV, where the hhZ mode is dominant, the hhh coupling may be measured with about 20% accuracy for relatively light Higgs bosons with $m_h \lesssim$ 150 GeV. For $\sqrt{s} \gtrsim$ 1 TeV, where the $hh\nu\bar{\nu}$ mode is dominant, higher sensitivity ($\delta\lambda_3/\lambda_3 \lesssim$ 10%) can be expected by using the invariant mass cut $M_{hh} < 600$ GeV for the hhZ mode and a 100% polarized electron beam for the $hh\nu\bar{\nu}$ mode.
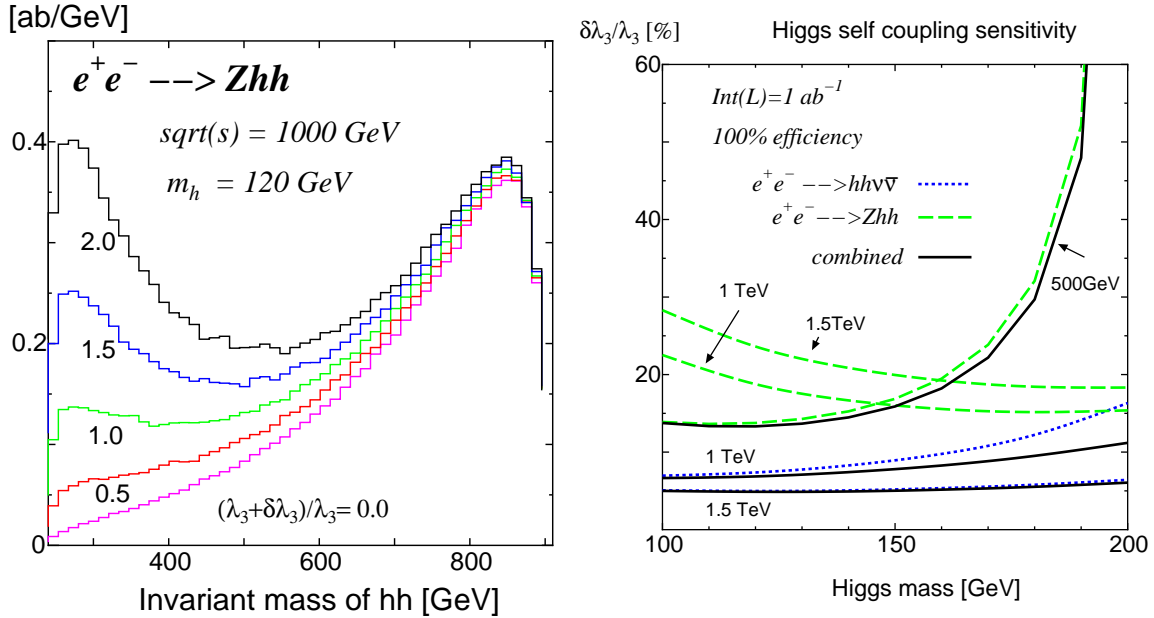
Figure 3.8: (Left figure) The hh invariant mass dependence of the hhZ mode for several values of $\delta\lambda_3$. (Right figure) The λ_3 measurement sensitivity; hhZ (dashed line), $hh\nu\bar{\nu}$ (dotted line) and combined results (solid line) [77].

The full calculation of the SM electroweak radiative corrections to the double Higgs-strahlung process $e^+e^- \to Zhh$ has been presented in Ref. [80].

3.4 Higgs Boson Width Measurement

At Higgs masses below approximately $2M_W$, the detector resolution on the Higgs boson mass for the main decay channels, $H \to b\bar{b}$ and $H \to WW$, is significantly larger than the natural width of the Higgs boson. Γ_H. As a consequence, no direct measurement of the Higgs width is possible through the analysis of the reconstructed Higgs boson mass lineshape. However, using the relation

$$\Gamma_H = \frac{\Gamma(H \to X)}{\mathrm{BR}(H \to X)} \tag{3.2}$$

with $X = WW$ or $\gamma\gamma$, the width can be determined indirectly. For example, the partial width $\Gamma(H \to \gamma\gamma)$ can be measured with the $\gamma\gamma$ collider whereas the branching fraction $\mathrm{BR}(H \to \gamma\gamma)$ is accessible in e^+e^- collisions from the diphoton invariant mass spectrum. The same procedure can be performed for the WW-fusion process and the $H \to WW$ decay mode. An accuracy in the determination of Γ_H between 4% and 15% can be achieved [58] for m_H up to 160 GeV.

The natural width of heavy Higgs boson with mass above $2M_Z$ becomes as large as few GeV and can be directly measured from the mass lineshape analysis [57]. Fig. 3.9 presents the spectra of reconstructed Higgs mass in the $HZ \to WW\ell^+\ell^-$ and $HZ \to ZZ\ell^+\ell^-$ channels with subsequent hadronic decays of weak bosons for $m_H = 200$ GeV. From the fit of the spectra with convolution of the detector resolution functions and Breit-Wigner function, the Higgs width can be determined with the relative precision of about 30% for $m_H = 200-320$ GeV.
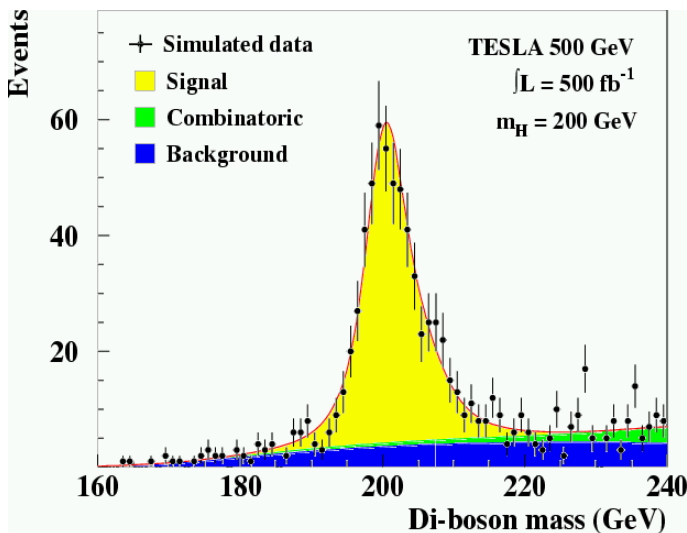
Figure 3.9: Reconstructed Higgs boson mass lineshape in the $HZ \to WW\ell^+\ell^-$ and $HZ \to ZZ\ell^+\ell^-$ channels with subsequent hadronic decays of weak bosons for $m_H = 200$ GeV. Selected sample corresponds to 500 fb^{-1} of luminosity collected at center-of-mass energy of 500 GeV.

3.5 Spin and CP Quantum Numbers of Higgs Boson

Full establishment of the Higgs mechanism implies measurements of Higgs spin and CP quantum numbers. The SM Higgs boson (like the CP-even MSSM Higgs bosons) has spin and CP-quantum numbers $J^{PC} = 0^{++}$. Information on CP-quantum numbers can be extracted by studying angular dependences of the Higgs-strahlung process. The analysis for the SM Higgs boson can also be applied to a SM-like MSSM Higgs boson.

The following quantities are sensitive to the CP quantum numbers of the Higgs: the polar production angle of the Higgs boson, θ; the angle between the Z momentum vector and the momentum vector of the fermion stemming from Z decay, θ^*; and the angle between the production and decay planes of the Z boson, ϕ^*. The latter two angles are defined in the Z boson rest frame. The definitions of these angles are illustrated in Fig. 3.10.

Studies presented in Refs. [81, 82] investigated the general case of a mixed scalar state Φ containing both CP-even and CP-odd components. In the presence of a CP-odd admixture in the scalar field, the amplitude for the Higgs-strahlung process reads:

$$\mathcal{M}_{Z\Phi} = \mathcal{M}_{ZH} + i\eta\mathcal{M}_{ZA}, \tag{3.3}$$

where $\mathcal{M}_{ZH}$ is the CP-even SM-like s-wave amplitude, and $\mathcal{M}_{ZA}$ is a new CP-odd p-wave amplitude contributing with strength η to the Higgs-strahlung process. The presence of the latter modifies the three-fold differential cross section $d^3\sigma/d(\cos\theta)d(\cos\theta^*)d(\cos\phi^*)$ with respect to the SM prediction. The parameter η can be determined using the method of optimal observables [81]. Neglecting terms quadratic in η, the optimal observable is chosen to be

$$\mathcal{O} = \frac{2\mathrm{Re}\left(\mathcal{M}_{ZA}^*\mathcal{M}_{ZH}\right)}{|\mathcal{M}_{ZH}|^2}. \tag{3.4}$$

The choice of the observable is very close to optimal for small η. At the next step, a "gauge" curve is produced, which quantifies the dependence of the mean value of the optimal observable and its error on the parameter η. This is done using reference distributions of the optimal observable corresponding to different values of η. Reference distributions are obtained for the selected samples in the $HZ \to X\ell^+\ell^-$ channel. The parameter η can then be read from this "gauge" curve including the confidence band. The analyzing power of this method can be enhanced by taking into account the dependence of the Higgs-strahlung cross section on η. Technically, the parameter η is calculated by minimizing the χ^2,

$$\chi^2 = \frac{(\langle\mathcal{O}_{meas}\rangle - E(\langle\mathcal{O}\rangle)(\eta))^2}{\sigma_{exp}(\eta)} + \frac{(N_{meas} - N_{exp}(\eta))^2}{N_{exp}(\eta)}, \tag{3.5}$$

where $\langle\mathcal{O}_{meas}\rangle$ and N_{meas} are the measured mean value of the optimal observable and the number of observed signal events in the hypothetical data sample, $E(\langle\mathcal{O}\rangle)(\eta)$ and $N_{exp}(\eta)$ are the expected mean value of the optimal observable and expected number of signal events, and $\sigma_{exp}(\eta)$ is the expected error on $E(\langle\mathcal{O}\rangle)(\eta)$. $E(\langle\mathcal{O}\rangle)(\eta)$, $N_{exp}(\eta)$ and $\sigma_{exp}(\eta)$ are determined from the "gauge" curves shown in Fig. 3.11. For small values of η, $\eta \leq 0.1$, this parameter can be measured with a precision of about 0.03.

An alternative method [82] consists of generating three-dimensional distributions in $\cos\theta$, $\cos\theta^*$ and $\cos\phi^*$ for various values of η. These distributions are generated for the selected $HZ \to X\ell^+\ell^-$ signal samples corresponding to 500 fb^{-1} of data collected at $\sqrt{s} = 350$ GeV. In the next step, the likelihood

$$\mathcal{L} = \prod_{(\cos\theta)_i(\cos\theta)_j(\cos\phi^*)_k} \frac{\mu_{ijk}^{N_{data}(i,j,k)}e^{-\mu_{ijk}}}{N_{data}(i,j,k)!} \tag{3.6}$$

is maximized, where $N_{data}(i,j,k)$ is the number of events of the hypothetical data sample and μ_{ijk} is the expected number in the ijk-th bin. μ_{ijk} is calculated assuming a linear combination of the number of events of three Monte Carlo samples, corresponding to the production of scalar Higgs (MC(ZH)), pseudoscalar Higgs (MC(ZA)) and events for the interference term (MC(IN)):

$$\mu_{ijk} = \alpha\mathrm{MC}(ZH)_{ijk} + \beta\mathrm{MC}(IN)_{ijk} + \gamma\mathrm{MC}(ZA)_{ijk}, \tag{3.7}$$

23

Figure 3.11: Gauge curve reflecting dependence of the mean value of the optimal observable and the Higgs-strahlung cross-section on the parameter η. Bands indicate 1σ confidence level intervals as obtained for a data sample corresponding to 500 fb^{-1} at $\sqrt{s} = 350$ GeV.

Figure 3.10: Definitions of the Z production and decay angles θ, θ^* and ϕ^* in the Higgs-strahlung process.

where α, γ and β quantify contributions from the production of the scalar state, pseudoscalar state and their interference, respectively. The likelihood is then maximized with respect to α, β and γ. The quantity η and its experimental error can then be determined by parameterizing the fraction of pseudoscalar component γ as a function of η. It has been shown that with this method, the parameter η can be measured with an accuracy of 0.015 for $|\eta| \leq 0.1$.

The Higgs boson parity can be established also by analyzing the spin correlation effects in the Higgs boson decay into fermion pairs [83]. The spin dependence of the decay probability is given by

$$\Gamma(H, A \to f\bar{f}) \sim 1 - s_z \bar{s}_z \pm s_\perp \bar{s}_\perp, \qquad (3.8)$$

where s and $\bar{s}$ denote spin vectors of fermion f and anti-fermion $\bar{f}$ in their respective rest frames (with the z axis oriented in the fermion flight direction). The positive sign in the transverse spin correlation term holds for the scalar particle (H) and the negative sign for the pseudoscalar (A). Although the dominant fermionic decay mode of the Higgs boson is into b quark pairs, it can hardly be utilized for measurement of the Higgs parity, as hadronization of quarks will inevitably dilute the spin information. The most promising channel is the Higgs decay into tau leptons, with their subsequent decay into ρ meson and neutrino [84]. The angle Φ^* between the planes spanned by the momentum vectors of the products of the $\rho^+ \to \pi^+ \pi^0$ and $\rho^- \to \pi^- \pi^0$ decays in the $\rho^+ \rho^-$ rest frame can be used to distinguish between the scalar and pseudoscalar states. Recently, a dedicated study [85] has been done which investigated the feasibility of measuring Higgs parity at ILC in the $H \to \tau^+ \tau^- \to \rho^+ \bar{\nu}_\tau \rho^- \nu_\tau \to \pi^+ \pi^0 \bar{\nu}_\tau \pi^- \pi^0 \nu_\tau$ channel. The analysis is performed at the level of detailed detector simulation and includes accurate estimates of the SM background. Higgs boson decays into tau leptons are selected using the Higgs-strahlung process with subsequent decays of the Z boson into electron and muon pairs and quarks. Even in the presence of SM backgrounds, the acoplanarity angle Φ^* clearly discriminates between CP-even and CP-odd states, as illustrated
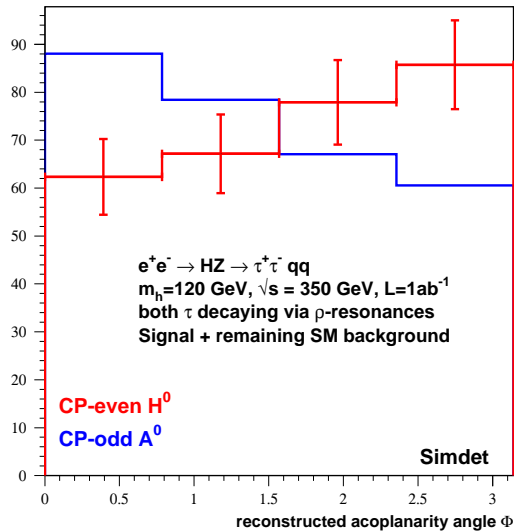
Figure 3.12: The distribution of the acoplanarity angle Φ^* as defined for the $H \to \tau^+\tau^- \to \rho^+\bar{\nu}_\tau\rho^-\nu_\tau \to \pi^+\pi^0\bar{\nu}_\tau\pi^-\pi^0\nu_\tau$ decay chain (see text) for the scalar state (error bars) and pseudoscalar state (histogram) in the selected sample of $HZ \to \tau^+\tau^- q\bar{q}$ events. Selected sample corresponds to 1 ab^{-1} of data collected at $\sqrt{s} = 350$ GeV. Higgs boson mass is 120 GeV.
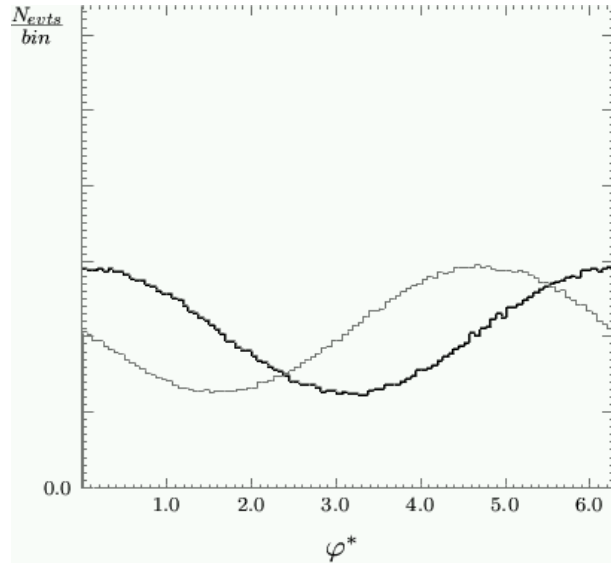
Figure 3.13: The acoplanarity angle Φ^* in the $H \to \tau^+\tau^- \to \rho^+\bar{\nu}_\tau\rho^-\nu_\tau \to \pi^+\pi^0\bar{\nu}_\tau\pi^-\pi^0\nu_\tau$ decay chain. Gaussian smearing of Φ^* and Higgs boson momenta are applied according to anticipated resolutions of the ILC detector. Thick line corresponds to a pure scalar state, while the thin line to a mixed one.

in Fig. 3.12.

With 1 ab^{-1} of data collected at $\sqrt{s} = 350$ GeV, scalar and pseudoscalar states can be distinguished at $\sim 4\sigma$ level. Furthermore, the method using the acoplanarity angle Φ^* can be applied in the general case of the mixed Higgs state, comprising both CP-even and CP-odd components.[3] The presence of a CP-odd admixture results in a phase shift in the distribution of the Φ^* angle as shown in Fig. 3.13. From the measurement of this shift the mixing angle between scalar and pseudoscalar components can be determined [86] with an accuracy of about 0.2 rad if one assumes 1 ab^{-1} of data collected at $\sqrt{s} = 350$ GeV.

Recently, a new method to measure CP violation in a light Higgs boson decay from τ-spin correlations has been proposed [87]. The method has been devised to be insensitive to beamstrahlung and exploits the information encoded in a unit vector $\vec{a}$, the τ polarization analyzer. The latter can be computed [88] from the measured decay products for the three hadronic decay modes, $\tau \to \pi\nu, \rho\nu, a_1\nu$, which constitute 55% of all decay channels of the τ lepton. For example, in the case of $\tau \to \pi\nu$ the polarization analyzer is represented by the pion direction. For $\tau \to \rho\nu$ and $\rho^\pm \to \pi^\pm\pi^0$,

$$a^i = \mathcal{N}\Big(2(q \cdot p_\nu)q^i - (q \cdot q)p_\nu^i\Big), \tag{3.9}$$

where $\mathcal{N}$ is a normalization factor, $p_\nu = p_\tau - p_\rho$ is the neutrino momentum and $q = p_{\pi^\pm} - p_{\pi^0}$ is the difference between the momenta of the charged pion and neutral pion. Once the vector $\vec{a}$ is

---

[3]This scenario requires redefinition of acoplanarity angle resulting in coverage of $[0, 2\pi]$ range. For details see Reference [86].

reconstructed, the information on the CP phase in the light Higgs state can be accessed through the distribution of the azimuthal angle

$$dN/d(\Delta\phi) \sim 1 - \frac{\pi^2}{16}\cos(\Delta\phi - 2\psi), \tag{3.10}$$

where ψ is the CP phase of the Higgs boson and $\Delta\phi$ is the difference in azimuthal angles of the $\vec{a}^\pm$ vectors in the $H \to \tau^+\tau^-$ rest frame. The reconstruction of $\Delta\phi$ is possible in the Higgs-strahlung process. It requires information on the visible decay products of the tau leptons, Z boson momentum, primary vertex position and the Higgs boson mass. The entire algorithm of reconstruction of $\Delta\phi$ is described in detail in Ref. [87]. Visible decay products of tau leptons are directly measured using only tracking in the case of the $\tau \to \pi\nu$ decay mode or using calorimeter and tracking information in the case of $\tau \to \rho\nu$. The momentum of the Z boson can be determined from the $Z \to e^+e^-, \mu^+\mu^-, q\bar{q}$ decays. The primary vertex position in $r\phi$ plane is constrained by the beam spot, whereas the z coordinate is determined from charged decay products of the Z boson. Finally, it is assumed that the Higgs mass will be determined with high precision prior to this analysis. Distributions of $\Delta\phi$ when only beamstrahlung is taken into account are shown in Figure 3.14. The sensitivity of the ψ measurement is expressed as
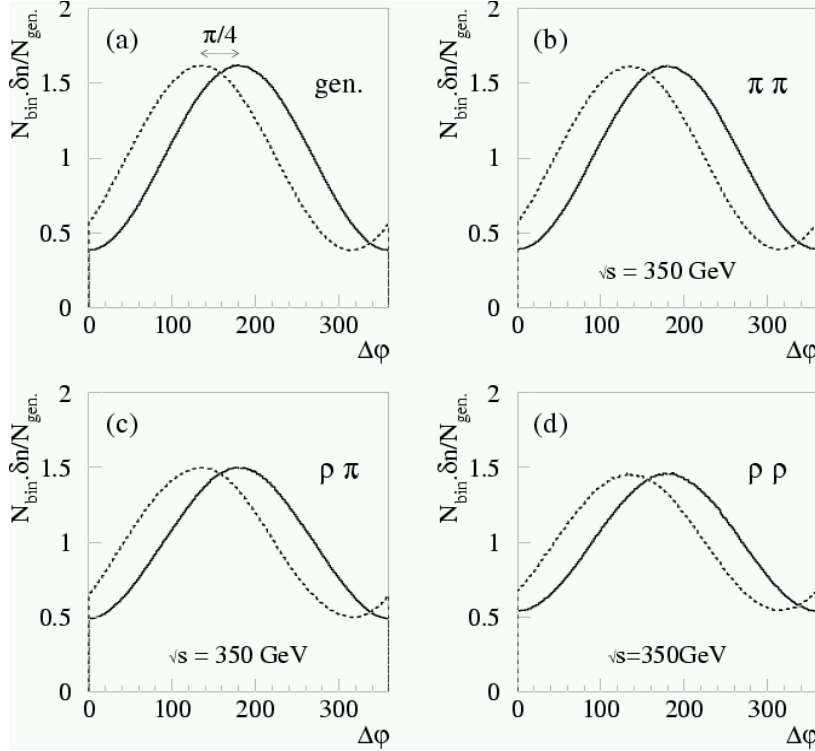
Figure 3.14: The distributions of $\Delta\phi$: a) at the generation level; b), c) and d) after dedicated reconstruction [87] for the three channels $\pi\nu\pi\nu$, $\pi\nu\rho\nu$ and $\rho\nu\rho\nu$ at center-of-mass energy of 350 GeV. Beamstrahlung effects only are taken into account. The histograms are normalized to the number of generated events and multiplied by the number of bins. The full lines correspond to a pure scalar Higgs state ($\psi = 0$), the dotted to a mixed state with $\psi = \pi/8$.

$$S_\psi = 1/\sigma_\psi\sqrt{N}, \tag{3.11}$$

where σ_ψ is the error on ψ expected from a maximum likelihood fit of the distribution for a sample of N events. Defined in such a way, the sensitivity measures the information per event on ψ contained in the distribution (3.10). Anticipated sensitivities in various decay channels for different center-of-mass energies are given in Table 3.6.

$\sqrt{s}$ (GeV)	Sensitivity (S_ψ)		
	$\pi\nu\pi\nu$	$\pi\nu\rho\nu$	$\rho\nu\rho\nu$
230	0.92	0.88	0.83
350	0.91	0.73	0.66
500	0.88	0.64	0.55

Table 3.6: Sensitivity for the determination of CP phase ψ of the Higgs boson for the three different channels $\pi\nu\pi\nu$, $\pi\nu\rho\nu$ and $\rho\nu\rho\nu$ at center-of-mass energies 230, 350 and 500 GeV.

To evaluate detector effects, a semi-realistic simulation of $H \to \tau\tau \to \pi\nu\pi\nu$ was performed. For the charged tracks an independent Gaussian smearing is performed on the five parameters: θ, ϕ, $1/p_T$ and the two components of impact parameter resolution. Assumed widths of the Gaussians are:

$$\sigma(\theta) = \sigma(\phi) = 0.1 \text{ mrad}$$
$$\sigma(1/p_T) = 5 \times 10^{-5} \text{ GeV}^{-1}$$
$$\sigma(r\phi) = \sigma(rz) = \left(4.2 \oplus 4.0/(p\sin^{3/2}\theta)\right) \mu\text{m}.$$

The jet energy resolution is assumed to be $0.3/\sqrt{E_{jet}}$. The reconstructed distributions of $\Delta\phi$ after inclusion of the detector effects are shown in Figure 3.15 for the decays of Z both into $\mu^+\mu^-$ and $q\bar{q}$. The corresponding sensitivities are given in Table 3.7.
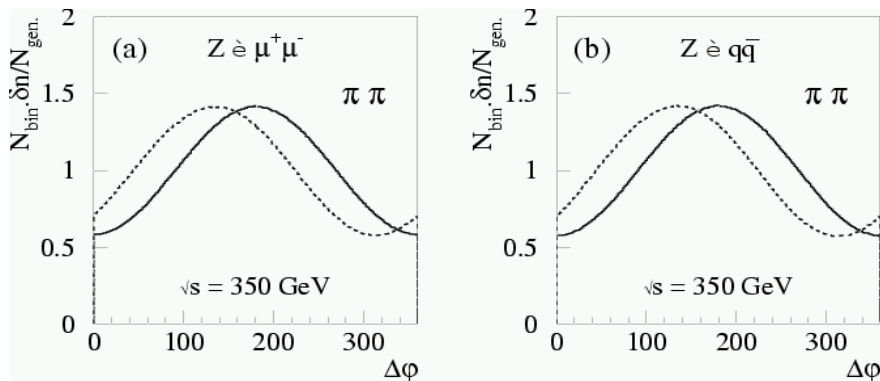
Figure 3.15: The distributions of $\Delta\phi$ in the $\pi\nu\pi\nu$ channel for the a) $Z \to \mu^+\mu^-$ and b) $Z \to q\bar{q}$ decays at center-of-mass energy 350 GeV. All experimental effects are included. The full lines correspond to a pure scalar Higgs state ($\psi = 0$), the dotted to a mixed state with $\psi = \pi/8$.

$\sqrt{s}$ (GeV)	Sensitivity (S_ψ)	
	$Z \to \mu^+\mu^-$	$Z \to q\bar{q}$
230	0.69	0.71
350	0.60	0.61
500	0.58	0.58

Table 3.7: Sensitivity of the determination of CP phase ψ of the Higgs boson for the $\pi\nu\pi\nu$ channel when all experimental effects are included.

The analyses of other decay modes, including the study of detector effects and π^0 reconstruction, have yet to be performed; nevertheless it appears that a reasonable goal for the measurement of

the phase ψ should be to use all the above mentioned channels and reach a sensitivity better than 0.5, i.e., $\sigma_\psi < 0.6\pi/\sqrt{N_{\text{event}}}$.

Finally, Higgs boson parity can determined in $\gamma\gamma$ collisions of linearly polarized photon beams [83]. The matrix elements for the production of scalar and pseudoscalar Higgs bosons in $\gamma\gamma$ collisions can be expressed as:

$$\mathcal{M}(\gamma\gamma \to H[0^{++}]) \sim \vec{\epsilon}_1 \cdot \vec{\epsilon}_2, \quad \mathcal{M}(\gamma\gamma \to A[0^{-+}]) \sim \vec{\epsilon}_1 \times \vec{\epsilon}_2 \cdot \vec{k}_\gamma \tag{3.12}$$

where $\vec{\epsilon}_1$ and $\vec{\epsilon}_2$ denote polarization vectors of colliding photons and $\vec{k}_\gamma$ is the momentum vector of one of the colliding photons. Hence, the parity of the produced Higgs state can be extracted by measuring the dependence of the production rate on the relative orientation of the polarization vectors of the linearly polarized photon beams.

The measurement of Higgs spin can be performed by analyzing the energy dependence of the Higgs boson production cross section just above the kinematic threshold [89, 90]. For a spin zero particle the rise of the cross section is expected to be $\sim \beta$, where β is the velocity of the boson in the center-of-mass system. For a spin-one particle the rise is $\sim \beta^3$ and for spin-two like $\sim \beta^5$. With
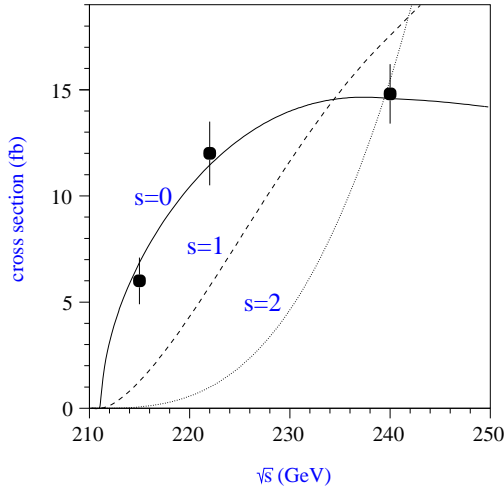
Figure 3.16: The cross section of $HZ \to q\bar{q}\ell^+\ell^-$ just above the threshold assuming $m_H = 120$ GeV. The dots correspond to a measurement and the curves are predictions for several spins.

a very small luminosity of about 20 fb^{-1} per energy point the scalar nature of the Higgs boson can be established and other spin hypotheses are disfavored, as shown in Fig. 3.16. It should be noted, however, that there are particular scenarios for spin-1 and -2 particles which show a threshold behavior similar in shape to the spin-0 case. This can be disentangled using angular information in addition.

3.6 Heavy SM-like Higgs boson

Most analyses for SM-like Higgs bosons have been performed for Higgs masses below ~ 150 GeV. However, higher masses are still allowed by the electroweak fits; see Sect. 2.1.2. Alternatively, new physics could compensate the effects of a heavier Higgs boson in the electroweak precision observables [22, 23]. For heavy SM-like Higgs bosons, $M_H \gtrsim 150$ GeV, the main decay channels are into WW and ZZ. Most analysis performed for lower masses can therefore not be taken over to this case.

3.6.1 Heavy Higgs Production

In addition to the treatment of different decay modes, a very heavy SM-like Higgs demands special theoretical treatment, because its width becomes non-negligible. For large M_H, the width of the Higgs is dominated by decays into longitudinal gauge bosons, and grows as M_H^3,

$$\Gamma\left(H \rightarrow VV\right) \quad \simeq \quad \frac{G_F\left(|Q_V|+1\right)}{\sqrt{2}16\pi}M_H^3\left(1-\frac{4M_V^2}{M_H^2}+3\frac{4M_V^4}{M_H^4}\right)\left(1-\frac{4M_V^2}{M_H^2}\right)^{1/2}, \qquad (3.13)$$

where $V = W, Z$, and Q_V is the electric charge of V. This behavior may be simply understood from the fact that the would-be Goldstone bosons are part of the Higgs doublet, and couple to the Higgs proportionally to the Higgs quartic $\lambda = M_H/v$ (at tree level). It is worth noting that the partial width into top quarks grows only as a single power of M_H, which explains why the decay into tops never dominates.
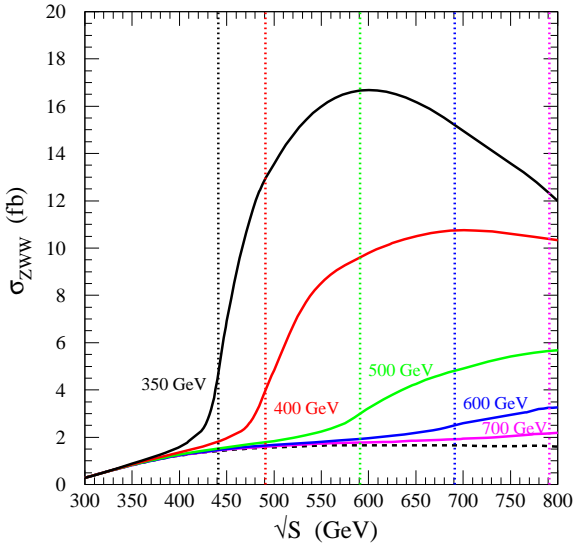
Figure 3.17: Cross sections for ZW^+W^- production as a function of $\sqrt{S}$ for a variety of Higgs masses. The solid lines of each curve include the appropriate SM Higgs width effects, whereas the dotted lines indicate the nominal threshold for HZ production.

Once the width is large, the Higgs production signal and the SM background processes can interfere in an important way. As a result, the Higgs contribution in a given channel may be important below the putative threshold energy for on-shell Higgs production, and the behavior of the signal slightly above threshold may be modified in an important way by the width [23]. This is illustrated in Figure 3.17 for the reaction $e^+e^- \rightarrow W^+W^-Z$, including the Higgs resonant production via $e^+e^- \rightarrow HZ$ followed by $H \rightarrow W^+W^-$, as well as all of the SM non-resonant production processes. For heavy Higgses, typically the associated production with a Z boson, $e^+e^- \rightarrow HZ$, and the W-fusion process $e^+e^- \rightarrow \nu_e\bar{\nu}_eH$ have roughly similar rates. The exception is when the Higgs is heavy enough that on-shell H and Z cannot be produced, in which case the W-fusion rate may dominate (see Figure 2.4).

3.6.2 Existing analyses

A heavy SM-like Higgs boson decays predominantly into WW and ZZ. For a Higgs boson with mass $2M_Z < m_H < 2m_t$, these final states constitute almost 100% of all decay modes. This scenario

has been investigated separately [57]. In this study Higgs events are selected exploiting the Higgs-strahlung process with $Z \to \ell^+\ell^-$. Only hadronic decays of W and Z bosons are considered. Separation of WW and ZZ decay modes is done on the basis of mass information. The hadronic system assigned to the decay of the Higgs is clustered into four jets. For each possible jet-pairing a kinematical fit is performed imposing four-momentum conservation, taking into account the center-of-mass energy ($\sqrt{s} = 500$ GeV) and the measured momenta of the two leptons stemming from Z decay. An additional constraint is imposed forcing the invariant masses of the two dijet systems to be equal, leading to a five constraint (5C) fitting procedure. With this procedure, the WW and ZZ decay modes can be efficiently separated by the mass obtained with the 5C kinematical fit. This is illustrated in Fig. 3.18.
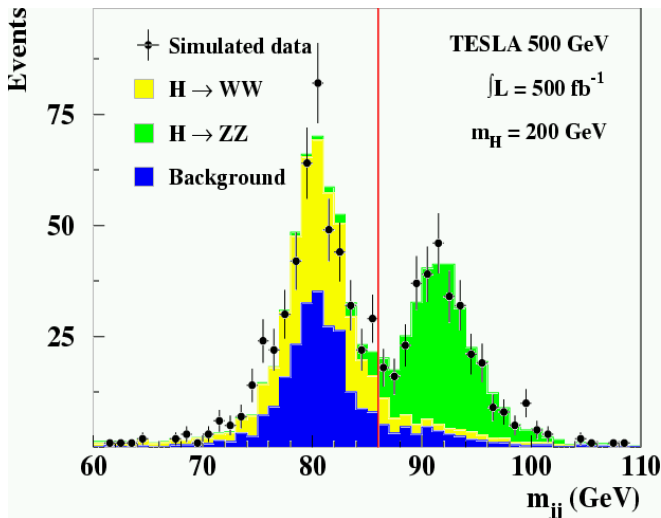
Figure 3.18: The distribution of the reconstructed vector boson mass in the sample of selected Higgs-strahlung events with $H \to WW$ or $H \to ZZ$ and $Z \to \ell^+\ell^-$. Distribution is obtained with 5C kinematic fit as described in text. The WW and ZZ decays of the Higgs boson are clearly separated. The Higgs mass is 200 GeV. The sample corresponds to integrated luminosity of 500 fb^{-1} collected at $\sqrt{s} = 500$ GeV.

With clear separation of the WW and ZZ decay channels, the measurement of the corresponding branching ratios of heavy Higgs can be performed. Results are given in Table 3.8.

m_H (GeV)	$H \to WW$	$H \to ZZ$
	Relative precision (%)	
200	3.5	9.9
240	5.0	10.8
280	7.7	16.2
320	8.6	17.3

Table 3.8: Precision on $H \to WW$ and $H \to ZZ$ branching ratio measurements for a heavy Higgs boson [57]. Results are obtained assuming 500 fb^{-1} of luminosity collected at $\sqrt{s} = 500$ GeV.

The prospect of measuring Higgs branching ratios with 1 ab^{-1} of e^+e^- collision data collected at 1 TeV center-of-mass energy has been investigated in Ref. [91]. The analysis is based on the measurement of topological cross sections $\sigma_{WW-\text{fusion}}\text{BR}(H \to X)$ with $X = b\bar{b}, WW, gg, \gamma\gamma$ and makes use of results for the Higgs branching ratio measurements into $b\bar{b}$ and WW at lower center-of-mass energies. Electron and positron beam polarization of 80% and 50%, respectively, is assumed. The study makes use of the following relations:

$$\text{BR}(H \to X) = \left(\sigma_{WW-\text{fusion}}\text{BR}(H \to X)\right)\left(\sigma_{WW-\text{fusion}}\text{BR}(H \to WW)\right)^{-1}\text{BR}^*(H \to WW)$$

$$= \left(\sigma_{WW-\text{fusion}}\text{BR}(H \to X)\right)\left(\sigma_{WW-\text{fusion}}\text{BR}(H \to b\bar{b})\right)^{-1}\text{BR}^*(H \to b\bar{b}), \quad (3.14)$$

where $\sigma_{WW-\text{fusion}}\text{BR}(H \to X)$ is the topological cross section measured at 1 TeV and $\text{BR}^*(H \to WW)$ and $\text{BR}^*(H \to bb)$ are branching ratios measured at 350 GeV center-of-mass energies. Using

these relations, a least-squares fit is performed to obtain measurement errors for $\text{BR}(H \rightarrow b\bar{b})$, $\text{BR}(H \rightarrow WW)$, $\text{BR}(H \rightarrow gg)$ and $\text{BR}(H \rightarrow \gamma\gamma)$. This procedure provide significant improvement (by a factor of two or more) for decay modes with small branching fractions, such as $\text{BR}(H \rightarrow b\bar{b})$ for 160 GeV $< m_H <$ 200 GeV, $\text{BR}(H \rightarrow WW)$ for 120 GeV $< m_H <$ 140 GeV, and $\text{BR}(H \rightarrow gg)$ and $\text{BR}(H \rightarrow \gamma\gamma)$ for all Higgs masses. More details can be found in Ref. [91].

Another study [92], making use of the large number of Higgs bosons produced in the WW fusion channel, obtained the following results. For 1 ab^{-1} of data at $\sqrt{s} = 800$ GeV a 5σ sensitivity to the bottom Yukawa coupling is achievable for $M_H < 210$ GeV. A measurement of the branching ratio $\text{BR}(H \rightarrow b\bar{b})$ is possible with the accuracies given in Tab. 3.9.

m_H (GeV)	$H \rightarrow b\bar{b}$
	Relative precision (%)
160	6.5
180	12.0
200	17.0
220	28.0

Table 3.9: Precision on $H \rightarrow b\bar{b}$ branching ratio measurements for a heavy Higgs boson [93]. Results are obtained assuming 1 ab^{-1} of luminosity collected at $\sqrt{s} = 800$ GeV.

Another analysis concerns the top Yukawa coupling measurement for Higgs bosons heavier than $2 m_t$. In this case the top Yukawa coupling could be determined from the Higgs decay into $t\bar{t}$ pairs. This decay can be studied at the ILC using the Higgs resonant contribution to the process $W^+W^- \rightarrow t\bar{t}$. While this electroweak $t\bar{t}$ production process cannot be observed at the LHC due to the huge QCD background of $t\bar{t}$ production by gluon fusion, it can be measured via a high energy e^+e^- linear collider. A complete simulation study of the $W^+W^- \rightarrow H \rightarrow t\bar{t}$ process from e^+e^- collisions has been performed including realistic backgrounds and experimental effects [94]. The helicity cross sections for the $e^+e^- \rightarrow t\bar{t}\nu\bar{\nu}$ signal process, including ISR and beamstrahlung effects, are given in Table 3.10 for a collider energy of $\sqrt{s} = 1$ TeV and different Higgs boson masses.

m_H	$\sigma(LL) = \sigma(RR)$	$\sigma(LR)$	$\sigma(RL)$	Total
100	0.11	0.22	0.21	0.65
400	1.89	0.34	0.33	4.45
600	0.89	0.22	0.21	2.21
800	0.33	0.22	0.21	1.09

Table 3.10: Helicity cross sections (in fb) for the $e^+e^- \rightarrow t\bar{t}\nu\bar{\nu}$ process, at $\sqrt{s} = 1$ TeV and for different Higgs boson masses (in GeV). $\sigma(\lambda, \lambda')$ denotes the cross section for production of a top quark with helicity λ and an antitop with helicity λ'. CP invariance implies $\sigma(RR) = \sigma(LL)$.

The relevant signal is a $t\bar{t}$ pair with missing transverse momentum carried by the neutrinos or from beam electrons not observed by the detector. The largest background is direct $t\bar{t}$ production. It can be suppressed by requiring missing mass greater than some minimal value, and further by choosing the jet association that best reconstructs the t and W masses. Another significant background is $e^+e^-t\bar{t}$, which can be reduced by requiring the missing transverse energy to be greater than some value such as 50 GeV as used in Ref. [94]. The background from $\gamma t\bar{t}$ can be mostly eliminated with an appropriate cut on the $p_T^{t\bar{t}}$ of the $t\bar{t}$ pair [95]. The expected number of reconstructed 6-jet events as a function of the visible mass at $\sqrt{s} = 1$ TeV with $\mathcal{L} = 1$ ab^{-1} is shown in Fig. 3.19 (left), and the expected relative precision in the top Yukawa measurement is shown in Fig. 3.19 (right) [94]. The QCD corrections of $\mathcal{O}(\alpha_s)$ to the $V_L V_L \rightarrow t\bar{t}$ scattering have been studied in Ref. [96], where V_L represents the longitudinally polarized vector boson $V = W^\pm$
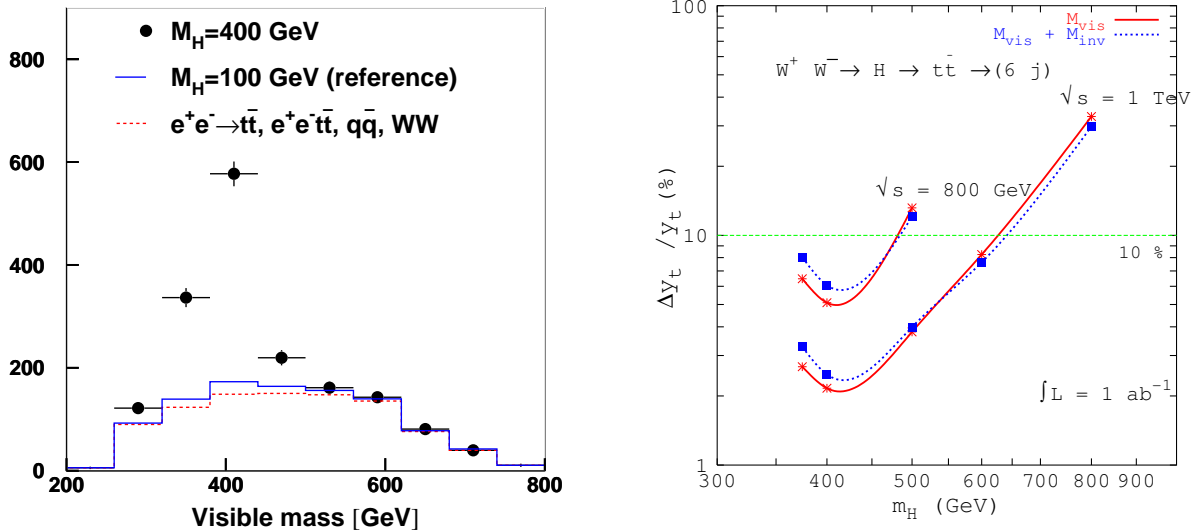
Figure 3.19: [Left figure] Expected number of reconstructed 6-jet events as a function of the visible mass, at $\sqrt{s} = 1$ TeV and with $\mathcal{L} = 1$ ab^{-1} after all cuts, for a Higgs boson of 400 GeV (dots) and for the backgrounds (dashed). The expectations (including background) for a Higgs of 100 GeV (solid) are also shown for comparison. [Right figure] Expected relative precision in the top Yukawa coupling mesurement as a function of the Higgs boson mass, from 6-jet events.

or Z. It has been found that corrections to the cross sections can be as large as 30% and must be accounted for in any precision measurement of $VV \to t\bar{t}$.

The second question about heavier Higgs bosons is whether the Higgs line-shape parameters (mass, decay width, Higgs-strahlung production cross section) can be measured. A complete study of the mass range 200 GeV $< m_H < 320$ GeV has been performed [97]. The final state $q\bar{q}q\bar{q}\ell^+\ell^-$ resulting from $HZ \to ZZZ$ and from $HZ \to W^+W^-Z$ is selected. A kinematic fit is used to assign the possible di-jet combinations to bosons (W^+W^- or ZZ). The resulting di-boson mass spectrum can be fitted by a Breit-Wigner distribution convolved with a detector resolution function. A relative uncertainty on the Higgs mass of 0.11–0.36% is achievable from 500 fb^{-1}at 500 GeV for Higgs masses between 200 and 320 GeV. The resolution on the total width varies between 22 and 34% for the same mass range. Finally, the total Higgs-strahlung cross-section can be measured with 3.5–6.3% precision. Under the assumption that only $H \to WW$ and $H \to ZZ$ decays are relevant, their branching ratios can be extracted with 3.5–8.6% and 9.9–17.3%, respectively (see Table 3.11). The expected mass spectra for $m_H = 200$ GeV and $m_H = 320$ GeV are shown in Fig. 3.20.

3.6.3 Open questions

In the field of heavy SM-like Higgs bosons many questions remain for future studies. Besides extending the results quoted above to other (possibly) higher Higgs mass values the following issues should be addressed:

- What are the chances to observe couplings of the heavy Higgs bosons other than those already investigated?

32
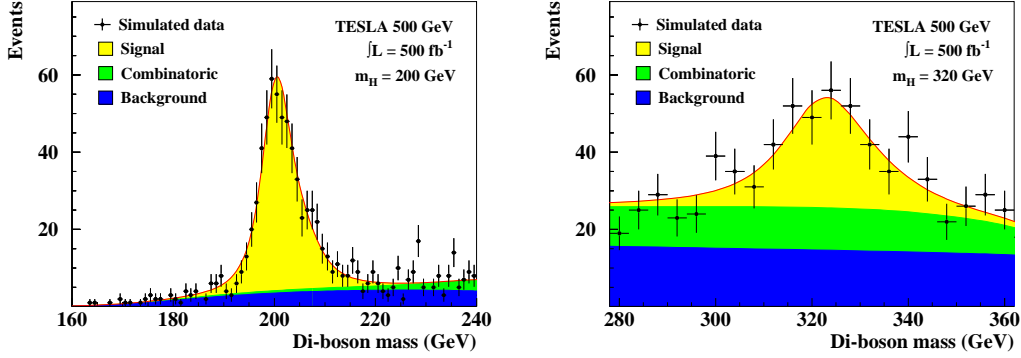
Figure 3.20: Expected reconstructed Higgs boson mass spectra for $m_H = 200$ GeV and $m_H = 320$ GeV from 500 fb^{-1} at 500 GeV (from [97]).

m_H (GeV)	$\Delta\sigma$ (%)	Δm_H (%)	$\Delta\Gamma_H$ (%)
200	3.6	0.11	34
240	3.8	0.17	27
280	4.4	0.24	23
320	6.3	0.36	26

Table 3.11: Expected precision on Higgs boson line-shape parameters for $200 < m_H < 320$ GeV at the ILC with $\sqrt{s} = 500$ GeV.

- What can be learned about the quantum numbers and the spin of heavy (SM-like) Higgs bosons?

- Do these additional measurements pose new requirements for the detector?

3.7   Heavy Neutral Higgs Bosons in the MSSM

Besides the light CP-even Higgs boson in the MSSM there are two other neutral Higgs bosons: the heavier CP-even H and the CP-odd A. For $M_A \gtrsim 150$ GeV the two heavy Higgs bosons are very similar in mass. The couplings of the Higgses to gauge bosons is either strongly suppressed (for HVV) or even zero at the tree-level (for AVV). Therefore the analyses performed for a heavy SM-like Higgs boson as outlined in the previous section cannot be taken over to the case of heavy MSSM Higgs bosons.

Similar to the light CP-even Higgs boson, the heavy neutral CP-even Higgs boson of MSSM can be produced in e^+e^- collisions via Higgs-strahlung and weak boson fusion processes. Neutral Higgs bosons of MSSM can be also produced in pairs, $e^+e^- \to hA$ and $e^+e^- \to HA$, and singly through Yukawa processes, e.g., $e^+e^- \to h(A,H)b\bar{b}$; see Fig. 2.6. In the decoupling limit of the MSSM, the Higgs-strahlung and weak boson fusion processes involving H, as well as pair production process involving h, get strongly suppressed (see, however, Ref. [49]). Hence, in this scenario the main production mechanisms of H and A bosons at an e^+e^- collider will be Yukawa processes and $e^+e^- \to HA$. The pair production of heavy neutral Higgs bosons at an e^+e^- collider has been studied in Ref. [98]. The analysis is based on selection of $b\bar{b}b\bar{b}$ and $b\bar{b}\tau^+\tau^-$ final states, which are expected to be dominant channels for $e^+e^- \to HA$ process for a large part of MSSM parameter

space. For the reconstruction of these final states, efficient b-tagging is important. The analysis employs the same flavor-tagging tools [99] as used in the study of the hadronic decays of the light Higgs boson [70]. The potential of the linear e^+e^- collider for detecting heavy neutral Higgs bosons and measuring their properties has been evaluated for various Higgs boson mass hypotheses. Although in large parts of the MSSM parameter space H and A are almost degenerate in mass, scenarios with large mass splitting between neutral Higgs bosons may occur. This feature is present in CP-conserving as well as in CP-violating scenarios.

Studies have been performed for a linear collider operated at center-of-mass energies of 500 and 800 GeV. An integrated luminosity of 500 fb^{-1} is assumed for each energy. The branching fractions
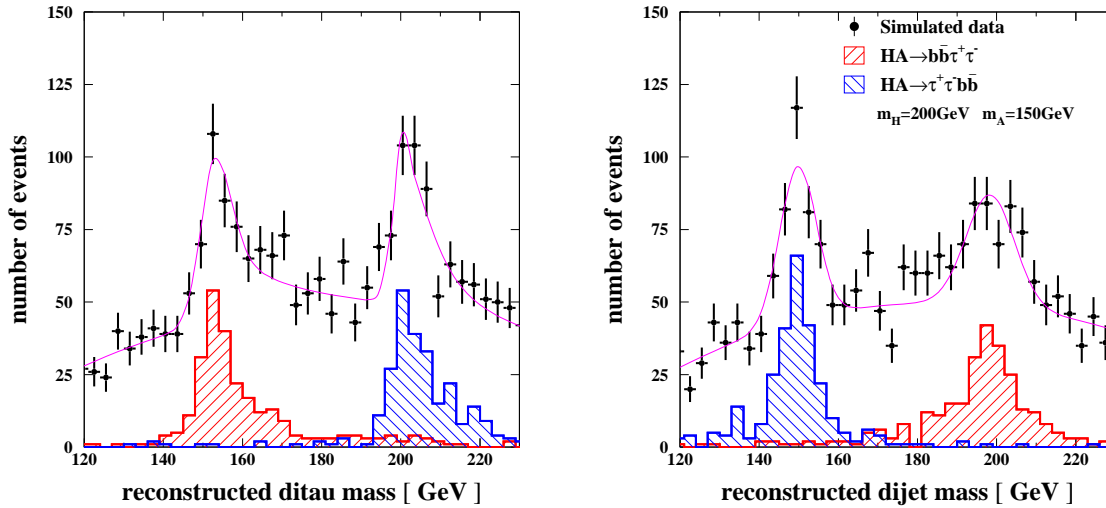
Figure 3.21: Distributions of the reconstructed di-tau mass (left plot) and di-jet mass (right plot) in the $HA \to b\bar{b}\tau^+\tau^-, \tau^+\tau^-b\bar{b}$ channels for $(m_H, m_A) = (200,150)$ GeV at $\sqrt{s} = 500$ GeV. Assumed integrated luminosity is 500 fb^{-1}.

of the Higgs bosons into b-quarks and τ-lepton pairs are set to their typical values in the MSSM: $\mathrm{BR}(H \to b\bar{b}) = \mathrm{BR}(A \to b\bar{b}) = 90\%$, $\mathrm{BR}(H \to \tau\tau) = \mathrm{BR}(A \to \tau\tau) = 10\%$. Furthermore, the maximal allowed cross section for $e^+e^- \to HA$ is assumed, corresponding to $|\sin(\alpha-\beta)| = 1$. These assumptions, however, do not restrict the generality of the study, and results of the analysis can be applied for arbitrary values of Higgs branching fractions by appropriate rescaling the expected number of signal events in each analyzed channel. As an example Fig. 3.21 presents reconstructed ditau and dijet mass spectra in the $b\bar{b}\tau^+\tau^-$ channel for the Higgs boson mass hypothesis (m_H, m_A) $= (200,150)$ GeV. For the same mass hypothesis the distribution of the reconstructed Higgs boson mass sum and mass difference in the $b\bar{b}b\bar{b}$ channel is presented in Fig. 3.22. Exploiting these two channels, the precision on Higgs boson masses and production cross sections is evaluated as a function of the Higgs masses. Higgs boson masses can be measured with accuracy ranging from 0.1 to 1 GeV for Higgs pair production far above and close to the kinematic limit, respectively. The topological cross section $\sigma_{e^+e^- \to HA \to b\bar{b}b\bar{b}}$ can be determined with relative precision of 1.5−7% and cross sections $\sigma_{e^+e^- \to HA \to b\bar{b}\tau^+\tau^-}$ and $\sigma_{e^+e^- \to HA \to \tau^+\tau^-b\bar{b}}$ with a precision of 4−30%. Furthermore, Higgs boson widths can be determined with relative accuracy ranging from 20 to 40%, depending on the Higgs masses. In the case of mass degenerate H and A bosons, the 5σ discovery reach corresponds to a common Higgs boson mass of about 385 GeV in the $HA \to b\bar{b}b\bar{b}$ channel at $\sqrt{s} =$ 800 GeV, assuming an integrated luminosity of 500 fb^{-1}. The mass reach for heavy neutral Higgs
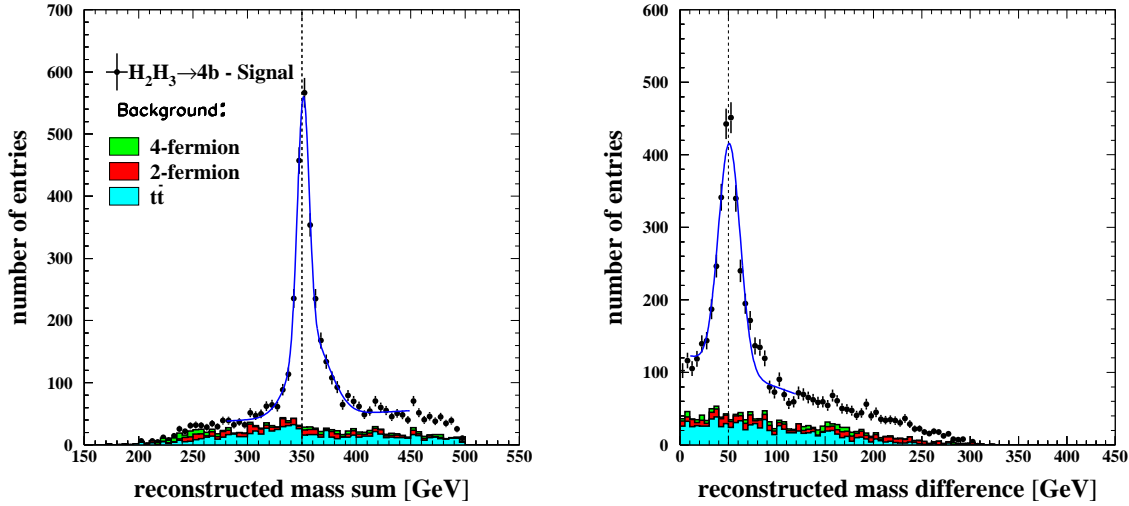
Figure 3.22: Distributions of the reconstructed Higgs boson mass sum, $m_A + m_H$, (left plot) and mass difference, $|m_H - m_A|$, (right plot) in the $HA \to b\bar{b}b\bar{b}$ channel for $(m_H, m_A) = (200,150)$ GeV at $\sqrt{s} = 500$ GeV. Assumed integrated luminosity is 500 fb^{-1}.

bosons can be extended by operating the linear collider at higher centre-of-mass energies. Fig. 3.23 shows as an example the signal in the $HA \to b\bar{b}b\bar{b}$ channel at $\sqrt{s} = 1$ TeV for the Higgs boson mass hypothesis $(m_H, m_A) = (394.6, 394.9)$ GeV, which corresponds to the SPS 1a benchmark point. With 1 ab^{-1} of data collected at $\sqrt{s} = 1$ TeV, m_H and m_A can be measured with an accuracy of 1.3 GeV, and the topological cross section with precision of 9% [98].
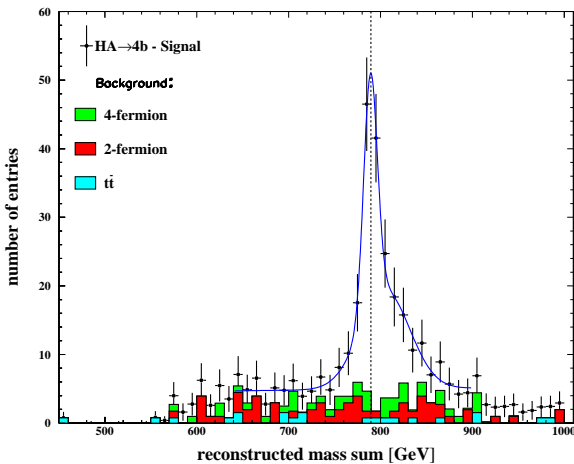
Figure 3.23: Distribution of the reconstructed Higgs boson mass sum, $m_H + m_A$, for the SPS 1a benchmark point. Higgs boson mass hypothesis is $(m_H, m_A) = (394.6, 394.9)$ GeV. Distribution corresponds to an integrated luminosity of 1 ab^{-1} collected at $\sqrt{s} = 1$ TeV.

Alternatively, heavy neutral Higgs bosons can be produced resonantly in $\gamma\gamma$ collisions. The main advantage of the photon collider with respect to the e^+e^- machine is its higher mass reach for heavy neutral Higgs particles. Neutral Higgs bosons with masses up to 350 GeV can be detected with high statistical significance at a photon collider operated at a modest center-of-mass energy of $\sqrt{s_{ee}}$ of 420 GeV [100]. More generally, Higgs bosons can be produced with masses up to 80% of the total e^+e^- energy. An example of the signal in the $\gamma\gamma \to H, A \to b\bar{b}$ channel is presented
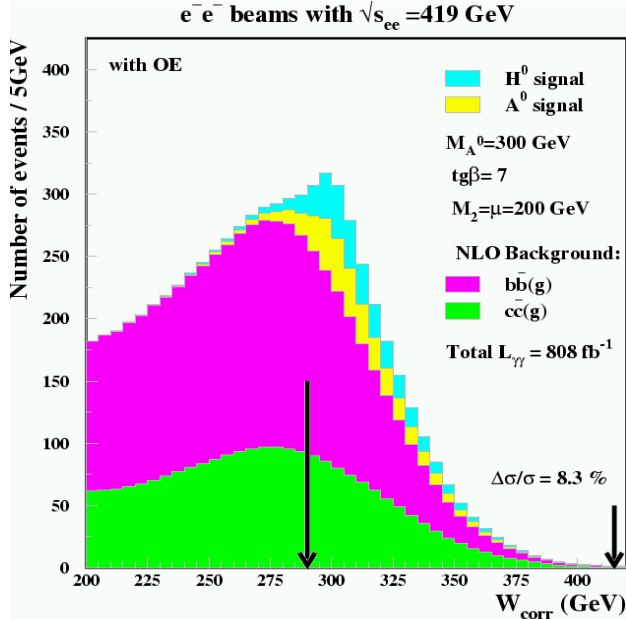
Figure 3.24: Distribution of the invariant mass of the hadronic system in the $\gamma\gamma \to H, A \to b\bar{b}$ channel. Distribution corresponds to 808 fb^{-1} of luminosity collected with photon collider operated at center-of-mass energy of $\sqrt{s_{ee}} = 419$ GeV [100]. Higgs boson masses are $m_H = m_A = 300$ GeV.

in Fig. 3.24. With this process a γC can, e.g., cover the "LHC wedge" where only a SM-like Higgs boson is within the reach of other colliders.

As was discussed above, in the decoupling limit of MSSM one of the most promising channels to detect heavy neutral Higgs bosons will be associated Higgs boson production, $e^+e^- \to HA$. Unfortunately, the mass reach for neutral Higgs bosons in this channel is limited: the Higgs bosons can be produced only if $m_H + m_A < \sqrt{s}$. H and A bosons can be also produced in Yukawa processes, such as $e^+e^- \to H(A)b\bar{b}$. In this case the mass reach is extended almost up to collision energy. Although a number of theoretical studies have been performed which investigated the prospects of detecting heavy neutral Higgs states at e^+e^- collider in Yukawa processes, no related experimental analysis including realistic detector simulation and SM background estimates has been done so far. We hope that this issue will be addressed by future studies.

3.8 Charged Higgs Bosons

The charged Higgs boson ($H^\pm$) is clear evidence of extended Higgs sectors beyond the SM. In the MSSM, the mass of the charged Higgs boson is related to that of the CP-odd Higgs boson by $m_{H^\pm}^2 = M_A^2 + M_W^2 + \delta_{\text{loop}}$, so that $H^\pm$ and A are almost degenerate in the large mass limit. By measuring this mass relation, the MSSM may be distinguished from the general two Higgs doublet model in which no such stringent relationship holds. While the derivative couplings VH^+H^-, $W^\pm H^\mp A$ and $W^\pm H^\mp H$ appear at tree level, there is no tree level $H^\pm W^\mp V$ ($V = \gamma$ or Z) coupling due to the $U(1)_{\text{em}}$ gauge invariance and also the global $SU(2)_V$ symmetry in two Higgs doublet models including the MSSM.

At the ILC, a relatively light charged Higgs boson is produced in pairs, $e^+e^- \to H^+H^-$, as long as the mass is smaller than one half of the collider energy, $m_{H^\pm} < \sqrt{s}/2$. A complete simulation of this process with the decay $H^+ \to t\bar{b}$ and $H^- \to b\bar{t}$ has been performed in Ref. [101] for $\sqrt{s} = 800$ GeV. The mass reconstruction is done by selecting the final state to be the four b jets plus four non-b tagged jets from the two W bosons from top decay. The expected signal and background are shown in Fig. 3.25 for $m_{H^\pm} = 300$ GeV, assuming the integrated luminosity to
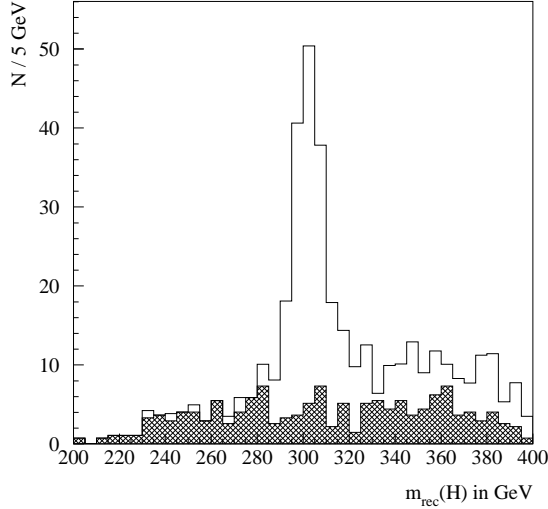
Figure 3.25: Fitted charged Higgs boson mass for $H^+H^- \to (t\bar{b})(\bar{t}b)$ with $m_{H^\pm} = 300$ GeV. The histogram is normalized to an integrated luminosity of 1 ab^{-1}, with a 100% branching ratio in the analyzed decay mode. The contribution of the $tbtb$ background events is shown by the dark histogram.

be 1 ab^{-1}. The mass resolution is approximately 1.5%. A 5σ level discovery will be possible for $m_{H^\pm} < 350$ GeV for $\sqrt{s} = 800$ GeV.

While the mass reach of pair production is limited to $\sqrt{s}/2$, the rare processes of single charged Higgs production may be useful for the search of heavier charged Higgs bosons. The dominant processes are $e^+e^- \to b\bar{t}H^+$, $e^+e^- \to \tau\bar{\nu}_\tau H^+$, $e^+e^- \to W^-H^+$ and $e^+e^- \to H^+e^-\bar{\nu}_e$ (one-loop induced). Their production rates have been calculated at leading order in Refs. [31–34]. QCD corrections to $e^+e^- \to b\bar{t}H^+$ have been studied in Ref. [32], and have turned out to be sizable. For more details about the progress in the cross section calculations, see Sect. 4.2. In Ref. [102], the simulation for the process $e^+e^- \to t\bar{b}H^- + $ c.c. $\to 4b+$jj$+\ell+p_T^{\rm miss}$ ($\ell = e, \mu$) has been performed for a charged Higgs boson mass above half of the collider energy, where the pair production channel $e^+e^- \to H^-H^+$ is no longer available. It has been shown that one can establish a statistically significant $H^\pm$ signal only over a rather limited mass region, of 20 GeV or so beyond $M_{H^\pm} \approx \sqrt{s}/2$, for very large or very small values of $\tan\beta$ and provided high b-tagging efficiency can be achieved; see Fig. 3.26.
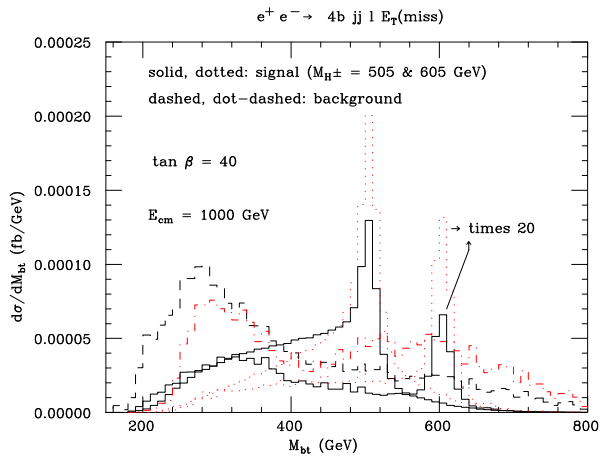
Figure 3.26: (Solid and dashed lines) Differential distribution in the reconstructed Higgs mass from both b-jets not generated in top decays and the two top systems for the signal $e^+e^- \to b\bar{t}H^+ + t\bar{b}H^- \to t\bar{t}b\bar{b}$ and the background $e^+e^- \to t\bar{t}g^* \to t\bar{t}b\bar{b}$, yielding the signature, after the kinematic cuts, including all decay BRs. (Dotted and dot-dashed lines) Same as above, but using only the b-jet with highest transverse momentum of the two not generated in top decays. See Ref. [102] for details.

The situation is different for charged Higgs masses smaller than m_t. A precise measurement of $M_{H^\pm}$ in that range is a challenging task for any collider. In this case the charged Higgs decays dominantly to a tau lepton and neutrino ($H^\pm \to \tau^\pm\nu$), and it is impossible to reconstruct directly

the invariant mass of the di-tau final state. However, due to the polarization of the $\tau^\pm$ leptons, the energy of the $\tau^\pm$ decay products depends strongly on $M_{H^\pm}$, a feature that can be exploited to extract $M_{H^\pm}$ indirectly. The main background to a $H^\pm$ signal in the $\tau^\pm$ decay mode comes from the W-boson decays $W^\pm \to \tau^\pm \nu$. However, thanks to the different structure of the $H^\pm$ and $W^\pm$ electroweak interactions to $\tau^\pm$-leptons, the tau polarization is very different which will allow a separation of $H^\pm \to \tau^\pm \nu$ and $W^\pm \to \tau^\pm \nu$ on a statistical basis. More specifically, the $\tau^\pm$ decay products ($\tau^+ \to \pi^+ \bar\nu$, or $\tau^+ \to \rho^+ \bar\nu$, etc.) have strikingly different topologies according as to whether they originate from a parent $W^\pm$ or $H^\pm$.

The key point is that τ^- leptons arising from $H^- \to \tau^- \nu$ decays are almost purely right-handed, in contrast to the left-handed τ^- leptons which arise from W^- decays. This contrast follows from the helicity flip nature of the Yukawa couplings of the Higgs fields, and the helicity conserving nature of the gauge interactions. The most dramatic difference is seen in the energy distribution for the single pion channel ($H^+/W^+ \to \tau^+ \nu \to \pi^+ \nu \bar\nu$) in the rest frame of the parent boson ($W^\pm$ or $H^\pm$) [103]. In practice, it is nearly impossible to reconstruct the rest frame of the W^+ or H^+ bosons because the momentum of the neutrinos cannot be measured. Instead, one can use the top quark pair production channel with top quark decays ($t \to H^+ b$) and reconstruct the top quark rest frame.

The distributions for the energy of the single pion in the top rest frame has the following form for $H^\pm$ and $W^\pm$ cases, respectively [104–106],

$$\frac{1}{\Gamma}\frac{d\Gamma}{dy_\pi} = \frac{1}{x_{max} - x_{min}} \begin{cases} (1 - P_\tau)log\frac{x_{max}}{x_{min}} + 2P_\tau y_\pi(\frac{1}{x_{min}} - \frac{1}{x_{max}}), & 0 < y_\pi < x_{min} \\ (1 - P_\tau)log\frac{x_{max}}{y_\pi} + 2P_\tau(1 - \frac{y_\pi}{x_{max}}), & x_{min} < y_\pi \end{cases} \tag{3.15}$$

where $y_\pi = \frac{2E_\pi^{top}}{M_{top}}$, $x_{min} = \frac{2E_\tau^{min}}{M_{top}}$, $x_{max} = \frac{2E_\tau^{max}}{M_{top}}$, $E_\tau^{min} = \frac{M_R^2}{2M_{top}}$, $E_\tau^{max} = \frac{M_{top}}{2}$. For the W boson, $P_\tau = -1$, and for the charged Higgs boson, $P_\tau = 1$.

The energy distribution for a pion from $H^\pm$ decay has a maximum at the point $E(\pi^\pm) = M_{H^\pm}^2/(2M_t)$. This dependence allows one to extract $M_{H^\pm}$ from the shape of the spectrum.

The QCD corrected top-quark decay width (in terms of $q_{H^+} = m_{H^+}^2/m_t^2$) is given by [107],

$$\Gamma_{QCD}^{imp}(t \to bH^+) = \frac{g^2}{64\pi M_W^2} m_t(1 - q_{H^+})^2 \bar{m}_b^2(m_t^2) \tan^2\beta \times$$
$$\left\{ 1 + \frac{\alpha_S(m_t^2)}{\pi}\left[7 - \frac{8\pi^2}{9} - 2\log(1 - q_{H^+}) + 2(1 - q_{H^+}) \right.\right.$$
$$\left.\left. + \left(\frac{4}{9} + \frac{2}{3}\log(1 - q_{H^+})\right)(1 - q_{H^+})^2 \right] \right\} \tag{3.16}$$

The Δm_b corrections have been included using `CPsuperH` [108]. The numerical simulations have been performed assuming a center of mass energy $\sqrt{s} = 500$ GeV and a total integrated luminosity $\mathcal{L} = 500$ fb^{-1}. We have performed detailed computations and Monte Carlo simulations for different sets of MSSM parameters, all leading to light charged Higgs bosons [103]. Here we present two scenarios, based on the mass parameters $M_Q = M_U = M_D = 1$ TeV, $M_{\tilde{g}} = M_2 = 1$ TeV, $A_t = 500$, $\mu = \pm 500$ GeV, and $\tan\beta = 50$, which give $M_{H^\pm} = 130$ GeV. The branching ratio BR($t \to H^\pm b$) will be enhanced or suppressed depending on the sign of μ. The branching ratios for these examples are

(i)	$M_{H^\pm} = 130$ GeV,	$\mu < 0$ and $\tan\beta = 50$:	$BR(t \to H^+ b) = 0.24$
(ii)	$M_{H^\pm} = 130$ GeV,	$\mu > 0$ and $\tan\beta = 50$:	$BR(t \to H^+ b) = 0.091$

The couplings have been implemented in CompHEP [109], which has been used to compute the cross sections for signal and background processes, including decays of top to $W^\pm$ and $H^\pm$ which

subsequently decay to polarized $\tau^{\pm}$ leptons. CompHEP was also used to generate events, and effects from initial state radiation and Beamstrahlung were included. Polarized $\tau^{\pm}$ decays have been simulated using TAUOLA [110] interfaced to CompHEP. Hadronization and energy smearing in the final state are accounted for by means of PYTHIA [111] using the CompHEP-PYTHIA [112] interface based on Les Houches Accord [113]. Effects from final state radiation have been implemented using the PHOTOS library [114].

A brief description of the fitting procedure is given in Ref [103]. We use the method of maximum likelihood to fit a spectrum created from simulated signal and background events, and obtained the following results for the cases described above:

$$(i) \quad M_{H^{\pm}} = 129.7 \pm 0.5 \text{ GeV},$$
$$(ii) \quad M_{H^{\pm}} = 129.4 \pm 0.9 \text{ GeV},$$

Figure 3.27 shows results of the simulations and fits. The charged Higgs mass may be determined, in both cases, with an uncertainty of the order of 1 GeV. This study is a theoretical level analysis, and no systematics or detector effects have been included. A full detector simulation will be necessary to test the robustness of this result.
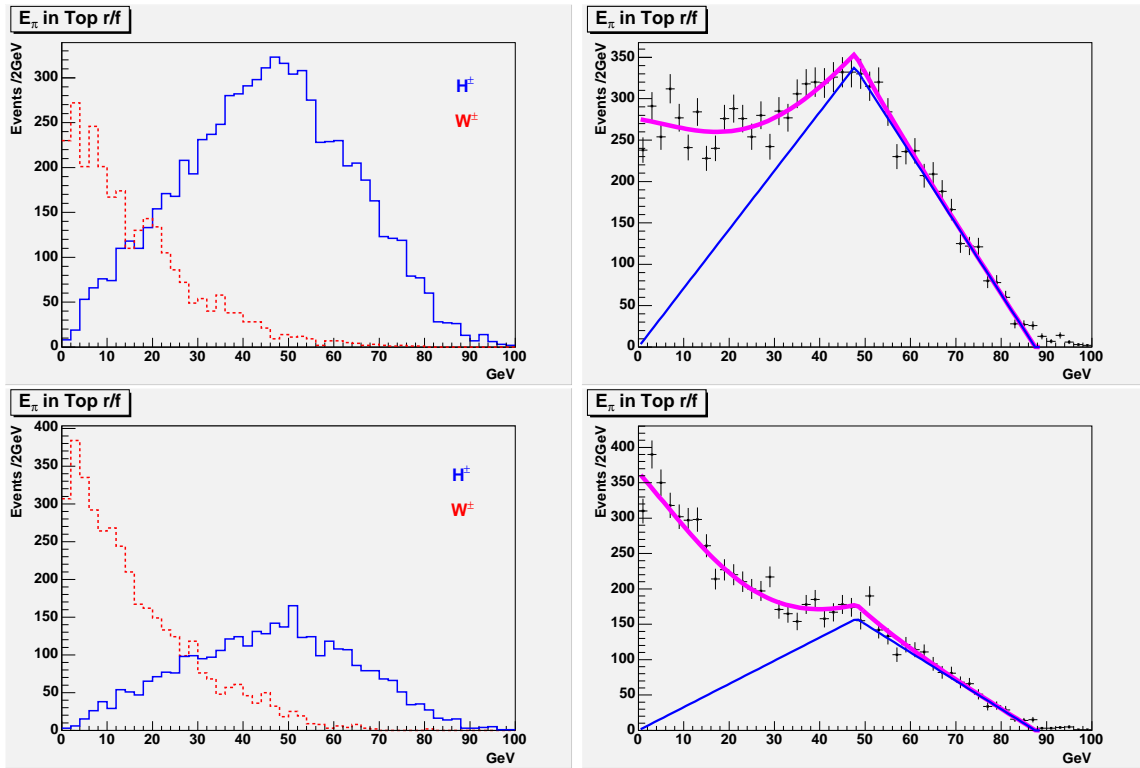
Figure 3.27: Generated $\pi^{\pm}$ energy spectra (left plots) and the fit (right plots) for the two sets of MSSM parameters described in the text.

3.9 Measuring $\tan\beta$ in $\gamma\gamma$ Collisions

The measurement of the mixing parameter $\tan\beta$, one of the fundamental parameters in the Higgs sector of supersymmetric theories, is a difficult task, especially if $\tan\beta$ is large. In this section two methods are described to measure $\tan\beta$ at the γC.

$\tau\tau$ fusion to Higgs bosons at a photon collider [115] can provide a valuable method for measuring this parameter. The couplings in the limit of large $\tan\beta$ (and moderate values of M_A in the case of the h) are given by (see e.g. Ref. [116])

$$\begin{aligned}
g_{\Phi\tau\tau} &= \tan\beta && \text{for } \Phi = A \\
g_{\Phi\tau\tau} &\simeq \tan\beta && \text{for } \Phi = h, H
\end{aligned} \tag{3.17}$$

[normalized to the Standard Model Higgs coupling to a tau pair, m_τ/v]. Thus the entire Higgs mass range up to the kinematical limit can be covered for large $\tan\beta$ by this method.

We consider the process

$$\gamma\gamma \to \tau\tau\ \tau\tau \to \tau\tau + h/H/A \ . \tag{3.18}$$

For large $\tan\beta$ all the Higgs bosons decay almost exclusively [80 to 90%] to a pair of b quarks, and the final state consists of a pair of τ's and a pair of resonant b quark jets. The main background channels are $\tau^+\tau^-$ annihilation into a pair of b-quarks, via s-channel γ/Z exchanges, naturally suppressed as a higher-order electroweak process, and diffractive $\gamma\gamma \to (\tau^+\tau^-)(b\bar{b})$ events, reduced kinematically by choosing proper cuts. The SUSY parameters have been chosen according to the SPS 1b scenario [117], but M_A has been varied.
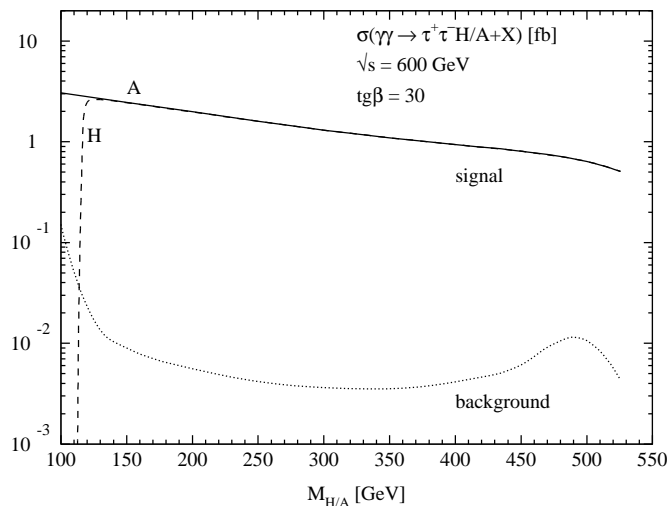
Figure 3.28: The cross sections for the production of the H/A Higgs bosons in the $\tau\tau$ fusion process at a $\gamma\gamma$ collider for $\tan\beta = 30$. The other parameters have been chosen according to the SPS 1b scenario (but with M_A varied). Also shown is the background cross section for properly chosen experimental cuts. $\sqrt{s}$ denotes the $\gamma\gamma$ collider c.m. energy, corresponding to approximately 80% of the $e^\pm e^-$ linear collider energy.

The cross sections for the signals of H and A Higgs-boson production in the $\tau\tau$ fusion process, together with the background processes, are presented in Fig. 3.28, including proper cuts. The cross section for $\tau\tau$ fusion to the light Higgs boson h is of the same size.

The statistical accuracy with which large $\tan\beta$ values can be measured in $\tau\tau$ fusion to $h/H/A$ Higgs bosons is exemplified for three $\tan\beta$ values, $\tan\beta = 10$, 30 and 50, in Table 3.12. Results for scalar H production are identical to pseudoscalar A in the mass range above 120 GeV. The two channels h and A, and H and A are combined in the overlapping mass ranges in which the respective two states cannot be discriminated. In Table 3.12 the relative errors $\Delta\tan\beta/\tan\beta$ are

M_{Higgs} [GeV]	$E_{\gamma\gamma} = 400$ GeV			$E_{\gamma\gamma} = 600$ GeV				
	$A \oplus h$	$A \oplus H$		$A \oplus h$	$A \oplus H$			
	100	200	300	100	200	300	400	500
$\tan\beta$	I	II	III	IV	V	VI	VII	VIII
10	8.4%	10.7%	13.9%	8.0%	9.0%	11.2%	13.2%	16.5%
30	2.6%	3.5%	4.6%	2.4%	3.0%	3.7%	4.4%	5.3%
50	1.5%	2.1%	2.7%	1.5%	1.8%	2.2%	2.6%	3.2%

Table 3.12: Relative errors $\Delta\tan\beta/\tan\beta$ on $\tan\beta$ in measurements for $\tan\beta = 10$, 30 and 50, based on: combined $A \oplus h$ [I,IV] and $A \oplus H$ [II,III,V–VIII] production, assuming [$E_{\gamma\gamma} = 400$ GeV, $\mathcal{L} = 100$ fb^{-1}] and [$E_{\gamma\gamma} = 600$ GeV, $\mathcal{L} = 200$ fb^{-1}]. Proper cuts and efficiencies are applied on the final–state τ's and b jets.

presented. Since in the region of interest the $\tau\tau$ fusion cross sections are proportional to $\tan^2\beta$ and the background is small, the absolute errors $\Delta\tan\beta$ are nearly independent of $\tan\beta$, varying between

$$\Delta\tan\beta \simeq 0.9 \quad \text{and} \quad 1.3 \tag{3.19}$$

for Higgs mass values away from the kinematical limits.

This analysis compares favorably well with the corresponding b-quark fusion process at the LHC [118]. Moreover, the method can be applied readily for a large range of Higgs mass values and thus is competitive with complementary methods in the e^+e^- mode of a linear collider [119].

An alternative method to measure $\tan\beta$ is provided by the associated $tH^\pm$ production in $\gamma\gamma$ collisions [120]. The subprocess $b\gamma \to H^- t$ utilizes the b-quark content of the photon. $\tan\beta$ enters through the $tbH^\pm$ vertex, so that the amplitude squared for the subprocess $b\gamma \to tH^-$ is given by:

$$\sum |M(b\gamma \to tH^\pm)|^2 \propto \sqrt{2}G_F\pi\alpha(m_b^2\tan^2\beta + m_t^2/\tan^2\beta). \tag{3.20}$$

Fig. 3.29 shows the cross section as a function of $\tan\beta$ with the measurement precision superimposed. It has been found that $\gamma\gamma \to tH^\pm + X$ can be used to make a good determination of $\tan\beta$ for most of the parameter space with the exception of the region around $\tan\beta \simeq 7$ where the cross section is at a point of inflection. This measurement provides an additional constraint on $\tan\beta$ which complements other processes.

3.10 Measurements in Exotic Scenarios

An interesting possibility is that the Higgs decays into particles not present in the Standard Model. In particular, if there are exotic light objects which did not obtain their mass directly from the Higgs mechanism, their couplings to the Higgs may be large despite their small masses, and they may dominate over the standard Higgs decay modes. Such a scenario depends very strongly on how these new objects manifest themselves inside the detector, and can play a very significant role in how well both the LHC and the ILC can determine the Higgs properties. In fact, the tiny expectation for the SM Higgs width (provided $M_H \lesssim 150$ GeV) implies that the Higgs is particularly sensitive to new decay modes, even if they are not very strongly coupled.
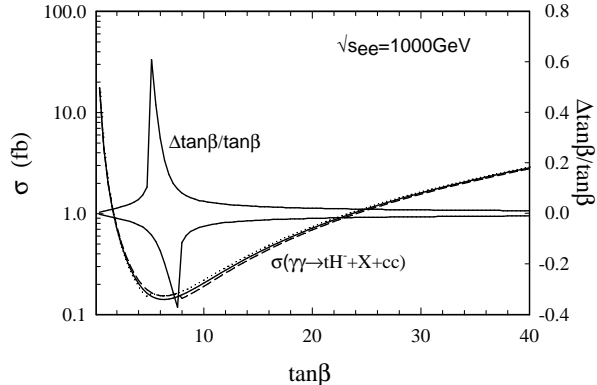
Figure 3.29: $\sigma(\gamma\gamma \rightarrow tH^- + X)$ vs. $\tan\beta$ for the backscattered laser case and the sensitivities to $\tan\beta$ based only on statistical errors (solid lines) for $\sqrt{s}_{ee} = 1$ TeV and $M_H = 200$ GeV. For the cross sections, the solid line represents the expected cross section at the nominal value of $\tan\beta$, while the dashed (dotted) line represents the expected cross section at $\tan\beta - \Delta\tan\beta$ ($\tan\beta + \Delta\tan\beta$). From Ref. [120].

3.10.1 Higgs decaying into unflavored jets

The first such scenario arises when the Higgs decays primarily into light hadrons, without any particular bottom or charm content. This actually occurs in some limits of the minimal supersymmetric standard model [121]. If, for example, the pseudo-scalar Higgs A is light enough, the dominant decay mode of the SM-like Higgs may be $H \rightarrow AA$. If the A mass is less than $2m_b$, and $\tan\beta$ is larger than 10 or so, the dominant A decay will be into strange quarks, with separation too small to be resolved as separate jets. Thus, the decay $H \rightarrow AA \rightarrow s\bar{s}s\bar{s}$ results in two hard jets of energy roughly $M_H/2$ in the Higgs rest frame[4].

A second possibility is that the Higgs decays into down-type squarks [123]. The most likely candidate is the scalar bottom $\tilde{b}$, which could further decay into a pair of anti-quarks through a baryon-number violating interaction of the type UDD. Again, if the mass of the $\tilde{b}$ is relatively small, the two quarks may not be sufficiently separated to be resolved as individual jets, and the Higgs decays effectively into two jets. Such a light bottom squark was postulated in [124] to address an excess in the open bottom quark production cross section at run I of the Tevatron. The MSSM Higgs width into a pair of scalar bottoms can be compared with the SM width into $b\bar{b}$ as,

$$\frac{\Gamma_{\tilde{b}}}{\Gamma_b} = \frac{(\mu\tan\beta)^2}{2m_h^2}\sin^2 2\theta_b \left(1 - 4\frac{m_{\tilde{b}}^2}{m_h^2}\right)^{\frac{1}{2}} \tag{3.21}$$

where μ is the higgsino mass parameter, $\tan\beta$ is the ratio of Higgs VEVs, and θ_b is the sbottom mixing angle. The decay into $\tilde{b}$ dominates whenever $\mu\tan\beta/m_h$ is large, and the mixing angle is not too small and the $\tilde{b}$ mass not too large.

However the new decay mode arises, this scenario can be modelled by assuming that the Higgs receives a new contribution to its width into jets (and assuming the width into other SM particles remains SM-like). For definiteness, we discuss the case with the light $\tilde{b}$, but the results are largely insensitive to this choice. As the width into the new decay mode becomes large, it eventually overwhelms the SM decay modes, driving their branching ratios to be small. Figure 3.30 shows the branching ratios for all of the important decay modes as a function of $\mu\tan\beta/m_h$. One should note that the light $\tilde{b}$ *have* been included in the loop-generated H-g-g and H-γ-γ couplings, and thus there is some model-dependence in those curves. As can be seen from the figure, once $\mu\tan\beta/m_h$ is larger than about 10, the decay into $\tilde{b}$ completely dominates, with the canonical SM decay into $b\bar{b}$ having a branching ratio of less than 10%.

The primary feature of the new decay mode is that, by reducing the decay into SM particles while leaving the Higgs production cross sections unchanged, it reduces the statistics available to

---

[4]This situation is also likely to arise in the NMSSM for regions of parameter space with small fine-tuning [122].
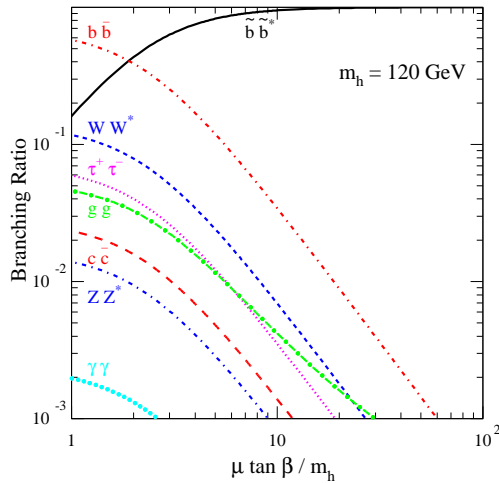
Figure 3.30: Branching fractions for various Higgs boson decay channels as a function of the ratio $\mu \tan\beta/m_h$, with $m_h = 120$ GeV. The sbottom mass is fixed to $m_{\tilde{b}} = 5$ GeV.

measure the Higgs interactions with SM particles and thus limits the precision with which they may be measured. At the same time, the decay into jets is experimentally very challenging, and can prevent the LHC from discovering the Higgs by depressing the decay into observable SM particles below LHC sensitivities and opening a new decay channel which cannot be seen at the LHC because of huge QCD jet backgrounds. A careful analysis shows that if the width into the new hadronic state is more than a few times the width into bottom quarks, the LHC completely loses the ability to detect the light CP-even Higgs [123]. This could lead one to the perplexing situation in which supersymmetry and perhaps one or more of the MSSM heavy Higgses are discovered, but the Higgs actually responsible for electroweak symmetry breaking is too difficult to extract from the large hadronic backgrounds.

The ILC will easily detect such a Higgs, because its primary search mode is not sensitive to the Higgs decay mode (see Sect. 3.1). At the same time, the high sensitivity expected at the ILC will help allow it to make important measurements of the Higgs. As the decay width into jets increases, the statistics for SM decays decreases, and some measurements are degraded. However, since the decay into jets can in general be extracted from the background, measurements of the couplings associated with Higgs production remain accessible and precise. Figure 3.31 plots the projected uncertainties in the Higgs couplings as a function of the ratio of widths $\Gamma(H \to jj)/\Gamma(H \to b\bar{b})$. Note that $H \to jj$ includes the SM decay into bottom quarks as well as the new contribution into unflavored jets.

3.10.2   Invisibly decaying Higgs

The Higgs might also decay predominantly into a neutral exotic particle, such as the lightest neutralino of a supersymmetric theory. In such a case, the Higgs becomes effectively invisible, because the decay products do not interact with the detector material. However, even in this case a precise mass measurement is possible with the recoil method down to the level of about ~ 100 MeV [8]. Concerning the other (now rare) decay channels, the existing studies apply with appropriately scaled signal rates; see Sects. 3.3, 3.6.

43
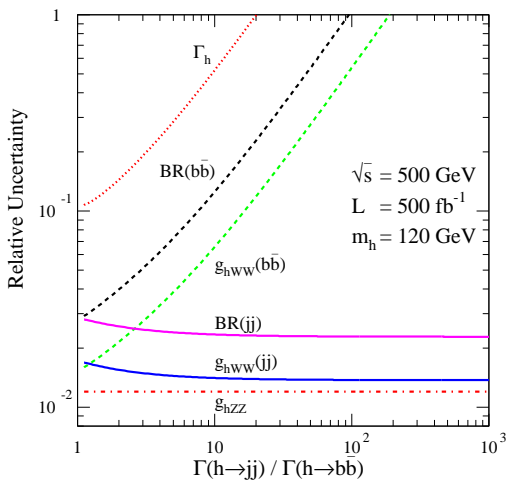
Figure 3.31: Expected accuracy in the measurements of the $b\bar{b}$ and jet-jet branching fractions, the hZZ and hWW coupling strengths, and the total width of the Higgs boson, as a function of the ratio of the jet-jet and the $b\bar{b}$ widths, assuming the Higgs boson couplings to $b\bar{b}$, ZZ, and WW^* are standard.

Chapter 4

Theoretical Developments

The ILC does not only offer an even greater physics potential, but in turn represents a great challenge for theorists to understand phenomena at the experimentally achievable level of precision.

At energies exceeding the reach of LEP2, many new processes will be accessible, such as top-quark pair production, Higgs production, or reactions with new-physics particles, as predicted, e.g., by SUSY models. To exploit the potential of the ILC, predictions for such reactions should be based on full transition matrix elements and improved by radiative corrections as much as possible. The higher level of accuracy at the ILC requires a corresponding level of precision in the theoretical predictions.

In the following we focus directly on Higgs physics, but there are other important areas (related to EWSB) where higher-order corrections are indispensable. This comprises precision calculations for M_W (i.e., for μ decay); precision observables on the Z resonance (e.g., for the effective leptonic weak mixing angle, $\sin^2 \theta_{\text{eff}}$); radiative corrections to $2 \to 3, 4, \ldots$ processes in general; single W production; etc.

4.1 Radiative corrections to Higgs masses and couplings in the MSSM

Within the MSSM the masses of the $\mathcal{CP}$-even neutral Higgs bosons as well as the masses of the charged Higgs bosons are calculable in terms of the other MSSM parameters. The status of the available corrections to the masses and mixing angles in the MSSM Higgs sector (with real parameters) can be summarized as follows. For the one-loop part, the complete result within the MSSM is known [15, 125–127]. The by far dominant one-loop contribution is the $\mathcal{O}(\alpha_t)$ term due to top and stop loops ($\alpha_t \equiv h_t^2/(4\pi)$, h_t being the superpotential top coupling). Concerning the two-loop effects, their computation is quite advanced and has now reached a stage such that all the presumably dominant contributions are known. They include the strong corrections, usually indicated as $\mathcal{O}(\alpha_t\alpha_s)$, and Yukawa corrections, $\mathcal{O}(\alpha_t^2)$, to the dominant one-loop $\mathcal{O}(\alpha_t)$ term, as well as the strong corrections to the bottom/sbottom one-loop $\mathcal{O}(\alpha_b)$ term ($\alpha_b \equiv h_b^2/(4\pi)$), i.e., the $\mathcal{O}(\alpha_b\alpha_s)$ contribution. The latter can be relevant for large values of $\tan\beta$. Presently, the $\mathcal{O}(\alpha_t\alpha_s)$ [16, 128–131], $\mathcal{O}(\alpha_t^2)$ [128, 132, 133] and the $\mathcal{O}(\alpha_b\alpha_s)$ [134, 135] contributions to the self-energies are known for vanishing external momenta. In the (s)bottom corrections the all-order resummation of the $\tan\beta$-enhanced terms, $\mathcal{O}(\alpha_b(\alpha_s \tan\beta)^n)$, is also performed [107, 136]. Recently the $\mathcal{O}(\alpha_t\alpha_b)$ and $\mathcal{O}(\alpha_b^2)$ corrections became available [137]. Finally a full two-loop effective potential calculation (including even the momentum dependence for the leading pieces) has been published [138]. However, no computer code is publicly available.

In the case of the MSSM with complex parameters (cMSSM) the higher order corrections have so far been restricted, after the first more general investigations [139], to evaluations in the effective potential (EP) approach [140, 141] and to the renormalization group (RG) improved one-loop EP method [142, 143]. These results have been restricted to the corrections coming from the (s)fermion sector and some leading logarithmic corrections from the gaugino sector. A more complete one-loop calculation has been attempted in Ref. [144]. More recently the leading one-loop corrections have also been evaluated in the Feynman-diagrammatic (FD) method, using the on-shell renormalization scheme [145]. The full one-loop result can be found in Ref. [146, 147].

The upper limit is estimated to be $m_h \lesssim 135$ GeV [16,17]. The remaining theoretical uncertainty on the lightest $\mathcal{CP}$-even Higgs boson mass has been estimated to be below ~ 3 GeV [17,52]. The above calculations have been implemented into public codes. The program `FeynHiggs` [16, 17, 37, 148] is based on the results obtained in the FD approach, it includes all available corrections. The code `CPsuperH` [108] is based on the RG improved effective potential approach. For the MSSM with real parameters the two codes can differ by up to ~ 4 GeV for the light $\mathcal{CP}$-even Higgs boson mass due to subleading higher-order corrections that are included only in `FeynHiggs`.

4.2 Single Higgs production at one-loop in $2 \to 3$ processes

Recently some one-loop calculations of electroweak radiative corrections have been presented for $2 \to 3$ processes that are interesting at the ILC: $e^+e^- \to \nu\bar{\nu}H$ [149,150] and $e^+e^- \to t\bar{t}H$ [151–153]. The results of Refs. [149, 152] were obtained with the GRACE-LOOP [154] system (see below). In Refs. [150, 151, 153] the technique [155] for treating tensor 5-point integrals was employed. While Refs. [149, 151, 152] make use of the slicing approach for treating soft-photon emission, the results of Refs. [150, 153] have been obtained by dipole subtraction and checked by phase-space slicing for soft and collinear bremsstrahlung.

In e^+e^- annihilation there are two main production mechanisms for the SM Higgs boson. In the Higgs-strahlung process, $e^+e^- \to ZH$, a virtual Z boson decays into a Z boson and a Higgs boson. The corresponding cross section rises sharply at threshold ($\sqrt{s} \gtrsim M_Z + M_H$) to a maximum at a few tens of GeV above $M_Z + M_H$ and then falls off as s^{-1}, where $\sqrt{s}$ is the CM energy of the e^+e^- system. In the W-boson-fusion process, $e^+e^- \to \nu_e\bar{\nu}_eH$, the incoming e^+ and e^- each emit a virtual W boson which fuse into a Higgs boson. The cross section of the W-boson-fusion process grows as $\ln s$ and thus is the dominant production mechanism for $\sqrt{s} \gg M_H$. A complete calculation of the $\mathcal{O}(\alpha)$ electroweak corrections to $e^+e^- \to \nu\bar{\nu}H$ in the SM has been performed in Refs. [149, 150]. The results of Refs. [149, 150] are in good agreement, see, e.g., [156]. The agreement of the correction is within 0.2% or better with respect to the lowest-order cross sections.

Sample results taken from Ref. [150] are shown in Fig. 4.1 for two Higgs boson masses, $M_H = 115, 150$ GeV. The higher-order corrections are of the order of a few percent if the tree-level result is expressed in terms of G_μ [150].

The Yukawa coupling of the top quark could be measured at a future ILC with high energy and luminosity at the level of $\sim 5\%$ [8] by analyzing the process $e^+e^- \to t\bar{t}H$. A thorough prediction for this process, thus, has to control QCD [157] (possibly SUSY QCD [158]) and electroweak corrections [152, 153]. The results of Refs. [152, 153] have been compared with other calculations, see e.g. Ref. [156]. Agreement within $\sim 0.1\%$ is found. This also holds for other energies and Higgs-boson masses. The results of the previous calculation [151] roughly agree with the ones of Refs. [152, 153] at intermediate values of $\sqrt{s}$ and M_H, but are at variance at high energies (TeV range) and close to threshold (large M_H).

Sample results taken from Ref. [152] are shown in Fig. 4.2 for $M_H = 120$ GeV. The higher-order corrections are of the order of 10 percent if the tree-level result is expressed in terms of G_μ [150].
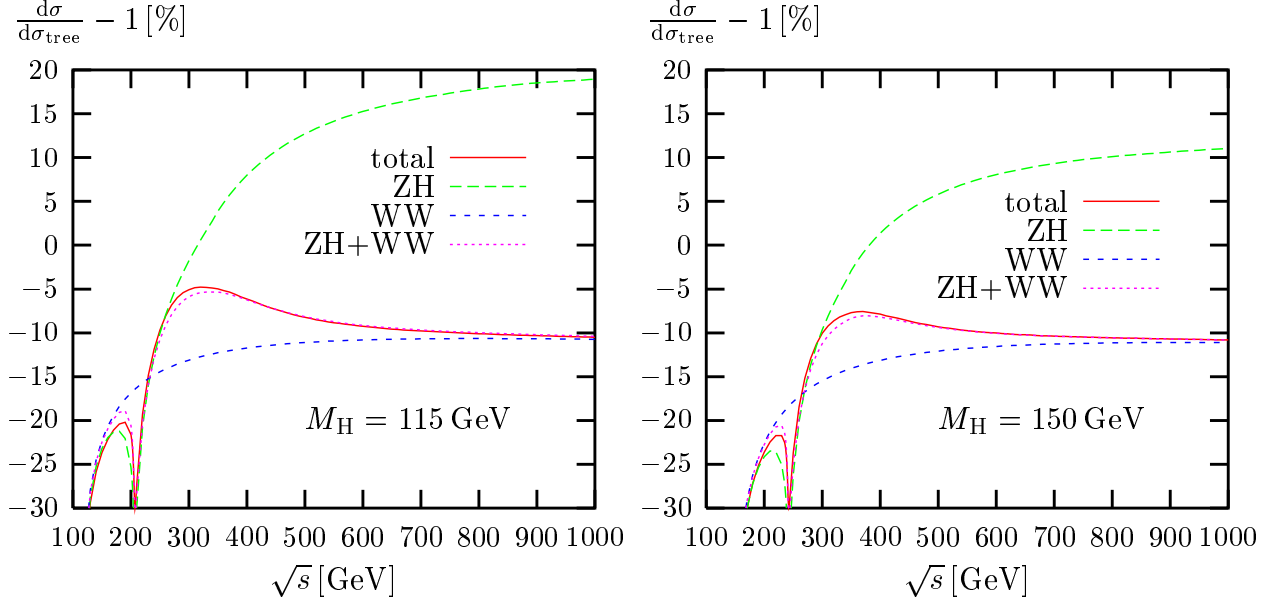
Figure 4.1: Relative electroweak corrections to the complete process $e^+e^- \rightarrow \nu\bar{\nu}H$ and to the contributions from ZH-production and WW-fusion channels for $M_H = 115$ GeV and $M_H = 150$ GeV [150].
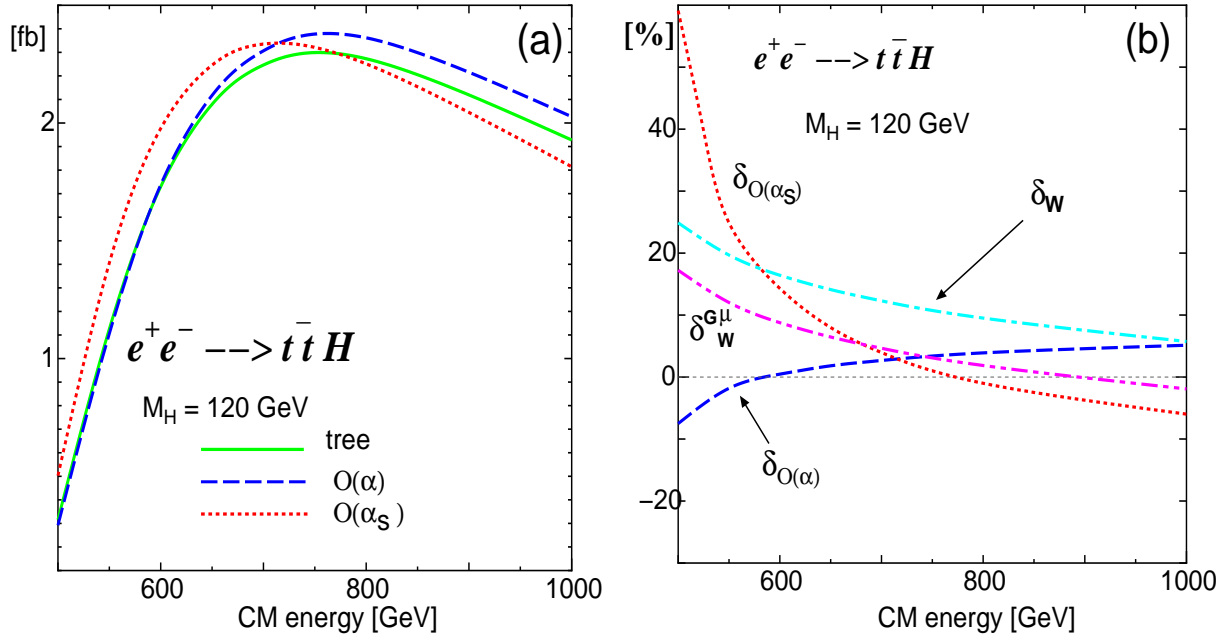
Figure 4.2: (a) Total cross section as a function of the CMS energy for $M_H = 120$ GeV. Shown are the results for the total cross sections for the tree level, full $\mathcal{O}(\alpha)$ and $\mathcal{O}(\alpha_s)$ level in (a). The relative corrections are shown in (b). Solid lines are tree level, dashed lines are the full $\mathcal{O}(\alpha)$ and dotted lines are the $\mathcal{O}(\alpha_s)$ corrections. In addition, the genuine weak correction δ_W and the relative correction $\delta_W^{G_\mu}$ in the G_μ scheme are presented. For more details see Ref. [152].

47

More higher-order corrections possibly have to be evaluated in order to reach the required ILC accuracy.

We now turn to the corresponding predictions within the MSSM At the one-loop level, first the contributions of fermion and sfermion loops in the MSSM to $e^+e^- \to \nu\bar{\nu}h$ have been evaluated in Ref. [49, 159]. The corrections to the light Higgs boson production have been found to be at the percent level [49].

Since at the tree level and in the decoupling limit the heavy neutral MSSM Higgs bosons decouple from the Z, the mass reach for their discovery at the ILC is limited to approximately $\sqrt{s}/2$ from the pair production process. It has been investigated how single production mechanisms could extend the mass reach of the ILC. In particular, the WW-fusion process $e^+e^- \to \nu_e\bar{\nu}_e H$ has been investigated [49]. Its tree level cross-section is proportional to $\cos(\beta - \alpha)$. Depending on the SUSY parameters, radiative corrections might increase the cross-section for $e^+e^- \to \nu_e\bar{\nu}_e H$, possibly allowing discovery beyond the pair production kinematic limit for certain choices of the MSSM parameters. Using left-polarized electron beams and right-polarized positron beams the cross-section can further be enhanced. A particular scenario where this is the case has been chosen in [49] ($M_{\mathrm{SUSY}} = 350$ GeV, $\mu = 1000$ GeV, $M_2 = 200$ GeV and large stop mixing). Cross-section contours for this scenario are shown in Fig. 4.3.
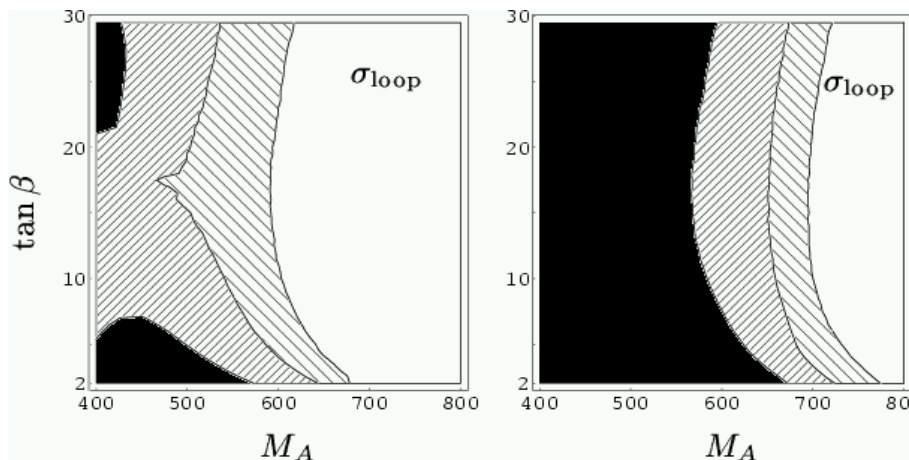
Figure 4.3: Cross-section contours for $e^+e^- \to H\nu\bar{\nu}$ for a particular MSSM scenario (see text) in the $m_A - \tan\beta$ plane for $\sqrt{s} = 1$ TeV. The different shadings correspond to: white: $\sigma \leq 0.01$ fb^{-1}, light shaded: 0.01 fb$^{-1} \leq \sigma \leq 0.02$ fb^{-1}, dark shaded: 0.02 fb$^{-1} \leq \sigma \leq 0.05$ fb^{-1}, black: $\sigma \geq 0.05$ fb^{-1}(from [49]). The left figure is for unpolarized beams, the right figure for an electron (positron) polarization of 0.8 (0.6).

In a CP violating scenario the three neutral Higgs bosons, H_1, H_2, H_3, are mixtures of the CP even and CP odd Higgs fields. Consequently, they all couple to the Z boson and to each other. These couplings may be very different from those of the CP conserving case. In the CP violating scenario the Higgs-strahlung processes $e^+e^- \to H_iZ$ ($i = 1, 2, 3$) and pair production processes $e^+e^- \to H_iH_j$ ($i \neq j$) may all occur, with widely varying cross-sections.

4.3 Higgs production at one-loop in $2 \to 2$ processes

The most promising channels for the production of the $\mathcal{CP}$-even neutral MSSM Higgs bosons in the first phase of an ILC are the Higgs-strahlung processes [160],

$$e^+ e^- \to Z\, H_i \ , \qquad (4.1)$$

$(H_{1,2} = h, H)$ and the associated production of a scalar and a pseudoscalar Higgs boson,

$$e^+ e^- \to A\, H_i \ . \qquad (4.2)$$

The full one-loop corrections [161] and the leading two-loop corrections [162] are available. They have been combined to obtain the currently most accurate results for these production cross sections. The results have been implemented into the code `FeynHiggsXS` [162].

In Fig. 4.4 the dependence of σ_{Zh} and σ_{Ah} on M_A are shown in the "no-mixing" benchmark scenario [163] ($M_{\mathrm{SUSY}} = 2$ TeV, $X_t = 0$, $A_t = A_b$, $\mu = 200$ GeV, $M_2 = 200$ GeV, $m_{\tilde{g}} = 0.8\, M_{\mathrm{SUSY}}$) for $\tan\beta = 5$ and $\tan\beta = 50$. The solid (dot-dashed) line represents the two-loop result including (excluding) box contributions, the dotted line shows an effective coupling approximation and the dashed line shows the one-loop result. For σ_{Zh}, the A boson decouples quickly; the dependence on M_A becomes very weak for $M_A \gtrsim 250$ GeV, when σ_{Zh} is already practically constant. In the same limit, σ_{Ah} goes quickly to zero due to suppression of the effective ZhA coupling, which is $\sim \cos(\alpha_{\mathrm{eff}} - \beta)$; also the kinematical suppression plays a role, but this becomes significant only for sufficiently large M_A, $M_A > 350$ GeV. For large $\tan\beta$ the decoupling of M_A is even more rapid. The differences between the FD two-loop result and the effective coupling approximation for the Higgs-strahlung cross section tend also to a constant, but they increase with M_A for the associated production. The latter can be explained by the growing relative importance of 3- and 4-point vertex function contributions compared to the strongly suppressed Born-like diagrams. As can be seen from Fig. 4.4, for $\tan\beta = 50$ and $M_A \geq 300$ GeV the two-loop result is almost an order of magnitude larger than the result of the effective coupling approximation, and starts to saturate. This can be attributed to the fact that the (non-decoupling) vertex and box contributions begin to dominate the cross section value. However, such a situation occurs only for very small σ_{Ah} values, $\sigma_{Ah} \approx 10^{-3}$ fb, below the expected experimental ILC sensitivities.

Comparing the one-loop and two-loop results an uncertainty larger than $\sim 5\%$ can be attributed to the theory evaluation of the production cross sections. Another type of possibly large corrections in the MSSM are the so-called Sudakov logs (see Ref. [164] and references therein). They appear in the form of $\log(q^2/M_{\mathrm{SUSY}}^2)$ (where q is the momentum transfer) in the production cross sections of SUSY particles at $e^+ e^-$ colliders. In order to reach the required level of accuracy of 1-2% further two-loop corrections as well as the corresponding Sudakov logs will have to be calculated.

4.4 Double Higgs production processes at one-loop order

Full electroweak radiative corrections to the double Higgs-strahlung $e^+ e^- \to ZHH$ has been calculated in Refs. [80,165]. The two results are in good agreement, within 0.1%, for $\sqrt{s} \lesssim 800$ GeV for $m_H = 115, 150, 200$ GeV. In Ref. [80], the computation is performed with the help of `GRACE-loop`.

It has been shown that the QED corrections are large especially around the threshold, so that a proper resummation of the initial state radiation needs to be performed in this case. At energies where the cross section can be substantial, however, the corrections are modest, especially for a Higgs boson mass of $M_H \simeq 120$ GeV. The genuine weak corrections near the peak of the cross sections are also not large, not exceeding $\sim 5\%$, and therefore are below the expected experimental
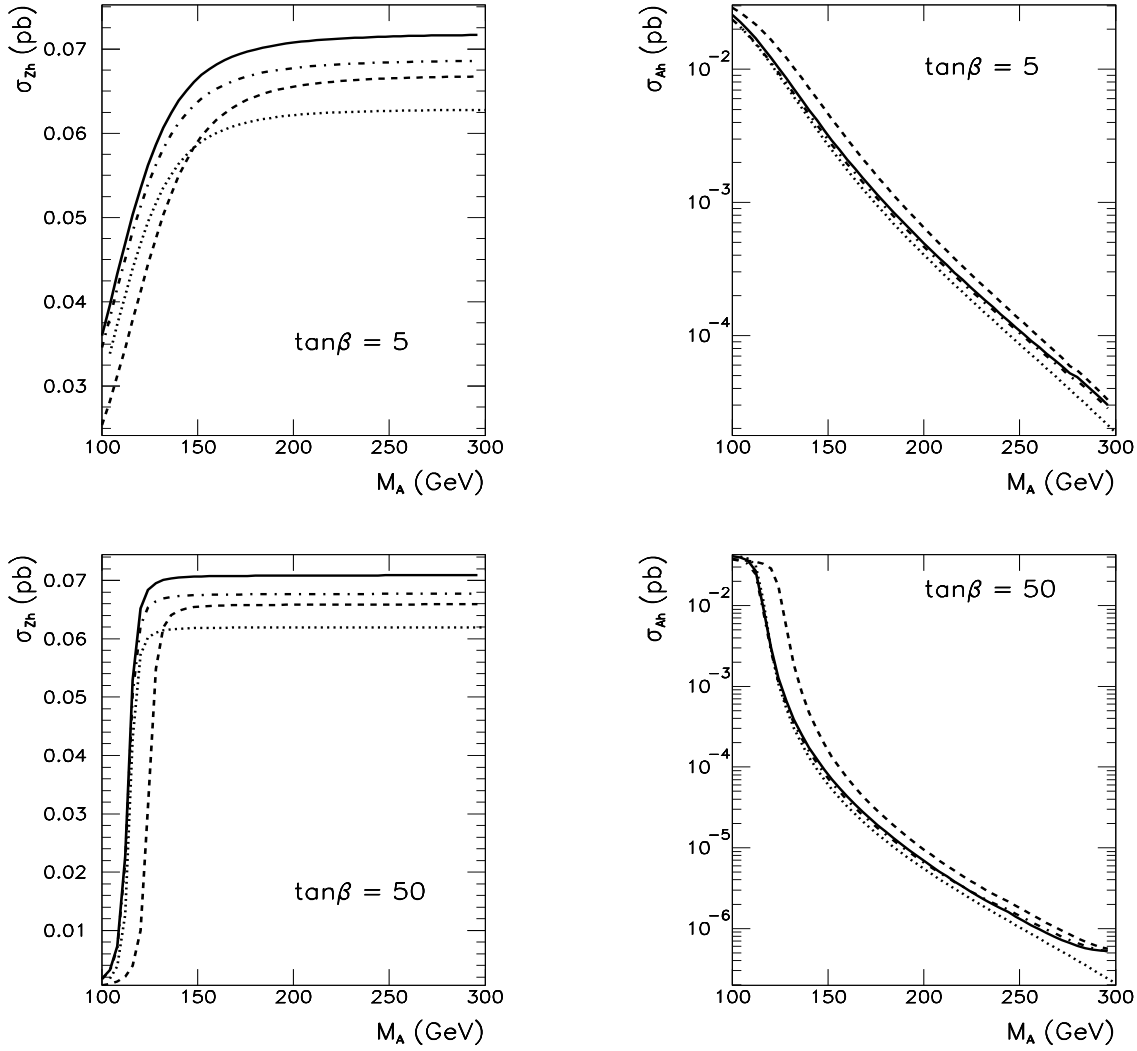
Figure 4.4: σ_{Zh} and σ_{Ah} as a function of M_A at $\sqrt{s} = 500$ GeV, shown for $\tan\beta = 5$ and $\tan\beta = 50$, in the no-mixing scenario (see text), as evaluated with `FeynHiggsXS`. The solid (dot-dashed) line represents the two-loop result including (excluding) box contributions, the dotted line shows an effective coupling approximation and the dashed line shows the one-loop result.

precision. As discussed in Ref. [77,78], the invariant mass M_{HH} distribution can be useful to extract the triple Higgs boson coupling. It is found that the genuine weak corrections, contrary to the QED corrections, hardly affect the shape of the distribution at least for energies where this distribution is to be exploited [80]: see Figure 4.5 and also Figure 3.8 (left). Therefore, an anomalous triple Higgs boson coupling could still be distinguished, if large enough, in this distribution provided that a proper inclusion of the initial QED corrections is allowed in the experimental simulation.

Recently, the corrections to the double Higgs production were also calculated in Ref. [166].
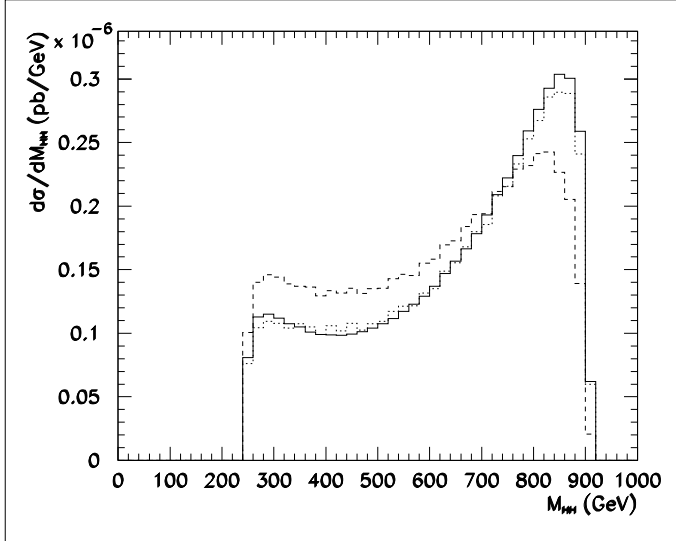
Figure 4.5: $d\sigma/dM_{HH}$ for $M_H = 120$ GeV at $\sqrt{s} = 1$ TeV. We show the tree-level (full curve), the effect of including only the genuine weak corrections (dotted curve) and the effect of including the full $\mathcal{O}(\alpha)$ corrections (dashed curve) [80].

4.5 Heavy MSSM Higgs bosons with CP violation at the $\gamma\gamma$ collider

The 2-doublet Higgs sector of the MSSM is automatically CP conserving at the tree level. However, CP violation can be induced by radiative corrections transmitting CP violating phases from the soft SUSY breaking Lagrangian to the Higgs system, in particular the relative phases between the higgsino mass parameter μ and the trilinear sfermion-Higgs parameters A_f. The Higgs system in 2-doublet models is generally described by a 3×3 complex mass matrix, composed of a real dissipative part and an imaginary absorptive part. The real dissipative part includes the parameters of the Higgs potential extended by loop corrections. The imaginary part includes the corresponding absorptive contributions of the loops, i.e., the widths in the diagonal elements.

CP asymmetries are naturally enhanced [167, 168] in the decoupling regime where $M_A \simeq M_H$. Near mass degeneracy of the scalar and pseudoscalar states in CP violating theories allows for frequent mutual transitions which induce large CP-odd mixing effects. In this limit the CP violation effects are located in the heavy Higgs sector and the light Higgs field can be ignored[1]. The mass matrix of the heavy Higgs sector can be reduced to a 2×2 form:

$$\mathcal{M}^2_{HA} = \begin{pmatrix} M_H^2 - iM_H\Gamma_H & \Delta^2_{HA} \\ \Delta^2_{HA} & M_A^2 - iM_A\Gamma_A \end{pmatrix} \tag{4.3}$$

The CP violation effects are encoded in Δ^2_{HA} connecting the scalar H and the pseudoscalar A fields through dissipative and absorptive contributions. Diagonalizing this mass matrix leads to the CP-mixed mass eigenstates H_2 and H_3. The rotation is described by the complex mixing parameter

$$X = \frac{1}{2}\tan 2\theta = \frac{\Delta^2_{HA}}{M_H^2 - M_A^2 - i[M_H\Gamma_H - M_A\Gamma_A]} \tag{4.4}$$

The shift in the masses and widths and the CP coupling of the states are quantitatively accounted for by the mixing parameter X:

$$\left[M_{H_3}^2 - iM_{H_3}\Gamma_{H_3}\right] \mp \left[M_{H_2}^2 - iM_{H_2}\Gamma_{H_2}\right] = \left\{\left[M_A^2 - iM_A\Gamma_A\right] \mp \left[M_H^2 - iM_H\Gamma_H\right]\right\} \begin{cases} \times \sqrt{1 + 4X^2} \\ \times \quad 1 \end{cases} \tag{4.5}$$

---

[1]In general, however, it would be desirable to include the full 3×3 mixing (with complex entries).

For a typical SUSY scenario,

$$M_{\text{SUSY}} = 0.5 \text{ TeV} \approx M_A, \quad |A_t| = 1.0 \text{ TeV}, \quad |\mu| = 1.0 \text{ TeV}, \quad \phi_\mu = 0; \quad \tan\beta = 5 \tag{4.6}$$

the mixing parameter X and the shifts of masses and widths are illustrated in Figs. 4.6(a), (b) and (c). ϕ_A denotes the CP-violating phase of A_t.
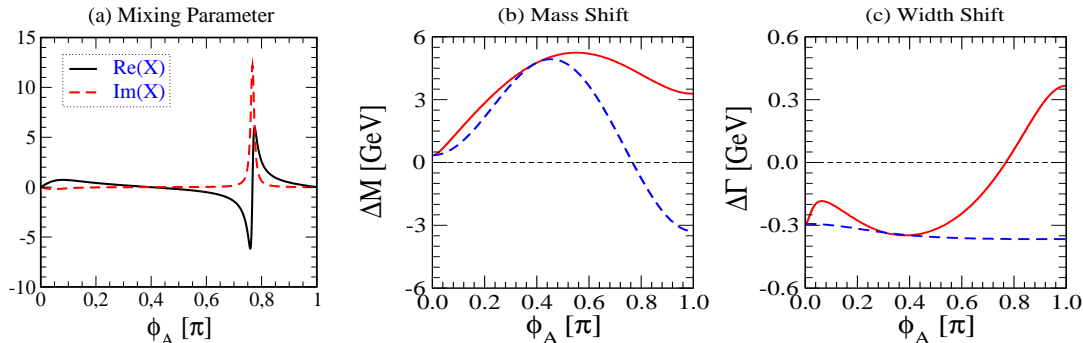
Figure 4.6: The dependence on the phase of A_t, ϕ_A, of (a) the mixing parameter X and of the shifts of (b) masses and (c) widths for the parameter set (4.6); in (b,c) the mass and width differences without mixing are shown by the broken lines. $\Re\mathrm{e}/\Im\mathrm{m}X(2\pi - \phi_A) = +\Re\mathrm{e}/-\Im\mathrm{m}X(\phi_A)$ for angles above π (taken from Ref. [167]).

Several asymmetries can be defined which reflect the presence of CP violating mixing effects either indirectly or directly. Direct CP violation can be studied in a classical way by measuring asymmetries of inclusive cross sections between left- and right-polarized photons [167]. At a photon collider, the circular polarization of laser photons is transferred completely to the high energy photons in Compton back-scattering of laser light near the maximum of the photon energy [8, 169, 170].

The CP violating asymmetry is defined by

$$A_{\text{hel}} = \frac{\sigma_{++} - \sigma_{--}}{\sigma_{++} + \sigma_{--}} , \tag{4.7}$$

where the subscripts denote the helicities of the two colliding photons. On top of the H_2, H_3 Higgs states the asymmetries are parameterized by the complex mixing parameter,

$$A_{\text{hel}}[H_2] \simeq \mathcal{A}_{\text{hel}}[H_3] \simeq \frac{2 \, \text{Im}(\cos\theta \sin\theta^*)}{|\cos\theta|^2 + |\sin\theta|^2} \tag{4.8}$$

in the asymptotic decoupling limit. Even though corrections due to non-asymptotic Higgs masses are still quite significant for the SUSY scenario introduced above, remarkably large asymmetries are predicted nevertheless in $\gamma\gamma$ fusion, shown in Fig. 4.7 as a function of the CP violating phase of the trilinear stop-Higgs coupling A_t.

Thus a photon collider provides an instrument that allows us to perform a unique classical experiment on CP violation in the Higgs sector of supersymmetric theories.

4.6 Charged Higgs Bosons

Charged Higgs bosons can be pair-produced at the ILC via $e^+e^- \to H^+H^-$ if $m_{H^\pm} < \sqrt{s}/2$ [171]. A complete simulation of this process for the decay $H^+ \to t\bar{b}$ has been performed for $\sqrt{s} = 800$
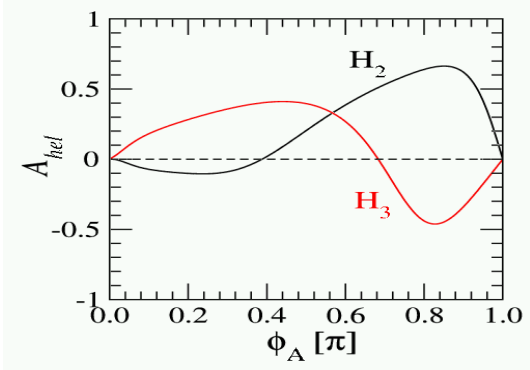
Figure 4.7: The ϕ_A dependence of the CP–violating asymmetry $\mathcal{A}_{\text{hel}}$ on top of the H_2, H_3 Higgs states, respectively.

GeV, 1 ab^{-1}, and $m_{H^\pm} = 300$ GeV [101]. The mass resolution is approximately 1.5%. A 5σ discovery will be possible for $m_{H^\pm} < 350$ GeV.

Since in pair production the mass reach for charged Higgs bosons is limited to $\sqrt{s}/2$, also the rare processes of single charged Higgs production may be considered. The dominant processes for single charged Higgs production are $e^+e^- \to b\bar{t}H^+, e^+e^- \to \tau^-\bar{\nu}_\tau H^+$, and $e^+e^- \to W^-H^+$. Their cross-sections have been calculated at leading order in Refs. [31,32]. Although the $H^\pm W^\mp$ production is a $2 \to 2$ process [33], the cross section is suppressed because of the absence of the tree level $H^\pm W^\mp Z$ coupling in multi Higgs doublet models. QCD corrections to $e^+e^- \to b\bar{t}H^+$ have recently become available [32] and are sizable. In general, parameter regions for which the production cross-section exceeds 0.1 fb are rather small for charged Higgs masses beyond the pair production threshold. Cross-section contours for $\sqrt{s} = 500$ GeV and 800 GeV are shown in Fig. 4.8.
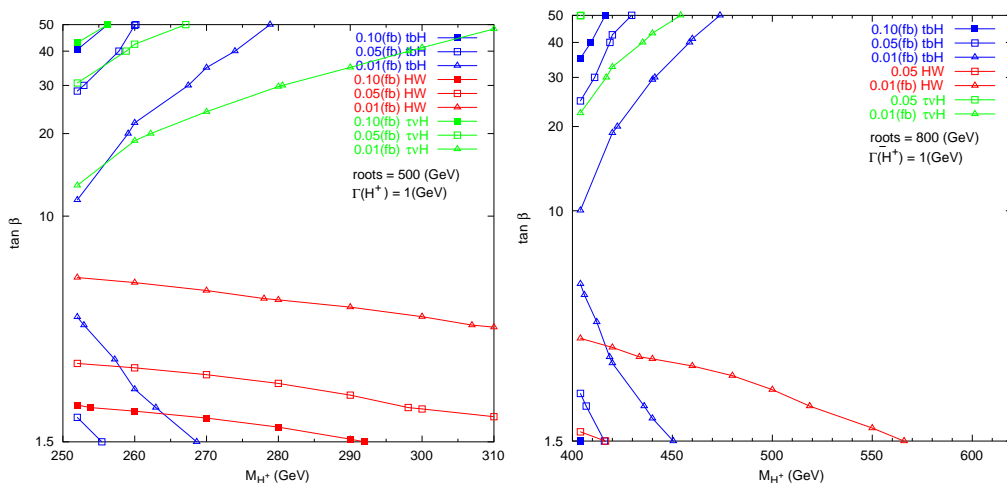
Figure 4.8: Cross-section contours for the processes $e^+e^- \to b\bar{t}H^+$ (blue/dark), $e^+e^- \to \tau^-\bar{\nu}_\tau H^+$ (green/light grey), and $e^+e^- \to W^-H^+$ (red/medium grey) at $\sqrt{s} = 500$ GeV (left) and at 800 GeV (right) [93].

At a $\gamma\gamma$ collider, production of a heavy charged Higgs boson is typically one order of magnitude larger than the production of the same final state at an e^+e^- collider with the same collision energy due to the t-channel nature. For $\sqrt{s}_{\gamma\gamma} > 2m_{H^\pm}$, pair production is dominant similarly to the electron-positron collision [171,172]. When the mass of the charged Higgs boson is larger than the threshold of pair production, single production processes become important. Cross sections of various single production processes have been calculated in Ref. [173]. Moreover, a polarized

$\gamma\gamma$ collider can determine the chirality of the Yukawa couplings of fermions with the charged Higgs boson via single charged Higgs boson production and, thus, discriminate models of new physics [174].

4.7 NMSSM

4.7.1 Overview

One attractive supersymmetric model is the Next to Minimal Supersymmetric Standard Model (NMSSM) [175, 176] which extends the MSSM by the introduction of just one singlet superfield, $\widehat{S}$, in addition to the Higgs up- and down-type superfields $\widehat{H}_u$ and $\widehat{H}_d$. [Hatted (unhatted) capital letters denote superfields (scalar superfield components).] When the scalar component of $\widehat{S}$ acquires a TeV scale vacuum expectation value (a very natural result in the context of the model), the superpotential term $\lambda \widehat{S}\widehat{H}_u\widehat{H}_d$ generates an effective $\mu\widehat{H}_u\widehat{H}_d$ interaction for the Higgs doublet superfields with $\mu \equiv \mu_{\text{eff}} = \lambda\langle S\rangle \equiv \lambda s$. Such a term is essential for acceptable phenomenology. No other SUSY model generates this crucial component of the superpotential in as natural a fashion. At the same time, the NMSSM preserves all the most attractive features of the MSSM. First, since the NMSSM introduces only an additional singlet superfield, the $SU(3)$, $SU(2)_L$ and $U(1)$ coupling constants continue to unify at the unification scale, $M_U \sim$ few $\times 10^{16}$ GeV, just as in the MSSM. Further, radiative electroweak symmetry breaking remains a natural possibility within the NMSSM. The electroweak symmetry breaking generates non-zero vevs for all the Higgs fields, $\langle H_u\rangle = h_u$, $\langle H_d\rangle = h_d$ and $\langle S\rangle = s$. A possible cosmological domain wall problem [177] can be avoided by introducing suitable non-renormalizable operators [178] that do not generate dangerously large singlet tadpole diagrams [179]. Alternatively, it has been argued that the domain walls are themselves the source of dark energy [180].

The trilinear term in the Higgs potential reads

$$\lambda A_\lambda S H_u H_d + \frac{\kappa}{3} A_\kappa S^3 \,. \tag{4.9}$$

Aside from λ, κ, μ_{eff}, A_κ and A_λ, the final Higgs sector parameter is $\tan\beta = h_u/h_d$. Thus, as compared to the three independent parameters needed in the MSSM context (often chosen as μ, $\tan\beta$ and m_A), the Higgs sector of the NMSSM is described by the six parameters

$$\lambda \,,\; \kappa \,,\; A_\lambda \,,\; A_\kappa,\; \tan\beta \,,\; \mu_{\text{eff}} \,. \tag{4.10}$$

A possible sign convention [181] is such that λ and $\tan\beta$ are positive, while κ, A_λ, A_κ and μ_{eff} should be allowed to have either sign.

The particle content of the NMSSM differs from the MSSM by the addition of one CP-even and one CP-odd state in the neutral Higgs sector (assuming CP conservation), and one additional neutralino. Altogether, in the Higgs sector we have the CP-even Higgs bosons h_1, h_2, h_3, the CP-odd Higgs bosons a_1, a_2 and the usual charged Higgs pair $H^\pm$. The five neutralinos ($\widetilde{\chi}^0_{1,2,3,4,5}$) are typically mixtures of the gauginos, higgsinos and the singlino. In some limits, the singlino can be a fairly pure state and it can either be the heaviest or the lightest of the neutralinos.

4.7.2 The Higgs boson mass spectrum

The mass of the lightest CP-even Higgs boson at the tree-level is given by

$$m_{h,\text{tree}}^2 \le M_Z^2 \left(\cos^2 2\beta + \frac{2\,\lambda^2}{g^2 + g'^2}\sin^2 2\beta\right) \,, \tag{4.11}$$

where λ should be below $\lambda \lesssim 0.7$ to remain perturbative up to the GUT scale. The evaluation of higher-order corrections to Higgs boson masses and mixing angles is less advanced than in the MSSM. No full one-loop calculation is available so far although there has been much work [182–187]. Most recently the leading two-loop Yukawa corrections have become available [188]. All available corrections have been implemented into the code `NMHDECAY` [181]. No genuine higher-order corrections to Higgs boson production and decay are available. However, in many cases (especially if the new singlet mass scale is large) the results from the MSSM can be taken over to the NMSSM case.

An important issue for NMSSM Higgs phenomenology is the mass and nature of the lightest CP-even and CP-odd Higgs bosons. In particular, if the a_1 is very light or even just moderately light there are dramatic modifications in the phenomenology of Higgs discovery at both the LHC and ILC [121, 181, 187, 189–194]. A light a_1 is natural in the context of the model, see Ref. [121] for a discussion. A very light a_1 is experimentally not ruled out, especially if it has a large singlet component. In some regions of the NMSSM parameter space, one can also get the lightest CP-even state, h_1, to be very light as well.

Another interesting feature of the NMSSM is that the standard measure of fine-tuning

$$F = \text{Max}_p F_p \equiv \text{Max}_p \left| \frac{d \log M_Z}{d \log p} \right|, \tag{4.12}$$

where the parameters p comprise all GUT-scale soft-SUSY-breaking parameters, can be very low for Higgs boson mass values above the LEP limit [122, 176, 195, 196].

4.7.3 LEP Higgs searches

Within the NMSSM it is also possible to have a Higgs boson with a mass below the LEP limits [122]. It escapes LEP constraints by virtue of having unusual decay modes for which LEP limits are weaker. In particular, parameters for which $h_1 \to a_1 a_1$ decays are dominant over $h_1 \to b\bar{b}$ decays must be carefully considered[2]. Particular care is required if there is a mixture of $h_1 \to a_1 a_1$ and $h_1 \to b\bar{b}$ decays, and the dominant a_1 decay is to $b\bar{b}$. In this situation, the single channel $Z2b$ and $Z4b$ rate limits from LEP are less sensitive than the combination of both channels, since in the $Z2b$ interpretation the $Z4b$ final state is ignored, and vice versa, which leads to a loss in sensitivity compared with the full combination.

This has particular relevance to the NMSSM scenarios with the very lowest fine-tuning, $F < 10$, as examined in Ref. [199]. Two types of scenarios emerge for $F < 10$. In both, $\text{BR}(h_1 \to b\bar{b}) \sim 0.1 \div 0.2$ and $\text{BR}(h_1 \to a_1 a_1) \sim 0.85 \div 0.75$. In scenarios of type I (II), $m_{a_1} > 2m_b$ ($m_{a_1} < 2m_b$) and $\text{BR}(a_1 \to b\bar{b}) \sim 0.92$ (0). More details can be found in Refs. [198, 199]. It has been found that the only $F < 10$ scenarios consistent with the full LEP Higgs Working Group (LHWG) analysis are of type II. Type I scenarios are typically excluded at about the $98 \div 99\%$ CL after data from all experiments are combined.

A very important feature of the type-II $F < 10$ scenarios is that a significant fraction of them can easily explain the well-known excess in the $Zh \to Zb\bar{b}$ final state in the vicinity of $m_h \sim 100$ GeV. This is illustrated in Fig. 4.9 [199], where all $F < 10$ NMSSM parameter choices (from a lengthy scan) with $m_{a_1} < 2m_b$ are shown to predict $m_{h_1} \sim 96 \div 105$ GeV along with a $C_{\text{eff}} = [g_{ZZh}^2/g_{ZZh_{\text{SM}}}^2]\text{BR}(h \to b\bar{b})$ that would explain the observed excess with respect to the expected limit. The statistical significance of this excess is of order 2σ. The properties of the four most ideal points for describing the excess are given in Table 4.1. Note that for point 3, $m_{a_1} < 2m_\tau$

---

[2]This is also possible in the MSSM [197]; corresponding holes from the LEP Higgs searches in the MSSM parameter planes exist [198].

implying that $a_1 \rightarrow$ quarks and gluons. A general feature with $F < 10$ is that they predict the Higgs boson properties needed to describe the LEP $Zh \rightarrow Z + b$'s excess. Another possibility, occuring at higher F values, is that the h_1 has a ZZh_1 coupling that is reduced in strength relative to the SM ZZ-Higgs coupling. This can give rise to other scenarios with light Higgs bosons that are consistent with the LHWG limits on the $Z + b$'s final state.
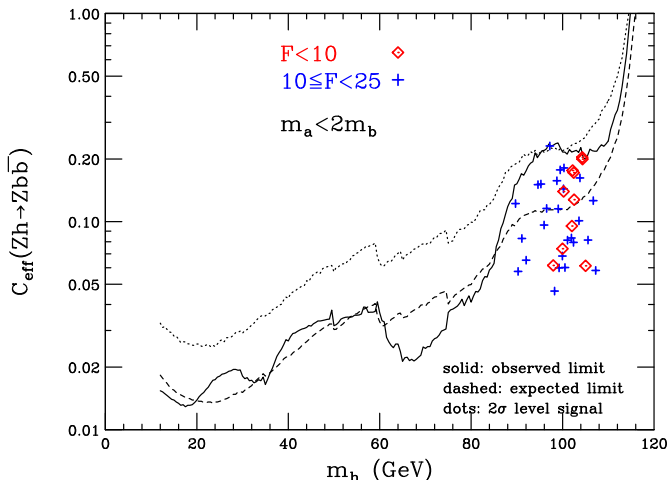
Figure 4.9: Expected and observed 95% CL limits on $C_{\text{eff}} = [g_{ZZh}^2/g_{ZZh_{\text{SM}}}^2]\text{BR}(h \rightarrow b\bar{b})$ from Ref. [4] are shown vs. m_h. Also plotted are the predictions for NMSSM parameter choices in our scan that give fine-tuning measure $F < 25$ and $m_{a_1} < 2m_b$ with fixed $\tan\beta = 10$ and gaugino masses of $M_{1,2,3}(M_Z) = 100, 200, 300$ GeV. [199]

| m_{h_1} | m_{a_1} | Branching Ratios | | | $N_{\text{SD}}^{\text{max}}$ |
(GeV)	(GeV)	$h_1 \rightarrow b\bar{b}$	$h_1 \rightarrow a_1 a_1$	$a_1 \rightarrow \tau^+\tau^-$	300 fb^{-1}
102.4	9.0	0.173	0.793	0.875	3.6
102.5	5.4	0.128	0.848	0.938	2.4
100.2	3.1	0.141	0.832	0.0	2.5
102.2	3.6	0.177	0.789	0.814	3.3

Table 4.1: Some properties of the h_1 and a_1 for four points with $F < 10$ and $m_{a_1} < 2m_b$ from a $\tan\beta = 10$, $M_{1,2,3}(M_Z) = 100, 200, 300$ GeV NMSSM scan. $N_{\text{SD}}^{\text{max}}(300$ fb$^{-1})$ is the statistical significance of the best "standard" LHC Higgs detection channel after accumulating integrated luminosity of $L = 300$ fb^{-1}.

4.7.4 ILC measurements

In this section we analyze the implications for the ILC of an NMSSM scenario in which there is a Higgs with fairly SM-like couplings, but that decays to two lighter Higgs bosons, emphasizing the most probable case of $h \rightarrow aa$ and m_h near 100 GeV.

To set the stage for the ILC, an important question is the extent to which the type of $h \rightarrow aa$ Higgs scenario (whether NMSSM or other) described here can be explored at the Tevatron and the LHC. This has been examined in the case of the NMSSM in [189–192, 194], with the conclusion that observation of any of the NMSSM Higgs bosons may be very difficult at hadron colliders if the decay mode $h_1 \rightarrow a_1 a_1$ is dominant. For example, the largest statistical significance in any of the "standard" search channels at the LHC, given in the last column of Table 4.1 for the four sample type-II scenario points, is below 5σ even after $L = 300$ fb^{-1} of integrated luminosity is accumulated. In this case, if any signals are observed at the Tevatron or LHC, it seems very possible that they will be quite tenuous, perhaps difficult to interpret, and possibly of quite low

statistical significance. In such a circumstance, the ILC becomes essential. It is the ideal machine for detecting a $m_h \sim 100$ GeV Higgs boson with unusual decays. One simply employs the search channel of inclusive $e^+e^- \to Z^* \to Zh \to \ell^+\ell^- X$ in which M_X is computed from the incoming and outgoing lepton information. An unmistakable peak in M_X is predicted, and it is completely independent of the h decay mode. Detection of $\gamma\gamma \to h \to aa$ is also predicted to be completely straightforward (regardless of the dominant a decay mode) at the $\gamma\gamma$ collider facility that will probably accompany the ILC [200]. Typical signal and background plots are shown in Ref. [200] assuming that the $\gamma\gamma$ collider is operated at an electron beam energy of 75 GeV and with laser and electron polarizations chosen to produce the general purpose broad spectrum in $E_{\gamma\gamma}$.

It should be noted that much of the discussion above regarding Higgs discovery is quite generic. Whether the a is truly the NMSSM CP-odd a_1 or just a lighter Higgs boson into which the SM-like h pair-decays, hadron collider detection of the h in its $h \to aa$ decay mode will be very challenging — only the ILC can currently guarantee its discovery.

4.7.5 Open questions

As mentioned above, the NMSSM studies are in general less advanced than the corresponding MSSM studies. The following open questions should be answered so that the ILC results can be fully exploited in the context of the NMSSM:

- Calculations for the Higgs masses, mixing angles and couplings have to be refined to reach the required level of accuracy. This task is similar to the MSSM case, where, however, already more precise calculations exist. Also the renormalization in the NMSSM Higgs sector is less advanced than in the MSSM. More precise calculations are also needed for the NMSSM Higgs boson production cross sections and branching ratios.

- In the important low fine-tuning case that $h_1 \to a_1 a_1$ with $a_1 \to \tau^+\tau^-$ is dominant, excellent τ-tagging capabilities at the ILC are necessary. Further experimental studies are needed. In a more general case where $h_1 \to a_1 a_1$ and $a_1 \to b\bar{b}$, excellent b-tagging capabilities would be crucial. This includes the distinction between b and $\bar{b}$ in order to reduce the number of b-jet combinations in multi-b final states.

- As in the MSSM, also in the NMSSM the lightest neutralino is a good candidate for cold dark matter, see e.g. [201, 202] and references therein. It is possible that Higgs physics plays an important role here if the LSPs annihilate via a Higgs boson to SM particles. More precise calculations for the Higgs boson couplings are necessary to reach the required precision. More experimental efforts have to be undertaken to extract the corresponding Higgs boson masses and widths with the required accuracies. This is discussed further in Sect. 7. There, the difficult scenario of annihilation of the lightest neutralino via a rather light singlet-like CP-odd Higgs boson (as possible in the low-F NMSSM scenarios) is discussed.

- There are other, non-Higgs-sector-related issues. These comprise the question of baryogenesis within the NMSSM, the investigation of the LSP quantities at the ILC, and the determination of neutralino sector observables in order to reconstruct all corresponding fundamental parameters.

4.8 Gauge Extensions of the MSSM

Another way to increase the mass of the lightest SUSY Higgs boson can arise from theories with extended gauge interactions. If the Higgs is charged under one or more of the new gauge groups,

there are additional D-term contributions to its quartic term in the Higgs potential, and thus the light CP even Higgs may be considerably heavier than the tree-level MSSM expectation. Early efforts in this direction included additional $U(1)$ gauge groups [203]. These are effective, but the possibility of large Higgs masses is limited if one requires perturbativity up to the grand unification scale. More recently, non-Abelian gauge groups which are asymptotically free have appeared which allow for large Higgs masses, but whose interactions are free from Landau poles to arbitrarily high scales [204, 205].

A simple example is provided by supersymmetric topflavor, which has gauge structure $SU(3)_C \times SU(2)_1 \times SU(2)_2 \times U(1)_Y$. The MSSM Higgses and the third family are charged under $SU(2)_1$ whereas the first two generations are charged under $SU(2)_2$. Precision EW constraints require the masses of the extra gauge bosons to be greater than a few TeV. The Higgs mass at tree level may be expressed as,

$$m_{h^0}^2 \leq \frac{1}{2}\left(g^2\Delta + g_Y^2\right)v^2\cos^2\beta \tag{4.13}$$

where g and g_Y are the usual MSSM $SU(2)_L$ and $U(1)_Y$ gauge couplings, and Δ parameterizes the new contribution from the extended $SU(2)$ structure,

$$\Delta \equiv \frac{1 + \frac{2m^2}{u^2}\frac{1}{g_2^2}}{1 + \frac{2m^2}{u^2}\frac{1}{g_1^2+g_2^2}} \tag{4.14}$$

where m^2 is a soft mass for the Higgs which breaks $SU(2)_1 \times SU(2)_2 \to SU(2)_L$, u is the breaking scale, and g_1 and g_2 are the underlying $SU(2)$ couplings, satisfying $1/g_1^2 + 1/g_2^2 = 1/g_L^2$. Tree level Higgs masses on the order of 350 GeV are relatively easy to obtain in this model, which clearly evades the LEP bounds [4]. This motivates studies of heavier (SM-like) Higgs bosons, see Sect. 3.6.

The model contains the extra Z' and W's from the broken extended gauge symmetry. These couple more strongly to the third family than to the first two and the W' is expected to be discovered at the LHC if this model is realized in nature [206]. The ILC could further potentially pin down the model and its parameters by indirectly measuring the properties of the Z', and studying the neutralino and chargino sectors, which now include the partners of these new gauge bosons as well as the usual MSSM components. Detailed studies of the branching ratios, production cross sections, etc., would be interesting to pursue.

The presence of extra asymptotically free gauge interactions may also result in an interesting modification of the NMSSM. The new strong gauge interactions may drive the coupling λ small at high energies, effectively removing the perturbative unification bound on the value of λ (see Sect. 4.7.2), and realizing an otherwise theoretically unmotivated region of parameter space [207]. A sample Higgs spectrum (at one loop) is presented in Figure 4.10, and shows several interesting features including a rather heavy set of CP even fields, and a charged scalar as the lightest of all of the Higgses.

4.9 Fat Higgs Models

A final possibility is to interpret the strongly coupled NMSSM as composite theory which confines at the strong coupling scale [208–210]. The original Fat Higgs [208] introduces an additional $SU(2)$ interaction and a number of *preons* charged under it. At an intermediate scale, Λ, the $SU(2)$ theory confines, forming a singlet superfield S and Higgs-like superfields H and $\bar{H}$ which play the role of the two MSSM Higgses. There is a dynamical super-potential induced of the form,

$$W_{dyn} = \lambda S\left(H\bar{H} - v_0^2\right) \tag{4.15}$$
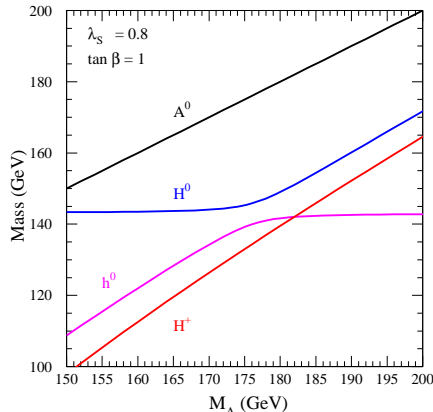
Figure 4.10: Higgs spectrum in an NMSSM-like model with large λ [207].

where naive dimensional analysis predicts $\lambda \sim 4\pi$ at the confinement scale, and $v_0^2 \sim m\Lambda/4\pi$ is related to the mass of the pair of underlying preon fields (m) which bind into S. The mass parameter m is ultimately what determines the electroweak scale.

Notably different from the NMSSM, the contribution to the Higgs quartic λ is much larger because the effective cut-off is much lower than the unification scale[3]. In addition, the electroweak symmetry is broken even in the supersymmetric limit. Higgs spectra similar to those expected from the gauge extensions with large λ result, with similar phenomenology quite distinct from the MSSM and usual NMSSM; see Figure 4.10 for an example.

Variations of the original Fat Higgs either restrict the composite sector to include only the gauge singlet [209] or generate the top quark from the strong dynamics as well as the Higgses [210], motivating the fact that the top mass is much larger than any of the other fermions by postulting that the large top Yukawa interaction is a residual of the force that bound a set of preons into both top and Higgs.

4.10 The Significance of $\tan\beta$ in Two-Higgs-Doublet Models

There are a number of discussions in this report about the measurement of the parameter $\tan\beta$ at the ILC. A precise theoretical understanding of the significance of this parameter is important. Recent progress in this direction is reviewed.

4.10.1 $\tan\beta$ as an (un)physical parameter

In the two-Higgs-doublet model (2HDM), the Higgs sector of the Standard Model is extended to include two complex hypercharge-one Higgs doublets [25, 211]. After the breaking of electroweak symmetry (preserving the electromagnetic U(1)$_{\mathrm{EM}}$ symmetry group), the Higgs fields' vacuum expectation values (vevs) can be chosen to take the following form:

$$\langle\Phi_1\rangle = \frac{1}{\sqrt{2}}\begin{pmatrix} 0 \\ v_1 \end{pmatrix}, \qquad \langle\Phi_2\rangle = \frac{1}{\sqrt{2}}\begin{pmatrix} 0 \\ v_2 e^{i\xi} \end{pmatrix}, \tag{4.16}$$

---

[3]Unification of the MSSM gauge couplings remains possible (and calculable, despite the strong dynamics) provided some addtional matter is included to arrange for the unification.

where $0 \leq \xi < 2\pi$ and the v_i are real and positive and normalized such that $v^2 \equiv v_1^2 + v_2^2 = 4m_W^2/g^2 = (246 \text{ GeV})^2$. In addition, the ratio of the magnitudes of the two vevs is denoted by $\tan\beta \equiv v_2/v_1$, where $0 \leq \beta \leq \pi/2$.

The relative phase ξ is clearly not a physical parameter of the model, since one is free to rephase the Φ_2 field to absorb this phase. Perhaps more surprisingly, $\tan\beta$ is also not generally a physical parameter. Since the two Higgs fields Φ_1 and Φ_2 possess identical gauge quantum numbers, one is free to redefine the scalar fields via an arbitrary U(2) transformation [212, 213], $\Phi_i \to U_{ij}\Phi_j$. Different choices of the unitary matrix U correspond to different basis choices for the scalar fields. Physical predictions of the model must, of course, be basis independent.

If $\tan\beta$ is not a physical parameter, what is the meaning of $\tan\beta$ that appears so often in this report? In fact, $\tan\beta$ can be promoted to a physical parameter by imposing some restrictions on possible terms that appear in the 2HDM Lagrangian. For example, by imposing supersymmetry on the model, the two Higgs fields Φ_1 and Φ_2 are distinguishable in a particular basis, and this basis provides a physical definition of $\tan\beta$. However, if phenomena consistent with a two-Higgs-doublet sector are observed, it may not be immediately obvious what theoretical constraints govern the underlying 2HDM. Thus, in order to carry out a truly model-independent study of 2HDM phenomena, one cannot employ $\tan\beta$ as defined below eq. (4.16).

Here we consider the most general 2HDM. One natural basis choice that exists is the so-called Higgs basis [213–218], consisting of the scalar fields Φ_a and Φ_b, in which only one of the neutral Higgs fields (which by convention will be denoted by Φ_a^0) has a non-zero vacuum expectation value. This basis choice is not unique, since one is always free to independently rephase the individual Higgs fields. One linear combination of these two rephasing transformations (corresponding to $\Phi_a \to e^{i\psi}\Phi_a$, $\Phi_b \to e^{i\psi}\Phi_b$) is the global hypercharge transformation U(1)$_Y$. This transformation does not modify any of the scalar potential parameters. However, we shall employ it simply to remove the phase from the vacuum expectation value of Φ_a^0. In this convention, the Higgs basis is parameterized by one angle χ:

$$\Phi_a = \Phi_1 \cos\beta + e^{-i\xi}\Phi_2 \sin\beta, \tag{4.17}$$

$$e^{i\chi}\Phi_b = -e^{i\xi}\Phi_1 \sin\beta + \Phi_2 \cos\beta. \tag{4.18}$$

One then obtains

$$\Phi_a = \begin{pmatrix} G^+ \\ \frac{1}{\sqrt{2}}(v + \varphi_1^0 + iG^0) \end{pmatrix}, \qquad e^{i\chi}\Phi_b = \begin{pmatrix} H^+ \\ \frac{1}{\sqrt{2}}(\varphi_2^0 + iA) \end{pmatrix}. \tag{4.19}$$

Indeed only Φ_a^0 develops a vacuum expectation value, which by convention is chosen to be real and positive. Of the original eight scalar degrees of freedom, three Goldstone bosons ($G^\pm$ and G^0) are absorbed ("eaten") by the $W^\pm$ and Z. In eq. (4.19), φ_1^0, φ_2^0 are CP-even neutral Higgs fields, A is a CP-odd neutral Higgs field, and $H^\pm$ is the physical charged Higgs boson pair. If CP is conserved, then A is the physical CP-odd Higgs scalar and φ_1^0 and φ_2^0 mix to produce two physical neutral CP-even Higgs states h and H. If the Higgs sector is CP-violating, then φ_1^0, φ_2^0, and A all mix to produce three physical neutral Higgs states of mixed CP properties.

In the Higgs basis, the scalar potential takes the following form:

$$\begin{aligned}
\mathcal{V} = {}& M_{11}^2 \Phi_a^\dagger \Phi_a + M_{22}^2 \Phi_b^\dagger \Phi_b - [M_{12}^2\, e^{i\chi}\Phi_a^\dagger \Phi_b + \text{h.c.}] \\
& + \frac{1}{2}\Lambda_1(\Phi_a^\dagger\Phi_a)^2 + \frac{1}{2}\Lambda_2(\Phi_b^\dagger\Phi_b)^2 + \Lambda_3(\Phi_a^\dagger\Phi_a)(\Phi_b^\dagger\Phi_b) + \Lambda_4(\Phi_a^\dagger\Phi_b)(\Phi_b^\dagger\Phi_a) \\
& + \left\{ \frac{1}{2}\Lambda_5\, e^{2i\chi}(\Phi_a^\dagger\Phi_b)^2 + [\Lambda_6\, e^{i\chi}(\Phi_a^\dagger\Phi_a) + \Lambda_7\, e^{i\chi}(\Phi_b^\dagger\Phi_b)]\Phi_a^\dagger\Phi_b + \text{h.c.} \right\},
\end{aligned} \tag{4.20}$$

M_{11}^2 and M_{12}^2 are fixed by the scalar potential minimum conditions, and M_{22}^2 is directly related to the physical charged Higgs boson squared-mass:

$$m_{H^\pm}^2 = M_{22}^2 + \frac{1}{2}v^2\Lambda_3\,. \tag{4.21}$$

The conditions for CP-invariance of the Higgs sector are very simple. The 2HDM is CP-conserving if and only if the Higgs basis scalar potential parameters satisfy [213, 217]

$$\text{Im}\,(\Lambda_5^*\Lambda_6^2) = \text{Im}\,(\Lambda_5^*\Lambda_7^2) = \text{Im}\,(\Lambda_6^*\Lambda_7) = 0\,. \tag{4.22}$$

If eq. (4.22) is satisfied, then there exists a choice of χ such that all the Higgs basis scalar potential parameters are simultaneously real [219–221]. By working in the Higgs basis, it is clear that $\tan\beta$ never appears. Thus, the couplings of the Higgs bosons to the vector bosons and the Higgs self-couplings can depend only on the scalar potential parameters (in the Higgs basis), the gauge couplings and the mixing angles that determine the neutral Higgs boson mass eigenstates in terms of φ_1^0, φ_2^0 and A.

In practice, the parameter $\tan\beta$ is most often associated with the Higgs-fermion Yukawa couplings. Thus, we now focus on the coupling of the 2HDM to three generations of quarks and leptons. The Higgs couplings to fermions are model dependent. The most general structure for the 2HDM Higgs-quark Yukawa couplings, often referred to as the type-III model [222], is given in the Higgs basis by (with an analogous form for the Higgs-lepton Yukawa couplings):

$$-\mathcal{L}_Y = \overline{Q}_L^0 \widetilde{\Phi}_a \kappa^{U,0} U_R^0 + \overline{Q}_L^0 \Phi_a \kappa^{D,0} D_R^0 + \overline{Q}_L^0 \widetilde{\Phi}_b \rho^{U,0} U_R^0 + \overline{Q}_L^0 \Phi_b \rho^{D,0} D_R^0 + \text{h.c.}\,, \tag{4.23}$$

where $\widetilde{\Phi} \equiv i\sigma_2\Phi^*$, Q_L^0 is the weak isospin quark doublet, and U_R^0, D_R^0 are weak isospin quark singlets. $\kappa^{Q,0}$ and $\rho^{Q,0}$ ($Q = U$, D) are Yukawa coupling matrices in quark flavor space.

The fermion mass eigenstates are related to the interaction eigenstates by the following unitary transformations:

$$U_L = V_L^U U_L^0\,, \qquad U_R = V_R^U U_R^0\,, \qquad D_L = V_L^D D_L^0\,, \qquad D_R = V_R^D D_R^0\,, \tag{4.24}$$

and the Cabibbo-Kobayashi-Maskawa matrix is defined as $K \equiv V_L^U V_L^{D\,\dagger}$. It is also convenient to define "rotated" linear combinations of the Yukawa coupling matrices:

$$\kappa^U \equiv V_L^U \kappa^{U,0} V_R^{U\,\dagger}\,, \qquad \rho^U \equiv V_L^U \rho^{U,0} V_R^{U\,\dagger}\,, \qquad \kappa^D \equiv V_L^D \kappa^{D,0} V_R^{D\,\dagger}\,, \qquad \rho^D \equiv V_L^D \rho^{D,0} V_R^{D\,\dagger}\,. \tag{4.25}$$

The quark mass terms are identified by replacing the scalar fields with their vacuum expectation values. The unitary matrices V_L^U, V_L^D, V_R^U and V_R^D are chosen so that κ^D and κ^U are diagonal with real non-negative entries. These quantities are proportional to the *diagonal* quark mass matrices:

$$M_D = \frac{v}{\sqrt{2}}\kappa^D\,, \qquad M_U = \frac{v}{\sqrt{2}}\kappa^U\,. \tag{4.26}$$

However, the matrices ρ^D and ρ^U are *complex* non-diagonal matrices, which are not constrained in a general model.

The Higgs-fermion interaction, expressed in terms of quark mass eigenstates, takes the following form [211, 213, 223]:

$$-\mathcal{L}_Y = \frac{1}{v}\overline{D}M_D D\varphi_1^0 + \frac{1}{\sqrt{2}}\overline{D}(\rho^D P_R + \rho^{D\dagger} P_L)D\varphi_2^0 + \frac{i}{\sqrt{2}}\overline{D}(\rho^D P_R - \rho^{D\dagger} P_L)DA + \frac{i}{v}\overline{D}M_D\gamma_5 DG^0$$

$$+ \frac{1}{v}\overline{U}M_U U\varphi_1^0 + \frac{1}{\sqrt{2}}\overline{U}(\rho^U P_R + \rho^{U\dagger} P_L)U\varphi_2^0 - \frac{i}{\sqrt{2}}\overline{U}(\rho^U P_R - \rho^{U\dagger} P_L)UA - \frac{i}{v}\overline{U}M_D\gamma_5 UG^0$$

$$+ \left\{\overline{U}\left[K\rho^D P_R - \rho^{U\dagger} KP_L\right]DH^+ + \frac{\sqrt{2}}{v}\overline{U}\left[KM_D P_R - M_U KP_L\right]DG^+ + \text{h.c.}\right\}\,, \tag{4.27}$$

where $P_{R,L} = \frac{1}{2}(1 \pm \gamma_5)$. The physical couplings of the quarks to the Higgs fields are then obtained by expressing φ_1^0, φ_2^0 and A in terms of the neutral Higgs mass eigenstates. Once again, the parameter $\tan\beta$ does not appear.

The most general 2HDM is phenomenologically untenable over most of its parameter space. In particular, since ρ^D and ρ^U are non-diagonal, eq. (4.27) [even when expressed in terms of the neutral Higgs mass eigenstates] exhibits tree-level Higgs-mediated flavor changing neutral currents (FCNCs). One way to avoid this problem is to go the region of parameter space where M_{22}^2 is very large (or equivalently $m_{H^\pm} \ll m_Z$). In this *decoupling limit*, the second doublet Φ_2 is very heavy and decouples from the effective low-energy theory. To a very good approximation, φ_1^0 is a CP-even Higgs mass eigenstate with couplings nearly indistinguishable from those of the Standard Model Higgs boson [224, 225]. In particular, tree-level Higgs-mediated FCNCs are suppressed, and the corresponding 2HDM is phenomenologically viable (at the expense of the fine-tuning necessary to guarantee that the second Higgs doublet is very heavy).

The more common procedure for avoiding FCNCs is to impose a symmetry on the theory in order to restrict the form of the Higgs-fermion interactions in a particular basis [226]. This procedure then establishes the *symmetry basis*. If the scalar fields of the symmetry basis are denoted by Φ_1 and Φ_2, whose relation to the Higgs basis is given by eqs. (4.17) – (4.18), then the parameter $\tan\beta$ is promoted to a physical parameter of the theory. For example, a discrete symmetry can be imposed such that Φ_2 decouples from the fermions in the symmetry basis. This yields the so-called type-I Higgs-fermion couplings [227, 228]. Another discrete symmetry can be found in which down-type right-handed fermions couple exclusively to Φ_1 and up-type right-handed fermions couple exclusively to Φ_2. This yields the so-called type-II Higgs-fermion couplings [215, 228]. As a final example, the MSSM also exhibits type-II Higgs-fermion couplings [229].

For simplicity, consider a *one-generation* type-II CP-conserving model. It is straightforward to show that the Higgs basis Yukawa couplings satisfy the following equation [213]:

$$\kappa^U \kappa^D + \rho^U \rho^D = 0 \,. \tag{4.28}$$

Moreover, one can compute $\tan\beta$ (where β is the relative orientation of the Higgs basis and the symmetry basis):

$$\tan\beta = \frac{-\rho^D}{\kappa^D} = \frac{\kappa^U}{\rho^U} \,, \tag{4.29}$$

where $\kappa^Q = \sqrt{2}M_Q/v$. Thus, it follows that:

$$\rho^D = -\frac{\sqrt{2}m_d}{v}\tan\beta \,, \qquad \rho^U = \frac{\sqrt{2}m_u}{v}\cot\beta \,. \tag{4.30}$$

Inserting this result into eq. (4.27), and expressing φ_1^0 and φ_2^0 in terms of the CP-even Higgs mass eigenstates h and H yields the well-known Feynman rules for the type-II Higgs-quark interactions.

4.10.2   Interpretation of ILC measurements

How should one interpret precision measurements of 2HDM Yukawa couplings? A priori, one does not know whether a symmetry basis exists. Thus, one should attempt to determine experimentally the ρ^U and ρ^D coupling matrices. Testing relations such as eq. (4.28) could reveal the presence of a symmetry basis, in which case one can determine $\tan\beta$ from eq. (4.29). However, one could discover that the equality of eq. (4.29) does not hold. For example, in a one-generation type-III CP-conserving model, a more general procedure would consist of defining three $\tan\beta$-like parameters:

$$\tan\beta_d \equiv \frac{-\rho^D}{\kappa^D} \,, \qquad \tan\beta_u \equiv \frac{\kappa^U}{\rho^U} \,, \tag{4.31}$$

and a third parameter $\tan\beta_e \equiv -\rho^E/\kappa^E$ corresponding to the Higgs-lepton interaction. The equality of these three $\tan\beta$-like parameters would imply the existence of a symmetry basis (and an underlying type-II Higgs-Yukawa coupling). Deviations from these equalities would imply a more complex realization of the electroweak symmetry breaking dynamics.

We can illustrate this procedure in a very simple model approximation. In the MSSM at large $\tan\beta$ (and supersymmetric masses significantly larger than m_Z), the effective Lagrangian that describes the coupling of the Higgs bosons to the third generation quarks is given by:

$$-\mathcal{L}_{\text{eff}} = h_b(\overline{q}_L \Phi_1)b_R + h_t(\overline{q}_L \widetilde{\Phi}_2)t_R + \Delta h_b\,(\overline{q}_L \Phi_2)b_R + \text{h.c.}\,, \tag{4.32}$$

where $\overline{q}_L \equiv (\overline{u}_L\,,\,\overline{d}_L)$. The term proportional to Δh_b is generated at one-loop due to supersymmetry-breaking effects. The tree-level relation between m_b and h_b is modified [107, 136]:

$$m_b = \frac{h_b v}{\sqrt{2}}\,\cos\beta(1+\Delta_b)\,, \tag{4.33}$$

where $\Delta_b \equiv (\Delta h_b/h_b)\tan\beta$. That is, Δ_b is $\tan\beta$-enhanced, and governs the leading one-loop correction to the physical Higgs couplings to third generation quarks. In typical models at large $\tan\beta$, Δ_b can be of order 0.1 or larger and of either sign. An explicit expression for Δ_b is given in Refs. [107, 136, 230]. In the approximation scheme above, $\kappa^U \simeq h_t\sin\beta$, $\rho^U \simeq h_t\cos\beta$, and [213]

$$\kappa^D \simeq h_b\cos\beta(1+\Delta_b)\,, \qquad \rho^D \simeq -h_b\sin\beta\left(1 - \frac{\Delta_b}{\tan^2\beta}\right) \simeq -h_b\sin\beta\,. \tag{4.34}$$

It follows that:

$$\tan\beta_d \simeq \frac{\tan\beta}{1+\Delta_b}\,, \qquad \tan\beta_u \simeq \tan\beta\,. \tag{4.35}$$

Thus, supersymmetry-breaking loop-effects can yield observable differences between $\tan\beta$-like parameters that probe the underlying nature of supersymmetry-breaking.

4.11 Lepton Flavor Violation in the Higgs boson decay at ILC

Lepton flavor violation (LFV) in charged leptons directly indicates new physics beyond the SM. In the models such as based on SUSY, in addition to the gauge boson mediated LFV process, the LFV Yukawa couplings are naturally induced by slepton mixing [231]. The direct search for such LFV Yukawa couplings would be possible by measuring the Higgs decay process $h, (H, A) \to \tau^\pm\mu^\mp$ at collider experiments [232–234]. Such a possibility has been examined at the LHC in Ref. [235]. In Ref. [236], this possibility has been discussed and the feasibility of this process at a ILC via the Higgs-strahlung process has been studied under the constraints from current data on LFV rare tau decay processes. A possibility of a search for the LFV Yukawa interaction via the deep inelastic scattering process $e^- N \to \tau^- X$ at the fixed target option of ILC has also been studied [237].

4.12 Dimension-Six Higgs Operators

4.12.1 The SM as a low energy effective theory of new physics models

Under the constraint from the current precision data, the SM with a light Higgs boson would be an effective theory to the cutoff scale which could be considered to be as high as the Planck scale without contradicting theoretical arguments such as vacuum stability and triviality. On the other hand, such scenario of the SM with very high cutoff scale has been considered to be unnatural,

because due to quantum corrections the Higgs boson mass is quadratically sensitive to the cutoff (new physics) scale ($\sim \Lambda^2$). Demanding relatively small (less than 90%) hierarchy, the scale of the new physics naturally would be expected to be of the order of 1-10 TeV. The effect of new physics would then enter into the low energy theory as higher dimensional operators. If a light Higgs boson is discovered at the LHC but no additional particles are seen at the LHC or the ILC, it is important to search for small deviations of the Higgs boson potential from the SM predictions to probe new physics scales. If the reason for such small deviations is beyond-the-SM physics at large scales Λ, the effective operator approach can be chosen to parameterize the low-energy behavior of such models.

The effective Lagrangian of the SM with the cutoff Λ can be described as

$$\mathcal{L}_{\text{eff}} = \mathcal{L}_{\text{SM}} + \sum_n \frac{f_n}{\Lambda^2} \mathcal{O}_n + O(1/\Lambda^{n+2}), \tag{4.36}$$

where $\mathcal{O}_n$ are dimension six operators, and f_n's are dimensionless "anomalous couplings". It is expected that f_n's are of order of unity at the cutoff scale Λ. There are eleven SM gauge invariant bosonic operators in dimension six (dim-6) terms [238], and eight of them are relevant to the Higgs boson field:

$$\mathcal{O}_{BW} = \Phi^\dagger B_{\mu\nu} W^{\mu\nu} \Phi, \tag{4.37}$$

$$\mathcal{O}_{\Phi,3} = (D_\mu \Phi)^\dagger \Phi^\dagger \Phi (D^\mu \Phi), \tag{4.38}$$

$$\mathcal{O}_{WW} = \Phi^\dagger W_{\mu\nu} W^{\mu\nu} \Phi, \tag{4.39}$$

$$\mathcal{O}_{BB} = \Phi^\dagger B_{\mu\nu} B^{\mu\nu} \Phi, \tag{4.40}$$

$$\mathcal{O}_W = (D_\mu \Phi)^\dagger W^{\mu\nu} (D_\nu \Phi), \tag{4.41}$$

$$\mathcal{O}_B = (D_\mu \Phi)^\dagger B^{\mu\nu} (D_\nu \Phi), \tag{4.42}$$

$$\mathcal{O}_{\Phi,1} = \frac{1}{2} \partial^\mu (\Phi^\dagger \Phi) \partial_\mu (\Phi^\dagger \Phi), \tag{4.43}$$

$$\mathcal{O}_{\Phi,2} = \frac{1}{3} (\Phi^\dagger \Phi)^3. \tag{4.44}$$

These operators are separated to the following three categories.

[Class I] $(\mathcal{O}_{BW}, \mathcal{O}_{\Phi,3})$
These operators contribute to the gauge boson two point functions $(\mathcal{O}_{BW} \Rightarrow S, \mathcal{O}_{\Phi,3} \Rightarrow T)$, so that they receive tight constraints from the current precision data: their coefficients are bounded at the 95% C.L. as [239]

$$-0.07 < \frac{f_{BW}}{(\Lambda/\text{TeV})^2} < 0.04, \quad -0.02 < \frac{f_{\Phi,3}}{(\Lambda/\text{TeV})^2} < 0.02. \tag{4.45}$$

[Class II] $(\mathcal{O}_{WW}, \mathcal{O}_{BB}, \mathcal{O}_W, \mathcal{O}_B)$
These four operators lead to interactions of the Higgs boson with gauge bosons such as

$$\mathcal{L}_{\text{eff}}^H = g_{H\gamma\gamma} H A_\mu A^\nu + g_{HZ\gamma}^{(1)} A_{\mu\nu} Z^\mu \partial^\nu H + g_{HZ\gamma}^{(2)} H A_{\mu\nu} Z^{\mu\nu} + g_{HZZ}^{(1)} Z_{\mu\nu} Z^\mu \partial^\nu H$$
$$+ g_{HZZ}^{(2)} H Z_{\mu\nu} Z^{\mu\nu} + g_{HWW}^{(1)} (W_{\mu\nu}^+ W^{-\mu} \partial^\nu H + h.c.) + g_{HWW}^{(2)} H W_{\mu\nu}^+ W^{-\mu\nu}. \tag{4.46}$$

Combinations of the coefficients of $\mathcal{O}_{WW}$, $\mathcal{O}_{BB}$, $\mathcal{O}_W$ and $\mathcal{O}_B$ contribute to these V-H couplings $g_{HVV'}$. Theoretical bounds from partial wave unitarity on these coefficients are rather weak. By using the precision data for the LEP II Higgs search results and one-loop corrections, these coefficients

are constrained not so strongly as

$$-4 < \frac{f_B}{(\Lambda/\text{TeV})^2} < 2, \quad -6 < \frac{f_W}{(\Lambda/\text{TeV})^2} < 5,$$

$$-17 < \frac{f_{BB}}{(\Lambda/\text{TeV})^2} < 20, \quad -5 < \frac{f_{WW}}{(\Lambda/\text{TeV})^2} < 6. \tag{4.47}$$

The measurement of the triple gauge boson couplings can also contribute to constrain these anomalous couplings, but the present results give weaker bounds. They are expected to be constrained more precisely at future collider experiments; for example, via $WW \rightarrow WW$ [239] at the LHC, via $e^+e^- \rightarrow W^+W^-\gamma$ ($ZZ\gamma$) at the ILC [240], and $\gamma\gamma \rightarrow ZZ$ at a $\gamma\gamma$ collider [241]. The effects of the anomalous couplings of this class modify the production and decay of the Higgs boson, so that they can be well tested via these processes at the LHC and the ILC after the Higgs boson is detected.

[Class III] ($\mathcal{O}_{\Phi,1}$, $\mathcal{O}_{\Phi,2}$)
The last two are genuine dim-6 interactions of the Higgs boson, which are not severely constrained by the current precision electroweak data: see next subsection.

4.12.2 Genuine Dimension Six Higgs Operators

Recently, phenomenological consequences of the genuine dim-6 Higgs interactions have been studied [242]. The operators $\mathcal{O}_{\Phi,1}$ and $\mathcal{O}_{\Phi,2}$ lead to a Lagrangian

$$\mathcal{L}' = \sum_i^2 \frac{a_i}{v^2} \mathcal{O}_{\Phi,i}, \tag{4.48}$$

where $a_i = f_{\Phi,i} v^2/\Lambda^2$. This is the consistent formulation respecting the SM gauge symmetry. These operators contribute to the HVV and $HHVV$ interactions and the Higgs boson self-interactions H^3 and H^4. In terms of the canonically normalized Higgs field and the physical Higgs boson mass, the interactions are expressed by

$$\mathcal{L}_{HVV} = \left(M_W^2 W_\mu^+ W^{-\mu} + \frac{1}{2} M_Z^2 Z_\mu Z^\mu \right) \left((1 - \frac{a_1}{2}) \frac{2H}{v} + (1 - a_1) \frac{H^2}{v^2} \right), \tag{4.49}$$

$$\mathcal{L}_{H^3} = -\frac{m_H^2}{2v} \left((1 - \frac{a_1}{2} + \frac{2a_2}{3} \frac{v^2}{m_H^2}) H^3 - \frac{2a_1 H \partial_\mu H \partial^\mu H}{m_H^2} \right), \tag{4.50}$$

$$\mathcal{L}_{H^4} = -\frac{m_H^2}{8v} \left((1 - a_1 + 4a_2 \frac{v^2}{m_H^2}) H^3 - \frac{4a_1 H \partial_\mu H \partial^\mu H}{m_H^2} \right). \tag{4.51}$$

The measurement of HVV vertices can test a_1 while by measuring the Higgs self-coupling constants a_2 (as well as a_1) can be probed. For H^3 and H^4 interactions, the effect of a_2 not only changes the Higgs potential, but also gives kinetic corrections which are enhanced at high energies.

In [242], it has been shown that the parameter a_1 can be well measured at the ILC to an accuracy of 0.005 (0.003) corresponding to a scale $\Lambda \approx 4$ TeV, from 1 ab^{-1}of data at 500 (800) GeV through the measurement of the production cross-sections from Higgs-strahlung and WW/ZZ-fusion for $m_H = 120$ GeV. The parameter a_2 modifies the form of the Higgs potential and thus the Higgs pair production cross-section. At the LHC the measurement of the HH production cross section is difficult because of the small rate with huge backgrounds [243]. At the ILC with the same integrated luminosity (1 ab^{-1}), for $m_H = 120$ GeV, a_2 can be measured to 0.13 (0.07) at 500 (800) GeV corresponding to a scale $\Lambda \approx 1$ TeV [79]; see Fig. 4.11.

65
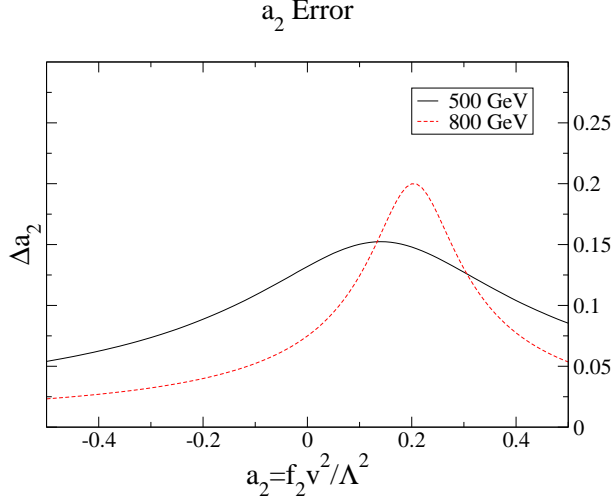
Figure 4.11: Combined statistical accuracy on a_2 with an integrated luminosity of 1 ab^{-1} for $\sqrt{s} = 500$ GeV and 800 GeV for $m_H = 120$ GeV, using the Higgs-strahlung and the WW-fusion channels.

4.12.3   Open questions

In order to exhaust the possibilities of the physics of dimension six operators, the following items should be considered in future studies.

- Fermionic operators should be included in the analysis.

- It is also important to calculate the anomalous coupling in various new physics scenarios. By classifying models in terms of anomalous couplings, a systematic search for new physics beyond the SM is possible with the future precision data at the ILC, even when only a light Higgs boson is found at the LHC.

4.13   Little Higgs

Recently, a new class of models for electroweak symmetry breaking has been proposed, the "Little Higgs" models [244]. Similar to supersymmetry as a model-building principle, the Little-Higgs mechanism stabilizes the mass of scalar particles against its quadratic cut-off sensitivity. The Higgs boson appears as a member of the Goldstone boson multiplet pertaining to a global symmetry that is spontaneously broken at some scale $\Lambda \sim \mathcal{O}(10$ TeV$)$. Naive dimensional analysis connects the cutoff Λ of such models with the decay constant of these bosons F by $F \sim \Lambda/4\pi$. This scale F is supposed to be above the electroweak scale $v = 246$ GeV, presumably in the TeV-region.

Being Goldstone bosons, the scalars in Little-Higgs models have neither a mass nor a potential as long as the global symmetry is exact. However, the SM gauge and Yukawa interactions of the Higgs explicitly break the global symmetry, thereby radiatively generating a potential for the Higgs by the Coleman-Weinberg mechanism. This idea dates back to the 1970s [245], but at that time no mechanism was known that suppressed the one-loop corrections to the Higgs self-energy without fine-tuning among the couplings.

This drawback is cured by the mechanism of collective symmetry breaking, originally observed in the context of deconstructed extra dimensions [246]. The structure of gauge and Yukawa interactions can be arranged such that if any one of their couplings is set to zero, the emerging global

symmetry makes the Higgs an exact Goldstone boson. Only if all couplings are different from zero, a potential is generated. If the global symmetry is broken in this particular way, one-loop contributions to the Higgs potential depend only logarithmically on the cut-off, while a quadratic divergence appears only at two-loop order. This allows for a three-scale hierarchy without fine-tuning: $v \sim F/4\pi \sim \Lambda/(4\pi)^2$.

To fully implement collective symmetry breaking in all sectors and thus cancel all one-loop quadratic cutoff sensitivity, a complete set of new gauge bosons, scalars and fermions is needed. Just like the MSSM extends the SM by new weakly-interacting particles with a characteristic soft-SUSY-breaking mass scale, Little-Higgs models thus lead to an extended weakly-interacting effective theory, where most of the new particles are expected with masses of order $F \gtrsim 1$ TeV.

In order to successfully implement collective symmetry breaking, either the global symmetry representation must be reducible or the gauge group must be non-simple. Consequently, there are two basic lines of model building. Particularly economic models emerge from a simple global symmetry group with an irreducible representation, such as the "Littlest Higgs" with its $SU(5) \to SO(5)$ breaking chain [247]. The non-simple gauge structure of such models generically introduces W' and γ'/Z' recurrences of the SM vector bosons (for additional U(1) factors there always is the freedom not to gauge it, see the discussion at the end of this subsection). By contrast, simple-(gauge-)group models tend to have a proliferation of scalar states in multiple representations and typically lead to a two-Higgs-doublet model at low energies, while the extra gauge bosons corresponding to nondiagonal generators of the extended EW gauge group are nontrivial to detect [248]. Finally, the "moose models" that were found first [249] establish a relation to higher-dimensional gauge theories [250] and feature factorized symmetries both in the scalar and vector sectors.

Collective symmetry breaking in the fermion sector requires the introduction of extra fermions, most notably heavy top-like states that implement a see-saw mechanism for the top mass in conjunction with the cancellation of fermion loops in the Higgs potential. In simple-group models, the irreducibility of the gauge group calls for extra fermion partners in all three generations.

By construction, Little-Higgs models involve tree-level mixing between the SM fields and their heavy partners. This leads to shifts in electroweak precision observables of the order v^2/F^2 which are at variance with data if F is below the TeV range. Detailed analyses [251] generically constrain the model parameters to $F \gtrsim 2 - 3$ TeV. An elegant way of removing some of the dangerous contributions is the implementation of a custodial $SU(2)$ symmetry [252]. Incidentally, in some models the problem is also ameliorated if the Higgs boson is rather heavy while the hierarchy $v \ll F \ll \Lambda$ is kept [253]. The mixing of states is eliminated by the implementation of a discrete symmetry, T-parity [254]. Analogous to R-parity in the MSSM and KK-parity in extra-dimension models, this leads to a one-loop suppression of shifts in precision observables and makes the lightest T-odd particle a suitable dark-matter candidate. Finally, embedding the little-Higgs mechanism in a supersymmetric model [255] can nicely remove the fine-tuning problems that are present both in the MSSM and in non-supersymmetric models.

If the Little-Higgs mechanism is realized in nature, we need experimental means to verify this fact and to identify the particular model. If possible, we should observe the new particles, the symmetry structure in the couplings that is responsible for stabilizing the Higgs potential, and the non-linearity of the representation that is characteristic for Goldstone scalars at low energies. This can be achieved by a combined analysis of LHC and ILC data [251, 256, 257], while flavor data will play a minor role [258]. The prospects for uncovering the ultimate UV completion of the model [255, 259] remain uncertain.

The LHC provides us with a considerable detection reach for new vector bosons. If found, their properties (masses, mixing angles and branching ratios) can be determined with considerable accuracy. Simultaneously, new vector bosons can be studied by their indirect effect on contact

interactions at the ILC, where the search limit extends into the 10 TeV range. New quarks can also be searched for at the LHC, although with less sensitivity, and they affect top-quark precision observables that can be measured at the ILC.

For the scalar sector of Little Higgs models we have to consider a wide range of possibilities, essentially arbitrary combinations of singlets, doublets, triplets, and more. While such particles may be nontrivial to isolate in LHC data, at least the lighter part of the Higgs spectrum can be covered by searches at the ILC. Precision studies of vector-boson and Higgs anomalous couplings can even uncover traces of the nonlinear Goldstone-boson representation and thus establish the main ingredient of the Little-Higgs paradigm.

Finally, a rather generic feature of Little-Higgs phenomenology originates from the enlarged global symmetry. This symmetry necessarily involves spontaneously broken $U(1)$ subgroups. Consequently, the spectrum contains either Z' bosons (gauged $U(1)$) [251], or light pseudoscalar particles otherwise [260]. The latter can be studied in diphotons at the LHC, in top-quark production at the ILC, and as resonances in $\gamma\gamma$ fusion at a photon collider.

4.14 Models with Higgs Triplets

Some of the "Little Higgs" models discussed in Sect. 4.13 postulate the existence of an $SU(2)_L$ triplet of scalar fields in addition to the conventional doublet. Unfortunately, the physical states associated with this triplet are expected to be too heavy for direct observation at a TeV linear collider. Nonetheless, "Little Higgs" models do not exhaust all possible models predicting triplets of scalar fields. These may occur, for example, in the models with extra spatial dimensions [261] (see also Sect. 4.15) and in other scenarios. Even the Standard Model Higgs sector can be extended to contain both doublet and triplet fields without contradicting existing experimental data [262]. Models with Higgs triplets predict an enriched spectrum of physical states, including not only neutral and singly charged particles, but also doubly charged states. These can be directly produced and detected at the linear e^+e^- collider. One shouldn't also exclude the possibility to detect a doubly charged Higgs boson, H^{--}, as a resonance at an e^-e^- collider, though this will require an anomalously strong Hee coupling. The existence of scenarios in which the H^{--} state can be produced in e^-e^- collisions with sufficiently high rate enabling its detection would emphasize the importance of a future ILC facility with several collision options. Clearly, rich phenomenology of the models with Higgs triplets invites investigation of the ILC potential for probing such a models.

4.15 Higgs Bosons and Extra Dimensions

In recent years, models with extra spatial dimensions have become very popular. They primarily address the electroweak hierarchy problem either by diluting gravity in a large extra dimensional volume that the SM interactions do not feel (as in the large or ADD extra dimensions [263]) or by explaining the apparent difference in scales by a warped metric in a small extra dimension (as in the warped or RS models [264]). Large extra dimensions necessarily have the Standard Model confined to a three dimensional sub-manifold, or brane, whereas RS exists in several versions which primarily differ as to how much of the SM is in the bulk.

The 'classic' signatures involve the effects of the Kaluza-Klein (KK) tower of gravitons. In the large extra dimension case, the size of the extra dimensions is expected to be large enough that the KK states are extremely tightly spaced and thus appear as a continuum of objects, each one of which interacts only with ordinary gravitational strength. Relevant impact on collider observables occurs because there are so many states that they collectively have a large effect. In the case of

warped extra dimensions the states have masses with spacing on the order of TeV. However, each is much more strongly coupled than the ordinary graviton, and so individually they can have a large impact on processes at colliders. The upshot is that both theories can induce deviations of SM processes like $e^+e^- \to f\bar{f}$ and $e^+e^- \to W^+W^-$ from the virtual exchange of KK modes [265, 266], or their real emission together with SM fermions or gauge bosons [267]. These modes have been studied with experimental models of detectors, see e.g. Ref. [8].

More recently, also the impact of extra dimensions on the Higgs boson phenomenology has been studied. In the ADD scenario, three effects have been analyzed (for another analysis, see Ref. [268]):

1. A modification of the quasi-resonant $W^+W^- \to H$ production process through interference of the SM amplitude with the imaginary part of the graviton/graviscalar KK exchange amplitude [269]. In order to yield a significant modification, a large total Higgs width is needed (i.e., large m_H), which implies on the other hand a large center-of-mass energy. While the graviscalar contribution only modifies the normalization of the cross-section (by few percent for $\sqrt{s} = 1$ TeV, $m_H = 500$ GeV and 2 extra dimensions at a fundamental Planck scale of 1 TeV), a significant change of the angular distribution is expected from the spin-2 graviton exchange.
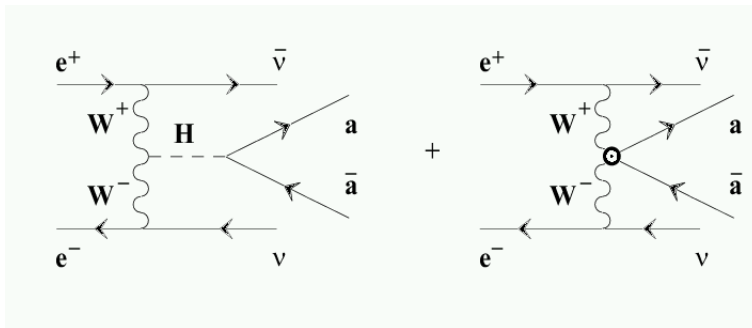
Figure 4.12: Effective Feynman diagrams from Equation (4.52) corresponding to single Higgs production with the subsequent Higgs decay into $a\bar{a}$, where a is a heavy particle, such as W, Z or t [270].

2. A modification of the process $e^+e^- \to HHZ$ and the existence of the process $e^+e^- \to HH\gamma$ which is absent at tree level in the SM [271]. For a 1 TeV ILC and $m_H = 120$ GeV, a sizable correction to $e^+e^- \to HHZ$ both in normalization and angular distribution is expected for fundamental Planck scale up to a few TeV. Furthermore, the cross-section for $e^+e^- \to HH\gamma$ exceeds 0.1 fb for a fundamental Planck scale below approximately 2 TeV. In [271], expected 5σ discovery limits on the fundamental Planck scale of 880–1560 (1640–2850) GeV have been derived at $\sqrt{s} = 500$ (1000) GeV for 6–3 extra dimensions.

3. Direct Higgs pair production $e^+e^- \to HH$ [272, 273]. The signature of this channel is two pairs of b-jets with an invariant mass close to the Higgs mass. The main SM backgrounds are $e^+e^- \to W^+W^-$, ZZ, ZH and $b\bar{b}b\bar{b}$. The differential cross section gives a characteristic signal of the spin 2 interaction. For an ILC operating at 1 TeV and a fundamental Planck scale of 2 TeV, the cross section is of the same order as the SM $e^+e^- \to ZH$ for $m_H = 120$ GeV. Indeed, 700 Higgs pair events can be generated with an integrated luminosity of 500 fb^{-1}.
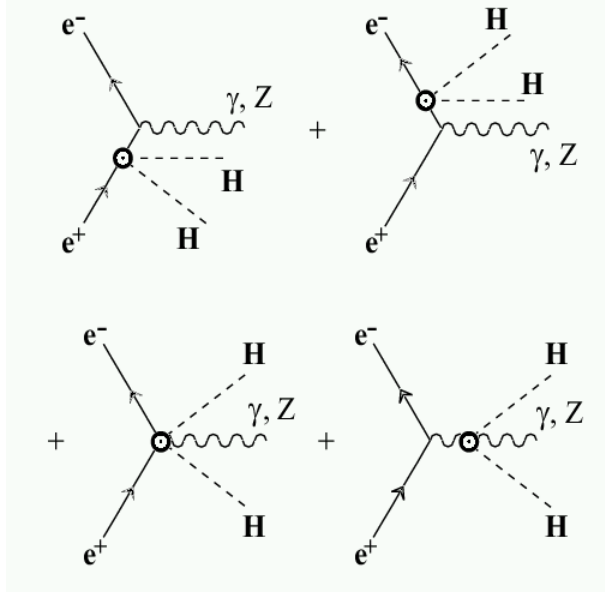
Figure 4.13: Feynman diagrams which contribute to the processes $e^+e^- \to ZHH$ or $e^+e^- \to \gamma HH$ [271]. In this case, a five particle effective vertex generated by the virtual graviton exchange or branon radiative corrections has to be taken into account, which is also provided by the Lagrangian (4.52).
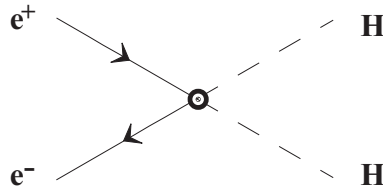
Figure 4.14: Feynman diagrams associated with the Higgs pair production $e^+e^- \to HH$ [273]. The effective four particle vertex is provided by the exchange of virtual KK-graviton in the rigid ADD and by a branon loop for flexible branes (See Equation (4.52)).

4.15.1 Radion Effects

Extra dimensional models contain moduli which describe the size and shape of the extra dimensions. These scalar fields, usually called the radion, can be understood as a zero mass component of the higher dimensional metric, i.e., g_{xy} where x and y are two of the compactified directions. In the case of a five dimensional model, there is a single scalar field which parameterizes the size of the extra dimension. In order to stabilize the size of the extra dimensions, these fields must acquire masses, and the specifics of the stabilization mechanism will in general play some role in determining the properties of the radion [274]. Generically, they are expected to couple to SM particles through the trace of the energy-momentum tensor, i.e., very similar to the SM Higgs boson, up to the trace anomaly of QCD. The lightest radion might in fact be lighter than the lightest graviton excitation and thus could be the discovery channel for the model.

In flat space, the radion is not usually relevant for colliders (see however Ref. [275]). The couplings are too small and not compensated by a large number of fields. They may nonetheless play an important role in cosmology and could even make up a fraction of the dark matter [276]. In warped backgrounds, the radion is much more relevant, because it picks up the same enhancement of its couplings as the graviton KK modes. Thus, the influence on the Higgs sector could be quite dramatic through mixing of the radion with the Higgs. This leads to mass eigenstates which are a mixture of both, and thus a strong modification of both the Higgs boson and radion properties, in particular their couplings to gauge bosons and fermions. For a review of the radion phenomenology, see e.g. [277]. Analyses of radion physics at the LHC and the ILC can be found in Ref. [12]. The radion sector is governed by 3 parameters: the strength of the radion-matter interactions described by an energy scale Λ_ϕ, the mass of physical radion m_ϕ, and the radion-Higgs mixing parameter ξ. In Fig. 4.15, the effective couplings squared of the Higgs boson and the radion (relative to those of a SM Higgs boson) are shown for the choice $\Lambda_\phi = 5$ TeV, and three values of the radion mass (20, 55, 200 GeV) as a function of ξ. Large deviations of the Higgs couplings from their SM values are expected if there is large radion-Higgs mixing present. The radion itself has couplings which are reduced by a factor v/Λ_ϕ with respect to those of a SM Higgs in the case of no mixing, which requires high luminosity for direct discovery. The sensitivity of the trilinear Higgs coupling to radion admixtures has been studied as well in [277].
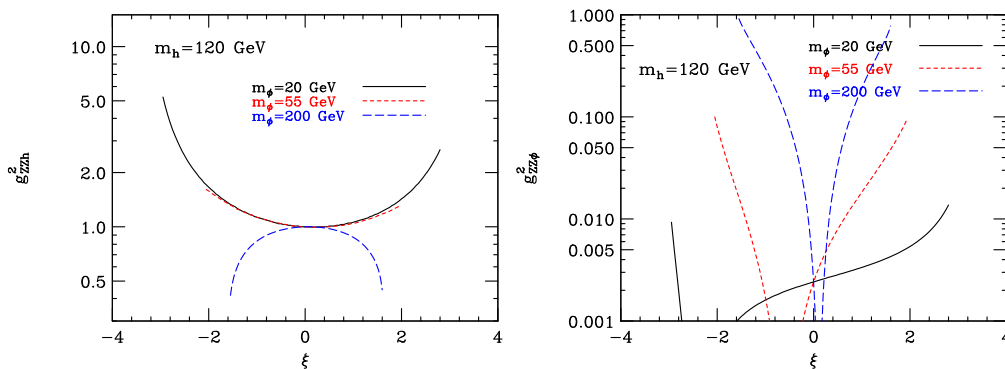
Figure 4.15: Effective coupling of the Higgs boson (left) and the radion (right) to Z boson (from [277]).

4.15.2 Branon Effects

The previous discussion has assumed that the branes are perfectly rigid. However, it is expected that the dynamics responsible for generating the brane will in fact leave it with a finite tension which will allow it to oscillate. The brane fluctuations are manifest as new pseudo-scalar particles, which are called branons [278]. For appropriate choices of parameters, branons are natural dark matter candidates, being stable and weakly coupled to Standard Model fields [279]. The collider signature for branons is missing energy; in particular, the mono-jet and single photon signals for hadron colliders [280] and the single Z and single photon channels for e^+e^- colliders [281]. This last signature has been studied experimentally by LEP [282], finding the most constraining bound for the brane tension scale: $f > 180$ GeV, for light branons. These collider searches are complementary to astrophysical and cosmological ones [283] and they need to be completed with branon radiative correction analyses. Indeed, these quantum corrections are very similar to the virtual KK-graviton

effects in the rigid ADD model since the two effects predict the same effective Lagrangian [284]:

$$\triangle \mathcal{L}_{\text{eff}} = W_1 T_{\mu\nu} T^{\mu\nu} + W_2 T^{\mu}_{\mu} T^{\nu}_{\nu} \, , \tag{4.52}$$

where W_1 and W_2 are two constants which depends on the renormalization procedure. This means that branons lead to analogous four body interactions and Higgs boson phenomenology.

Chapter 5

Analysis Tools

In this section we give a brief overview about the state-of-the-art tools that are available for the evaluation of Higgs boson observables. The first subsection summarizes the computer codes that have been developed for the calculation of Higgs boson mass spectra and branching fractions. The second subsection briefly describes event generators available for Higgs boson physics. All codes are listed in Tab. 5.1, together with their corresponding web address (see also the Les Houches Web Repository for BSM Tools [285]).

HDECAY	people.web.psi.ch/spira/hdecay/
FeynHiggs	www.feynhiggs.de/
CPsuperH	www.hep.man.ac.uk/u/jslee/CPsuperH.html
NMHDECAY	www.th.u-psud.fr/NMHDECAY/nmhdecay.html
HERWIG	hepwww.rl.ac.uk/theory/seymour/herwig/
ISAJET	www.phy.bnl.gov/~isajet/
MADGRAPH	madgraph.hep.uiuc.edu/
PYTHIA	www.thep.lu.se/~torbjorn/Pythia.html
SHERPA	www.physik.tu-dresden.de/~krauss/hep/
WHIZARD	www-ttp.physik.uni-karlsruhe.de/whizard/

Table 5.1: Web links for Higgs-related tools.

5.1   Higgs spectra and branching fractions

5.1.1   Standard Model Higgs

The Standard Model Higgs decay branching fractions and total width are computed by the packages HDECAY [38] and FeynHiggs [37, 148, 286]. We outline here the known radiative corrections and sources of theoretical uncertainty in the SM Higgs branching ratios. We focus here on HDECAY: for some of the decays to $b\bar{b}$, $c\bar{c}$, $s\bar{s}$, we believe that HDECAY is slightly better than FeynHiggs in terms of containing SM higher order radiative corrections to the decay widths; however, the other decays are treated to comparable accuracy.

The radiative corrections to Higgs decays to fermion and boson pairs have been reviewed in Ref. [287]; we give here a brief sketch of the known corrections and refer to Ref. [287] for references to the original calculations. The full QCD corrections to the Higgs decay to $q\bar{q}$ are known up to

three loops neglecting the quark mass in the kinematics; at the two loop level they are known for massive final-state quarks in the leading-N_F approximation. The electroweak corrections to the Higgs decay to quark or lepton pairs are known at one-loop; in addition, the QCD corrections to the leading top-mass-enhanced electroweak correction term are known up to three loops, to order $G_F m_t^2 \alpha_s^2$. All of these corrections to the Higgs partial widths to fermions are included in a consistent way in the program HDECAY [38].

For the Higgs masses below the WW threshold, $M_H \lesssim 160$ GeV, decays into off-shell gauge bosons (WW, ZZ) are important and affect the total Higgs width, thus feeding in to the Higgs branching fractions. Off-shell decays to W and Z bosons are taken into account. One-loop electroweak corrections to Higgs decays to WW and ZZ are known, together with the QCD corrections to the leading $\mathcal{O}(G_F m_t^2)$ result up to three loops. These corrections to $\Gamma_{W,Z}$ amount to less than about 5% in the intermediate Higgs mass range [287] (translating to less than roughly 2% in BR($H \to b\bar{b}$) for $M_H \simeq 120$ GeV) and have been neglected in HDECAY, although their inclusion would seem straightforward.

The Higgs decay into gluon pairs, $H \to gg$, is of order $\mathcal{O}(G_F \alpha_s^2)$ at the leading one-loop order and therefore suffers a large scale dependence. In the SM, the state of the art is the $\mathcal{O}(G_F \alpha_s^4)$ contribution in the large m_t limit computed in Ref. [288]. This correction is of order 20% for a light Higgs, increasing the total Higgs hadronic width by only about 1%, and the remaining scale uncertainty from varying the renormalization scale between $M_H/2$ and $2M_H$ is roughly $\pm 5\%$. This correction appears not to be included in HDECAY, although its inclusion would be trivial.

The SM $H \to \gamma\gamma$ decay partial width receives QCD corrections, which of course only affect the quark loop diagrams. Because the external particles in the $\gamma\gamma H$ vertex are color neutral, the virtual QCD corrections are finite by themselves. Since no real radiation diagrams contribute, the QCD corrections to $H \to \gamma\gamma$ are equivalent to those to the inverse process $\gamma\gamma \to H$. This is in contrast to the QCD corrections to the ggH vertex. The QCD corrections to Γ_γ in the SM are known analytically at the two-loop [$\mathcal{O}(G_F \alpha_s)$] order [289] and as a power expansion up to third order in M_H/m_t at three-loop [$\mathcal{O}(G_F \alpha_s^2)$] order [290]. They are small for Higgs masses $M_H < 2m_t$; the $\mathcal{O}(\alpha_s)$ corrections are only of order 2% for $M_H < 2M_W$, and the $\mathcal{O}(\alpha_s^2)$ corrections are negligible, demonstrating that the QCD corrections are well under control. The SM $H \to \gamma\gamma$ decay partial width also receives electroweak radiative corrections. The electroweak corrections are much more difficult to compute than the QCD corrections and a full two-loop calculation does not yet exist. The electroweak correction due to two-loop diagrams containing light fermion loops and W or Z bosons (with the Higgs boson coupled to the W or Z boson, because the light fermion Yukawa couplings are neglected) was computed recently in Ref. [291] and contributes between -1% and -2% for $M_H \lesssim 140$ GeV. The leading $\mathcal{O}(G_F m_t^2)$ electroweak correction due to top-mass-enhanced two-loop diagrams containing third-generation quarks was also computed recently in Ref. [292] as an expansion to fourth order in the ratio $M_H^2/(2M_W)^2$.[1] The expansion appears to be under good control for $M_H \lesssim 140$ GeV, where this correction contributes about -2.5% almost independent of M_H. The leading $\mathcal{O}(G_F M_H^2)$ correction was computed in Ref. [294] for large M_H; however, this limit is not useful for a light Higgs boson. We conclude that the electroweak radiative corrections to $H \to \gamma\gamma$ appear to be under control at the 1–2% level.

The Higgs branching ratios in the SM also have a parametric uncertainty due to the experimental uncertainties in the SM input parameters. The largest sources of parametric uncertainty are the bottom and charm quark masses and (to a lesser extent) the strong coupling α_s, which contributes via the QCD corrections to the $Hq\bar{q}$ couplings. These parametric uncertainties were evaluated in, e.g., Refs. [295, 296]. Ref. [296] found a parametric uncertainty in BR($H \to b\bar{b}$) of about 1.4%

---

[1]The $\mathcal{O}(G_F m_t^2)$ electroweak correction was also considered in Ref. [293], whose results disagree with that of Ref. [292]. The source of this disagreement is addressed in Ref. [292].

for $M_H = 120$ GeV, using the standard $\alpha_s = 0.1185 \pm 0.0020$ [297] and a somewhat optimistic $m_b(m_b) = 4.17 \pm 0.05$ GeV ($\overline{\text{MS}}$) [298]. The parametric uncertainty in $\text{BR}(H \to b\bar{b})$ is suppressed due to the fact that Γ_b makes up about 2/3 of the Higgs total width at $M_H = 120$ GeV, leading to a partial cancellation of the uncertainty in the branching ratio; the uncertainty instead feeds into the other Higgs branching ratios to W^+W^-, $\tau\tau$, etc. We also expect the parametric uncertainty in $\text{BR}(H \to b\bar{b})$ to be somewhat larger at higher Higgs masses, where Γ_b no longer dominates the total width.

The best measurements of α_s come from LEP-I and II; the Tevatron and LHC are unlikely to improve on this. The ILC is expected to improve the precision of α_s by about a factor of two [53, 299]. The bottom quark mass is extracted from heavy quarkonium spectroscopy and B meson decays with a precision limited by theoretical uncertainty. There are prospects to improve the bottom quark mass extraction through better perturbative and lattice calculations [300] and more precise measurements of the upsilon meson properties from CLEO [301].

5.1.2 MSSM Higgs

CP-conserving MSSM

The three major codes used to compute the Higgs spectrum and branching fractions in the CP-conserving MSSM are `HDECAY` [38], `FeynHiggs` [37, 148], and `CPsuperH` [108].

`HDECAY` computes the MSSM Higgs spectrum and mixing angles with the user's choice of packages: `Subh` [302] and `Subhpole` [303] (now subsumed into `CPsuperH` [108, 143, 304]) as well as Haber et al. [305], which use a renormalization-group-improved effective field theory approach to compute Higgs masses and mixing angles; and `FeynHiggsFast`[2] [37], which contains the two-loop diagrammatic computation (the most recent version uses `FeynHiggsFast` by default). A reconciliation between the two-loop diagrammatic computation of the mass of the lightest CP-even Higgs boson and the effective field theory computation was performed in Ref. [306]. The code contains, in addition to the SM modes, Higgs decays to SUSY particles and SUSY contributions to loop-induced decays. In the case of Higgs decays to SM particles through tree-level couplings, the MSSM rates are computed by scaling the SM couplings by the appropriate Higgs mixing angles.

`FeynHiggs`, in addition to computing the MSSM Higgs mass spectrum and mixing angles using the on-shell Feynman-diagrammatic approach at the two-loop level, also computes the Higgs decay branching fractions and the Higgs boson production cross sections at the Tevatron and the LHC for all relevant channels (in a simplified parametric approach). In some of the SUSY decays, `FeynHiggs` includes corrections that are not in `HDECAY`, e.g., the Δ_b corrections in the charged Higgs decay to $t\bar{b}$. Details and references were given in Sec. 4.1.

`CPsuperH` contains a computation of the MSSM Higgs boson pole masses and mixing angles based on the renormalization-group-improved effective potential computation in the MSSM [304]. Since the case with real parameters is only a special case of the complex MSSM, more details about the two codes will be discussed further in the next subsection.

CP-violating MSSM

The two major codes used to compute the Higgs spectrum and branching fractions in the MSSM with explicit CP violation are `FeynHiggs` [37, 145, 147, 148] and `CPsuperH` [108].

The program `FeynHiggs` [37, 148, 286] is based on the results obtained in the Feynman-diagrammatic (FD) approach [16, 17, 129, 137]. It computes the MSSM Higgs spectrum and mixing angles, taking into account the full phase dependence at the one-loop and a partial phase dependence at the

---

[2]`FeynHiggsFast`, though still available, has been superseded by `FeynHiggs2.2`.

two-loop level. The code `CPsuperH` [108] is based on the renormalization group (RG) improved effective potential approach [303, 306–308]. For the MSSM with real parameters the two codes can differ by up to ~ 4 GeV for the light CP-even Higgs boson mass, mostly due to formally subleading two-loop corrections that are included only in `FeynHiggs`. For the MSSM with complex parameters the phase dependence at the two-loop level is included in a more advanced way [143, 309] in `CPsuperH`, but, on the other hand, `CPsuperH` does not contain all the subleading one-loop contributions that are included [145–147] in `FeynHiggs`. In the case of real parameters, the remaining theoretical uncertainty on the light CP-even Higgs boson mass has been estimated to be below ~ 3 GeV [17, 52], if `FeynHiggs` is used. In the case of complex parameters, no detailed estimate for the additional theory uncertainty due to the complex phases has been performed. However, the intrinsic uncertainties should be larger than for real parameters by at most a factor of two.

5.1.3 Beyond the MSSM

The NMSSM

The Next-to-Minimal Supersymmetric Standard Model (NMSSM) contains a Higgs sector enlarged by a singlet chiral superfield compared to the MSSM. The Higgs masses, couplings and decay widths in this model are computed by the Fortran code `NMHDECAY` [181, 310]. The computation of the Higgs spectrum includes leading electroweak corrections and leading two-loop terms. The computation of the decay widths is carried out as in `HDECAY` [38] (temporarily without three-body decays); Higgs-to-Higgs decays are included and can be important. Each point in parameter space can be checked against low-energy observables, as well as negative Higgs boson searches at LEP and negative sparticle searches at LEP and the Tevatron, including unconventional channels relevant for the NMSSM. Version 2.0 [310] allows to compute the dark matter relic density via a link to a NMSSM version of the `MicrOmegas` code [311].

Other extended models

There are many extended Higgs models in the literature for which no public codes exist. The Higgs couplings have been studied in detail using private codes for some of these models, as follows:

- Randall-Sundrum model: mixed radion and Higgs [312, 313],

- Randall-Sundrum model: Higgs with a profile in the warped extra dimension [314],

- Universal extra dimensions and Kaluza-Klein effects [315],

- Littlest Higgs model [256, 257, 316, 317].

5.2 Event generators

Here we give brief descriptions of Monte Carlo event generators that produce Higgs events for the ILC. Many of these rest upon the spectrum and branching fraction calculators like `FeynHiggs` and/or `HDECAY` discussed in the previous sections.[3]

- HERWIG

---

[3]The depth of the descriptions does not reflect the importance of the respective generator, but the information provided to the authors.

`HERWIG` [318–322] is a general-purpose Monte Carlo (MC) event generator for high-energy collider processes within the SM and MSSM [323, 324]. The `HERWIG` source codes and related information can be found in [325].

Higgs production and decay is available within the SM and MSSM. While the SM implementation is built-in, the MSSM generation relies on input information provided by other programs. As the `HERWIG` generator does not contain any built-in models for SUSY-breaking scenarios, in all cases the general MSSM particle spectrum and decay tables must be provided just like those for any other object, with the following caveats: (i) (coloured) SUSY particles do not radiate (which is reasonable if their decay lifetimes are much shorter than the QCD confinement scale); (ii) CP-violating SUSY phases are not included. A package, `ISAWIG`, has been created to work with `ISAJET` [326] to produce a file containing the SUSY (and Higgs) particle masses, lifetimes, couplings and mixing parameters. This package takes the outputs of the `ISAJET` MSSM programs and produces a data file in a format that can be read into `HERWIG` for the subsequent process generation. Of particular relevance to Higgs production and decay is also the interface to the `HDECAY` program [327]. As of 2005, also a link to `FeynHiggs` is available. However, the user can produce her/his own file provided that the correct format is used; see the corresponding web page, where examples of input files can be found (the SUSY benchmark points recommended in Ref. [117] are also uploaded). Finally, the implementation of the SUSY Les Houches accord of Ref. [328] will soon be available.

The SM and MSSM Higgs production and decay processes of relevance for the physics of an ILC [329] currently implemented in `HERWIG` are are associated with the process numbers $\mathtt{IPROC} = 300, 400, 900, 1000$ and 1100 (i.e., Higgs-strahlung, vector-boson fusion, pair production and associated production with heavy fermions). Also the decay of SUSY particles to Higgs bosons is considered [323, 324].

- `ISAJET 7.73`

  The event generator `Isajet` [326] can be used to generate SM Higgs boson production via the process $e^+e^- \to ZH_{SM}$ using the `E+E-` reaction type, and stipulating the final state to be `'Z0'` and `'HIGGS'`. The Higgs mass is input using the `HMASS` keyword. The H_{SM} decay modes are calculated internally at tree level. The beam polarization can be adjusted using the `EPOL` keyword, which allows input of $P_L(e^-)$ and/or $P_L(e^+)$. The events can be generated with initial state photon bremsstrahlung and/or beamstrahlung using the `EEBREM` or `EEBEAM` keywords. Input of the beamstrahlung parameter Υ and bunch length σ_z is needed. Then an effective electron and positron distribution function is calculated, and the hard scattering events are convolved with the $e^\pm$ PDFs, to give a variable CM energy for the hard scattering. Fox-Wolfram QCD showers and independent hadronization are used to convert final state quarks and gluons into jets of hadrons.

  `Isajet` can also generate Higgs production in the MSSM. One may either run with weak scale MSSM input parameters, or with high scale parameters in supergravity models, GMSB models or AMSB models. The full SUSY and Higgs mass spectrum is calculated using 2-loop RGEs to obtain an iterative solution, and full one-loop radiative corrections are included. The various Higgs masses are computed using the RG improved one-loop effective potential evaluated at an optimized scale to account for leading two-loop terms. Agreement for the Higgs boson masses with `FeynHiggs` is in the few GeV range, typically. The production reactions include $e^+e^- \to Zh$, ZH, Ah, AH and H^+H^- (along with the various SM and MSSM $2 \to 2$ processes). The sparticle mass spectrum and decay table can be output separately using the `isasugra` or `isasusy` subprograms. Leading QCD corrections are included for Higgs decay

to heavy quarks. It should be noted that the various MSSM Higgs bosons can be produced at large rates via sparticle cascade decays. Also, the `Isajet` decay table includes Higgs boson decays to sparticles, which can sometimes modify and even improve prospects for MSSM Higgs boson discovery.

As with SM Higgs production, beam polarization and brems/beamstrahlung effects can be included in the event generation. While spin correlation effects are neglected, full decay matrix elements are used for three-body sparticle decays. Decays to left and right tau lepton helicity states are computed, to give on average the correct energy distributions from decays to tau leptons.

- `MadGraph`

  `MadGraph` [330] is an automated tree-level matrix element generator based on helicity amplitudes as implemented in the `HELAS` library [331]. The associated event generator `MadEvent` [332] can then be used to generate unweighted events. For showering/hadronization, interfaces to `PYTHIA` and `HERWIG` are available.

  Higgs production in both the SM and MSSM [333] is handled at tree-level. In the MSSM, the Higgs spectrum and mixing angles are supplied from a SUSY Les Houches Accord (SLHA) [328] input file, which can be generated with the user's choice of spectrum calculator. Higgs decay widths in both the SM and MSSM are taken from `HDECAY`, which is integrated into the `HELAS` library.

- `PYTHIA`

  `PYTHIA` [111, 334] is a general-purpose event generator for hadronic events in e^+e^-, eh, and hh collisions (where h is any hadron or photon). For a recent brief introduction to this and many other codes, see [335]. The current version is always available from the `PYTHIA` web page with update notes and a number of useful examples.

  `PYTHIA` contains a large number of Higgs boson processes, both for production (in many cases with polarisation effects included, see [111], Section 8.8) and decay. The partial widths of the Higgs bosons are very strongly dependent on the mass, and are calculated as a function of the actual Higgs mass, i.e., not just at the nominal mass. Leading order expressions are used, with running fermion masses and, in some cases, overall K-factors, to absorb the leading radiative corrections. Other higher-order effects are not included. Since the Higgs is a spin-0 particle, it decays isotropically. In decay processes such as $h^0 \to W^+W^-/Z^0Z^0 \to 4$ fermions, angular correlations are included [336]. In decays to 2 jets, the parton shower off the final state is merged with the 3-jet matrix elements for hard jet emission [337], thus incorporating part of the NLO correction.

  The relevant physics scenarios included in `PYTHIA` can be categorised as follows:

  - Light Standard Model Higgs (narrow-width approximation): In e^+e^- annihilation, the main processes are $e^+e^- \to h^0Z^0$, usually dominant close to threshold, and vector boson (Z^0Z^0 and W^+W^-) fusion which is important at high energies. The vector boson fusion process is a full $2 \to 3$ body calculation. The loop-induced $\gamma\gamma$ fusion process may also be of interest, in particular when the effects of beamstrahlung photons and backscattered photons are included. For details, see [111], Section 8.5.1.
  - Heavy Standard Model Higgs: for details, see [111], Section 8.5.2.
  - SUSY/2HDM: the Higgs sector in Supersymmetric models is a special case of the general 2-Higgs Doublet Model included in `PYTHIA`. The internal `PYTHIA` routines for fixing the

MSSM Higgs sector rely on the effective potential approach of [302, 303], including the important radiative corrections at large $\tan\beta$. Other Higgs boson spectrum calculations can be interfaced, either via the SUSY Les Houches Accord [328, 338], or via the run-time interfaces to both `Isasusy` [339] and `FeynHiggs` [37, 148]. Recently, an interface to NMSSM models via the Les Houches Accords [113, 328] has also been implemented [340]. The additional production processes possible in a 2HDM are included, such as Higgs boson pair production. In production and decay, however, the effects of virtual superpartners are *not* included. For details, see [111], Sections 8.5.3–8.5.5 (2HDM) and 8.7 (SUSY).

– Left–Right symmetry / Higgs Triplets: the particle content is expanded by right-handed Z_R^0 and $W_R^\pm$ and right-handed neutrinos. The Higgs fields are in a triplet representation, leading to doubly-charged Higgs particles, one set for each of the two SU(2) groups. Also the number of neutral and singly-charged Higgs states is increased relative to the Standard Model. `PYTHIA` implements the scenario of [341, 342]. The main decay modes implemented are $H_L^{++} \to W_L^+ W_L^+, \ell_i^+ \ell_j^+$ (i, j generation indices) and $H_R^{++} \to W_R^+ W_R^+, \ell_i^+ \ell_j^+$. For details, see [111], Section 8.6.3

– Technicolor: while not a model with a fundamental Higgs boson, Technicolor still belongs to the category of Higgs-related topics. Techni-rho production is possible using the Heavy Standard Model Higgs processes or through a vector dominance mechanism [343]; see [111], Section 8.6.7.

– Little Higgs: Standard `PYTHIA` does not explicitly include a Little Higgs model, but important features can be handled using the options for 4th generation fermions and possibly Z'/W' bosons. For example, single heavy top quark T production and decay can be simulated using the t'. See [111], Sections 8.6.1 and 8.6.2.

- `SHERPA`

`SHERPA` [344] is a full event generator which is capable of describing events in e^+e^-, pp, $p\bar{p}$, and $\gamma\gamma$ collisions; for the latter the photon spectra produced through laser-backscattering are parametrised according to `CompAZ`. For the description of the perturbative aspects of such events, it includes a fully automated matrix element generator for the calculation of cross sections at the tree-level (`AMEGIC++` [345]), a module for the simulation of subsequent soft QCD radiation through the parton shower (`APACIC++` [346]) and a merging of both according to the prescription of [347–349].

All production and decay processes in the SM and the MSSM are treated at tree-level, including processes involving Higgs bosons. In the case of the MSSM, the particle spectra and mixing angles are taken from a SUSY Les Houches Accord (SLHA) [328] input file. Additional interfaces to `IsaSUSY`, `HDECAY` and `FeynHiggs` are available.

- `WHIZARD`

`WHIZARD` [350] is a program system designed for the efficient calculation of multi-particle scattering cross sections and simulated event samples. Tree-level matrix elements are generated automatically for arbitrary partonic processes by calling one of the external programs `O'Mega` [351], `MADGRAPH` or `CompHEP` [109]. Matrix elements obtained by alternative methods (e.g., including loop corrections) may be interfaced as well. The program is able to calculate numerically stable signal and background cross sections and generate unweighted event samples with reasonable efficiency for processes with up to six final-state particles.

Polarization is treated exactly for both the initial and final states. Final-state quark or lepton flavors can be summed over automatically where needed. For ILC physics, beamstrahlung (`CIRCE`) and initial-state radiation spectra are included for electrons and photons. Exact color flow information is maintained, which is used when fragmenting and hadronizing events with the built-in `PYTHIA` interface. The events can be written to file in STDHEP or ASCII format.

Currently, `WHIZARD` supports the Standard Model and the MSSM, optionally with anomalous couplings, but model extensions or completely different models can be added. Higgs production and decay couplings, and spectra in the case of the MSSM, are adopted from the corresponding matrix element generator.

Chapter 6

Interplay between LHC and ILC in the Higgs Sector

If a Higgs-like state is discovered at the LHC and the ILC, independent of the realization of the Higgs mechanism, important synergistic effects arise from the interplay of LHC and ILC [12].

6.1   Overview

If a state resembling a Higgs boson is detected, it is crucial to experimentally test its nature as a Higgs boson. To this end the couplings of the new state to as many particles as possible must be precisely determined, which requires observation of the candidate Higgs boson in several different production and decay channels. Furthermore the spin and the other CP-properties of the new state need to be measured, and it must be clarified whether there is more than one Higgs state. The LHC will be able to address some of these questions, but in order to make further progress a comprehensive program of precision Higgs measurements at the ILC will be necessary. While the ILC will provide a wealth of precise experimental information on a light Higgs boson, the LHC may be able to detect heavy Higgs bosons which lie outside the kinematic reach of the ILC (it is also possible, however, that the ILC will detect a heavy Higgs boson that is not experimentally observable at the LHC due to overwhelming backgrounds). Even in the case where only one scalar state is accessible at both colliders, important synergistic effects arise from the interplay of LHC and ILC. This has been demonstrated for the example of the Yukawa coupling of the Higgs boson to a pair of top quarks, see below.

The LHC and the ILC can successfully work together in determining the CP properties of the Higgs bosons. In an extended Higgs sector with CP violation there is a non-trivial mixing between all neutral Higgs states. Different measurements at the LHC and the ILC (in both the electron–positron and the photon–photon collider options) have sensitivity to different coupling parameters. In the decoupling limit, the lightest Higgs boson is an almost pure CP-even state, while the heavier Higgs states may contain large CP-even and CP-odd components. Also in this case, high-precision measurements of the properties of the light Higgs boson at the ILC may reveal small deviations from the SM case, while the heavy Higgs bosons might only be accessible at the LHC. In many scenarios, for instance the MSSM, CP-violating effects are induced via loop corrections. The CP properties therefore depend on the particle spectrum. The interplay of precision measurements in the Higgs sector from the ILC and information on the SUSY spectrum from the LHC can therefore be important for revealing the CP structure. As an example, if CP-violating effects in the Higgs sector in a SUSY scenario are established at the ILC, one would expect CP-violating couplings in

the scalar top and bottom sector. The experimental strategy at the LHC could therefore focus on the CP properties of scalar tops and bottoms.

While the most studied Higgs boson models are the SM and the MSSM, more exotic realisations of the Higgs sector cannot be ruled out. Thus, it is important to explore the extent to which search strategies need to be altered in such a case.

A possible scenario giving rise to non-standard properties of the Higgs sector is the presence of large extra dimensions, motivated for instance by a "fine-tuning" and "little hierarchy" problem of the MSSM, see Sect. 4.15. A popular class of such models comprise those in which some or all of the SM particles live on 3-branes in the extra dimensions. Such models inevitably require the existence of a radion (the quantum degree of freedom associated with fluctuations of the distance between the 3-branes or the size of the extra dimension(s)). The radion has the same quantum numbers as the Higgs boson, and in general the two will mix. Since the radion has couplings that are very different from those of the SM Higgs boson, the two physical eigenstates will have unusual properties corresponding to a mixture of the Higgs and radion properties; the prospects for detecting them at the LHC and ILC must be carefully analysed. In cases of this kind the ILC can observe both the Higgs boson and the radion, and covers most of the parameter space where detection of either state at the LHC is difficult.

A case where the LHC detects a heavy (500 GeV–1 TeV) SM-like Higgs boson rather than a light CP-even Higgs boson, as apparently needed to satisfy precision electroweak constraints, can also occur in a general two-Higgs-doublet model. The source of the extra contributions mimicking the effect of a light Higgs boson in the electroweak precision tests may remain obscure in this case. The significant improvement in the accuracy of the electroweak precision observables obtainable at the ILC running in the GigaZ mode and at the WW threshold will be crucial to narrow down the possible scenarios.

Another challenging SUSY scenario is the MSSM with an extra singlet (NMSSM, see Sect. 4.7), especially if the extra singlet dominates the lightest Higgs. While such a state has reasonably large production cross sections at the LHC, it would be difficult to detect as it mainly decays hadronically. Such a state could be discovered at the ILC. From the measurement of its properties, the masses of the heavier Higgs bosons could be predicted, guiding in this way the searches at the LHC. For a very heavy singlet-dominated Higgs state, on the other hand, the kinematic reach of the LHC will be crucial in order to verify that a non-minimal Higgs sector is realised. Thus, input from both the LHC and the ILC will be needed in order to provide complete coverage of the NMSSM parameter space.

If no light Higgs boson exists, quasi-elastic scattering processes of W and Z bosons at high energies provide a direct probe of the dynamics of electroweak symmetry breaking. The amplitudes can be measured in 6-fermion processes both at the LHC and the ILC. The two colliders are sensitive to different scattering channels and yield complementary information. The combination of LHC and ILC data will considerably increase the LHC resolving power. In the low-energy range it will be possible to measure anomalous triple gauge couplings down to the natural value of $1/16\pi^2$. The high-energy region where resonances may appear can be accessed at the LHC only. The ILC, on the other hand, has an indirect sensitivity to the effects of heavy resonances even in excess of the direct search reach of the LHC. Detailed measurements of cross sections and angular distributions at the ILC will be crucial for making full use of the LHC data.

6.2 Higgs coupling determination

6.2.1 Combined LHC/ILC analysis

At the LHC, without any theory assumption, no coupling measurement of a Higgs boson can be performed. With "mild" theory assumptions one might hope for a $t\bar{t}H$ coupling measurement at the level of 12-19% [7]. At the ILC, on the other hand, the $t\bar{t}H$ coupling can be measured only at high energies, $\sqrt{s} \gtrsim 800$ GeV. However, even in the first stage of the ILC, the $\sqrt{s} = 500$ GeV data can be combined with the LHC data on Higgs branching ratios to obtain information about the $t\bar{t}H$ coupling (see Ref. [352] for a first evaluation). Using information from all Higgs production and decay modes at the LHC [7] and from the ILC, i.e.,

- M_H,

- $\sigma_{\mathrm{tot}}(e^+ e^- \to HZ)$,

- $\sigma_{\mathrm{tot}}(e^+ e^- \to HZ) \times \mathrm{BR}(H \to X)$ ($X = b\bar{b}$, $\tau^+ \tau^-$, gg, WW^*), and

- $\sigma_{\mathrm{tot}}(e^+ e^- \to \nu\bar{\nu}H) \times \mathrm{BR}(H \to b\bar{b})$,

a determination of $g_{t\bar{t}H}$ down to the level of 11-14% can be performed without any additional assumptions on the underlying theory (for $m_H \lesssim 200$ GeV, and assuming SM-like BR measurements) [353].

In a similar way the coupling of the Higgs boson to photons can be constrained in a better way than with the LHC or the ILC results alone. In the combined analysis of LHC and ILC data [353] (with the ILC running at $\sqrt{s} = 500$ GeV and without the $\gamma\gamma$ collider option) the $\gamma\gamma H$ coupling can be determined to the level of 7-8% for $m_H \lesssim 200$ GeV (and assuming SM-like BR measurements).

6.2.2 Model-Independent Analysis for the Higgs Boson Couplings

Once the (lightest) Higgs boson is found at the LHC, its mass, production cross section, and decay branching ratios will be measured as precisely as possible at the LHC and the ILC in order to determine the Higgs boson couplings to gauge bosons and fermions. The predictions for these couplings differ among various models beyond the SM. By determining these couplings accurately, these models may be distinguished, even when no further new particle is found.

These Higgs boson couplings may be written in a model-independent way as [10, 35],

$$\mathcal{L} = x\frac{m_b}{v}h\bar{b}b + y(\frac{m_t}{v}h\bar{t}t + \frac{m_c}{v}h\bar{c}c) + z\frac{m_\tau}{v}h\bar{\tau}\tau + u(gm_W hW_\mu W^\mu + \frac{g_Z}{2}m_Z hZ_\mu Z^\mu),$$

where the four parameters x, y, z, and u represent the multiplicative factors in the Higgs-boson coupling constants with down-type quarks, up-type quarks, charged-leptons and massive gauge bosons, respectively. The SM corresponds to $x = y = z = u = 1$. This expression is valid at lowest order in the SM, MSSM, NMSSM and multi Higgs doublet models without tree-level flavor mixing. The expected accuracy of the parameter determination has been evaluated with respect to the SM case. It has been shown that the u and x parameters are determined to the few-percent level, and y and z are constrained to less than 10%. From the correlation of the four parameters determined at the ILC, it may also be possible to distinguish various models. For example, the Type-I two-Higgs-doublet model, which predicts the relation $x=y$, and the MSSM lie in different regions of the x-y space. For a large $\tan\beta$ value, the allowed range of the x-z space can deviate from the $x=z$ line for the MSSM because of the SUSY corrections to the $hb\bar{b}$ vertex [107, 354].

6.3 What if Only a Light Higgs and Nothing Else is Found at the LHC?

If (only) a state resembling a Higgs boson is detected, it is crucial to experimentally test its nature as a Higgs boson. The couplings of the supposed Higgs boson to as many particles as possible must measured; see also the previous subsection. Furthermore the spin and the other CP-properties of the new state need to be measured. The LHC will be able to address some of these questions, but in order to make further progress a comprehensive program of precision Higgs measurements at the ILC will be necessary. The significance of the precision Higgs program is particularly evident from the fact that many extended Higgs theories over a wide part of their parameter space have a lightest Higgs scalar with nearly identical properties to those of the SM Higgs boson. In this decoupling limit additional states of the Higgs sector are heavy and may be difficult to detect both at the LHC and ILC.

6.3.1 Indirect Determination of the Heavy Higgs Boson Masses in the MSSM

In the MSSM, information on the heavy Higgs boson masses can be extracted from the experimental information on branching ratios of the lightest Higgs boson [355] (see also Ref. [356] for an earlier study).

The analysis has been performed in an SPS 1a–based scenario [117], where M_A has been kept as a free parameter, but so heavy that the LHC only detects one light Higgs boson. For the parameters of the SPS 1a scenario this corresponds to the region $M_A \gtrsim 400$ GeV.

The precise measurements of Higgs branching ratios at the ILC together with accurate determinations of (parts of) the SUSY spectrum at the LHC and the ILC (see Ref. [12]) will allow in this case to obtain indirect information on M_A (for a discussion of indirect constraints on M_A from electroweak precision observables, see Ref. [53]). When investigating the sensitivity to M_A it is crucial to take into account realistic experimental errors on the other SUSY parameters that enter the prediction of the Higgs branching ratios. In Ref. [355] all the SUSY parameters have been varied according to error estimates for the measurements at LHC and ILC in this scenario. The sbottom masses and the gluino mass can be obtained from mass reconstructions at the LHC with ILC input; see Ref. [12]; the precisions have been assumed to be $\Delta m_{\tilde{g}} = \pm 8$ GeV and $\Delta m_{\tilde{b}_{1,2}} \approx \pm 7.5$ GeV. The lighter stop (which in the SPS 1a scenario has a mass of about 400 GeV, see Ref. [117]) will be accessible at the ILC, leading to an accuracy of about $\Delta m_{\tilde{t}_1} = \pm 2$ GeV. The the stop mixing angle, $\theta_{\tilde{t}}$, can also be determined with high accuracy [355]. For $\tan\beta$ an uncertainty of $\Delta\tan\beta = 10\%$ has been used (this accuracy can be expected from measurements at the ILC in the gaugino sector for the SPS 1a value of $\tan\beta = 10$ [357]). Concerning the top quark mass an error of $\Delta m_t = \pm 0.1$ GeV has been assumed from the ILC, so that the parametric uncertainties on the m_h predictions become negligible. m_h is measured at the ILC with high accuracy, but a theory error from unknown higher-order corrections of ± 0.5 GeV has been included [17].

The analysis is based on the comparison of the theoretical prediction [52, 358] for the ratio of branching ratios

$$r \equiv \frac{[\mathrm{BR}(h \to b\bar{b})/\mathrm{BR}(h \to WW^*)]_{\mathrm{MSSM}}}{[\mathrm{BR}(h \to b\bar{b})/\mathrm{BR}(h \to WW^*)]_{\mathrm{SM}}} \tag{6.1}$$

with its prospective experimental measurement. Even though the experimental error on the ratio of the two BR's is larger than that of the individual BR's, the quantity r has a stronger sensitivity to M_A than any single branching ratio.

Assuming a certain precision of r, indirect bounds on M_A can be obtained. For the experimental accuracy of r two different values have been considered: a 4% accuracy resulting from a first phase of

ILC running with $\sqrt{s} \lesssim 500$ GeV [8–10,359], and a 1.5% accuracy which can be achieved from ILC running at $\sqrt{s} \approx 1$ TeV [91]. Fig. 6.1 shows that a 4% accuracy on r allows to establish an indirect upper bound on M_A for M_A values up to $M_A \lesssim 800$ GeV (corresponding to an r measurement of $r \gtrsim 1.1$). With an accuracy of 1.5%, on the other hand, a precision on $\Delta M_A / M_A$ of approximately 20% (30%) can be achieved for $M_A = 600$ (800) GeV. The indirect sensitivity extends to even higher values of M_A. The comparison with the idealized situation where all SUSY parameters (except M_A) were precisely known illustrates the importance of taking into account the parametric errors as well as the theory errors from unknown higher-order corrections. Detailed experimental information on the SUSY spectrum and a precision measurement of m_t are clearly indispensable for exploiting the experimental precision on r.
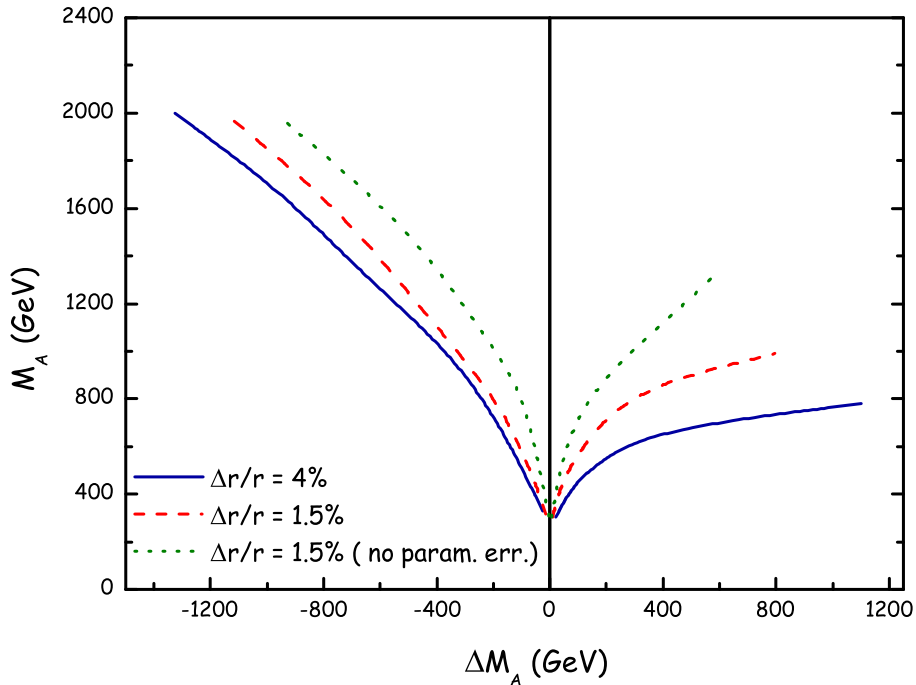
Figure 6.1: The 1σ bound on M_A, ΔM_A, versus M_A obtained from a comparison of the precision measurement of r (see text) at the ILC with the MSSM prediction. The results for ΔM_A are shown for a 4% accuracy of r (full line) and a 1.5% accuracy of r (dashed line). The parametric uncertainties in the prediction of r resulting from LHC/ILC measurement errors on $\tan\beta, m_{\tilde{b}_{1,2}}, m_{\tilde{t}_1}, m_{\tilde{g}}, m_h$, and m_t are taken into account. Also shown is the accuracy on M_A which would be obtained if these uncertainties were neglected (dotted line).

6.3.2 Distinction between the MSSM and the NMSSM

It is possible that the MSSM and the NMSSM result in similar low-energy phenomenology. Then neither the LHC nor the ILC alone can identify one or the other model. Especially the Higgs sector does not allow the identification of the NMSSM [187] if scalar and/or pseudoscalar Higgs bosons with dominant singlet character escape detection due to their suppressed couplings to the other MSSM particles. This is illustrated in one specific example. The scenario is fixed by $\mu_{\mathrm{eff}} = 457.5$ GeV, $\tan\beta = 10$, $\lambda = 0.5$ and $\kappa = 0.2$. A scan over the remaining parameters in the Higgs sector, the trilinear couplings A_λ and A_κ, has been performed using NMHDECAY [181]. The
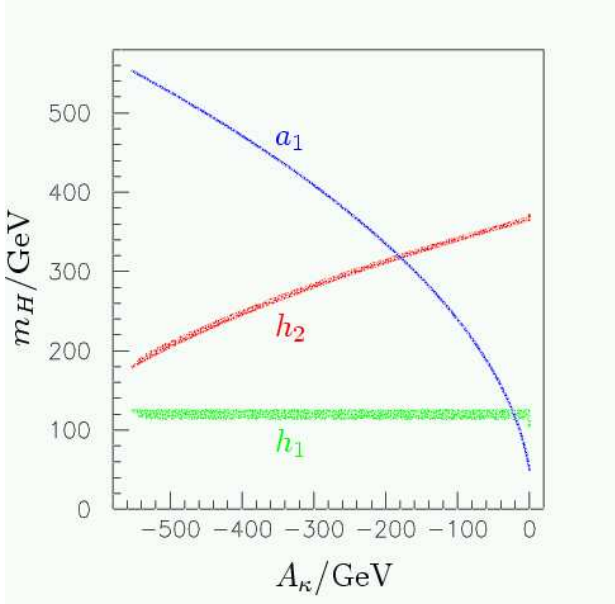
Figure 6.2: The masses of the two light scalar Higgs bosons, m_{h_1}, m_{h_2}, and of the lightest pseudoscalar Higgs boson m_{a_1} as function of the trilinear Higgs coupling A_κ in the NMSSM for $\mu_{\mathrm{eff}} = 457.5$ GeV, $\tan\beta = 10$, $\lambda = 0.5$ and $\kappa = 0.2$, while A_λ and A_κ have been scanned over all possible values. h_1 is MSSM-like whereas h_2 and a_1 are singlet-dominated Higgs particles.

parameter points which survive the theoretical and experimental constraints are in the region 2740 GeV $< A_\lambda <$ 5465 GeV and -553 GeV $< A_\kappa < 0$, see Fig. 6.2. In this parameter region the lightest scalar Higgs boson h_1 is always MSSM-like whereas the second lightest scalar h_2 and the lightest pseudoscalar a_1 are singlet-dominated. For -450 GeV $\lesssim A_\kappa \lesssim -100$ GeV h_2 and a_1 have very pure singlet character and masses $\gtrsim 200$ GeV, which excludes their appearance in chargino/neutralino decays in this scenario. All other heavier Higgs bosons have masses of $\mathcal{O}(A_\lambda)$, hence they cannot be produced at the LHC or the ILC. In this case a combined LHC/ILC analysis in the neutralino sector, as carried out in Ref. [360], is necessary. It can find the phenomenological differences between the two models and thus reveal also the nature of the Higgs sector.

For $A_\kappa \lesssim -450$ GeV the smaller mass of the h_2 and a stronger mixing between the singlet and MSSM-like states in h_1 and h_2 might allow a discrimination in the Higgs sector while for $A_\kappa \gtrsim -100$ GeV the existence of a light pseudoscalar a_1 may give the first hints of the NMSSM [361]. See Sect. 4.7 for further details.

Chapter 7

Cosmological connections

7.1 Cold dark matter and MSSM Higgs physics

A large fraction of the total amount of matter in the universe appears to be cold dark matter (CDM). The density of CDM in the universe is tightly constrained by WMAP and other astrophysical and cosmological data [362]. Within the MSSM (or other supersymmetric extensions of the SM) it is well known that the lightest supersymmetric particle (LSP) is an excellent candidate for cold dark matter [363], with a density that falls naturally within the range [362],

$$0.094 < \Omega_{\text{CDM}} h^2 < 0.129 \ . \tag{7.1}$$

Assuming that the cold dark matter is composed predominantly of the lightest neutralino, a value of $\Omega_{\text{CDM}} h^2 \sim 1$ can easily be obtained. However, in order to exactly match eq. (7.1) a mechanism in the early universe is needed that efficiently reduces the CDM density.

One possible mechanism is the rapid Higgs pole annihilation,

$$\tilde{\chi}_1^0 \, \tilde{\chi}_1^0 \to A \to b\bar{b} \ , \tag{7.2}$$

involving the pseudo-scalar MSSM Higgs boson. This mechanism is very efficient for $M_A \approx 2 \, m_{\tilde{\chi}_1^0}$. The role of the ILC is to determine with high accuracy the masses and couplings of the involved particles in the process in eq. (7.2). The corresponding theoretical determination of Ω_{CDM} then has to match the experimental value of eq. (7.1).

At leading order the annihilation cross section is given by

$$\sigma_{\tilde{\chi}\tilde{\chi} \to A \to \text{all}} \approx \frac{2 \, y_{A\tilde{\chi}\tilde{\chi}}^2 \, \Gamma_A}{M_A} \frac{s_{\tilde{\chi}\tilde{\chi}}}{(s_{\tilde{\chi}\tilde{\chi}} - M_A^2)^2 + \Gamma_A^2 M_A^2}, \tag{7.3}$$

where $s_{\tilde{\chi}\tilde{\chi}}$ is the invariant mass of the two LSPs in the initial state, and $y_{A\tilde{\chi}\tilde{\chi}}$ is the coupling of the A to the two lightest neutralinos, given by

$$y_{A\tilde{\chi}\tilde{\chi}} = \frac{1}{2} \left(g_1 N_{11} - g_2 N_{12} \right) \left(\sin\beta N_{13} - \cos\beta N_{14} \right) \ , \tag{7.4}$$

with N being the unitary matrix that diagonalizes the neutralino mass matrix.

The uncertainty of the experimental measurement of the CDM density as shown in eq. (7.1) is currently at the 10% level. How this accuracy can be matched by experimental analyses and theoretical evaluations will be discussed in the following subsections.

The next generation of CDM experiments like PLANCK [364] will improve the precision of Ω_{CDM} down to about 2%. This will require additional efforts both from the experimental as well as from the theoretical side.

7.2 Experimental issues

The main quantities that enter the theoretical calculation of eq. (7.2) are the mass of the CP-odd Higgs boson, M_A, and its width, Γ_A, see eq. (7.3). They have to be determined with the highest possible accuracy.

The ILC provides a unique tool to investigate the heavy MSSM Higgs bosons via the channels

$$e^+e^- \quad \rightarrow \quad AH \rightarrow b\bar{b}\,b\bar{b} \tag{7.5}$$

$$e^+e^- \quad \rightarrow \quad AH \rightarrow b\bar{b}\,\tau^+\tau^- \ . \tag{7.6}$$

Corresponding analyses can be found in Refs. [98, 365, 366]. The precision that can be reached in M_A depends on the mass splitting between H and A. In most cases this splitting is too small to be disentangled at the ILC. Assuming zero splitting a mass determination better than ~ 1 GeV can be reached [98]. The Higgs boson width, for realistic values of $\Gamma_A \gtrsim 10$ GeV could be determined at the 30-50% level only.

In Ref. [366] two CMSSM points with $M_H \approx M_A \approx 400$ GeV have been analyzed, assuming 1 ab^{-1}of integrated luminosity at $\sqrt{s} = 1$ TeV. Here the mass average, $1/2(M_A + M_H)$ could be determined to $\sim \pm 2.5$ GeV, whereas the mass difference, $1/2(M_A - M_H)$ could be measured to about ± 5 GeV. The Higgs boson width was determined better than about 25%. Assuming that all other relevant quantities, see Sect. 7.3, are known with negligible uncertainty, the authors used DarkSUSY [367] to evaluate the corresponding CDM density. The precision of $\Omega_{\mathrm{CDM}}h^2$ was in the 20% range, i.e., about a factor of two larger than the current experimental precision. This would become even worse if all other experimental uncertainties were included.

Other experimental aspects are the neutralino properties. In order to determine $s_{\tilde{\chi}\tilde{\chi}}$, a measurement of the LSP mass is necessary. However, this can be achieved at the ~ 50 MeV level [8]. Furthermore the coupling of the lightest neutralinos to the A has to be measured. Either $y_{A\tilde{\chi}\tilde{\chi}}$ has to be measured directly (which would be very difficult), or the various elements entering eq. (7.4) have to be measured. Further experimental studies in this directions are required.

The current experimental uncertainty of $\sim 10\%$ in $\Omega_{\mathrm{CDM}}h^2$ requires a precise determination of M_A and Γ_A down to the level of $\sim 1\%$ for the Higgs boson mass and of about $\sim 10\%$ for the Higgs boson width. While the first goal seems feasible [98], the second one is very challenging. The situation is complicated by the strong correlation which exists between the measured widths of the H and A bosons and the finite mass difference between these physical states. A more precise determination of heavy Higgs widths would require higher integrated luminosities as well as improved analyses. The latter should include the study of additional signal channels, e.g., the Yukawa process $e^+e^- \rightarrow Ab\bar{b}$, and a more sophisticated treatment of correlation between Γ_A, Γ_H and $M_A - M_H$. It was shown [98] that by combining analyses in the $HA \rightarrow b\bar{b}b\bar{b}$ and $HA \rightarrow b\bar{b}b\tau^+\tau^-$ channels, the A boson width can be determined with a relative accuracy of about 40% for $M_A \sim M_H$ = 300 GeV, assuming 500 fb^{-1} of integrated luminosity collected at 800 GeV centre-of-mass energy. Assuming a $1/\sqrt{N_{event}}$ dependence of the relative precision of this measurement, the accuracy can be improved to 20% if 2000 fb^{-1} of luminosity is accumulated at 800 GeV centre-of-mass energy. Further improvement can be achieved by inclusion of the Yukawa process $e^+e^- \rightarrow Ab\bar{b}(Hb\bar{b})$. Combining the mass lineshape analysis in the $e^+e^- \rightarrow Ab\bar{b}(Hb\bar{b})$ channel with the $HA \rightarrow b\bar{b}b\bar{b}$ and $HA \rightarrow b\bar{b}b\tau^+\tau^-$ channels would allow to improve the measurement of Γ_A, in particular at high $\tan\beta$ values where the $e^+e^- \rightarrow Ab\bar{b}$ process is expected to have an enhanced rate. On the other hand, Γ_A can be determined by combining mesurements of BR$(A \rightarrow b\bar{b})$ and the rate of the $e^+e^- \rightarrow Ab\bar{b}$ process. The first measurement can be performed by exploiting the $e^+e^- \rightarrow HA$ process, while the second provides direct access to the partial width $\Gamma_{A \rightarrow b\bar{b}}$. The total width is then calculated as $\Gamma_A = \Gamma_{A \rightarrow b\bar{b}}/BR(A \rightarrow b\bar{b})$. Again, the precision of measurement will crucially

depend on the expected rate in the $e^+e^- \to A b\bar{b}$ channel, which is governed by $\tan\beta$. Clearly, given the relatively poor precision on Γ_A predicted by currently existing analyses, the proposed ways to improve the experimental accuracy on Γ_A should be investigated by future studies.

In order to match the anticipated PLANCK accuracy for $\Omega_{\mathrm{CDM}}h^2$ of about 2%, a much better precision in M_A and Γ_A will be necessary. The mass will have to be known at the $\sim 0.25\%$ level, whereas the width would require a $\sim 3\%$ accuracy. These goals are extremely ambitious and invite further investigations.

7.3 Theoretical issues

The theoretical calculation of $\Omega_{\mathrm{CDM}}h^2$ also requires a precise evaluation of eq. (7.3). The one-loop corrections to eq. (7.3) are expeted at the $\mathcal{O}(\mathrm{few}\%)$. Consequently, they can be omitted at the present level of accuracy. However, in order to match the anticipated Planck precision of about $\sim 2\%$ a calculation of the leading one-loop corrections is necessary. Since for the 'inverse' process, $e^+e^- \to \tilde{\chi}^0_1\tilde{\chi}^0_1$, a full one-loop calculation exists [368], the tools for the required calculation appear to be available.

Even if the heavy Higgs boson are not observed at the LHC and the ILC, the additional information from the ILC can be valuable: the calculation of $\Omega_{\mathrm{CDM}}h^2$ can also incur large uncertainties due to the lack of sufficiently stringent lower bounds on the masses of A and H. We show this fact in Fig. 7.1 [369, 370]. Here we display the variation in $\Omega_{\mathrm{CDM}}h^2$ caused only by a variation in
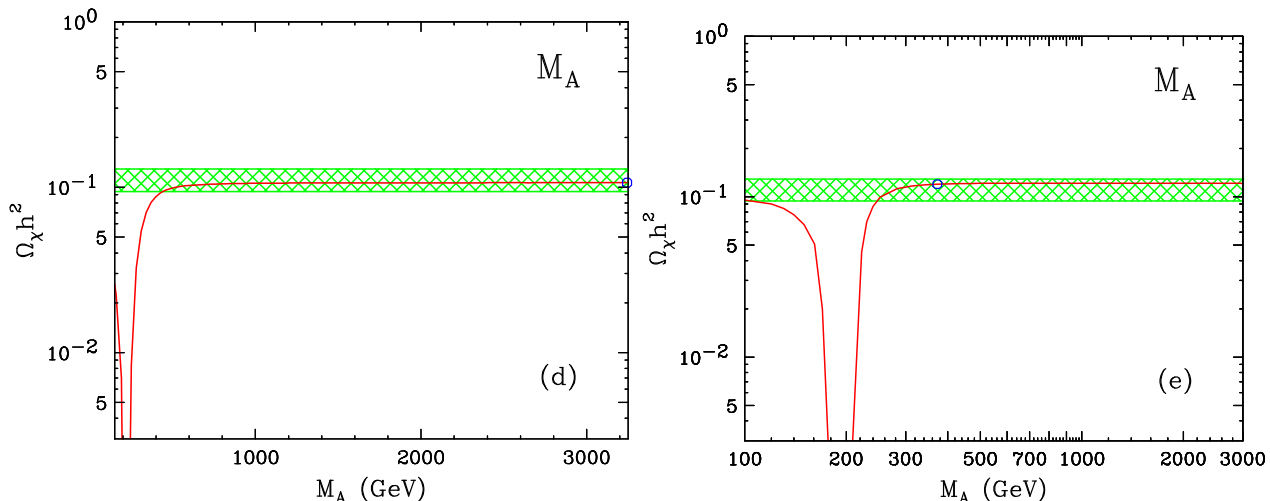
Figure 7.1: Effect on relic density of varying the SUSY mass parameter M_A for point B$'$ from the bulk region of mSUGRA (left plot) and the point LCC2 from the focus point region of mSUGRA (right plot). The horizontal (green-shaded) region denotes the 2σ WMAP limits on the dark matter relic density. The red line shows the variation of the relic density as a function of M_A. The blue dot in each plot denotes the nominal value for M_A at point B$'$ (left plot) and the point LCC2 (right plot). Taken from Refs. [369, 370].

M_A. In the left plot, we have chosen as our nominal point one from the 'bulk' region of mSUGRA parameter space. The blue circle identifies the nominal values of $\Omega_{\mathrm{CDM}}h^2$ and M_A for the point. The green cross-hatched region denotes values consistent with the WMAP determination of the relic density. The red line illustrates how the value of $\Omega_{\mathrm{CDM}}h^2$ changes as the parameter M_A is changed. Since the slope of the red line is small as it passes through the nominal value, $\Omega_{\mathrm{CDM}}h^2$

appears rather insensitive to the exact value of M_A. However, it is possible that the value of M_A cannot be determined at a collider (if $\sqrt{s} = 500$ GeV for example), and only a lower bound can be attained. If this is the case, when calculating $\Omega_{\mathrm{CDM}}h^2$, one must allow M_A to vary between its lower bound and infinity. From the plot, it is clear that this introduces large uncertainties in $\Omega_{\mathrm{CDM}}h^2$ if the lower bound is not much above 200 GeV. It is likely that this will be the best lower limit available from the LHC at this point [369, 370]. However, a 500 GeV linear collider will raise this lower limit to approximately 250 GeV (and higher energies can give rise to larger increases). From the plot, it can be seen that the extra 50 GeV gained from the ILC will vastly improve the uncertainty in the calculation of $\Omega_{\mathrm{CDM}}h^2$ due to experimental uncertainty in M_A. The right plot shows the same story for the case of a point [371] from the 'focus point' region [372]. If the value of M_A can be determined, $\Omega_{\mathrm{CDM}}h^2$ will be very insensitive to its exact numerical value. This is unlikely to happen since $M_A \sim 3$ TeV. However, $\Omega_{\mathrm{CDM}}h^2$ will be very sensitive to the lower experimental bound on M_A if it is around 200 GeV.

7.4 The NMSSM case

7.4.1 Cold dark matter and NMSSM Higgs physics

Since the NMSSM has five neutralinos and two CP-odd Higgs bosons, there are many new ways in which the relic density of the $\tilde\chi_1^0$ could match the observed dark matter density; see, e.g., [201,202]. The latter group has made their code publicly available. In the NMSSM the m_{a_1} and m_{a_2} masses are quite unconstrained by LEP data and theoretical model structure, implying that $\tilde\chi_1^0\tilde\chi_1^0 \to a_{1,2} \to X$ could be the primary annihilation mechanism for large swaths of parameter space. It is relatively easy to construct NMSSM models yielding the correct relic density even for a very light neutralino, $100\ \mathrm{MeV} < m_{\tilde\chi_1^0} < 20\ \mathrm{GeV}$. Even after including constraints from Upsilon decays, $b \to s\gamma$, $B_s \to \mu^+\mu^-$ and the magnetic moment of the muon, a light bino or singlino neutralino is allowed that can generate the appropriate relic density.

The LSP is a mixture of the bino, neutral wino, neutral higgsinos and singlino, which is the superpartner of the singlet Higgs. The lightest neutralino therefore has a singlino component in addition to the four MSSM components; its eigenvector $\tilde\chi_1^0$ can be written in terms of gauge eigenstates in the form

$$\tilde\chi_1^0 = \epsilon_u\tilde{H}_u^0 + \epsilon_d\tilde{H}_d^0 + \epsilon_W\tilde{W}^0 + \epsilon_B\tilde{B} + \epsilon_s\tilde{S}, \tag{7.7}$$

where ϵ_u, ϵ_d are the up-type and down-type higgsino components, ϵ_W, ϵ_B are the wino and bino components and ϵ_s is the singlet component of the lightest neutralino. Similarly, the CP-even and CP-odd Higgs states are mixtures of MSSM-like Higgses and singlets. For the lightest CP-even Higgs state we can define (see also Sect. 4.7.1)

$$h_1 = \frac{1}{\sqrt{2}}\left[\xi_u\mathrm{Re}\left(H_u^0 - v_u\right) + \xi_d\mathrm{Re}\left(H_d^0 - v_d\right) + \xi_s\mathrm{Re}\left(S - s\right)\right]. \tag{7.8}$$

Here, Re denotes the real component of the respective state. Lastly, the lightest CP-odd Higgs can be written as (a similar formula also applies for the heavier a_2)

$$a_1 = \cos\theta_{a_1}A_{\mathrm{MSSM}} + \sin\theta_{a_1}A_s, \tag{7.9}$$

where A_s is the CP-odd piece of the singlet and A_{MSSM} is the state that would be the MSSM pseudoscalar Higgs if the singlet were not present. Here, θ_{a_1} is the mixing angle between these two states.

In the NMSSM context, when annihilation proceeds via one of the CP-odd Higgs bosons the calculation of the relic $\tilde{\chi}_1^0$ density is much more flexible than in the MSSM; see Sect. 7.1. The general formula for the thermally averaged cross section takes the form

$$\langle \sigma v \rangle \approx \frac{g_2^4 c_f m_f^2 \cos^4 \theta_{a_1} \tan^2 \beta}{8\pi m_W^2} \frac{m_{\tilde{\chi}_1^0}^2 \sqrt{1 - m_f^2/m_{\tilde{\chi}_1^0}^2}}{(4m_{\tilde{\chi}_1^0}^2 - m_{a_1}^2)^2 + m_{a_1}^2 \Gamma_{a_1}^2} \tag{7.10}$$

$$\times \left[-\epsilon_u(\epsilon_W - \epsilon_B \tan\theta_W)\sin\beta + \epsilon_d(\epsilon_W - \epsilon_B \tan\theta_W)\cos\beta \right.$$

$$\left. + \sqrt{2}\frac{\lambda}{g_2}\epsilon_s(\epsilon_u \sin\beta + \epsilon_d \cos\beta) + \frac{\tan\theta_{a_1}}{g_2}\sqrt{2}(\lambda\epsilon_u\epsilon_d - \kappa\epsilon_s^2) \right]^2,$$

where c_f is a color factor, equal to 3 for quarks and 1 otherwise. For this result, we have assumed that the final state fermions are down-type. If they are instead up-type fermions, the $\tan^2\beta$ factor should be replaced by $\cot^2\beta$. For medium to large values of $\tan\beta$, neutralino dark matter can avoid being overproduced for any a_1 mass below $\sim 20-60$ GeV, as long as $m_{\tilde{\chi}_1^0} > m_b$. For smaller values of $\tan\beta$, a lower limit on m_{a_1} can apply as well.
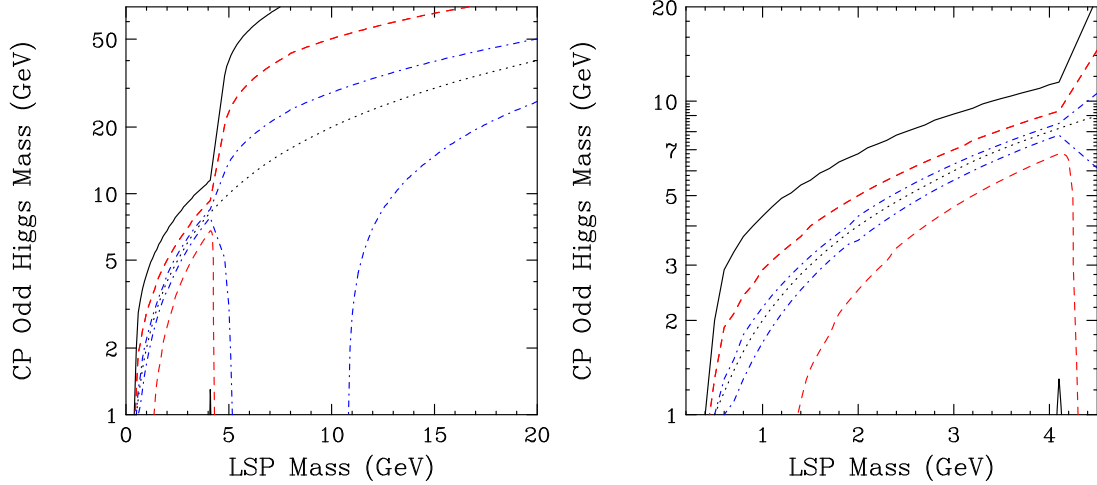
Figure 7.2: We display contours in $m_{a_1} - m_{\tilde{\chi}_1^0}$ parameter space for which $\Omega h^2 = 0.1$. Points above or below each pair of curves produce more dark matter than is observed; inside each set of curves less dark matter is produced than is observed. These results are for a bino-like neutralino with a small higgsino admixture ($\epsilon_B^2 = 0.94$, $\epsilon_u^2 = 0.06$). Three values of $\tan\beta$ (50, 15 and 3) have been used, shown as solid black, dashed red, and dot-dashed blue lines, respectively. The dotted line is the contour corresponding to $2m_{\tilde{\chi}_1^0} = m_{a_1}$. For each set of lines, we have set $\cos^2\theta_{a_1} = 0.6$.

Fig. 7.2 shows typical NMSSM results. There, the a_1 composition is chosen such that $\cos^2\theta_{a_1} = 0.6$ and the neutralino composition is specified by $\varepsilon_B^2 = 0.94$ and $\varepsilon_u^2 = 0.06$. These specific values are representative of those that can be achieved for various NMSSM parameter choices satisfying all constraints. For each pair of contours (solid black, dashed red, and dot-dashed blue), $\Omega h^2 = 0.1$ along the contours and the region between the lines is the space in which the neutralino's relic density obeys $\Omega h^2 < 0.1$. The solid black, dashed red, and dot-dashed blue lines correspond to $\tan\beta$=50, 15 and 3, respectively. Also shown as a dotted line is the contour corresponding to the resonance condition, $2m_{\tilde{\chi}_1^0} = m_{a_1}$. For the $\tan\beta$=50 or 15 cases, neutralino dark matter can avoid

being overproduced for any a_1 mass below $\sim 20-60$ GeV, as long as $m_{\tilde{\chi}_1^0} > m_b$. For smaller values of $\tan\beta$, a lower limit on m_{a_1} can apply as well.

For neutralinos lighter than the mass of the b-quark, annihilation is generally less efficient. This region is shown in detail in the right frame of Fig. 7.2. In this funnel region, annihilations to $c\bar{c}$, $\tau^+\tau^-$ and $s\bar{s}$ all contribute significantly. Despite the much smaller mass of the strange quark, its couplings are enhanced by a factor proportional to $\tan\beta$ (as with bottom quarks) and thus can play an important role in this mass range. In this mass range, constraints from Upsilon and J/ψ decays can be very important, often requiring fairly small values of $\cos\theta_{a_1}$.

The above discussion focused on the case of a mainly bino LSP. If the LSP is mostly singlino, it is also possible to generate the observed relic abundance in the NMSSM. A number of features differ for the singlino-like case in contrast to a bino-like LSP, however. Most importantly, an LSP mass that is chosen to be precisely at the Higgs resonance, $m_{a_1} \simeq 2m_{\tilde{\chi}_1^0}$, is not possible for this case: m_{a_1} is always less than $2m_{\tilde{\chi}_1^0}$ by a significant amount. Second, in models with a singlino-like LSP, the a_1 is generally also singlet-like and the product of $\tan^2\beta$ and $\cos^4\theta_{a_1}$, to which annihilation rates are proportional, see Eq. (7.10), is typically very small. This limits the ability of a singlino-like LSP to generate the observed relic abundance. The result is that annihilation is too inefficient for an LSP that is more than 80% singlino. However, there is no problem having $m_{\tilde{\chi}_1^0} \sim m_{a_1}/2$ so as to achieve the correct relic density when the $\tilde{\chi}_1^0$ is mainly bino while the a_1 is mainly singlet.

Finally, for the scenarios with a low F value (see eq. (4.12)), one has $m_{a_1} < 2m_b$ and the a_1 is very singlet-like, with $\cos^2\theta_{a_1} \lesssim 0.015$. In this case, adequate annihilation of a very light $\tilde{\chi}_1^0$ via $\tilde{\chi}_1^0\tilde{\chi}_1^0 \to a_1 \to X$ occurs only if $m_{\tilde{\chi}_1^0} \simeq m_{a_1}/2$. This requires a rather fine adjustment of the M_1 bino soft mass relative to m_{a_1}. Because the a_1 is so light in the low fine-tuning scenarios, if $m_{\tilde{\chi}_1^0}$ is significantly above $2m_b$ then consistency with relic abundance limits requires that $\tilde{\chi}_1^0\tilde{\chi}_1^0$ annihilation proceed via one of the more conventional co-annihilation channels or via $\tilde{\chi}_1^0\tilde{\chi}_1^0 \to a_2 \to X$. The latter case is only applicable if $m_{\tilde{\chi}_1^0} \gtrsim 200$ GeV (with typically $m_{a_2} \gtrsim 400$ GeV).

7.4.2 Direct dark matter detection

In Ref. [201] it is estimated that the neutralino-proton elastic scattering cross section is on the order of 4×10^{-42} cm^2 (4×10^{-3} fb) for either a bino-like or a singlino-like LSP. This value may be of interest to direct detection searches such as CDMS, DAMA, Edelweiss, ZEPLIN and CRESST. To account for the DAMA data, the cross section would have to be enhanced by a local over-density of dark matter.

Prospects for direct detection of dark matter in the low fine-tuning scenarios are rather constrained. Since the a_1 is so singlet in nature, the only exchange of importance is h_1 exchange. In the low-F scenarios, h_1 is almost entirely H_u. In particular, the H_d component of the h_1 is $\xi_d \sim 0.1$, and correspondingly $\xi_u \sim 0.99$. Whether or not $m_{\tilde{\chi}_1^0}$ is below m_b ($m_{\tilde{\chi}_1^0} < m_b$ requiring annihilation via $\tilde{\chi}_1^0\tilde{\chi}_1^0 \to a_1 \to X$), the typical composition of a bino-like $\tilde{\chi}_1^0$ is such that $\varepsilon_B > 0.8$ and ε_u and ε_d take a range of values from 0.1 up to 0.5. Keeping only the s-quark contribution and the dominant $\varepsilon_d\xi_u$ piece in the external factor, we obtain

$$\sigma_{\text{elastic}} \sim 5 \times 10^{-6}\varepsilon_B^2 \left(\frac{\varepsilon_d}{0.25}\right)^2 \left(\frac{100 \text{ GeV}}{m_{h_1}}\right)^4 \left(\frac{\tan\beta}{10}\right)^2 \quad \text{fb}. \tag{7.11}$$

Although $m_{\tilde{\chi}_1^0}$ can be chosen in the range $\gtrsim 20$ GeV (assuming appropriate coannihilation to achieve proper relic density), which is relatively optimal for experiments like ZEPLIN and CRESST, the predicted cross section is much below their expected sensitivity. If annihilation is via $\tilde{\chi}_1^0\tilde{\chi}_1^0 \to a_1 \to X$, the required mass $m_{\tilde{\chi}_1^0} \simeq m_{a_1}/2 < m_b$ is not very optimal and there would be no hope of direct detection at such experiments.

7.4.3　The role of the ILC

In the case where $m_{\tilde\chi_1^0} \lesssim 20 \div 30$ GeV, and especially if $m_{\tilde\chi_1^0} < m_b$, the best that a hadron collider can do will probably be to set an upper limit on $m_{\tilde\chi_1^0}$. Determining its composition is almost certain to be very difficult. Note that the $m_{\tilde\chi_2^0} - m_{\tilde\chi_1^0}$ mass difference should be large, implying adequate room for $\tilde\chi_2^0 \to Z\tilde\chi_1^0$ and a search for lepton kinematic edges and the like. (Of course, $\tilde\chi_2^0 \to h_1\tilde\chi_1^0$ will also probably be an allowed channel, with associated implications for h_1 detection in SUSY cascade decays.) If the dominant annihilation channel is $\tilde\chi_1^0\tilde\chi_1^0 \to a_1 \to X$, determination of the properties of the a_1 would also be critical. A light singlet-like a_1 is very hard to detect. At best, it might be possible to bound $\cos\theta_{a_1}$ by experimentally establishing an upper bound on the $WW \to a_1a_1$ rate (proportional to $\cos^4\theta_{a_1}$). Thus, the ILC would be absolutely essential. Precise measurement of the $\tilde\chi_1^0$ mass and composition using the standard ILC techniques should be straightforward. A bigger question is how best to learn about the a_1 at the precision level. Of course, we will have lots of a_1's to study from $h_1 \to a_1a_1$ decays. The events will give precise measurements of $g_{ZZh_1}^2\mathrm{BR}(h_1 \to a_1a_1)\mathrm{BR}(a_1 \to X)\mathrm{BR}(a_1 \to Y)$, where $X,Y = b\bar b, \tau^+\tau^-$. The problem will be to unfold the individual branching ratios so as to learn about the a_1 itself. Particularly crucial would be some sort of determination of $\cos\theta_{a_1}$ which enters so critically into the annihilation rate. (One can assume that a $\tan\beta$ measurement could come from other supersymmetry particle production measurements and so take it as given.) There is some chance that $WW \to a_1a_1$ and $Z^* \to Za_1a_1$, with rates proportional to $\cos^4\theta_{a_1}$, could be detected. The $\cos^2\theta_{a_1} = 1$ rates are very large, implying that observation might be possible despite the fact that the low-F scenarios have $\cos^2\theta_{a_1} \lesssim 0.01$. One could also consider whether $\gamma\gamma \to a_1$ production would have an observable signal despite the suppression due to the singlet nature of the a_1. Hopefully, enough precision could be achieved for the a_1 measurements that they could be combined with the $\tilde\chi_1^0$ precision measurements so as to allow a precision calculation of the expected $\tilde\chi_1^0\tilde\chi_1^0 \to a_1 \to X$ annihilation rate. A study of the errors in the dark matter density computation using the above measurements as compared to the expected experimental error for the Ωh^2 measurement is needed.

7.5　Electroweak Baryogenesis and quantum corrections to the triple Higgs boson coupling

Baryogenesis is one of the fundamental cosmological problems. Electroweak baryogenesis [30] is a scenario of baryogenesis at the electroweak phase transition, so that the Higgs sector plays an essentially important role. In the symmetric phase ($T > T_c$), where T_c is the critical temperature, baryon number is generated by sphaleron processes. For successful electroweak baryogenesis, it is required that the sphaleron decouples just after the phase transition. In the SM this condition implies $\varphi_c/T_c \gtrsim 1$, where φ_c is the vacuum expectation value at T_c: i.e., the phase transition is strongly first order. This is qualitatively described in the high temperature expansion, where the effective potential is expressed by

$$V_{\mathrm{eff}} = D(T^2 - T_0^2)\varphi^2 - ET\varphi^3 + \frac{\lambda_T}{4}\varphi^4 + \cdots . \tag{7.12}$$

One can see that $\varphi_c = 2ET_c/\lambda_T$. Hence, the sphaleron decoupling condition yields $E/\lambda_T \gtrsim 0.5$. In the SM, where $E = \frac{1}{4\pi v^3}(2m_W^3 + m_Z^3)$, this gives the upper bound for the mass of the Higgs boson $m_h \lesssim 46$ GeV. A more quantitative analysis shows that the phase transition turns into a smooth cross-over for $m_h \gtrsim 80$ GeV. Therefore, the electroweak baryogenesis cannot be realized in the framework of the SM with the present experimental limit $m_h \gtrsim 114$ GeV [4].

7.5.1 Strong first order phase transition by the additional bosonic loop contribution

The condition of the sphaleron decoupling is compatible with the current experimental results when we consider extensions of the SM, which give larger values of the coefficient E of the cubic term in Eq. (7.12) than in the SM prediction. Some additional bosons can contribute to enhance E at one-loop level when they show the non-decoupling property: i.e., when they receive masses mainly from the vacuum expectation value v. In the MSSM, light stops may be a candidate of such additional bosons [373]. An alternative viable model may be the Two-Higgs-Doublet Model (THDM) [374].

The phenomenological influence of such succesful baryogenesis scenarios on the Higgs physics has been discussed in the THDM and MSSM [75]. It was shown that the condition on the finite temperature effective potential for a successful scenario exactly corresponds to the condition of a large non-decoupling quantum effect due to extra Higgs boson loops on the hhh coupling of the lightest Higgs boson h. In the THDM the leading contributions to the one-loop corrections to the hhh coupling is given in the SM-like limit ($\sin(\alpha - \beta) \simeq -1$) by [74]

$$
\lambda_{hhh}^{\mathrm{eff}}(\mathrm{THDM}) \quad \simeq \quad \frac{3m_h^2}{v}\Big[1 + \frac{m_H^4}{12\pi^2 m_h^2 v^2}\left(1 - \frac{M^2}{m_H^2}\right)^3 + \frac{m_A^4}{12\pi^2 m_h^2 v^2}\left(1 - \frac{M^2}{m_A^2}\right)^3
$$
$$
+ \frac{m_{H^\pm}^4}{6\pi^2 m_h^2 v^2}\left(1 - \frac{M^2}{m_{H^\pm}^2}\right)^3 - \frac{m_t^4}{\pi^2 m_h^2 v^2}\Big], \tag{7.13}
$$

where M is the soft-breaking mass parameter of the discrete Z_2 symmetry.

At finite temperatures, in the case with $M^2 \ll m_\Phi^2$ ($\Phi = H, A, H^\pm$), the coefficient E of the cubic term in Eq. (7.12) is evaluated as $E = \frac{1}{12\pi v^3}(6m_W^3 + 3m_Z^3 + m_H^3 + m_A^3 + 2m_{H^\pm}^3)$, and the condition of sphaleron decoupling can be satisfied for $m_h \gtrsim 115$ GeV for large values of heavy Higgs boson masses. In this case, from Eq. (7.13) the effects of the heavy Higgs boson loops on the hhh coupling are enhanced by m_Φ^4. These loop effects do not decouple in the large mass limit, and yield large deviations in the hhh coupling from the SM prediction. Such large non-decoupling effects can modify the hhh coupling by more than 10% [74] (maximally $\simeq$ a few times 100% within the requirement from perturbative unitarity [375]), so that the deviation is expected to be detected at ILC [77,78]. In the same scenario, the effects on the quartic Higgs boson coupling are also discussed in Ref. [376].

This connection between the condition for successful electroweak baryogenesis and the large non-decoupling effect on the hhh coupling is a common feature, and can be seen in some other models such as the MSSM with light stops. In the MSSM, the effect of additional stop loop contributions to the hhh coupling is expressed by using the high temperature expansion as

$$
\frac{\Delta\lambda_{hhh}(\mathrm{MSSM})}{\lambda_{hhh}(\mathrm{SM})} \simeq \frac{2v^4}{m_t^2 m_h^2}(\Delta E_{\tilde{t}_1})^2, \tag{7.14}
$$

where $\Delta E_{\tilde{t}_1}$ is the contribution of the light stop loop to the cubic term in the finite temperature effective potnetial in Eq. (7.12).

Therefore, these scenarios of electroweak baryogenesis can be tested by precisely measuring the hhh coupling at an ILC (see Figure 7.3).

7.5.2 Strong first order phase transition in the SM with a low cutoff scenario

Recently the possibility of electroweak baryogenesis has been studied in the SM with a low cut-off scale, by adding the higher dimensional Higgs boson operators [377, 378]. In contrast to previous
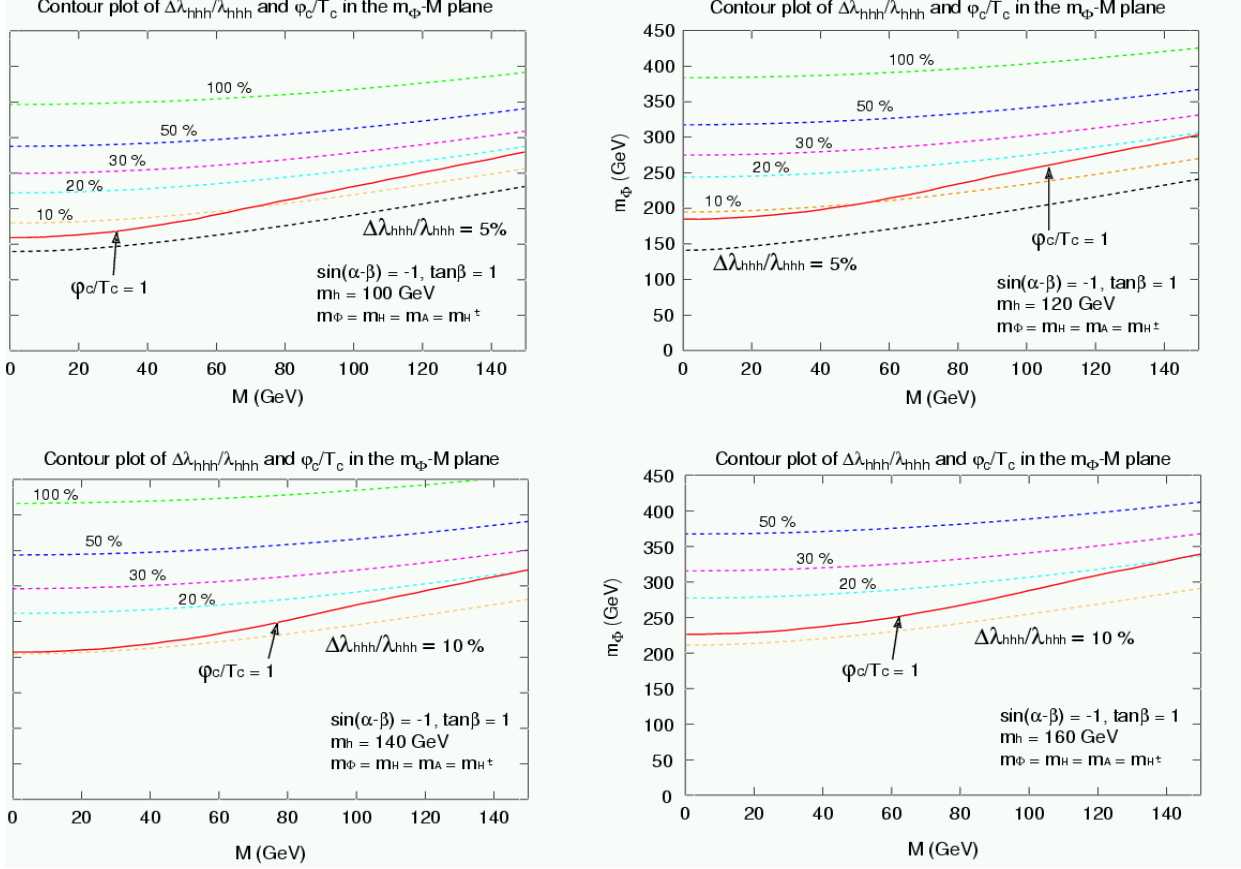
Figure 7.3: The contour of the radiative correction of the triple Higgs boson coupling constant overlaid with the line $\varphi_c/T_c = 1$ in the m_Φ-M plane for m_h=100, 120, 140 and 160 GeV. Above the critical line, the phase transition is strong enough for a successful electroweak baryogenesis scenario [75].

approaches which rely on large cubic Higgs interactions, they allow the possibility of a negative quartic coupling while the stability of the potential is restored by higher dimensional operators [378]:

$$V(\Phi) = \lambda \left(\Phi^\dagger \Phi - \frac{v^2}{2} \right)^2 + \frac{1}{\Lambda^2} \left(\Phi^\dagger \Phi - \frac{v^2}{2} \right)^3, \tag{7.15}$$

where Φ is the SM electroweak Higgs doublet. At zero temperature, the CP-even scalar state can be written in terms of the zero temperature vacuum expectation value $\langle \varphi \rangle = v_0 \simeq 246$ GeV and the physical Higgs boson H: $\Phi = \varphi/\sqrt{2} = (H + v_0)/\sqrt{2}$. One can minimize the zero temperature potential to find $\lambda = m_H^2/(2v_0^2)$ and $v = v_0$ in terms of physical parameters m_H and v_0.

The effective potential at finite temperatures is approximately obtained by adding the thermal mass to the zero temperature potential $V(\varphi, T) = cT^2\varphi^2/2 + V(\varphi, 0)$, where c is generated by the quadratic terms, $T^2 m_i^2$, in the high temperature expansion of the thermal potential. The quartic term, which is neglected here, is also induced but its contribution is a few percent in the physically interesting region where a strongly first-order electroweak phase transition occurs. The cubic interaction is also induced at finite temperatures but it has a smaller role in this scenario, thus neglected here. From the requirements of the global minimum of the vacuum at zero temprature, a first order phase transition, and positivity of the thermal mass term, the cutoff scale is constrained

as

$$\max\left(\frac{v_0^2}{m_H^2}, \frac{\sqrt{3}v_0^2}{\sqrt{m_H^2 + 2m_c^2}}\right) < \Lambda < \sqrt{3}\frac{v_0^2}{m_H^2}, \tag{7.16}$$

where $m_c = v_0\sqrt{(4y_t^2 + 3g^2 + g'^2)/8} \sim 200$ GeV, where g and g' are $SU(2)_L$ and $U(1)_Y$ gauge couplings, and y_t is the top Yukawa coupling. The left plot of Fig. 7.4 shows the contours of constant v_c/T_c in the Λ vs. m_H plane, where T_c is the critical temperature and v_c is the vacuum expectation value at T_c. The results are encouraging and motivate a full one-loop computation of the thermal potential embedded in a complete baryogenesis scenario.

The value of the cutoff scale Λ affects the prediction of the HHH and $HHHH$ couplings. Describing the zero temperature Higgs self-interations by $V(H) = m_H^2 H^2/2 + \mu H^3/3! + \eta H^4/4! + \cdots$, one has

$$\mu = 3\frac{m_H^2}{v_0} + 6\frac{v_0^3}{\Lambda^2}, \qquad \eta = 3\frac{m_H^2}{v_0^2} + 36\frac{v_0^2}{\Lambda^2}. \tag{7.17}$$

The right plot of Fig. 7.4 shows that the contours of $\mu/\mu_{\rm SM} - 1$ in the Λ vs. m_H plane.
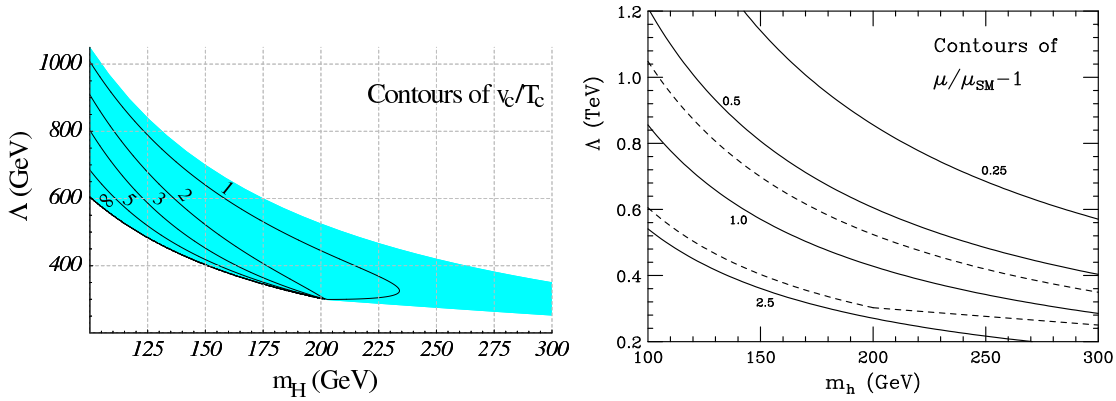

Figure 7.4: [Left] Contours of constant v_c/T_c from 1 to ∞. The shaded (blue) region satisfies the bounds of Eq. (7.16). [Right] Contours of constant $\mu/\mu_{\rm SM} - 1$ in the Λ vs. m_H plane. The dashed lines delimit the allowed region defined in Eq. (7.16). For details, see [378].

Chapter 8

Impact of Machine and Detector Performance on Precision of Measurements in the Higgs Sector

The physics processes at the ILC have been studied for about 15 years and resulted in a variety of studies for discovery and precision measurements. Many requirements on the detector and to a lesser extend on the machine development have been established. The impact of the detector (resolution, material budget, and coverage) and machine aspects which directly influence the physics performance (beam energy and luminosity spread, background induced in the detector) are important aspects to be studied further. In this chapter we collect the existing results and discuss how the detector could be optimized in view of Higgs boson physics. Finally we present a strategy for future studies to facilitate the final goal of Higgs precision measurements.

We start this section be recalling the main requirements for the ILC detector [379].

- *Momentum resolution:* $\sigma_{1/p} \sim 5 \times 10^{-5}$ GeV^{-1} (a factor of 10 better than that achieved at LEP). Good momentum resolution is important for the reconstruction of the leptonic decays of Z bosons. This is particularly relevant for $e^+ e^- \to HZ$, which is best suited to study the Higgs boson properties in detail. This works especially well by investigating the Higgs boson recoiling against the Z, with the clean decay $Z \to \mu^+ \mu^-$.

- *Impact parameter resolution:* Efficient b and c quark tagging is important, implying a good impact parameter (d_0) resolution:

$$\sigma_{d_0}^2 < (5.0 \ \mu\text{m})^2 + \left(\frac{5.0 \ \mu\text{m}}{p[\text{GeV}] \sin^{3/2} \theta} \right)^2 \ , \tag{8.1}$$

  where p is particle momentum and θ is the polar angle. This is a factor of three better than the resolution obtained at SLD.

- *Jet energy resolution:* $\sigma_E/E \sim 0.3/\sqrt{E[\text{GeV}]}$ in order to be able to directly reconstruct and identify gauge bosons from their hadronic decays to jets.

- *Hermiticity:* Hermiticity down to 5 mrad is needed for searches for missing energy signals from new physics.

- *High granularity:* Events at the ILC will have high local particle densities due to the boosted final states and the fact that many of the interesting physics processes result in final states with six or more jets, especially in the case of Higgs events. The ILC detector is required to have high granularity calorimeters to enable efficient separation of close-by showers and good pattern recognition in the tracking system.

8.1   Existing Analyses

A number of studies investigating the relation between machine and detector performance and the precision of measurements in the Higgs sector have been presented at this Snowmass workshop and documented as LC Notes or e-prints.

8.1.1   Beam related issues

In Ref. [56], discussing the prospects of the Higgs boson mass measurements at ILC, the impact of beam related systematic effects on the Higgs mass measurements have been evaluated. The following experimental effects have been investigated:

- uncertainty in the beam energy measurement;

- beam energy spread; and

- uncertainty in the differential luminosity spectrum measurements.

Since the analysis relies upon kinematic fits exploiting energy-momentum conservation, a shift in center-of-mass energy will inevitably introduce a bias in the measured Higgs mass. This is illustrated in Fig. 8.1. In order to keep systematic uncertainty due to a bias in the beam energy measurement below the statistical error on the Higgs mass, the beam energy has to be controlled with relative precision better than 10^{-4}.

To estimate the impact of the beam energy spread, Gaussian smearing of the beam energy has been applied at the stage of signal event generation. It has been shown that for the case of 1% energy spread for both electron and positron beams, the statistical precision in the Higgs boson mass measurement degrades from 45 to 50 MeV in the $HZ \to b\bar{b}q\bar{q}$ channel and from 85 to 90 MeV in the $HZ \to q\bar{q}\ell^+\ell^-$ channel. For a TESLA-like machine the expected energy spread amounts to 0.15% for the electron beam and 0.032% for the positron beam [8]. For these energy spreads no significant degradation of the precision in the Higgs boson mass measurement is observed.

The energy spectra of the colliding electrons and positrons at the linear collider will be significantly affected by photon radiation of an electron/positron in one bunch against the coherent field of the opposite bunch. This effect is referred to as beamstrahlung. To have a fast simulation of beamstrahlung, the program CIRCE [60] has been written. It assumes that the beamstrahlung in the two beams is equal and uncorrelated between the beams. The spectrum is parameterized according to

$$f(x) = a_0\delta(1 - x) + a_1 x^{a_2}(1 - x)^{a_3}, \tag{8.2}$$

where x is the ratio of the colliding electron/positron energy to the initial energy of the undisrupted beam. The parameters a_i depend on operational conditions of the linear collider. The normalization condition, $\int f(x)dx = 1$, fixes one of these parameters, leaving only three of them independent. The default parameters for the ILC (taken from TESLA) operated at the centre-of-mass energy of 350 GeV are:

$$a_0 = 0.55, \;\; a_1 = 0.59, \;\; a_2 = 20.3, \;\; a_3 = -0.63. \tag{8.3}$$

H→b$\bar{b}$, Z→e^+e^-+$\mu^+\mu^-$, √s=350GeV, L=500fb^{-1}

Legend:
- √s=350GeV, m_H = 120.003 GeV
- ΔE_{beam}=+25MeV, m_H = 119.977 GeV
- ΔE_{beam}=-25MeV, m_H = 120.030 GeV
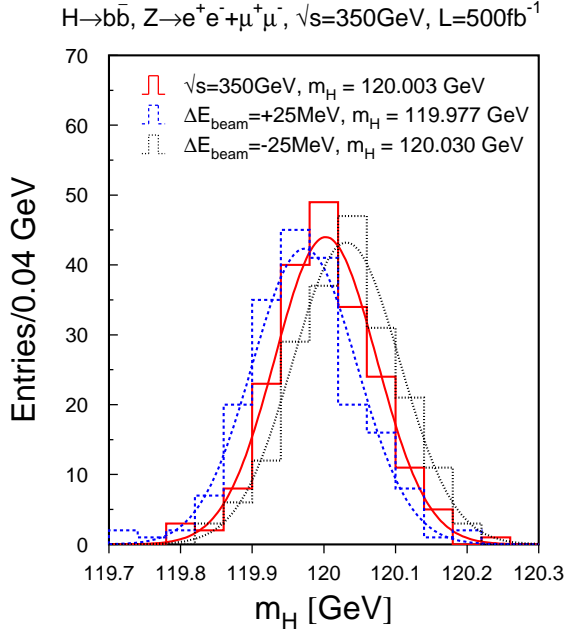
Y-axis: Entries/0.04 GeV
X-axis: m_H [GeV]

Figure 8.1: The spectrum of the fitted values of the Higgs boson mass as obtained from 200 independent signal samples in the $HZ \to q\bar{q}\ell^+\ell^-$ channel for the case when both electron and positron beam energies are overestimated by 25 MeV (dotted histogram), when they are underestimated by 25 MeV (dashed histogram) and when no shifts are introduced to the beam energies (solid histogram).

It was shown that from the analysis of the acolinearity spectrum of Bhabha scattering events, the parameters a_i can be determined with a precision of about 1% [380]. With such a precision on the parameters a_i, the uncertainty in the differential luminosity spectrum is expected to have a negligible effect on the Higgs mass measurement.

Beamstrahlung photons can interact and among others produce hadronic final states, $\gamma\gamma \to$ hadrons. At a cold machine, the average number of these interactions with the center-of-mass energy of colliding photons in excess of 5 GeV is expected to be about 0.25 (0.4) per bunch crossing in e^+e^- collisions at $\sqrt{s} = 500$ (800) GeV. This effect gets even stronger at a $\gamma\gamma$ collider. About two $\gamma\gamma \to$ hadrons events are expected on average per bunch crossing at the ILC photon collider (taken from TESLA) for $\sqrt{s}_{ee} = 400$ GeV at nominal luminosity[1]. These parasitic interactions will inevitably contaminate physics events and deteriorate the performance of physics analyses. The impact of the hadronic $\gamma\gamma$ background on selected Higgs analyses has been investigated in Reference [381]. Particles resulting from $\gamma\gamma \to$ hadrons interactions tend to be produced at low polar angles. Therefore, for processes like $e^+e^- \to HZ$, where mainly central production of bosons is expected, the contamination from parasitic interactions can be reduced by rejecting particles produced at low polar angles. This allows for a partial recovery of the analysis performance. With special rejection criteria, allowing for suppression of $\gamma\gamma \to$ hadrons background, the precision on the Higgs boson mass measurement in the $HZ \to b\bar{b}q\bar{q}$ channel at $\sqrt{s} = 500$ GeV with 500 fb^{-1} degrades only by a few MeV. However, for the WW-fusion process the effect is expected to be more severe. For the cold machine, the presence of the $\gamma\gamma \to$ hadrons background results in degradation of the signal-to-background ratio in the $e^+e^- \to W\nu\bar{\nu} \to b\bar{b}\nu\bar{\nu}$ channel by about 15% at $\sqrt{s} = 1$ TeV.

---

[1]This effect was taken into consideration in the dedicated analyses related to Higgs boson studies at a photon collider [63, 100]

8.1.2 Jet identification and resolution

Many signal signatures at ILC will involve multi-jet final states. For their analysis, accurate jet identification and measurement is crucial. Efficient separation of ZZ and WW decay modes of a heavy Higgs boson (Fig. 3.18) is possible with a jet energy resolution $\Delta E_{\rm jet}/E_{\rm jet} \leq 0.3/\sqrt{E_{\rm jet}}$. A recent study has investigated the impact of jet energy resolution on the measurement of the Higgs boson branching ratio to W bosons in the Higgs-strahlung process [382].
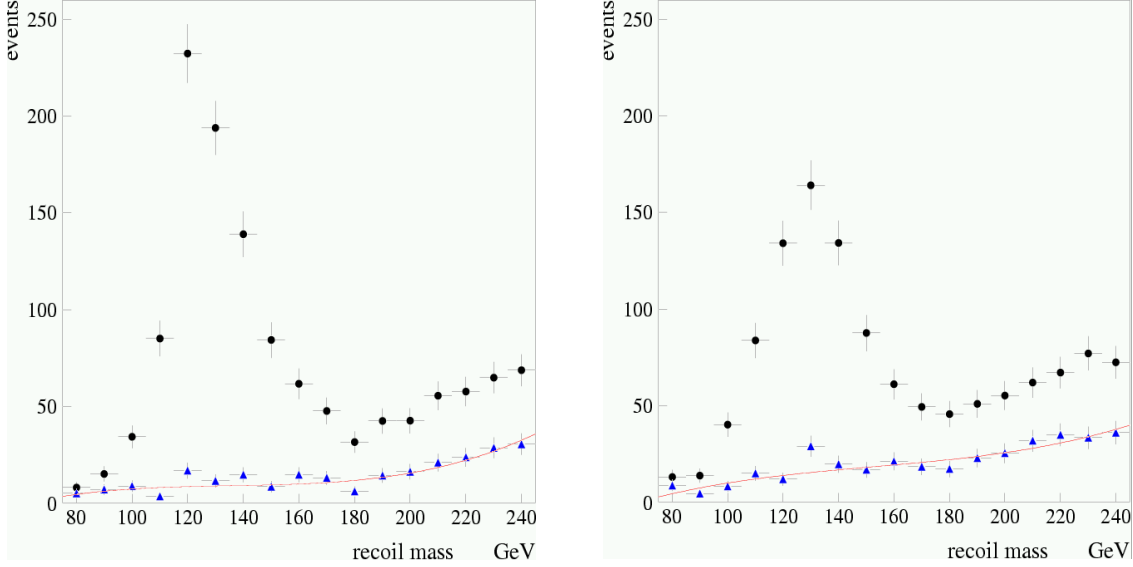

Figure 8.2: Distribution of the reconstructed Higgs boson mass in the sample of selected Higgs-strahlung events with subsequent decay of the Higgs into W boson pairs and hadronic decays of the Z boson. Only semileptonic decays of W pairs are considered. Left plot corresponds to jet energy resolution of $0.3/\sqrt{E_{\rm jet}}$, right plot corresponds to jet energy resolution of $0.6/\sqrt{E_{\rm jet}}$. Selected sample corresponds to an integrated luminosity of 500 fb^{-1} collected at $\sqrt{s} = 360$ GeV.

The analysis is based on selection of $e^+e^- \to HZ$ events with subsequent semileptonic decays of W pairs, $WW^* \to jj\ell\nu$, and hadronic decays of the Z boson, $Z \to q\bar{q}$. The study is done for a light Higgs boson, $m_H = 120$ GeV, assuming 500 fb^{-1} of data collected at $\sqrt{s} = 360$ GeV. Three scenarios are considered, corresponding to assumed jet energy resolution of $0.3/\sqrt{E_{\rm jet}}$ (benchmark goal for the ILC detector), $0.6/\sqrt{E_{\rm jet}}$ (jet energy resolution for a typical LEP detector) and $0.4/\sqrt{E_{\rm jet}}$ (some intermediate value between the first two scenarios). Fig. 8.2 presents the reconstructed Higgs boson mass for the first and second scenarios. A considerable degradation in the signal-to-background ratio from 5 to 2.5 is observed for jet energy resolution of $0.6/\sqrt{E_{\rm jet}}$ compared to $0.3/\sqrt{E_{\rm jet}}$. This results in deterioration of the precision in the $H \to WW^*$ branching fraction by 20% which is equivalent to 45% loss in the integrated luminosity.

A similar analysis [383] has been performed which investigated the impact of jet energy resolution on the Higgs boson mass measurement in the four-jet channel. It has been shown that a deterioration in the jet energy resolution from $30\%/\sqrt{E}$ to $60\%/\sqrt{E}$ results in a decrease in the Higgs mass accuracy from 42 MeV to 50 MeV. Like in the previous analysis, this roughly corresponds to an effective luminosity loss of 45%.

In Sect. 3.5 the method to determine the CP quantum number of the Higgs boson by studying transverse spin correlation effects in the $H \to \tau^+\tau^-$ decay has been described. Efficient identification of the tau decay mode is crucial for this measurement and sets stringent requirements on the performance of the electromagnetic calorimeter in combination with a dedicated pattern
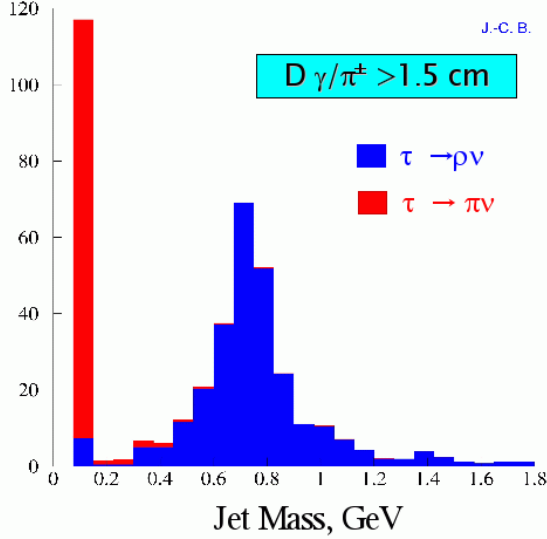
Figure 8.3: The distribution of the measured tau-jet mass for the $\tau^\pm \to \pi^\pm\nu$ and $\tau^\pm \to \rho^\pm\nu \to \pi^\pm\pi^0\nu$ channels.

recognition algorithm [384]. Fig. 8.3 illustrates the separation of $\tau \to \pi\nu$ and $\tau \to \rho\nu$ modes in the distribution of the reconstructed tau-jet mass. The result has been obtained with dedicated reconstruction tools aiming to identify and separate showers resulting from the charged pion and from the $\pi^0 \to \gamma\gamma$ decay. The simulation is performed for a TESLA-like detector with a high granularity tungsten-silicon ECAL. The quality of separation between $\tau^\pm \to \pi^\pm\nu$ and $\tau^\pm \to \rho^\pm\nu \to \pi^\pm\pi^0\nu$ modes is quantified in Tab. 8.1. These results set one of the benchmark conditions for the ECAL optimization studies.

Decay Mode	Jet mass < 0.2 GeV	0.2 GeV < Jet mass < 2 GeV
$\tau^\pm \to \pi^\pm\nu$	82%	17%
$\tau^\pm \to \rho^\pm\nu \to \pi^\pm\pi^0\nu$	2%	19%

Table 8.1: Fraction of the $\tau^\pm \to \pi^\pm\nu$ and $\tau^\pm \to \rho^\pm\nu \to \pi^\pm\pi^0\nu$ final states with the tau-jet mass below 0.2 GeV and in the window $0.2 - 2$ GeV. Distributions correspond to the samples in which the distance between π^+ entering calorimeter and the nearest photon is greater that 1.5 cm, one and a half calorimeter cell size.

8.1.3 Identification of *b*- and *c*-quarks

For the study of the hadronic branching fractions, an excellent *b*- and *c*-tagging capability of the detector is crucial. Tools have been developed which implement in detail the procedure of tagging *b*- and *c*-hadrons [99]. Fig. 8.4 illustrates performance of *b*- and *c*-tagging in terms of *b* (*c*) purity as a function of *b* (*c*) efficiency as obtained with dedicated tools for the micro-vertex detector configuration foreseen for a TESLA-like detector. Recently, a dedicated analysis based on these detailed flavor-tagging tools has been performed [70] to evaluate the ILC potential for the measurement of hadronic decays of a light Higgs boson with $m_H = 120$ GeV. The study is based on the the selection of an inclusive sample of hadronic Higgs decays using the Higgs-strahlung process and exploiting all possible decay modes of the Z boson. Each selected event is assigned quantities that quantify the probability to contain *b*- or *c*-jets. These quantities are referred to as *b*- and *c*-tag variables. The branching ratios $H \to b\bar{b}$, $H \to c\bar{c}$ and $H \to gg$ are determined from the
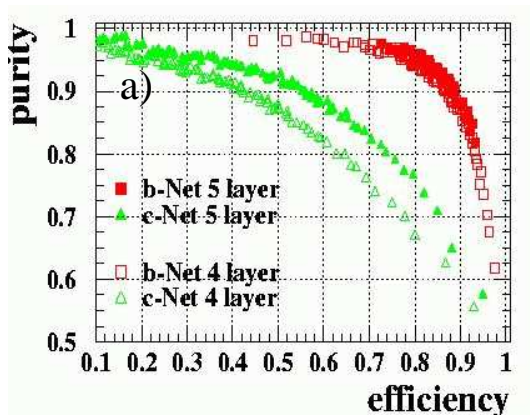
Figure 8.4: The performance of b- and c-tagging as envisaged for a vertex device of the TESLA detector. Performance is quantified in terms of b/c purity as a function of b/c efficiency.
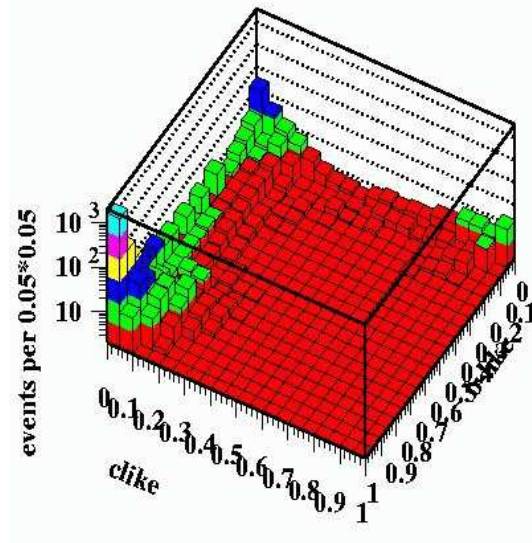
Figure 8.5: The 2D distribution of event b-tag vs. c-tag in the sample of the selected Higgs-strahlung events with $H \rightarrow$ hadrons and $Z \rightarrow q\bar{q}$ [70].

fit of 2D distribution of b-tag vs. c-tag variables (Fig. 8.5) with three free parameters, which are normalization factors quantifying the fractions of $H \rightarrow b\bar{b}$, $H \rightarrow c\bar{c}$ and $H \rightarrow gg$ events in the final selected samples. Results of this study are presented in Tab. 8.2.

Decay	$Z \rightarrow \ell^+\ell^-$	$Z \rightarrow \nu\bar{\nu}$	$Z \rightarrow q\bar{q}$	Combined
	Relative precision (%)			
$H \rightarrow b\bar{b}$	3.0	2.1	1.5	1.1
$H \rightarrow c\bar{c}$	33.0	20.5	17.5	12.1
$H \rightarrow gg$	18.5	12.3	14.4	8.3

Table 8.2: Relative precision on the measurement of the hadronic branching ratios of Higgs for m_H = 120 GeV. The analysis is performed for $\sqrt{s}$ = 350 GeV, assuming an integrated luminosity of 500 fb^{-1}.

Another study (reported at Snowmass) has evaluated the impact of the vertex detector parameters on the measurement of the hadronic branching fractions of the Higgs boson [385]. The analysis is performed for the SM Higgs boson with a mass of 127 GeV and for one representative MSSM parameter point giving the same mass for the light supersymmetric Higgs. The detector response is simulated with the SGV program [386]. Two configurations of the vertex detector are considered. The first configuration has five layers, located at the distance 15, 26, 37, 48, 60 mm away from the beam axis. In the second configuration the innermost layer is removed. For both configurations, the precision on $\Gamma(H \rightarrow c\bar{c})$ and $\Gamma(H \rightarrow b\bar{b})$ has been investigated as a function of the layer thickness and spatial resolution of a single layer. The analysis is based on the selection of Higgs-strahlung events. The prospective measurement is simulated assuming an integrated luminosity of 500 fb^{-1} collected at 350 GeV center-of-mass energy. The study revealed strong dependence of the relative precision of the $\Gamma(H \rightarrow c\bar{c})$ measurement on the vertex detector characteristics as illustrated in Fig. 8.6. The dependence is found to be less pronounced for the $H \rightarrow b\bar{b}$ channel.
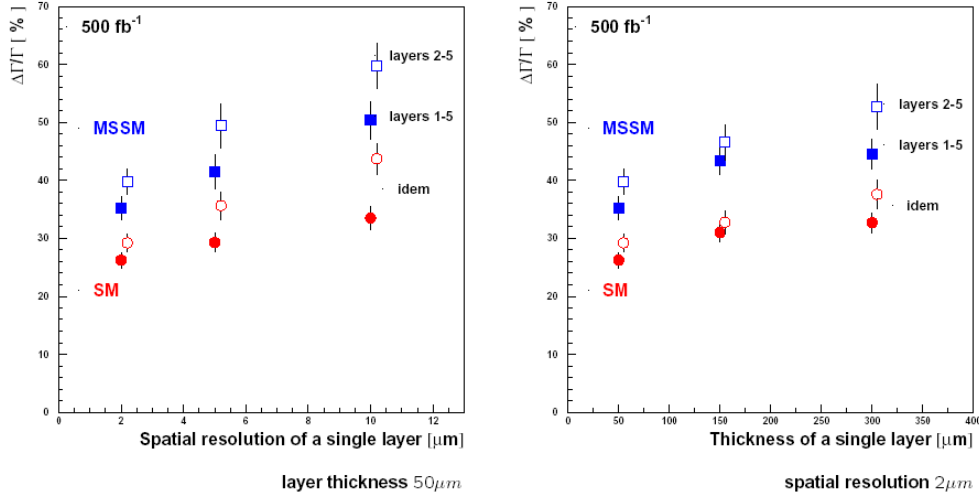
Figure 8.6: The dependence of relative precision on $\Gamma(H \to c\bar{c})$ as a function of spatial resolution of single layer (left plot) and layer thickness (right plot). In the left plot layer thickness is fixed to 50 μm. In the right plot spatial resolution is fixed to 2μm. Filled dots correspond to the vertex configuration with five layers. Open dots show results for the case when the innermost layer is removed. Results for the SM Higgs are indicated with circles, for MSSM Higgs with square markers.

8.2 Higgs Physics and Detector Optimization

The International Linear Collider project enters now the phase of detector design and optimization. At this stage, the detailed analyses studying the impact of the detector design and event reconstruction procedure on the precision of the measurements at ILC are of crucial importance. The studies discussed in previous sections have been performed using fast parametric Monte Carlo programs, in which the detector response and event reconstruction performance are simulated in an idealized manner for a specific detector configuration option. Such an approach is illustrated by the `Simdet` [387] program, which found wide acceptance within the ECFA studies. `Simdet` parameterizes the response of the ILC detector with fixed detector geometry and therefore is not appropriate for studies relating various detector configurations to the attainable precision of measurements in various physics channels. `Simdet` performs a fast Monte Carlo by smearing the particle momenta and energies according to subdetector resolutions obtained from studies with full simulation programs based on the `Geant3` or `Geant4` packages. Parameterization of the detector response in `Simdet` relies on Monte Carlo studies performed with the full `Geant3`-based simulation program `Brahms` on single particle samples. Results of these studies are then extrapolated to events with complex topology, e.g., multi-jet final states, assuming highly efficient pattern recognition in the tracking system and calorimeters in a high local particle density environment. Clearly, the physics potential of the ILC will depend on both detector performance and performance of the corresponding reconstruction software, and the issue is still open whether the performance of the detector and event reconstruction are realistically implemented in the fast parametric Monte Carlo programs. In order to answer this question and to perform detailed and reliable detector optimization studies, future analyses related to Higgs physics at the ILC should be done with a full detector simulation based on `Geant3` or `Geant4` implementations of existing detector

designs and with consistent and realistic reconstruction software.

8.2.1 Tools for Full Detector Simulation

Currently, activities are ongoing worldwide which aim at the development of realistic simulation tools based on the `Geant4` package as well as reconstruction software which can be used for the detector optimization studies. A big progress in the development of such tools has been reported at Snowmass. Most of these tools use the common output format realized in the LCIO data model [388]. This feature facilitates direct comparison between the various detector models implemented in the different simulators. The list of available full simulation programs for the linear collider detector is given below:

- **Brahms** [389]: `Geant3` based package which implements the TESLA TDR geometry in a hard-coded manner. The program reads HEPEVT files and produces an output in the ASCII or LCIO format. Since the detector geometry is fixed, the `Brahms` package cannot be utilized for detector optimization studies. However, it may still be useful for revision of currently existing Higgs analyses with the full realistic simulation.

- **SLIC** [390]: `Geant4` based simulation package that uses an XML geometry input format called LCDD. This package includes various detector models developed within the compact detector concept with the silicon tracker (SiD) as well as large detector (LDC) and huge detector (GLD) concepts with the TPC as the main tracking device. The program reads a StdHep file for the event input and produces an output in the form of a LCIO file.

- **Mokka** [391]: `Geant4` simulator that retrieves geometry information from a MySQL database. It reads binary StdHep or ASCII HEPEVT files and writes a LCIO file. Although originally `Mokka` was designed for simulation of the large detector with the TPC as the main tracking device, the latest release of `Mokka` contains also models with the silicon tracker. The package provides an option for coherent scaling of various detector components such as the TPC, ECAL and HCAL, which allows to optimize the length and radius of the tracker, the depth and sampling frequency of calorimeters, and other geometrical parameters of the detector.

- **Jupiter** [392]: `Geant4` based program for simulation of the GLD detector. This program uses as input StdHep or HEPEVT files. The geometry of the detector is specified using XML interfaces. The data flow controller is based on ROOT. However, work is ongoing to implement output in the LCIO format to enable comparison with other detector concepts.

8.2.2 Tools for Event Reconstruction

The most promising strategy for event reconstruction at the ILC is based on the particle flow concept, implying reconstruction of the four-vectors of all particles produced in an event. The particle flow algorithm works best at moderate energies of individual particles, below about 100 GeV. In this regime, the tracking system reconstructs the momentum of the charged particles with an accuracy better than that achievable for the energy measurements with calorimeters. This is illustrated in Figure 8.7. Hence, in order to attain a better reconstruction of events, the charged particle measurement must be solely based on the tracking information. The crucial step of the particle flow algorithm is the correct assignment of calorimeter hits to the charged particles, and efficient separation of close-by showers produced by charged and neutral particles. A clustering algorithm is then performed on calorimetric hits not assigned to the charged particles to reconstruct photons and neutral hadrons. The reconstruction of photons and neutral hadrons buried in jets is
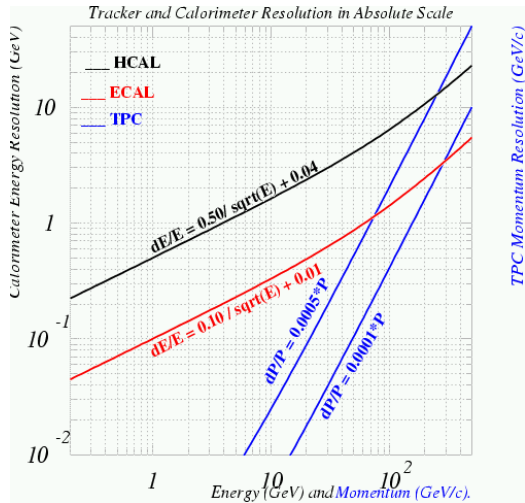
Figure 8.7: The track momentum resolution for charged objects and the energy resolution for photons and hadrons as a function of particle energy. Plotted curves correspond to the resolutions envisaged for the TESLA detector.

nearly impossible with a typical LEP detector. This explains why LEP detectors could reconstruct jet energy with something like $60\%/\sqrt{E}$ (where E represents the jet energy). The goals of the physics program at the linear collider requires however much better jet energy resolution in order to efficiently separate, e.g., ZZ and WW final states. Monte Carlo studies have shown that an ideal reconstruction algorithm [393], which finds each particle and measures its energy and direction with the detector resolution expected for single particles, could reach a jet energy resolution of $14\%/\sqrt{E}$. Over the years a jet energy resolution of $30\%/\sqrt{E}$ has become accepted as a good compromise between the theoretically possible and practically achievable resolution. The RERECO package [389], developed at DESY, represents the first complete software implementation of the event reconstruction following the particle flow concept. A good performance of this implementation was demonstrated in a number of Monte Carlo studies [393, 394]. The software includes pattern recognition in the vertex detector, TPC, and forward tracking system, followed by a track fitting procedure. The calorimeter clustering, track-cluster association and particle identification is done with the SNARK [395] package. The output is produced in the form of the reconstructed particle flow objects stored in the LCIO file. Despite the main advantage of being a complete and consistent implementation of the particle flow algorithm, the RERECO package has serious shortcomings. It is heavily bound to the TESLA TDR geometry implemented in `Brahms` and, therefore, cannot be used for detector optimization. Nevertheless, the revision of the Higgs analyses in the key channels can be done with this package for the TESLA TDR geometry.

The `MarlinReco` package [396], meant as a successor of RERECO, is currently being developed at DESY. Presently, this package includes track reconstruction and fitting in the TPC, calorimeter clustering, track-cluster matching and particle identification. Unlike RERECO, `MarlinReco` is not bound to any specific detector geometry and can be used for the detector optimization studies. Other reconstruction packages presented at the Snowmass workshop include `org.lcsim` [397] designed primarily for the SiD detector and the package designed for the GLD detector [398]. Both packages, `MarlinReco` and `org.lcsim`, use the same LCIO data model, which serves as an interface between the detector simulation and reconstruction software. The LCIO produced by full simulation contains a collection of hits recorded in various subdetectors. This information is used as an input for the reconstruction software. The reconstructed objects, namely tracks, calorimeter clusters and particle flow objects, are also stored in the LCIO file and can be used for further analysis. Currently, the event reconstruction package used for the GLD detector stores information on the reconstructed objects in a ROOT file, but efforts are ongoing to make this package also compatible with the LCIO data format.

Existing reconstruction packages provide an option to disentangle detector effects from the inefficiencies of the reconstruction algorithm. This is done by emulating perfect pattern recognition in the tracking system and calorimeters and constructing true Monte Carlo tracks and calorimeter clusters. This approach, referred to as "perfect particle flow", is very important at the stage of detector optimization since it allows to trace and eliminate possible systematic effects coming solely from the reconstruction algorithms.

8.2.3 Benchmarking Detector Performance with Measurements in the Higgs Sector

One of the main issues that has to be addressed by future studies is the relation between detector design and precision of measurements in the Higgs sector, going beyond the existing studies summarized in Sect. 8.1. We propose the following list of questions to be addressed by dedicated studies along with Higgs channels which can be used to benchmark the performance of the different detector components.

- **Vertex Detector**

  How does the precision of Higgs hadronic branching ratio measurements depend on the specific configuration of the micro-vertex detector (number of layers, position of the innermost layer, etc.)? How is the analysis performance in other channels, e.g. $HA \to b\bar{b}b\bar{b}$, influenced by the micro-vertex detector configuration? The first study addressing these questions is presented in Ref. [385]. Efficient determination of the charge of secondary vertices is important for the reduction of combinatorial background in the HHZ channel with the $H \to b\bar{b}$ decay and therefore crucial for the measurement of the Higgs self-coupling. How does the efficiency of the reconstruction of the vertex charge depend on the configuration of the vertex detector?

- **Tracking System**

  What charged particle momentum resolutions can be achieved with the currently considered options for the main tracking device (TPC, silicon tracker)? How does the geometry of the tracking system (radius and length of TPC, number and position of layers in the silicon tracker, etc.) affect the charged particle momentum resolution? What impact will the charged particle momentum resolution have on the performance of analyses which utilize the inclusive $HZ \to X\ell^+\ell^-$ channel? How will the pattern recognition capabilities provided by different configurations of the tracking system influence the reconstruction of multi-jet final states with high track multiplicity, e.g. $ZHH \to 6$ jets or $HZ \to WW(ZZ)qq \to 6$ jets?

- **Calorimeters**

  How does the precision on the Higgs photonic branching ratio measurement depend on the energy and angular resolution of the electromagnetic calorimeter? What impact will a specific option for electromagnetic and hadronic calorimeters (absorber material, active media, sampling fraction, transverse granularity) have on the efficiency of the reconstruction of multi-jet final states with high particle multiplicity in various Higgs channels? What jet energy resolution can be achieved with a given option for the calorimeter system? How does the efficiency of τ lepton identification via its hadronic decays depend on the configuration of the calorimeter system. What effects will it have on the identification of $H \to \tau\tau$ decays, which is crucial for the determination of the CP quantum numbers of Higgs bosons?

- **Muon System**

What improvement can be achieved in the identification of high energy the muons if tracking and calorimeter information is complemented by the muon system? Should the muon system be realized in a conventional way by instrumenting the magnet return yoke or are alternative ways of implementing the muon detector more favorable? What active element (Resistive Plate Chambers, scintillating strips/tiles) is preferable for the muon system? These studies should be based on the analysis of final states involving high energy muons ($HZ \to X\mu^+\mu^-$, $e^+e^- \to H\nu\bar{\nu} \to \mu^+\mu^-\nu\bar{\nu}$).

- **Overall Detector Performance and Performance of Reconstruction Software**

  The overall detector and reconstruction software performance can be expressed in terms of the jet energy resolution. Hence, it would be desirable to investigate the dependence of jet energy resolution on a given detector configuration and also to study the impact of the jet energy resolution on the precision of measurements in the various Higgs channels involving multi-jet final states.

The ultimate goal of these studies would be to establish a mapping between performance/configurations of different subdetectors and the precision of measurements in the Higgs sector.

8.3   Proposed Strategy

The detector optimization for the Higgs channels can be done in two steps. The first step is based on the simple MC smearing of the 4-momentum of isolated particles, jet energies and angles, and a parameterization of the heavy flavor tagging procedure. The resolution functions are extracted separately for each type of particle by running a full simulation program on single particle samples. For charged particles it implies the study of the performance of the tracking system and the parameterization of the momentum resolution and reconstruction efficiency as a function of particle momentum and polar angle θ. For neutral particles, detailed investigation of the calorimeter response has to be performed in order to quantify the energy, position and angular resolutions separately for photons and neutral hadrons. The Higgs analyses relying on flavor-tagging will need as an input the parameterization of the vertex detector performance in terms of b- and c- tagging efficiency versus purity. Realistic reconstruction packages can be employed to evaluate the jet energy resolutions for the case of perfect particle flow as well as for realistic particle flow algorithms. Once the main characteristics quantifying the detector response are extracted from the full simulation and reconstruction tools, fast Monte Carlo smearing can be applied to the generated background and signal samples relevant for a given Higgs channel. The program is supposed to emulate the measurements of the four-momenta of isolated particles and jets, heavy-flavor tagging, etc., using as an input the detector resolution functions extracted from the Monte Carlo studies with the full simulation. Results of the relevant analyses will directly reflect the potential of a specific detector model for measurements in the Higgs sector.

On the other hand, with this simple parametric approach, one can study the precision of measurements as a function of the main detector performance characteristics, such as jet energy resolution, momentum resolution of the tracking system, etc., without referring to a specific detector model. The main advantage of the parametric approach is that it provides a fast procedure for mapping the detector performance (described in terms of generic resolution functions and inefficiencies) into the precision of measurements in the key physics channels.

However, this strategy has a major shortcoming. Lacking detailed simulation of the detector response and realistic event reconstruction, it fails to predict in an accurate way the analysis performance in the physics channels where details of the pattern recognition in the detector play

a crucial role. This situation can be illustrated by two examples. Successful determination of Higgs CP quantum numbers in the $H \to \tau^+\tau^-$ channel will require efficient pattern recognition in the electromagnetic calorimeter in order to identify the tau decay mode and to measure precisely the decay products of the tau leptons. Accurate analysis in this channel is possible only with the full detector simulation and realistic reconstruction tools. The second example is given by measurements of Higgs self-couplings in the double Higgs-strahlung process, $e^+e^- \to HHZ$. The large combinatorial background in this channel can be reduced by identifying the vertex charge, which would allow to discriminate between b and $\bar{b}$ jets. Again, reliable prediction of the vertex charge identification efficiency requires a detailed study of the vertex detector performance with the full simulation and realistic reconstruction tools.

At this point one can conclude that it is reasonable to employ fast parametric simulation at the early stage of the detector optimization to reject those detector configurations that result in unacceptable deterioration of the precision of measurements in the Higgs sector.

For detector configurations passing the first step of optimization with the fast parametric simulation, a more detailed study is needed that employs the full detector simulation and reconstruction. The large-scale analyses including background estimates represent a time-consuming procedure in this case. Therefore, we propose first to run full simulation programs, implementing a chosen detector geometry, only on HEPEVT or StdHep files of signal samples. Performing event reconstruction, selection and analysis of only the signal samples, one can get a rough idea about the dependence of the analysis performance on a specific detector configuration. Variations in analyzing power of variables crucial for a given Higgs channel will serve as a major criterion to discriminate between different detector designs. An example of such an approach is illustrated in Fig. 8.8. It presents reconstructed Higgs boson mass spectra in the $e^+e^- \to H\nu\bar{\nu} \to b\bar{b}\nu\bar{\nu}$ channel after performing the full simulation of the TESLA TDR detector with `Mokka`. The figure compares results of the realistic reconstruction based on the `MarlinReco` package and the perfect particle flow algorithm. It is very important that the results of the realistic event reconstruction are cross checked with the simulation of perfect reconstruction. This is necessary to disentangle detector effects from the inefficiencies in pattern recognition algorithms and to guide the efforts of the developers of the reconstruction software. In this particular example, the obtained resolution on the reconstructed Higgs boson mass plays the role of a parameter evaluating the performance of the given detector model and event reconstruction package. Similar studies can be done in other channels for various detector options which may emerge in the future as a result of the detector R&D program for the ILC.
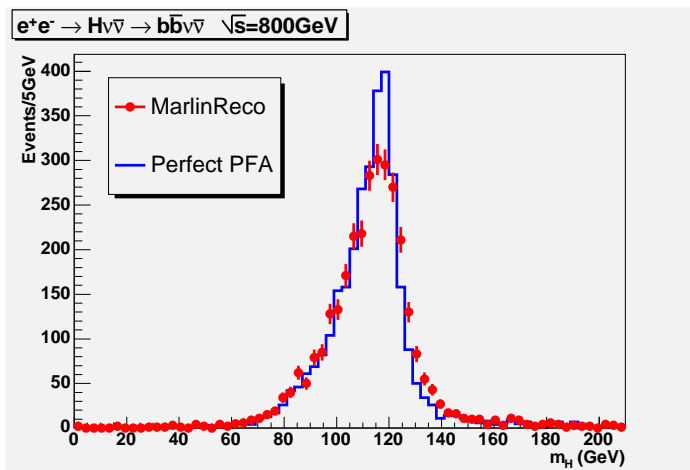

Figure 8.8: The distribution of the dijet mass in the $e^+e^- \to H\nu\bar{\nu} \to b\bar{b}\nu\bar{\nu}$ channel. Distribution is obtained after performing full simulation of the TESLA TDR detector with `Mokka`. The result of the realistic event reconstruction with the `MarlinReco` package (dots) is compared with perfect reconstruction (line).

Bibliography

[1] S. Glashow, *Nucl. Phys.* **22** (1961) 579;
S. Weinberg, *Phys. Rev. Lett.* **19** (1967) 1264;
A. Salam, *Elementary Particle Theory*, edited by N. Svartholm (Almqvist and Wiksell, Stockholm, 1968), p. 367.

[2] P. Higgs, *Phys. Lett.* **12** (1964) 132; *Phys. Rev. Lett.* **13** (1964) 508; *Phys. Rev.* **145** (1966) 1156;
F. Englert and R. Brout, *Phys. Rev. Lett.* **13** (1964) 321;
G. Guralnik, C. Hagen and T. Kibble, *Phys. Rev. Lett.* **13** (1964) 585.

[3] M. Grünewald, hep-ex/0511018;
C. Diaconu, talk given at "Lepton-Photon 2005", Uppsala, Sweden, June 2005, see:
`lp2005.tsl.uu.se/lp2005/LP2005/programme/presentationer/morning/`
`diaconu.pdf`; see also: `lepewwg.web.cern.ch/LEPEWWG/Welcome.html`.

[4] The LEP Working Group for Higgs Searches, ALEPH, DELPHI, L3 and OPAL Collaborations, *Phys. Lett.* **B 565** (2003) 61, hep-ex/0306033; hep-ex/0107030; hep-ex/0107031;
LHWG-Note 2004-01, see: `lephiggs.web.cern.ch/LEPHIGGS/papers/` .

[5] ATLAS Collaboration, *"ATLAS: Detector and Physics Performance Technical Design Report, Volume 2"*, CERN-LHCC-99-15, ATLAS-TDR-15 (1999);
CMS Collaboration, see: `cmsinfo.cern.ch/Welcome.html/CMSdocuments/CMSplots/` .

[6] D. Zeppenfeld, R. Kinnunen, A. Nikitenko and E. Richter-Was, *Phys. Rev.* **D 62** (2000) 013009, hep-ph/0002036;
A. Belyaev and L. Reina, *JHEP* **0208** (2002) 041, hep-ph/0205270;
M. Dührssen, ATL-PHYS-2003-030, available from `cdsweb.cern.ch` .

[7] M. Dührssen, S. Heinemeyer, H. Logan, D. Rainwater, G. Weiglein and D. Zeppenfeld, *Phys. Rev.* **D 70** (2004) 113009, hep-ph/0406323; hep-ph/0407190.

[8] J. Aguilar-Saavedra *et al.*, TESLA TDR Part 3: "Physics at an e^+e^- Linear Collider", hep-ph/0106315, see: `tesla.desy.de/tdr` .

[9] T. Abe *et al.* [American Linear Collider Working Group Collaboration], "Linear collider physics resource book for Snowmass 2001", hep-ex/0106056.

[10] K. Abe *et al.* [ACFA Linear Collider Working Group Collaboration], hep-ph/0109166, see: `lcdev.kek.jp/RMdraft` .

[11] B. Badelek et al. [ECFA/DESY Photon Collider Working Group], *Int. J. Mod. Phys.* **A 19** (2004) 5097, hep-ex/0108012.

[12] G. Weiglein et al. [LHC / ILC Study Group], hep-ph/0410364.

[13] N. Cabbibo, et al. *Nucl. Phys.* **B 158** (1979) 295;
M. Lindner, *Z. Phys.* **C 31** (1986) 295.

[14] T. Hambye and K. Riesselmann, *Phys. Rev.* **D 55** (1997) 7255, hep-ph/9610272.

[15] J. Ellis, G. Ridolfi and F. Zwirner, *Phys. Lett.* **B 257**, 83 (1991);
Y. Okada, M. Yamaguchi and T. Yanagida, *Prog. Theor. Phys.* **85**, 1 (1991);
H. Haber and R. Hempfling, *Phys. Rev. Lett.* **66**, 1815 (1991).

[16] S. Heinemeyer, W. Hollik and G. Weiglein, *Eur. Phys. J.* **C 9** (1999) 343, hep-ph/9812472.

[17] G. Degrassi, S. Heinemeyer, W. Hollik, P. Slavich and G. Weiglein, *Eur. Phys. J.* **C 28** (2003) 133, hep-ph/0212020.

[18] J. Espinosa, M. Quiros, *Phys. Rev. Lett.* **81** (1998) 516.

[19] S. Kanemura, T. Kasai and Y. Okada *Phys. Lett.* **B 471** (1999) 182.

[20] Y. Okada, hep-ph/0304286.

[21] [The Tevatron Electroweak Working Group], hep-ex/0507091.

[22] M. Peskin and J. Wells, *Phys. Rev.* **D 64** (2001) 093003, hep-ph/0101342.

[23] D. Choudhury, T. M. P. Tait and C. E. M. Wagner, Phys. Rev. D **65**, 115007 (2002), hep-ph/0202162.

[24] H. Nilles, *Phys. Rep.* **110** (1984) 1;
H. Haber and G. Kane, *Phys. Rep.* **117**, (1985) 75;
R. Barbieri, *Riv. Nuovo Cim.* **11**, (1988) 1.

[25] J. Gunion, H. Haber, G. Kane and S. Dawson, *The Higgs Hunter's Guide* (Perseus Publishing, Cambridge, MA, 1990).

[26] H.-J. He, C. Hill, T. Tait, *Phys. Rev.* **D 65** (2002) 055006.

[27] N. Arkani-Hamed et al., *J. High Energy Phys.* **08** (2002) 021;
M. Schmaltz, *Nucl. Phys. Proc. Suppl.* **117** (2003) 40.

[28] Y. Hosotani, S. Noda and K. Takenaga, *Phys. Lett.* **B 607** (2005) 276.

[29] A. Zee, *Phys. Lett.* **B 161** (1985) 141;
S. Kanemura et al., *Phys. Rev.* **D 64** (2001) 053007;
D. Dicus, H.-J. He, J. Ng, *Phys. Rev. Lett.* **87** (2001) 111803; *Phys. Lett.* **B 536** (2002) 83.

[30] V. Kuzmin, V. Rubakov and M. Shaposhnikov, *Phys. Lett.* **B 155**, 36 (1985);
A. Cohen, D.B. Kaplan and A. Nelson, *Phys. Lett.* **B 245**, 561 (1990);
A. Cohen, D.B. Kaplan and A. Nelson, *Ann. Rev. Nucl. Part. Sci.* **43**, 27 (1993).

[31] S. Kanemura, S. Moretti and K. Odagiri, *JHEP* **0102** (2001) 011;
H. Logan and S. Su, *Phys. Rev.* **D 67** (2003) 017703;
S. Moretti, hep-ph/0209210.

[32] B. Kniehl, F. Madricardo and M. Steinhauser, *Phys. Rev.* **D 66** (2002) 054016.

[33] S. Zhu, hep-ph/9901221;
S. Kanemura, *Eur. Phys. J.* **C17** (2000) 473;
A. Arhrib et al., *Nucl. Phys.* **B 581** (2000) 34;
H. Logan, S. Su, *Phys. Rev.* **D 66** (2002) 035001;
O. Brein, hep-ph/0209124.

[34] O. Brein, T. Hahn, S. Heinemeyer and G. Weiglein, hep-ph/0402053.

[35] S. Kiyoura, et al., hep-ph/0301172.

[36] GRACE: T. Ishikawa, T. Kaneko, K. Kato, S. Kawabata, Y. Shimizu and H. Tanaka, KEK Report 92-19 (1993);
F. Yuasa et al., *Prog. Theor. Phys. Suppl.* **138** (2000) 18;
GRACE/SUSY: J. Fujimoto et al., hep-ph/0208036.

[37] S. Heinemeyer, W. Hollik and G. Weiglein, *Comp. Phys. Comm.* **124** (2000) 76, hep-ph/9812320; hep-ph/0002213; see `www.feynhiggs.de` .

[38] A. Djouadi, J. Kalinowski and M. Spira, *Comput. Phys. Commun.* **108**, 56 (1998), hep-ph/9704448.

[39] J. Gunion and H. Haber, *Phys. Rev.* **D 48** (1993) 5109;
D. Borden, D. Bauer and D. Caldwell, *Phys. Rev.* **D 48** (1993) 4018.

[40] D. Asner, J. Gronberg, J. Gunion, hep-ph/0110320.

[41] D. Asner et al., *Eur. Phys. J.* **C 28** (2003) 27, hep-ex/0111056.

[42] S. Soldner-Rembold and G. Jikia, *Nucl. Instrum. Meth.* **A 472** (2001) 133, hep-ex/0101056.

[43] E. Asakawa, J. Kamoshita, A. Sugamoto, and I. Watanabe, *Eur. Phys. J.* **C 14**, 335 (2000);
E. Asakawa, S. Choi, K. Hagiwara, J. Lee, *Phys. Rev.* **D 62** (2000) 115005;
E. Asakawa, hep-ph/0101234.

[44] V. Telnov, *Nucl. Instr. Meth.* **A 472** (2001) 43.

[45] M. Galynskii, E. Kuraev, M. Levchuk and V. Telnov, *Nucl. Instr. Meth.* **A 472** (2001) 267.

[46] A. Rosca, *Eur. Phys. J.* **C 33** (2004) 1044.

[47] N. Walker, plenary talk given at Snowmass '05.

[48] G. Moortgat-Pick et al., hep-ph/0507011.

[49] T. Hahn, S. Heinemeyer and G. Weiglein, *Nucl. Phys.* **B 652** (2003) 229, hep-ph/0211204;
Nucl. Phys. Proc. Suppl. **116**, 336 (2003) hep-ph/0211384.

[50] R. Hawkings and K. Mönig, *Eur. Phys. J. direct* **C8** (1999) 1; hep-ex/9910022.

[51] U. Baur, R. Clare, J. Erler, S. Heinemeyer, D. Wackeroth, G. Weiglein and D. Wood, hep-ph/0111314.

[52] S. Heinemeyer, W. Hollik and G. Weiglein, hep-ph/0412214.

[53] J. Erler, S. Heinemeyer, W. Hollik, G. Weiglein and P. Zerwas, *Phys. Lett.* **B 486** (2000) 125; hep-ph/0005024.

[54] J.-C. Brient, LC-PHSM-2000-049, see: `www-flc.desy.de/lcnotes` .

[55] P. Garcia-Abia and W. Lohmann, *EPJdirect* **C 2** (2000) 1.

[56] P. Garcia-Abia, W. Lohmann and A. Raspereza, hep-ex/0505096.

[57] K. Desch and N. Meyer, *Eur. Phys. J.* **C 35** (2004) 171.

[58] K. Desch and N. Meyer, LC-PHSM-2001-025, see: `www-flc.desy.de/lcnotes` .

[59] A. Zarnecki, *Acta Phys. Polon.* **B 34** (2003) 2741.

[60] V. Telnov, talk presented at the 2nd ECFA/DESY Workshop on Physics and Detectors for Linear Collider, St. Malo, France, April 2002.
T. Ohl, see: `ftp://heplix.ikp.physik.tu-darmstadt.de/pub/ohl/circe2/doc/manual.pdf` .

[61] K. Mönig and A. Rosca, hep-ph/0310036; hep-ph/0506271.

[62] P. Niezurawski, A. Zarnecki and M. Krawczyk, *Acta Phys. Polon.* **B 34** (2003) 177.

[63] P. Niezurawski, A. Zarnecki and M. Krawczyk, hep-ph/0307183; P. Niezurawski, hep-ph/0507004 and this Proceedings ALCPG0503.

[64] Z. Sullivan, hep-ph/0509012 and this Proceedings ALCPG0402.

[65] M. Battaglia, hep-ph/9910271.

[66] G. Borisov and F. Richard, hep-ph/9905413;
E. Boos et al., *EPJdirect* **C 2** (2000) 5.

[67] E. Boos et al., *Eur.Phys. J.* **C 19** (2001) 455.

[68] M. Dubinin, H. Schreiber and A. Vologdin, *Eur. Phys. J.* **C 30** (2003) 337.

[69] J.-C. Brient, LC-PHSM-2002-003, see: `www-flc.desy.de/lcnotes` .

[70] T. Kuhl, talk given at International Conference on Linear Colliders, LCWS04, Paris, April 2004.

[71] M Battaglia, A. De Roeck, *eConf* **C010630**, hep-ph/0111307.

[72] H. Baer, S. Dawson and L. Reina, *Phys. Rev.* **D 61**, 013002 (2000).

[73] A. Juste, " Towards a precise measurement of the top-Higgs Yukawa coupling at 500 GeV", talk presented at the Snowmass workshop, 14-27 August 2005.

[74] S. Kanemura et al., *Phys. Lett.* **B 558** (2003) 157; *Phys. Rev.* **D 70** (2004) 115002.

[75] S. Kanemura, Y. Okada and E. Senaha, *Phys. Lett.* **B 606** (2005) 361; hep-ph/0507259.

[76] G. Gounaris, D. Schildknecht, F. Renard, *Phys. Lett.* **B83** (1979) 191;
V. Barger, T. Han, R. Phillips, *Phys. Rev.* **D 38**, 2766 (1988);
F. Boudjema, E. Chopin, *Z. Phys.* **C 73** (1996) 85;
V. Ilyin, A. Pukhov, Y. Kurihara, Y. Shimizu and T. Kaneko, *Phys. Rev.* **D 54** (1996) 6717;
J. Kamoshita, Y. Okada, M. Tanaka, I. Watanabe, hep-ph/9602224;
A. Djouadi, H. Haber, P. Zerwas, *Phys. Lett.* **B 373** (1996) 135;
A. Djouadi, W. Kilian, M. Mühlleitner, P.M. Zerwas, *Eur. Phys. J.* **C10** (1999) 27.

[77] M. Battaglia, E. Boos, W. Yao, hep-ph/0111276.

[78] Y. Yasui et al., hep-ph/0211047.

[79] C. Castanier, P. Gay, P. Lutz and J. Orloff, hep-ex/0101028.

[80] G. Bélanger et al., *Phys. Lett.* **B 576** (2003) 152, hep-ph/0309010.

[81] M. Schumacher, LC-PHSM-2001-003, see: `www-flc.desy.de/lcnotes` .

[82] M. Dova, S. Ferrari, *Phys. Lett.* **B 605** (2005) 376.

[83] M. Krämer, J. Kühn, M. Stong and P Zerwas, *Z. Phys.* **C 64** (1994) 21.

[84] G. Bower, T. Pierzchala, Z. Was and M. Worek, *Phys.Lett.* **B543** (2002) 227.

[85] A. Imhof, talk presented at LCWS05 Workshop, Stanford, March 2005.

[86] K. Desch, A. Imhof, Z. Was and M. Worek, *Phys. Lett.* **B 579** (2004) 157.

[87] A. Rouge, *Phys. Lett.* **B 619** (2005) 2005.

[88] H. Kühn and F. Wagner, *Nucl. Phys.* **B 236** (1984) 16;
S. Jadach, H. Kühn, Z. Was, *Comput. Phys. Commun.* **64** (1991) 275.

[89] D. Miller, S. Choi, B. Eberle, M. Muhlleitner and P. Zerwas, *Phys. Lett.* **B 505** (2001) 149, hep-ph/0102023.

[90] M. Dova, P. Garcia-Abia and W. Lohmann, hep-ph/0302113.

[91] T. Barklow, hep-ph/0312268.

[92] M. Battaglia, hep-ph/0211461.

[93] K. Desch, hep-ph/0311092.

[94] J. Alcaraz and E. Ruiz Morales, *Phys. Rev. Lett.* **86**, 3726 (2001).

[95] F. Larios, T. Tait and C. Yuan, *Phys. Rev.* **D 57**, 3106 (1998).

[96] S. Godfrey and S. Zhu, *Phys. Rev.* **D 72**, 074011 (2005).

[97] N. Meyer, hep-ph/0308142.

[98] K. Desch, T. Klimkovich, T. Kuhl and A. Raspereza, hep-ph/0406229.

[99] S. Xella Hansen et al., LC-PHSM-2003-061, see: `www-flc.desy.de/lcnotes` ;
S. Xella Hansen et al., LC-PHSM-2001-024, see: `www-flc.desy.de/lcnotes` ;
S. Xella Hansen, *Nucl. Instr. Meth.* **A 501** (2003) 106;
T. Kuhl, *Nucl. Instr. Meth.* **A 511** (2003) 221.

[100] M. Muhlleitner, M. Kramer, M. Spira and P. M. Zerwas, *Phys. Lett.* **B 508** (2001) 311,
hep-ph/0101083;
P. Niezurawski, A. Zarnecki and M. Krawczyk, hep-ph/0307180.

[101] M. Battaglia, A. Ferrari, A. Kiiskinen and T. Maki, hep-ex/0112015.

[102] S. Moretti, *Eur. Phys. J.* **C 34** (2004) 157, hep-ph/0306297.

[103] E. Boos, V. Bunichev, M. Carena and C. Wagner, hep-ph/0507100.

[104] M. Nojiri, *Phys. Rev.* **51**, 6281 (1995);

[105] E. Boos, H. Martyn, G. Moortgat-Pick, M. Sachwitz, A. Sherstnev and P. Zerwas, *Eur. Phys. J.* **C 30**, 395 (2003), hep-ph/0303110.

[106] E. Boos, G. Moortgat-Pick, H. Martyn, M. Sachwitz and A. Vologdin, hep-ph/0211040.

[107] M. Carena, D. Garcia, U. Nierste and C. Wagner, *Nucl. Phys.* **B 577** (2000) 577, hep-ph/9912516;
H. Eberl, K. Hidaka, S. Kraml, W. Majerotto and Y. Yamada, *Phys. Rev.* **D 62** (2000) 055006, hep-ph/9912463.

[108] J. Lee, A. Pilaftsis et al., *Comput. Phys. Comm.* **156** (2004) 283, hep-ph/0307377.

[109] A. Pukhov et al., hep-ph/9908288;
E. Boos et al. [CompHEP Collaboration], *Nucl. Instrum. Meth.* **A 534** (2004) 250, hep-ph/0403113.

[110] S. Jadach, Z. Was, R. Decker and J. Kuehn, *Comp. Phys. Commun.* **76** (1993) 361.

[111] T. Sjostrand, L. Lonnblad, S. Mrenna and P. Skands, hep-ph/0308153.

[112] A. Belyaev et al., hep-ph/0101232; see: `theory.sinp.msu.ru/comphep` .

[113] E. Boos et al., hep-ph/0109068.

[114] P. Golonka, B. Kersevan, T. Pierzchala, E. Richter-Was, Z. Was and M. Worek, hep-ph/0312240.

[115] S. Choi, J. Kalinowski, J. Lee, M. Muhlleitner, M. Spira and P. Zerwas, *Phys. Lett.* **B 606** (2005) 164, hep-ph/0404119.

[116] M. Gomez-Bock, M. Mondragon, M. Muhlleitner, R. Noriega-Papaqui, I. Pedraza, M. Spira and P. M. Zerwas, *J. Phys. Conf. Ser.* **18** (2005) 74, hep-ph/0509077.

[117] B. Allanach et al., *Eur. Phys. J.* **C 25** (2002) 113, hep-ph/0202233,
see: `www.ippp.dur.ac.uk/~georg/sps` .

[118] R. Kinnunen, S. Lehti, F. Moortgat, S. Nikitenko and M. Spira, *Eur. Phys. J.* **C 40N5** (2005) 23, hep-ph/0503075.

[119] J. Gunion et al., in [12];
see also Ref. [105].

[120] M. Doncheski, S. Godfrey and S. Zhu, *Phys. Rev.* **D 68** (2003) 053001, hep-ph/0306126.

[121] B. Dobrescu, G. Landsberg and K. Matchev, *Phys. Rev.* **D 63**, 075003 (2001), hep-ph/0005308;
B. Dobrescu and K. Matchev, *JHEP* **0009** (2000) 031, hep-ph/0008192.

[122] R. Dermisek and J. Gunion, *Phys. Rev. Lett.* **95** (2005) 041801, hep-ph/0502105.

[123] E. Berger, C. Chiang, J. Jiang, T. Tait and C. Wagner, *Phys. Rev.* **D 66**, 095001 (2002), hep-ph/0205342.

[124] E. Berger, B. Harris, D. Kaplan, Z. Sullivan, T. Tait and C. Wagner, *Phys. Rev. Lett.* **86** (2001) 4231, hep-ph/0012001.

[125] A. Brignole, *Phys. Lett.* **B 281** (1992) 284.

[126] P. Chankowski, S. Pokorski and J. Rosiek, *Phys. Lett.* **B 286** (1992) 307; *Nucl. Phys.* **B 423** (1994) 437, hep-ph/9303309.

[127] A. Dabelstein, *Nucl. Phys.* **B 456** (1995) 25, hep-ph/9503443; *Z. Phys.* **C 67** (1995) 495, hep-ph/9409375.

[128] R. Hempfling and A. Hoang, *Phys. Lett.* **B 331** (1994) 99, hep-ph/9401219.

[129] S. Heinemeyer, W. Hollik and G. Weiglein, *Phys. Rev.* **D 58** (1998) 091701, hep-ph/9803277; *Phys. Lett.* **B 440** (1998) 296, hep-ph/9807423.

[130] R. Zhang, *Phys. Lett.* **B 447** (1999) 89, hep-ph/9808299;
J. Espinosa and R. Zhang, *JHEP* **0003** (2000) 026, hep-ph/9912236.

[131] G. Degrassi, P. Slavich and F. Zwirner, *Nucl. Phys.* **B 611** (2001) 403, hep-ph/0105096.

[132] J. Espinosa and R. Zhang, *Nucl. Phys.* **B 586** (2000) 3, hep-ph/0003246.

[133] A. Brignole, G. Degrassi, P. Slavich and F. Zwirner, *Nucl. Phys.* **B 631** (2002) 195, hep-ph/0112177.

[134] A. Brignole, G. Degrassi, P. Slavich and F. Zwirner, *Nucl. Phys.* **B 643** (2002) 79, hep-ph/0206101.

[135] S. Heinemeyer, W. Hollik, H. Rzehak and G. Weiglein, *Eur. Phys. J.* **C 39** (2005) 465, hep-ph/0411114; hep-ph/0506254.

[136] R. Hempfling, *Phys. Rev.* **D 49** (1994) 6168;
L.J. Hall, R. Rattazzi and U. Sarid, *Phys. Rev.* **D 50** (1994) 7048, hep-ph/9306309;
M. Carena, M. Olechowski, S. Pokorski and C. Wagner, *Nucl. Phys.* **B 426** (1994) 269, hep-ph/9402253.

[137] G. Degrassi, A. Dedes and P. Slavich, *Nucl. Phys.* **B 672** (2003) 144, hep-ph/0305127.

[138] S. Martin, *Phys. Rev.* **D 65** (2002) 116003, hep-ph/0111209; *Phys. Rev.* **D 66** (2002) 096001, hep-ph/0206136; Phys. Rev. **D 67** (2003) 095012, hep-ph/0211366; *Phys. Rev.* **D 68** 075002 (2003), hep-ph/0307101; *Phys. Rev.* **D 70** (2004) 016005, hep-ph/0312092; *Phys. Rev.* **D 71** (2005) 016012, hep-ph/0405022; *Phys. Rev.* **D 71** (2005) 116004, hep-ph/0502168; S. Martin and D. Robertson, hep-ph/0501132.

[139] A. Pilaftsis, *Phys. Rev.* **D 58** (1998) 096010, hep-ph/9803297; A. Pilaftsis, *Phys. Lett.* **B 435** (1998) 88, hep-ph/9805373.

[140] D. Demir, *Phys. Rev.* **D 60** (1999) 055006, hep-ph/9901389.

[141] S. Choi, M. Drees and J. Lee, *Phys. Lett.* **B 481** (2000) 57, hep-ph/0002287.

[142] A. Pilaftsis and C. Wagner, *Nucl. Phys.* **B 553** (1999) 3, hep-ph/9902371.

[143] M. Carena, J. Ellis, A. Pilaftsis and C. Wagner, *Nucl. Phys.* **B 586** (2000) 92, hep-ph/0003180.

[144] T. Ibrahim and P. Nath, *Phys. Rev.* **D 63** (2001) 035009, hep-ph/0008237; *Phys. Rev.* **D 66** (2002) 015005, hep-ph/0204092.

[145] S. Heinemeyer, *Eur. Phys. Jour.* **C 22** (2001) 521, hep-ph/0108059.

[146] M. Frank, S. Heinemeyer, W. Hollik and G. Weiglein, hep-ph/0212037, appeared in the proceedings of SUSY02, DESY, Hamburg, Germany, July 2002.

[147] S. Heinemeyer, hep-ph/0407244.

[148] T. Hahn, S. Heinemeyer, W. Hollik and G. Weiglein, hep-ph/0507009; T. Hahn, M. Frank, S. Heinemeyer, W. Hollik, H. Rzehak and G. Weiglein, *in preparation*.

[149] G. Bélanger et al., *Phys. Lett.* **B 559** (2003) 252, hep-ph/0212261.

[150] A. Denner, S. Dittmaier, M. Roth and M. Weber, *Phys. Lett.* **B 560** (2003) 196, hep-ph/0301189; *Nucl. Phys.* **B 660** (2003) 289, hep-ph/0302198.

[151] Y. You et al., hep-ph/0306036.

[152] G. Bélanger et al., *Phys. Lett.* **B 571** (2003) 163, hep-ph/0307029.

[153] A. Denner, S. Dittmaier, M. Roth and M. Weber, *Phys. Lett.* **B 575** (2003) 290, hep-ph/0307193.

[154] J. Fujimoto el al., *Acta Phys. Polon.* **B 28** (1997) 945.

[155] A. Denner and S. Dittmaier, *Nucl. Phys.* **B 658** (2003) 175, hep-ph/0212259.

[156] S. Dittmaier, hep-ph/0308079.

[157] S. Dittmaier, M. Kramer, Y. Liao, M. Spira and P. Zerwas, *Phys. Lett.* **B 441** (1998) 383, hep-ph/9808433.

[158] S. Dittmaier, M. Kramer, Y. Liao, M. Spira and P. Zerwas, *Phys. Lett.* **B 478** (2000) 247, hep-ph/0002035.

[159] H. Eberl, W. Majerotto, and V. Spanos, *Phys. Lett.* **B 538** (2002) 353, hep-ph/0204280; *Nucl. Phys.* **B 657** (2003) 378, hep-ph/0210038.

[160] W. Kilian, M. Krämer and P. Zerwas, *Phys. Lett.* **B 373** (1996) 135, hep-ph/9512335.

[161] P. Chankowski, S. Pokorski and J. Rosiek, *Nucl. Phys.* **B 423** (1994) 497;
V. Driesen and W. Hollik, *Z. Phys.* **C 68** (1995), 485, hep-ph/9504335;
V. Driesen, W. Hollik and J. Rosiek, *Z. Phys.* **C 71** (1996) 259, hep-ph/9512441.

[162] S. Heinemeyer, W. Hollik, J. Rosiek, and G. Weiglein, *Eur. Phys. J.* **C 19** (2001) 535, hep-ph/0102081;
S. Heinemeyer and G. Weiglein, *Nucl. Phys. Proc. Suppl.* **89** (2000) 210; hep-ph/0102177.
The code is available at `www.feynhiggs.de` .

[163] M. Carena, S. Heinemeyer, C. Wagner and G. Weiglein, hep-ph/9912223; *Eur. Phys. J.* **C 26** (2003) 601, hep-ph/0202167; hep-ph/0511023.

[164] M. Beccaria, F. Renard and C. Verzegnassi, *Phys. Rev.* **D 63** (2001) 095010, hep-ph/0007224;
M. Beccaria, M. Melles, F. Renard and C. Verzegnassi, *Phys. Rev.* **D 65** (2002) 093007, hep-ph/0112273;
M. Beccaria, H. Eberl, F. Renard and C. Verzegnassi, *Phys. Rev.* **69** (2004) 091301, hep-ph/0403099.

[165] R. Zhang et al., *Phys. Lett.* **B 578** (2004) 349.

[166] Y. Yasui, talk at Durham 2004.

[167] S. Choi, J. Kalinowski, Y. Liao and P. Zerwas, *Eur. Phys. J.* **C 40** (2005) 555, hep-ph/0407347.

[168] J. Ellis, J. Lee and A. Pilaftsis, *Nucl. Phys.* **B 718** (2005) 247, hep-ph/0411379; hep-ph/0507046.

[169] B. Badelek et al. [ECFA/DESY Photon Collider Working Group], *Int. J. Mod. Phys.* **A 19** (2004) 5097 hep-ex/0108012.

[170] E. Boos et al., *Nucl. Instrum. Meth.* **A 472** (2001) 100, hep-ph/0103090.

[171] S. Komamiya, *Phys. Rev.* **D 38** (1988) 2158.
A. Djouadi, J. Kalinowski and P.M. Zerwas, *Z. Phys.* **C 74** (1993) 569;
A. Djouadi, J. Kalinowski, P. Ohmann and P. Zerwas, *Z. Phys.* **C 74** (1997) 93;
J. Guasch, W. Hollik and A. Kraft, *Nucl. Phys.* **B 596** (2001) 66.

[172] D. Bowser-Chao, K. Cheung and S. Thomas, *Phys. Lett.* **B 315** (1993) 399;
M. Drees, R. Godbole, M. Nowakowski and S. Rindani, *Phys. Rev.* **D 50** (1994) 2335.

[173] S. Moretti, S. Kanemura, *Eur. Phys. J.* **C 29** (2003) 19.

[174] H.-J. He, S. Kanemura and C.-P. Yuan, *Phys. Rev. Lett.* **89** (2002) 101803; *Phys. Rev. D* **68** (2003) 075010;

[175] H. Nilles, M. Srednicki and D. Wyler, *Phys. Lett.* **B 120** (1983) 346.
J. Frere, D. Jones and S. Raby, *Nucl. Phys.* **B 222** (1983) 11;
J. Derendinger and C. Savoy, *Nucl. Phys.* **B 237** (1984) 307;
J. Ellis, J. Gunion, H. Haber, L. Roszkowski and F. Zwirner, *Phys. Rev.* **D 39** (1989) 844;
M. Drees, *Int. J. Mod. Phys.* **A 4** (1989) 3635;
U. Ellwanger, M. Rausch de Traubenberg and C. Savoy, *Phys. Lett.* **B 315** (1993) 331, hep-ph/9307322; *Nucl. Phys.* **B 492** (1997) 21, hep-ph/9611251;
F. Franke and H. Fraas, *Int. J. Mod. Phys.* **A 12** (1997) 479, hep-ph/9512366.

[176] S. King and P. White, *Phys. Rev.* **D 52** (1995) 4183, hep-ph/9505326.

[177] S. Abel, S. Sarkar and P. White, *Nucl. Phys.* **B 454** (1995) 663, hep-ph/9506359.

[178] S. Abel, *Nucl. Phys.* **480** (1996) 55, hep-ph/9609323;
C. Panagiotakopoulos and K. Tamvakis, *Phys. Lett.* **B 446** (1999) 22, hep-ph/9809475.

[179] H. Nilles, M. Srednicki and D. Wyler, *Phys. Lett.* **124** (1983) 337;
U. Ellwanger, *Phys. Lett.* **133** (1983) 187;
J. Bagger and E. Poppitz, *Phys. Rev. Lett.* **71** (1993) 2380, hep-ph/9307317;
J. Bagger, E. Poppitz and L. Randall, *Nucl. Phys.* **B 455** (1995) 59, hep-ph/9505244.

[180] M. Bucher and D. Spergel, *Phys. Rev.* **D 60** (1999) 043505;
A. Friedland, H. Murayama and M. Perelstein, *Phys. Rev.* **D 67** (2003) 043519.

[181] U. Ellwanger, J. Gunion and C. Hugonie, *JHEP* **0502** (2005) 066, hep-ph/0406215.

[182] U. Ellwanger, *Phys. Lett.* **B 303** (1993) 271, hep-ph/9302224.

[183] P. Pandita, *Phys. Lett.* **B 318** (1993) 338;
T. Elliott, S. King and P. White, *Phys. Rev.* **D 49** (1994) 2435, hep-ph/9308309.

[184] G. Yeghian, hep-ph/9904488.

[185] U. Ellwanger and C. Hugonie, *Eur. Phys. J.* **C 25** (2002) 297, hep-ph/9909260.

[186] J. Kamoshita, Y. Okada and M. Tanaka, *Phys. Lett.* **B 328** (1994) 67, hep-ph/9402278;
U. Ellwanger, M. Rausch de Traubenberg and C. Savoy, *Z. Phys.* **C 67** (1995) 665, hep-ph/9502206;
S. King and P. White, *Phys. Rev.* **D 53** (1996) 4049, hep-ph/9508346;
S. Ham, S. Oh and B. Kim, *J. Phys.* **G 22** (1996) 1575, hep-ph/9604243;
G. Hiller, hep-ph/0404220.

[187] D. Miller, R. Nevzorov and P. Zerwas, *Nucl. Phys.* **B 681** (2004) 3, hep-ph/0304049.

[188] U. Ellwanger and C. Hugonie, *Phys. Lett.* **B 623** (2005) 93, hep-ph/0504269.

[189] J. Gunion, H. Haber and T. Moroi, hep-ph/9610337.

[190] U. Ellwanger, J. Gunion and C. Hugonie, hep-ph/0111179.

[191] U. Ellwanger, J. Gunion, C. Hugonie and S. Moretti, hep-ph/0305109.

[192] U. Ellwanger, J. Gunion, C. Hugonie and S. Moretti, hep-ph/0401228.

[193] D. Miller and S. Moretti, hep-ph/0403137.

[194] U. Ellwanger, J. Gunion and C. Hugonie, *JHEP* **0507** (2005) 041, hep-ph/0503203.

[195] G. Kane and S. King, *Phys. Lett.* **B451** (1999) 113. See also: S. Dimopoulos and G. Giudice, *Phys. Lett.* **B357** (1995) 573;
P. Chankowski, J. Ellis, S. Pokorski, *Phys. Lett.* **B 423** (1998) 327;
P. Chankowski, J. Ellis, M. Olechowski and S. Pokorski, *Nucl. Phys.* **B544** (1999) 39.

[196] M. Bastero-Gil, C. Hugonie, S. King, D. Roy and S. Vempati, *Phys. Lett.* **B 489** (2000) 359, hep-ph/0006198.

[197] S. Heinemeyer and W. Hollik, *Nucl. Phys.* **B 474** (1996) 32, hep-ph/9602318.

[198] [LEP Higgs Working Group], LHWG-Note 2005-01;
see also the talk by A. Sopczak, "MSSM Higgs boson searches at LEP", presented at SUSY 2005, Durham, England. Tabular numbers provided by A. Sopczak, Tom Junk and Philip Bechtle.

[199] R. Dermisek and J. Gunion, hep-ph/0510322;
see also: J.F. Gunion, presented at Berkeley, Oct. 11, 2005, and the TeV4LHC Workshop, Fermilab, Oct. 20, 2005.

[200] J. Gunion and M. Szleper, hep-ph/0409208.

[201] J. Gunion, D. Hooper and B. McElrath, hep-ph/0509024.

[202] G. Belanger, F. Boudjema, C. Hugonie, A. Pukhov and A. Semenov, *JCAP* **0509** (2005) 001, hep-ph/0505142.

[203] H. Haber and M. Sher, *Phys. Rev.* **D 35** (1987) 2206;
M. Drees, *Phys. Rev.* **D 35** (1987) 2910;
K. Babu, X. He and E. Ma, *Phys. Rev.* **D 36** (1987) 878;
J. Espinosa and M. Quiros, *Phys. Lett.* **B 279** (1992) 92;
J. Espinosa and M. Quiros, *Phys. Lett.* **B 302** (1993) 51, hep-ph/9212305;
M. Cvetic, D. Demir, J. Espinosa, L. Everett and P. Langacker, *Phys. Rev.* **D 56** (1997) 2861; [Erratum-ibid. **D 58**, 119905 (1998)] hep-ph/9703317;

[204] P. Batra, A. Delgado, D. Kaplan and T. Tait, *JHEP* **0402**, 043 (2004) hep-ph/0309149.

[205] R. Martinez, N. Poveda and J. Rodriguez, *Phys. Rev.* **D 69**, 075013 (2004);
A. Maloney, A. Pierce and J. Wacker, hep-ph/0409127;
K. Babu, I. Gogoladze and C. Kolda, hep-ph/0410085.

[206] T. Tait and C. Yuan, *Phys. Rev.* **D 63**, 014018 (2001), hep-ph/0007298;
Z. Sullivan, *Phys. Rev.* **D 66**, 075011 (2002), hep-ph/0207290.

[207] P. Batra, A. Delgado, D. Kaplan and T. Tait, *JHEP* **0406**, 032 (2004), hep-ph/0404251.

[208] R. Harnik, G. Kribs, D. Larson and H. Murayama, *Phys. Rev.* **D 70**, 015002 (2004), hep-ph/0311349.

[209] S. Chang, C. Kilic and R. Mahbubani, *Phys. Rev.* **D 71**, 015003 (2005), hep-ph/0405267.

[210] A. Delgado and T. Tait, *JHEP* **0507**, 023 (2005), hep-ph/0504224.

[211] G. Branco, L. Lavoura and J. Silva, *CP Violation* (Oxford University Press, Oxford, England, 1999), chapters 22 and 23.

[212] I. Ginzburg and M. Krawczyk, hep-ph/0408011.

[213] S. Davidson and H. Haber, *Phys. Rev.* **D 72**, 035004 (2005) [Erratum: **D 72**, 099902(E) (2005)], hep-ph/0504050.

[214] H. Georgi and D. Nanopoulos, *Phys. Lett.* **B 82**, 95 (1979).

[215] J. Donoghue and L. Li, *Phys. Rev.* **D 19**, 945 (1979).

[216] F. Botella and J. Silva, *Phys. Rev.* **D 51**, 3870 (1995).

[217] L. Lavoura and J. Silva, *Phys. Rev.* **D 50**, 4619 (1994).

[218] L. Lavoura, *Phys. Rev.* **D 50**, 7089 (1994), hep-ph/9405307.

[219] G. Branco, M. Rebelo and J. Silva-Marcos, *Phys. Lett.* **B 614**, 187 (2005), hep-ph/0502118.

[220] J. Gunion and H. Haber, *Phys. Rev.* **D 72**, 095002 (2005), hep-ph/0506227.

[221] I. Ivanov, hep-ph/0507132.

[222] W. Hou, *Phys. Lett.* **B 296**, 179 (1992);
D. Chang, W. Hou and W. Keung, *Phys. Rev.* **D 48**, 217 (1993);
D. Atwood, L. Reina and A. Soni, *Phys. Rev.* **D 55**, 3156 (1997).

[223] H. Haber and D. O'Neil, *in preparation.*

[224] J. Gunion and H. Haber, *Phys. Rev.* **D 67**, 075019 (2003), hep-ph/0207010.

[225] J. Gunion, H. Haber and J. Kalinowski, *in preparation.*

[226] S. Glashow and S. Weinberg, *Phys. Rev.* **D 15**, 1958 (1977).

[227] H. Haber, G. Kane and T. Sterling, *Nucl. Phys.* **B 161**, 493 (1979).

[228] L. Hall and M. Wise, *Nucl. Phys.* **B 187**, 397 (1981).

[229] P. Fayet, *Nucl. Phys.* **B 78**, 14 (1974); *Nucl. Phys.* **B 90**, 104 (1975);
K. Inoue, A. Kakuto, H. Komatsu and S. Takeshita, *Prog. Theor. Phys.* **67**, 1889 (1982);
R. Flores and M. Sher, *Annals Phys. (NY)* **148**, 95 (1983);
J. Gunion and H. Haber, *Nucl. Phys.* **B 272**, 1 (1986) [Erratum: **B 402**, 567 (1993)].

[230] M. Carena and H. Haber, *Prog. Part. Nucl. Phys.* **50**, 63 (2003), hep-ph/0208209.

[231] K.S. Babu, C. Kolda, *Phys. Rev. Lett.* **89** (2002) 241802;

[232] A. Pilaftsis, *Phys. Lett.* **B 285** (92) 68.

[233] A. Brignole, A. Rossi, *Phys. Lett.* **B 566** (2003) 217; *Nucl. Phys.* **B 701** (2004) 3;
E. Arganda, et al., *Phys. Rev.* **D 71** (2005) 035011.

[234] J. Diaz-Cruz, R. Noriega-Papaqui, A. Rosado, *Phys. Rev.* **D 69** (2004) 095002.

[235] K. Assamagan, A. Deandrea and P.-A. Delsart, *Phys. Rev.* **D 67** (2003) 035001.

[236] S. Kanemura, et al., *Phys. Lett.* **B 599** (2004) 83;
S. Kanemura, T. Ota, K. Tsumura, hep-ph/0505191.

[237] S. Kanemura, Y. Kuno, M. Kuze and T. Ota, *Phys. Lett.* **B 607** (2005) 165.

[238] K. Hagiwara, S. Ishihara, R. Szalapski, D. Zeppenfeld, *Phys. Lett.* **283** (1992) 353; *Phys. Rev.* **48** (1993) 2182.

[239] B. Zhang, Y.-P. Kuang, H.-J. He, C.-P. Yuan, *Phys. Rev.* **67** (2003) 114024.

[240] M. Gonzalez-Garcia, *Int. J. Mod. Phys.* **A 14** (1999) 3121.

[241] T. Han, Y. Kuang and B. Zhang, hep-ph/0512193.

[242] V. Barger, T. Han, P. Langacker, B. McElrath and P. Zerwas, *Phys. Rev.* **D 67** (2003) 115001, hep-ph/0301097.

[243] U. Baur, T. Plehn, D. Rainwater, *Phys. Rev.* **67** (2003) 033003; *Phys. Rev.* **68** (2003) 033001.

[244] For reviews, see: M. Schmaltz, *Nucl. Phys. Proc. Suppl.* **117**, 40 (2003), hep-ph/0210415;
M. Schmaltz and D. Tucker-Smith, hep-ph/0502182.

[245] H. Georgi and A. Pais, *Phys. Rev.* **D 10**, 539 (1974);
H. Georgi and A. Pais, *Phys. Rev.* **D 12**, 508 (1975);
D. Kaplan and H. Georgi, *Phys. Lett.* **B 136**, 183 (1984);
D. Kaplan, H. Georgi and S. Dimopoulos, *Phys. Lett.* **B 136**, 187 (1984);
H. Georgi and D. Kaplan, *Phys. Lett.* **B 145**, 216 (1984).

[246] N. Arkani-Hamed, A. Cohen and H. Georgi, *Phys. Rev. Lett.* **86**, 4757 (2001) hep-th/0104005;
N. Arkani-Hamed, A. Cohen and H. Georgi, *Phys. Lett.* **B 513**, 232 (2001) hep-ph/0105239;
N. Arkani-Hamed, A. Cohen, T. Gregoire and J. Wacker, *JHEP* **0208**, 020 (2002) hep-ph/0202089;
R. Chivukula, N. Evans and E. Simmons, *Phys. Rev.* **D 66**, 035008 (2002) hep-ph/0204193.

[247] N. Arkani-Hamed, A. Cohen, E. Katz and A. E. Nelson, *JHEP* **0207**, 034 (2002) hep-ph/0206021;
I. Low, W. Skiba and D. Smith, *Phys. Rev.* **D 66**, 072001 (2002) hep-ph/0207243;
W. Skiba and J. Terning, *Phys. Rev.* **D 68**, 075001 (2003) hep-ph/0305302;
J. Thaler and I. Yavin, *JHEP* **0508**, 022 (2005) hep-ph/0501036.

[248] D. Kaplan and M. Schmaltz, *JHEP* **0310**, 039 (2003) hep-ph/0302049;
M. Schmaltz, *JHEP* **0408**, 056 (2004) hep-ph/0407143.

[249] N. Arkani-Hamed, A. Cohen, E. Katz, A. Nelson, T. Gregoire and J. G. Wacker, *JHEP* **0208**, 021 (2002) hep-ph/0206020;
T. Gregoire and J. Wacker, *JHEP* **0208**, 019 (2002) hep-ph/0206023.

[250] R. Contino, Y. Nomura and A. Pomarol, *Nucl. Phys.* **B 671**, 148 (2003) hep-ph/0306259;
K. Agashe, R. Contino and A. Pomarol, *Nucl. Phys.* **B 719**, 165 (2005) hep-ph/0412089.

[251] C. Csaki, J. Hubisz, G. Kribs, P. Meade and J. Terning, *Phys. Rev.* **D 67**, 115002 (2003) hep-ph/0211124;
J. Hewett, F. Petriello and T. Rizzo, *JHEP* **0310**, 062 (2003) hep-ph/0211218;

G. Burdman, M. Perelstein and A. Pierce, *Phys. Rev. Lett.* **90**, 241802 (2003) [Erratum-ibid. **92**, 049903 (2004)] hep-ph/0212228;

C. Csaki, J. Hubisz, G. Kribs, P. Meade and J. Terning, *Phys. Rev.* **D 68**, 035009 (2003) hep-ph/0303236;

T. Gregoire, D. Smith and J. Wacker, *Phys. Rev.* **D 69**, 115008 (2004) hep-ph/0305275;

M. Perelstein, M. Peskin and A. Pierce, *Phys. Rev.* **D 69**, 075002 (2004) hep-ph/0310039.

M. Chen and S. Dawson, *Phys. Rev.* **D 70**, 015003 (2004) hep-ph/0311032;

R. Casalbuoni, A. Deandrea and M. Oertel, *JHEP* **0402**, 032 (2004) hep-ph/0311038;

C. Kilic and R. Mahbubani, *JHEP* **0407**, 013 (2004) hep-ph/0312053;

R. Casalbuoni, S. De Curtis and D. Dominici, *Phys. Rev.* **D 70**, 055010 (2004) hep-ph/0405188;

J. Conley, J. Hewett and M. Le, hep-ph/0507198.

[252] S. Chang and J. Wacker, *Phys. Rev.* **D 69**, 035002 (2004) hep-ph/0303001;
S. Chang, *JHEP* **0312**, 057 (2003) hep-ph/0306034.

[253] W. Kilian and J. Reuter, *Phys. Rev.* **D 70**, 015004 (2004) hep-ph/0311095.

[254] A. Birkedal-Hansen and J. Wacker, *Phys. Rev.* **D 69**, 065022 (2004) hep-ph/0306161;
H. Cheng and I. Low, *JHEP* **0309**, 051 (2003) hep-ph/0308199;
H. Cheng and I. Low, *JHEP* **0408**, 061 (2004) hep-ph/0405243;
I. Low, *JHEP* **0410**, 067 (2004) hep-ph/0409025;
J. Hubisz and P. Meade, hep-ph/0411264;
J. Hubisz, P. Meade, A. Noble and M. Perelstein, hep-ph/0506042;
H. Cheng, I. Low and L. Wang, hep-ph/0510225.

[255] A. Birkedal, Z. Chacko and M. Gaillard, *JHEP* **0410**, 036 (2004) hep-ph/0404197;
T. Roy and M. Schmaltz, hep-ph/0509357;
C. Csaki, G. Marandella, Y. Shirman and A. Strumia, hep-ph/0510294.

[256] T. Han, H. Logan, B. McElrath and L. Wang, *Phys. Lett.* **B 563**, 191 (2003) [Erratum-ibid. **B 603**, 257 (2004)] hep-ph/0302188;
C. Yue, S. Wang and D. Yu, *Phys. Rev.* **D 68**, 115004 (2003) hep-ph/0309113;
G. Azuelos et al., *Eur. Phys. J.* **C 39S2**, 13 (2005) hep-ph/0402037;
G. Gonzalez-Sprinberg, R. Martinez and J. Rodriguez, *Phys. Rev.* **D 71**, 035003 (2005) hep-ph/0406178;
J. Lee, *JHEP* **0412**, 065 (2004) hep-ph/0408362;
S. Park and J. Song, *Phys. Rev.* **D 69**, 115010 (2004);
G. Marandella, C. Schappacher and A. Strumia, *Phys. Rev.* **D 72**, 035014 (2005) hep-ph/0502096;
T. Han, H. Logan and L. Wang, hep-ph/0506313.

[257] H. Logan, *Phys. Rev.* **D 70**, 115003 (2004) hep-ph/0405072.

[258] W. Huo and S. Zhu, *Phys. Rev.* **D 68**, 097301 (2003) hep-ph/0306029;
S. Choudhury, N. Gaur, A. Goyal and N. Mahajan, *Phys. Lett.* **B 601**, 164 (2004) hep-ph/0407050;
S. Choudhury, N. Gaur, G. Joshi and B. McKellar, hep-ph/0408125;
A. Buras, A. Poschenrieder and S. Uhlig, *Nucl. Phys.* **B 716**, 173 (2005) hep-ph/0410309;
C. Yue and W. Wang, *Nucl. Phys.* **B 683**, 48 (2004) hep-ph/0401214;

T. Han, H. Logan, B. Mukhopadhyaya and R. Srikanth, *Phys. Rev.* **D 72**, 053007 (2005) hep-ph/0505260.

[259] E. Katz, J. Lee, A. Nelson and D. Walker, hep-ph/0312287;
D. Kaplan, M. Schmaltz and W. Skiba, *Phys. Rev.* **D 70**, 075009 (2004) hep-ph/0405257;
O. Kong, *Phys. Rev.* **D 70**, 075021 (2004) hep-ph/0409238;
P. Batra and D. Kaplan, hep-ph/0412267.

[260] W. Kilian, D. Rainwater and J. Reuter, *Phys. Rev.* **D 71**, 015008 (2005) hep-ph/0411213.

[261] N. Haba and N. Maru, *Phys. Lett.* **B 532** (2002) 93.

[262] J. Gunion, R. Vega and J. Wudka, *Phys. Rev.* **D 42** (1990) 1673.

[263] N. Arkani-Hamed, S. Dimopoulos and G. Dvali, *Phys. Lett.* **B429** (1998) 263.

[264] L. Randall and R. Sundrum, *Phys. Rev. Lett.* **83** (1999) 3370; *Phys. Rev. Lett.* **83** (1999) 4690.

[265] J. Hewett, *Phys. Rev. Lett.* **82** (1999) 4765.

[266] H. Davoudiasl, J. L. Hewett and T. Rizzo, *Phys. Rev. Lett.* **84** (2000) 2080.

[267] G. Giudice, R. Rattazzi and J. Wells, *Nucl. Phys.* **B 544** (1999) 3, hep-ph/9811291.

[268] L. Hall and C. Kolda, *Phys. Lett.* **B 459** (1999) 213, hep-ph/9904236.

[269] A. Datta, E. Gabrielli, B. Mele, hep-ph/0303259.

[270] A. Datta, E. Gabrielli and B. Mele, *JHEP* **0310**, 003 (2003).

[271] N. Deshpande and D. Ghosh, *Phys. Rev.* **D 67** (2003) 113006, hep-ph/0301272.

[272] T. Rizzo, *Phys. Rev.* **D 60** (1999) 075001, hep-ph/9903475.

[273] N. Delerue, K. Fujii and N. Okada, *Phys. Rev.* **D 70**, 091701 (2004).

[274] G. Giudice, R. Rattazzi and J. Wells, *Nucl. Phys.* **B595** (2001) 250;
C. Csaki, M. Graesser and G. Kribs, *Phys. Rev.* **D63** (2001) 065002;
W. Goldberger and M. Wise, *Phys. Rev. Lett.* **83**, 4922 (1999), hep-ph/9907447.

[275] M. Battaglia, D. Dominici, J. Gunion and J. Wells, hep-ph/0402062.

[276] E. Kolb, G. Servant and T. Tait, *JCAP* **0307**, 008 (2003), hep-ph/0306159.

[277] J. Hewett and T. Rizzo, *JHEP* **0308** (2003) 028, hep-ph/0202155;
D. Dominici, B. Grzadkowski, J. Gunion and M. Toharia, hep-ph/0206192.

[278] R. Sundrum, *Phys. Rev.* **D59**, 085009 (1999);
A. Dobado and A. Maroto, *Nucl. Phys.* **B592**, 203 (2001);
J. Cembranos, A. Dobado and A. Maroto, *Phys. Rev.* **D65** 026005 (2002).

[279] J. Cembranos, A. Dobado and A. Maroto, *Phys. Rev. Lett.* **90**, 241301 (2003); *Int. J. Mod. Phys.* **D13**, 2275 (2004).

[280] J. Cembranos, A. Dobado, A. Maroto, *Phys. Rev.* **D70**, 096001 (2004).

[281] J. Alcaraz et al., *Phys. Rev.* **D67**, 075010 (2003); J. Cembranos, A. Dobado, A. Maroto, *AIP Conf.Proc.* **670**, 235 (2003).

[282] P. Achard et al. [L3 Collaboration], *Phys.Lett.* **B597** (2004) 145.

[283] J. Cembranos, A. Dobado and A. Maroto, *Phys. Rev.* **D68**, 103505 (2003)

[284] J. Cembranos, A. Dobado and A. Maroto, hep-ph/0507066; hep-ph/0510399.

[285] P. Skands et al., FERMILAB-CONF-05-521-T, see: `www.ippp.dur.ac.uk/montecarlo/BSM/`; appeared in:
B. Allanach et al., hep-ph/0602198.

[286] M. Frank, S. Heinemeyer, W. Hollik and G. Weiglein, hep-ph/0202166.

[287] M. Spira, *Fortsch. Phys.* **46**, 203 (1998), hep-ph/9705337.

[288] K. Chetyrkin, B. Kniehl and M. Steinhauser, *Phys. Rev. Lett.* **79**, 353 (1997), hep-ph/9705240.

[289] H. Zheng and D. Wu, *Phys. Rev.* **D 42**, 3760 (1990);
A. Djouadi, M. Spira, J. van der Bij and P. Zerwas, *Phys. Lett.* **B 257**, 187 (1991);
S. Dawson and R. Kauffman, *Phys. Rev.* **D 47**, 1264 (1993);
A. Djouadi, M. Spira and P. Zerwas, *Phys. Lett.* **B 311**, 255 (1993), hep-ph/9305335;
K. Melnikov and O. Yakovlev, *Phys. Lett.* **B 312**, 179 (1993) hep-ph/9302281;
M. Inoue, R. Najima, T. Oka and J. Saito, *Mod. Phys. Lett.* **A 9**, 1189 (1994);
J. Fleischer, O. Tarasov and V. Tarasov, *Phys. Lett.* **B 584**, 294 (2004), hep-ph/0401090.

[290] M. Steinhauser, hep-ph/9612395.

[291] U. Aglietti, R. Bonciani, G. Degrassi and A. Vicini, hep-ph/0404071.

[292] F. Fugel, B. Kniehl and M. Steinhauser, hep-ph/0405232.

[293] Y. Liao and X. Li, *Phys. Lett.* **B 396**, 225 (1997), hep-ph/9605310;
A. Djouadi, P. Gambino and B. Kniehl, *Nucl. Phys.* **B 523**, 17 (1998), hep-ph/9712330.

[294] J. Korner, K. Melnikov and O. Yakovlev, *Phys. Rev.* **D 53**, 3737 (1996), hep-ph/9508334.

[295] A. Djouadi, M. Spira and P. Zerwas, *Z. Phys.* **C 70** (1996) 427, hep-ph/9511344.

[296] M. Carena, H. Haber, H. Logan and S. Mrenna, *Phys. Rev.* **D 65**, 055005 (2002) [Erratum-ibid. **D 65**, 099902 (2002)] hep-ph/0106116.

[297] S. Eidelman et al. [Particle Data Group Collaboration], *Phys. Lett.* **B 592** (2004) 1.

[298] A. Hoang, hep-ph/0008102.

[299] M. Winter, LC Note LC-PHSM-2001-016, see: `www-flc.desy.de/lcnotes`.

[300] A. El-Khadra and M. Luke, *Ann. Rev. Nucl. Part. Sci.* **52**, 201 (2002), hep-ph/0208114;
T. Lee, *JHEP* **0310**, 044 (2003), hep-ph/0304185.

[301] G. Corcella and A. Hoang, *Phys. Lett.* **B 554**, 133 (2003), hep-ph/0212297.

[302] M. Carena, J. Espinosa, M. Quiros and C. Wagner, *Phys. Lett.* **B 355**, 209 (1995), hep-ph/9504316.

[303] M. Carena, M. Quiros and C. Wagner, *Nucl. Phys.* **B 461**, 407 (1996), hep-ph/9508343.

[304] M. Carena, J. Ellis, A. Pilaftsis and C. Wagner, *Nucl. Phys.* **B 625**, 345 (2002), hep-ph/0111245.

[305] H. Haber, R. Hempfling and A. Hoang, *Z. Phys.* **C 75**, 539 (1997), hep-ph/9609331.

[306] M. Carena, H. Haber, S. Heinemeyer, W. Hollik, C. Wagner, and G. Weiglein, *Nucl. Phys.* **B 580** (2000) 29, hep-ph/0001002.

[307] J. Casas, J. Espinosa, M. Quirós and A. Riotto, *Nucl. Phys.* **B 436** (1995) 3, E: *ibid.* **B 439** (1995) 466, hep-ph/9407389.

[308] M. Carena, J. Espinosa, M. Quirós and C. Wagner, *Phys. Lett.* **B 355** (1995) 209, hep-ph/9504316.

[309] A. Pilaftsis, *Phys. Rev.* **D 58** (1998) 096010, hep-ph/9803297;
M. Carena, J. Ellis, S. Mrenna, A. Pilaftsis and C. Wagner, *Nucl. Phys.* **B 659** (2003) 145, hep-ph/0211467.
See also Refs. [141–143].

[310] U. Ellwanger and C. Hugonie, hep-ph/0508022.

[311] G. Belanger, F. Boudjema, A. Pukhov and A. Semenov, hep-ph/0405253.

[312] J. Hewett and T. Rizzo, *JHEP* **0308**, 028 (2003), hep-ph/0202155.

[313] D. Dominici, B. Grzadkowski, J. Gunion and M. Toharia, *Nucl. Phys.* **B 671**, 243 (2003), hep-ph/0206192.

[314] B. Lillie, hep-ph/0505074.

[315] F. Petriello, *JHEP* **0205** (2002) 003 hep-ph/0204067.

[316] H. Logan, hep-ph/0409004.

[317] G. Gonzalez-Sprinberg, R. Martinez and J. Rodriguez, *Phys. Rev.* **D 71**, 035003 (2005), hep-ph/0406178.

[318] G. Marchesini, B. Webber, G. Abbiendi, I. Knowles, M. H. Seymour and L. Stanco, *Comput. Phys. Commun.* **67**, 465 (1992).

[319] G. Corcella et al., hep-ph/9912396.

[320] G. Corcella et al., *JHEP* **0101**, 010 (2001), hep-ph/0011363;
see: `hepwww.rl.ac.uk/theory/seymour/herwig/`.

[321] G. Corcella et al., hep-ph/0107071.

[322] G. Corcella et al., hep-ph/0201201.

[323] S. Moretti, K. Odagiri, P. Richardson, M. Seymour and B. Webber, *JHEP* **0204**, 028 (2002), hep-ph/0204123.

[324] S. Moretti, hep-ph/0205105.

[325] See: `hepwww.rl.ac.uk/theory/seymour/herwig/` .

[326] F. Paige, S. Protopescu, H. Baer and X. Tata, hep-ph/0312045;
see: `www.phy.bnl.gov/~isajet/`.

[327] See: `www.hep.phy.cam.ac.uk/ richardn/HERWIG/ISAWIG/` .

[328] P. Skands et al., *JHEP* **0407**, 036 (2004) hep-ph/0311123;
see: `home.fnal.gov/~skands/slha/`.

[329] S. Moretti, hep-ph/0209209.

[330] T. Stelzer and W. Long, *Comput. Phys. Commun.* **81**, 357 (1994), hep-ph/9401258.

[331] H. Murayama, I. Watanabe and K. Hagiwara, KEK-91-11.

[332] F. Maltoni and T. Stelzer, *JHEP* **0302**, 027 (2003), hep-ph/0208156.

[333] G.-C. Cho, K. Hagiwara, J. Kanzaki, T. Plehn, D. Rainwater and T. Stelzer, *in preparation.*

[334] T. Sjostrand, P. Eden, C. Friberg, L. Lonnblad, G. Miu, S. Mrenna and E. Norrbin, *Comput. Phys. Commun.* **135**, 238 (2001), hep-ph/0010017;
see: `www.thep.lu.se/~torbjorn/Pythia.html`.

[335] M. Dobbs et al, hep-ph/0403045.

[336] V. Barger, K. Cheung, A. Djouadi, B. Kniehl and P. Zerwas, *Phys. Rev.* **D 49** (1994) 79, hep-ph/9306270.

[337] E. Norrbin and T. Sjostrand, *Nucl. Phys.* **B 603** (2001) 297, hep-ph/0010012.

[338] B. Allanach et al. [Beyond the Standard Model Working Group], hep-ph/0402295.

[339] H. Baer, F. Paige, S. Protopopescu and X. Tata, hep-ph/9305342.

[340] A. Pukhov and P. Skands, *in preparation.*

[341] K. Huitu, J. Maalampi, A. Pietila and M. Raidal, *Nucl. Phys.* **B 487** (1997) 27, hep-ph/9606311.

[342] G. Barenboim, K. Huitu, J. Maalampi and M. Raidal, *Phys. Lett.* **B 394** (1997) 132, hep-ph/9611362.

[343] K. Lane and S. Mrenna, *Phys. Rev.* **67** (2003) 115011, hep-ph/0210299.

[344] T. Gleisberg, S. Hoche, F. Krauss, A. Schalicke, S. Schumann and J. Winter, *JHEP* **0402**, 056 (2004), hep-ph/0311263;
see: `www.physik.tu-dresden.de/~krauss/hep/`.

[345] F. Krauss, R. Kuhn and G. Soff, *JHEP* **0202** (2002) 044, hep-ph/0109036.

[346] F. Krauss, A. Schalicke and G. Soff, hep-ph/0503087.

[347] S. Catani, F. Krauss, R. Kuhn and B. Webber, *JHEP* **0111** (2001) 063, hep-ph/0109231.

[348] F. Krauss, *JHEP* **0208** (2002) 015, hep-ph/0205283.

[349] A. Schalicke and F. Krauss, *JHEP* **0507** (2005) 018, hep-ph/0503281.

[350] W. Kilian, LC-TOOL-2001-039, see: `www-flc.desy.de/lcnotes`.
See also: `www-ttp.physik.uni-karlsruhe.de/whizard/`.

[351] T. Ohl, hep-ph/0011243;
M. Moretti, T. Ohl and J. Reuter, hep-ph/0102195.

[352] K. Desch and M. Schumacher, hep-ph/0407159.

[353] S. Heinemeyer, talk given at the LHC/ILC workshop, SLAC, April 2005;
K. Desch, M. Dührssen, S. Heinemeyer, H. Logan, D. Rainwater, G. Weiglein and D. Zeppenfeld, *in preparation.*

[354] M. Carena, S. Mrenna and C. Wagner, *Phys. Rev.* **D 60**, 075010 (1999);
K. Babu and C. Kolda, *Phys. Lett.* **B451**, 77 (1999);
H. Haber, M. Herrero, H. Logan, S. Peñaranda, S. Rigolin and D. Temes, *Phys. Rev.* **D 63**, 055004 (2001).

[355] K. Desch, E. Gross, S. Heinemeyer, G. Weiglein and L. Zivkovic, *JHEP* **0409** (2004) 062, hep-ph/0406322.

[356] J. Kamoshita, Y. Okada and M. Tanaka, in *Proceedings of the Workshop on Physics and Experiments with Linear Colliders*, Morioka-Appi, Iwate, Japan 1995 edited by A. Miyamoto *et al.* (World Scientific, Singapore, 1996); *Phys. Lett.* **B 391**, 124 (1997);
I. Nakamura and K. Kawagoe, in *Proceedings of the Workshop on Physics and Experiments with Linear Colliders*, Morioka-Appi, Iwate, Japan 1995 edited by A. Miyamoto *et al.* (World Scientific, Singapore, 1996); *Phys. Rev.* **D 54**, 3634 (1996); S. Kiyoura and Y. Okada, hep-ph/0101172.

[357] K. Desch, J. Kalinowski, G. Moortgat-Pick, M. Nojiri and G. Polesello, *JHEP* **0402** (2004) 035, hep-ph/0312069.

[358] S. Heinemeyer, W. Hollik and G. Weiglein, *Eur. Phys. J.* **C 16** (2000) 139, hep-ph/0003022.

[359] J.-C. Brient, LC-PHSM-2004-002, see: `www-flc.desy.de/lcnotes` .

[360] G. Moortgat-Pick, S. Hesselbach, F. Franke and H. Fraas, *JHEP* **0506** (2005) 048, hep-ph/0502036; hep-ph/0508313.

[361] U. Ellwanger, J. Gunion and C. Hugonie, *JHEP* **0507** (2005) 041, hep-ph/0503203.

[362] C. Bennett et al., *Astrophys. J. Suppl.* **148** (2003) 1, astro-ph/0302207;
D. Spergel et al. [WMAP Collaboration], *Astrophys. J. Suppl.* **148** (2003) 175, astro-ph/0302209.

[363] H. Goldberg, *Phys. Rev. Lett.* **50** (1983) 1419;
J. Ellis, J. Hagelin, D. Nanopoulos, K. Olive and M. Srednicki, *Nucl. Phys.* **B 238** (1984) 453.

[364] See: `www.rssd.esa.int/index.php?project=PLANCK&page=index` .

[365] M. Battaglia and M. Peskin, hep-ph/0509135.

[366] T. Moroi and Y. Shimizu, hep-ph/0509196.

[367] P. Gondolo, J. Edsjo, P. Ullio, L. Bergstrom, M. Schelke and E. Baltz, *JCAP* **0407** (2004) 008, astro-ph/0406204.

[368] W. Oller, H. Eberl and W. Majerotto, *Phys. Lett.* **B 590** (2004) 273, hep-ph/0402134; T. Fritzsche and W. Hollik, *Nucl. Phys. Proc. Suppl.* **135** (2004) 102, hep-ph/0407095.

[369] A. Birkedal, "Testing Cosmology at the LHC and NLC", talk given at the ALCPG Workshop, SLAC, Jan. 7-10, 2004.

[370] A. Birkedal et al., hep-ph/0507214.

[371] R. Gray et al., hep-ex/0507008.

[372] J. Feng, K. Matchev and T. Moroi, *Phys. Rev. Lett.* **84** (2000) 2322, hep-ph/9908309; *Phys. Rev.* **D 61** (2000) 075005, hep-ph/9909334; J. Feng, K. Matchev and F. Wilczek, *Phys. Lett.* **B 482** (2000) 388, hep-ph/0004043; J. Feng and K. Matchev, *Phys. Rev.* **D 63** (2001) 095003, hep-ph/0011356.

[373] M. Carena, M. Quiros and C. Wagner, *Phys. Lett.* **B 380**, 81 (1996); D. Delepine, J. Gerard, R. Gonzalez Felipe and J. Weyers, *Phys. Lett.* **B 386**, 183 (1996).

[374] N. Turok and J. Zadrozny, *Phys. Rev. Lett.* **65**, 2331 (1990); *Nucl. Phys.* **B 358**, 471 (1991); *Nucl. Phys.* **B 369**, 729 (1992); A. Bochkarev, S. Kuzmin and M. Shaposhnikov, *Phys. Lett.* **B 244**, 275 (1990); *Phys. Rev.* **D 43**, 369 (1991); A. Nelson, D.B. Kaplan and A. Cohen, *Nucl. Phys.* **B 373**, 453 (1992); P. Huet and A. Nelson, *Phys. Rev.* **D 53**, 4578 (1996); J. Cline, K. Kainulainen and A. Vischer, *Phys. Rev.* **D 54**, 2451 (1996); K. Funakubo, A. Kakuto, S. Otsuki and F. Toyoda, *Prog. Theor. Phys.* **96**, 771 (1996).

[375] S. Kanemura, T. Kubota and E. Takasugi, *Phys. Lett.* **B 313**, 155 (1993); A. Akeroyd, A. Arhrib and E. Naimi, *Phys. Lett.* **B 490**, 119 (2000).

[376] S. Ham and S. Oh, hep-ph/0502116.

[377] D. Bodeker, L. Fromme, S. Huber and M. Seniuch, *JHEP* **0502**, 026 (2005), hep-ph/0412366.

[378] C. Grojean, G. Servant and J. Wells, *Phys. Rev.* **71**, 036001 (2005), hep-ph/0407019.

[379] M. Thomson, proceedings of the LCWS Amsterdam, 2003, see: `www.desy.de/conferences/ecfa-desy-lcext.html` (click on "Proceedings").

[380] K.Mönig, LC Note LC-PHSM-2000-060, see: `www-flc.desy.de/lcnotes` .

[381] K. Desch, A. Imhof, N. Meyer and A. Raspereza, LC-PHSM-2004-009, see: `www-flc.desy.de/lcnotes` .

[382] J.C. Brient, LC-PHSM-2004-001, see: `www-flc.desy.de/lcnotes` .

[383] T. Barklow, "Physics Impact of Detector Performance", talk presented at LCWS05 Workshop, Stanford, 18-22 March 2005.

[384] J.C. Brient, "Higgs measurements and Constraints for the Calorimeter", talk presented at the Snowmass workshop, 14-27 August 2005.

[385] J. Ciborowsky, "Study of VXD Geometry on Favour Tagging", talk presented at the Snowmass workshop, 14-27 August 2005.

[386] See: `berggren.home.cern.ch/berggren/sgv.html` .

[387] SIMDET V3.2, M. Pohl and H. Schreiber, DESY-99-030 (1999).

[388] F. Gaede with T. Behnke, N. Graf, T. Johnson, LC Note LC-TOOL-2003-053,
see: `www-flc.desy.de/lcnotes` .
See also: `lcio.desy.de/` .

[389] T.Behnke et al., LC Note LC-TOOL-2001-005, see: `www-flc.desy.de/lcnotes` .

[390] J. McCormick, "Full Detector Simulation Using SLIC and LCDD", talk presented at the Snowmass workshop, 14-27 August 2005;
see: `lcsim.org/software/index.html#sim.full.slic` .

[391] see: `polywww.in2p3.fr/geant4/tesla/www/mokka/mokka.html` .

[392] A. Miyamoto, "Jupiter and Sattelites", talk presented at the Snowmass workshop, 14-27 August 2005.

[393] V. Morgunov, *"Calorimetry Design With Energy Flow Concept (Imaging Detector for High Energy Physics)"*, 10th International Conference on Calorimetry in High Energy Physics (CALOR 2002), Pasadena, California, 25-30 Mar 2002, published in Pasadena 2002, "Calorimetry in particle physics" 70-84.

[394] S. Chekanov and V. Morgunov, *Phys. Rev.* **D 67** 074011 (2003).

[395] V. Morgunov, SNARK package, available at `www-zeuthen.desy.de/lc_repository/detector_simulation/dev/BRAHMS/tex/snark_html/index.html` .

[396] S. Aplin, "MarlinReco : A Marlin based Reconstruction", talk presented at the Snowmass workshop, 14-27 August 2005.

[397] T. Johnson, "org.lcsim : Reconstruction and Analysis Package", talk presented at the Snowmass workshop, 14-27 August 2005.

[398] T. Yoshiaka, "Particle Flow Algorithm for GLD", talk presented at the Snowmass workshop, 14-27 August 2005.